VOLUME 118 NUMBER 1

THE ASTROPHYSICAL JOURNAL

AN INTERNATIONAL REVIEW OF SPECTROSCOPY
AND ASTRONOMICAL PHYSICS

JULY 1953

THE CRAB NEBULA AS A RADIO SOURCE . *Jesse L. Greenstein and Rudolph Minkowski* 1
RAPID VARIABLES IN THE ORION NEBULA . . *Guillermo Haro and W. W. Morgan* 16
INTERCOMPARISON OF SHELL SPECTRA . . *Paul W. Merrill and A. Louise Lowen* 18
THE RED CORONAL LINE IN THE SPECTRA OF NOVAE . . . *Dean B. McLaughlin* 27
THE ORBIT OF BOSS 1074 . . . . *Roscoe F. Sanford* 35
BETA CEPHEI . . . . *O. Struve, D. H. McNamara, S. M. Kung, and C. Beymer* 39
THE SYSTEM OF ALPHA CORONAE BOREALIS *Gerald E. Kron and Katherine C. Gordon* 55
STELLAR SPECTRA AND COLORS IN AN IRREGULAR REGION IN CYGNUS *Paul R. Annear* 77
SOME CHARACTERISTICS OF COLOR SYSTEMS *W. W. Morgan, D. L. Harris, and H. L. Johnson* 92
THE POSSIBLE INFLUENCE OF INTERSTELLAR CLOUDS ON STELLAR VELOCITIES. II . . . . *Lyman Spitzer, Jr., and Martin Schwarzschild* 106
MAGNETIC FIELDS IN SPIRAL ARMS . . . . *S. Chandrasekhar and E. Fermi* 113
PROBLEMS OF GRAVITATIONAL STABILITY IN THE PRESENCE OF A MAGNETIC FIELD . . . . *S. Chandrasekhar and E. Fermi* 116
THE EFFECT OF ELECTRON SCREENING ON THERMONUCLEAR ENERGY GENERATION . . . . *Geoffrey Keller* 142
THE APSIDAL MOTION AND RADIUS OF GYRATION OF THE PROTON-PROTON SOLAR MODEL . . . . *Lloyd Motz* 147
VARIATIONS IN ATMOSPHERIC ABSORPTION OVER THE DISKS OF JUPITER AND SATURN . . . . *Seymour L. Hess* 151

NOTES

A Probable Clustering of Blue Giants in Cygnus . . . *Luis Münch and W. W. Morgan* 161
The Nebula Near 10 Lacertae . . . . *Hugh M. Johnson* 162
Photoelectric Magnitudes and Colors in NGC 6231 *Robert R. Brownlee and Arthur N. Cox* 165

THE UNIVERSITY OF CHICAGO PRESS
CHICAGO, ILLINOIS, U.S.A.

July 1953 Vol. 118, No. 1

THE ASTROPHYSICAL JOURNAL

AN INTERNATIONAL REVIEW OF SPECTROSCOPY AND ASTRONOMICAL PHYSICS

Published in Collaboration with the American Astronomical Society

S. CHANDRASEKHAR
Managing Editor

GERARD P. KUIPER
Associate Editor

Yerkes Observatory of the University of Chicago

EDITORIAL BOARD

H. W. BABCOCK (1953-57)
Mount Wilson Observatory of the Carnegie Institution of Washington

FRED L. WHIPPLE (1952-54)
Harvard College Observatory

C. D. SHANE (1952-55)
Lick Observatory, University of California

G. HERZBERG (1952-56)
National Research Council, Ottawa

LYMAN SPITZER, JR. (1952-53)
Princeton University Observatory

The Astrophysical Journal is published bimonthly by the University of Chicago at the University of Chicago Press, 5750 Ellis Avenue, Chicago 37, Illinois, during January, March, May, July, September, and November. ¶Two volumes are published per year, one beginning with the January issue and the other beginning with the July issue. The subscription price is $6.00 per volume or $12.00 per year; the price of single copies is $3.00. (Orders for service of less than a volume will be charged at the single copy rate.) ¶Postage is prepaid by the publishers on all orders from the United States and its possessions. No extra charge is made for postage to countries in the Pan American Postal Union. ¶Postage is charged extra as follows: for Canada, 20 cents per volume, 40 cents per year (total $6.20 per volume, $12.40 per year); on single copies 5 cents (total $3.05); for all other countries in the Postal Union, 40 cents per volume, 75 cents per year (total $6.40 per volume, $12.75 per year), on single copies 10 cents (total $3.10). ¶Subscriptions are payable in advance. Please make all remittances payable to The University of Chicago Press, in United States currency or its equivalent by postal or express money orders or bank drafts.

The following is an authorized agent:

For the British Empire, except North America and Australasia: The Cambridge University Press, Bentley House, 200 Euston Road, London, N.W. 1, England. Prices of yearly subscriptions and of single copies may be had on application.

Claims for missing numbers should be made within the month following the regular month of publication. The publishers expect to supply missing numbers free only when losses have been sustained in transit, and when the reserve stock will permit.

Business correspondence should be addressed to The University of Chicago Press, Chicago 37, Illinois.

Communications for the editors and manuscripts should be addressed to: S. Chandrasekhar, Editor of THE ASTROPHYSICAL JOURNAL, Yerkes Observatory, Williams Bay, Wisconsin.

Line drawings and photographs should be made by the author, and all marginal notes such as co-ordinates, wave lengths, etc., should be included in the cuts. It will not be possible to set up such material in type.

One copy of the corrected galley proof should be returned as soon as possible to the editor, Yerkes Observatory, Williams Bay, Wisconsin. Authors should take notice that the manuscript will not be sent to them with the proof.

The cable address is "Observatory, Williamsbay, Wisconsin."

The articles in this journal are indexed in the *International Index to Periodicals*, New York, N.Y.

Applications for permission to quote from this journal should be addressed to The University of Chicago Press, and will be freely granted.

Microfilms of complete journal volumes are available to regular subscribers only and may be obtained at the end of the year. Orders and inquiries should be addressed to University Microfilms, 313 North First Street, Ann Arbor, Michigan.

Notice to subscribers: If you change your address, please notify us and your local postmaster immediately.

Entered as second-class matter, July 31, 1940, at the Post-Office at Chicago, Ill., under the Act of March 3, 1879.

Acceptance for mailing at special rate of postage provided for in United States Postal Act of October 3, 1917, Section 1103, amended February 28, 1925.

[PRINTED IN U.S.A.]

THE ASTROPHYSICAL JOURNAL

AN INTERNATIONAL REVIEW OF SPECTROSCOPY AND
ASTRONOMICAL PHYSICS

VOLUME 118 JULY 1953 NUMBER 1

THE CRAB NEBULA AS A RADIO SOURCE

Jesse L. Greenstein and Rudolph Minkowski
Mount Wilson and Palomar Observatories
Carnegie Institution of Washington
California Institute of Technology

Received December 19, 1952

ABSTRACT

The optical continuous spectrum of the Crab nebula is rediscussed to ascertain whether the electron temperature in the amorphous mass can be very high. Table 1 contains revised data. The level of ionization maintained by electron impacts is given in Tables 2 and 3. The optical radiation might persist even without a central star. Certain nuclear reactions in a "collapsed" star might produce excess *Li* and *C;* broadened lines of ionized carbon should be searched for in the spectrum of the amorphous mass.

The thermal emission at radio frequencies is computed on the basis of Elwert's evaluation of the logarithmic term in the free-free opacity. The Crab nebula is found to be optically thick (Table 1) below 100 Mc. It is not possible to reconcile the observed radio flux from Taurus A with the optical flux at any temperature; the thermal emission is about one-ninetieth of the observed radio flux.

Any nonthermal radio-generation process, like those in other gaseous "point sources," will have its energy distribution changed by the opacity of the surrounding ion-electron cloud. Models in which nonthermal sources suffer absorption prove to have flattened energy distributions (Figs. 1 and 2) at low frequencies, as does the radio source in the Crab nebula.

The radio-frequency opacity of other ionized hydrogen regions is found to be appreciable, and distant nonthermal sources seen through bright *H* II regions will also have flattened spectra. This opacity is proportional to the "emission measure" of the region; the Orion nebula, planetary nebulae, and long paths through weak *H* II regions are optically thick. The Orion nebula should be detectable as a thermal emitter at high frequencies; *H* II regions toward the galactic center may also be detectable in a narrow range of galactic latitude.

The identification of the Crab nebula as a radio source raises the question of whether the radio emission is the low-frequency extension of the optical continuous spectrum observed in the central part of the nebula. The optical spectrum can be interpreted as temperature radiation of the ionized gas, but the values of electron temperature and density resulting from this interpretation do not explain the observed radio emission. Since some of the optical data cannot be determined with high accuracy, a rediscussion of the optical spectrum seemed desirable. The aim of this discussion is to find the astronomically acceptable extreme values of electron temperature and density, to compute the expected line spectrum, and then to explore the possible interpretation of the energy distribution of the radio emission.

THE OPTICAL CONTINUOUS SPECTRUM

One of us (Minkowski) has already attempted to describe the spectrum and estimate the electron temperature of the inner amorphous mass of the Crab nebula;[1] N. U. Mayall[2]

---

[1] R. Minkowski, *Mt. W. Contr.*, No. 666; *Ap. J.*, **96**, 199, 1942.

[2] *Pub. A.S.P.*, **49**, 10, 1937.

[Copyright 1953 by the University of Chicago]

described the line emission of the outer filamentary structures. The continuous spectrum of the inner mass was ascribed by Minkowski to free-free emission of the ionized gas. This same process could possibly produce the radio-frequency emission. It is now necessary to re-examine and extend his computations, for several reasons. His rough measures of the color temperature of the continuum determined the electron temperature. The measured gradient ϕ was 1.75 at $\lambda = 0.45\ \mu$. But if ϕ actually equals 1.35, T_e would be infinite. This difference of 0.40 in ϕ corresponds to about 0.09 on the C_1 photoelectric scale of color excesses. Such an error is quite within the bounds of the observational uncertainty of ϕ; furthermore, 48-inch Schmidt plates show that the field near the Crab nebula is covered by patches of interstellar absorption. Thus it is quite possible that T_e is much higher than given by Minkowski. It is also possible that the Balmer discontinuity, D, was overestimated.[3] Consequently, we now wish to rediscuss the data, allowing for the possibility of a very high electron temperature.

Since it is possible that a supernova outburst occurs in a star that has substantially exhausted its hydrogen, the ratio of helium in the ejected material to the heavier elements may be nearly normal, but the ratio H/He may be somewhat smaller than normal. From the spectra of the filaments, one may estimate that H/He is possibly less than one-tenth its normal value. Let a_Z be the fractional abundance, by number of atoms, of the nucleus of charge Z. We compute the properties of models of composition pure hydrogen, $a_1 = 1$; pure helium, $a_2 = 1$; and the probable "standard mixture," $a_1 = 0.15$, $a_2 = 0.80$, $a_4 = 0.05$. The actual nuclear Z of the elements in the last group (C, N, O, etc.) exceeds 4, but they are only partially ionized. The atomic weights adopted are $\mu_1 = 1$, $\mu_2 = 4$, $\mu_4 = 27$. Under all probable conditions H and He are completely ionized.

Several errata should be noted in the earlier published computations[1] of the Balmer jump. Equation (6) should have a term $3.14 \times 10^5 T_e^{-1}$; equation (8) should have $\Sigma a_Z Z^2$ in the denominator. An error was made in the computations of D for all cases except $a_1 = 1$. The main result of the error is that we must increase the electron temperature required to produce a given Balmer jump for models in which helium or the heavy elements are abundant. We have therefore recomputed D, as well as M, the mass of the nebula, and n_i and n_e, in Table 1, from the theory of recombination and free-free emission by hydrogen-like ions. The equations can be conveniently rewritten as follows:

$$D - 1 = \frac{10^{3.39\theta_e} \Sigma a_Z Z}{2.5 \times 10^{-5} T_e \Sigma a_Z Z^2 + 8 \Sigma a_Z Z^4 \sum_{2Z+1}^{\infty} \frac{1}{s^3} 10^{\theta_e R Z^2 / s^2}}, \qquad (1)$$

$$M = 2.6 \times 10^{-30} A^{1/2} \frac{\Sigma a_Z \mu_Z}{(\Sigma a_Z Z)^{1/2}}, \qquad (2)$$

where, if J_ν is the emission into 4π solid angle,

$$A = \frac{J_\nu (\lambda\ 4250)}{n_i n_e V} = \frac{1.44 \times 10^{37} T_e^{1/2} 10^{2.9\theta_e} J_\nu (\lambda\ 4250)}{\Sigma a_Z Z^2 + 3.14 \times 10^5 T_e^{-1} \Sigma a_Z Z^4 \sum_{2Z+1}^{\infty} \frac{1}{s^3} 10^{\theta_e R Z^2 / s^2}}. \qquad (3)$$

Minkowski estimated that $J_\nu(\lambda\ 4250) = 3.4 \times 10^{21}$. Table 1 is based on his estimate of the volume occupied by the nebula, V, as 10^{55} cm^3. Note that the effect of admixture of heavy elements with H is to diminish D, since, at very high T_e,

$$D - 1 \rightarrow \frac{\Sigma a_Z Z}{2.55 \times 10^{-5} T_e \Sigma a_Z Z^2}. \qquad (4)$$

---

[3] D. Barbier, *Ann. d'ap.*, **8**, 35, 1945; R. Minkowski, *Ann. d'ap.*, **9**, 97, 1946.

The term in the denominator represents the effect of the free-free transitions and results in small Balmer jumps for $T_e > 2 \times 10^5$, especially if Z is large. If the absolute magnitude of the nebula has been underestimated, because of the interstellar absorption, the masses and electron densities are higher than in Table 1. The Gaunt factor, g_{III}, has been taken as unity. The densities n_i and n_e are per cubic centimeter. (Only values of D are given for pure H and pure He.) The predicted gradients at $\lambda = 0.45\ \mu$ are given. While they are all smaller than the observed $\phi = 1.75$, a small allowance for interstellar reddening makes them plausible. If any Balmer jump was, in fact, detectable on the original plates, then $T_e < 4 \times 10^5$; if no Balmer jump exists, then the only limitation is the probable upper limit to the original stellar mass. If we assume that the mass could be $36\ M_\odot$, T_e might be as high as two million degrees[4] We will see that the large uncertainty of T_e does not affect the predicted radio noise of thermal origin.

TABLE 1

PHYSICAL PARAMETERS AS A FUNCTION OF ELECTRON TEMPERATURE OF THE AMORPHOUS MASS

$10^{-4}T_e$	STANDARD MIXTURE				$a_1 = 1.0$ D	$a_2 = 1.0$ D	ϕ	τ_0 AT 100 Mc
	D	n_i	n_e	$M/M_\odot$				
10	1.20	450	880	17.3	1.43	1.10	1.48	2.1
20	1.10	530	1030	20.4	1.20	1.05	1.41	1.1
40	1.05	620	1210	24.1	1.09	1.02	1.37	0.56
100	1.02	770	1500	30.0	1.04	1.01	1.35	0.22
200	1.01	930	1810	36.0	1.02	1.01	1.35	0.12

At such high temperatures, the energy content of the nebula is large, and the emission rate is low. The total luminosity per cubic centimeter, largely free-free, is

$$L_{ff} = \frac{2^7 \pi^3 e^6}{(6\pi)^{3/2} m h c^3} \left(\frac{k}{m}\right)^{1/2} T_e^{1/2} n_i n_e \Sigma a_Z Z^2 . \tag{5}$$

For our standard mixture the radiation is

$$L_{ff} = 6 \times 10^{-27} T_e^{1/2} n_i n_e \qquad (\text{erg/cm}^3\ \text{sec}) . \tag{6}$$

At $T_e = 10^6$, $L_{ff} = 7 \times 10^{-18}$ erg/cm³ sec; since the outburst in A.D. 1054, the total radiation (computed at its present rate) would have been 2×10^{-7} erg/cm³. The thermal energy content is $(n_i + n_e)kT$, which is 3.7×10^{-7} erg/cm³. Other sources of energy include ionization (which is of the same order of magnitude) and the macroscopic kinetic energy content. The Reynolds number is so large that the expansion must be highly irregular or turbulent. The kinetic energy in the expansion (neglecting the electrons) is $\frac{1}{2} n_i v^2 m_H \Sigma a_Z \mu_Z$, which is 2.4×10^{-5} erg/cm³, at the observed[2] radial velocity of 1100 km/sec. Thus dissipation of only 1 per cent of the kinetic energy of expansion would supply the nebular radiation for a thousand years. That the expansion velocities are not purely radial, and not single-valued, is highly probable. The amorphous mass does not seem to be hollow, and significant ejection cannot still be going on. Consequently, an appreciable velocity spread must exist. The velocity of sound even at 10⁶° K in helium is only about 100 km/sec, so that the expansion is highly supersonic. Shock phenomena will occur, and energy conversion from mass motion, via shocks, turbulence, and viscosity, will maintain the high temperature. It would be dangerous to assert positively that the present luminosity of the Crab nebula would persist even if nothing is left of the central star. But at its present expansion velocity and at $T_e = 10^6\,^\circ$ K, the energy content of the nebula is so large that such a hypothesis could be seriously considered.

THE OUTER FILAMENTARY NEBULOSITY

The spectra of the filaments resemble those of filaments in ordinary diffuse and planetary nebulae. However, the weakness of the hydrogen lines is outstanding. $H\beta$ is weaker than the lines of either *He* I or *He* II, and this cannot be a temperature effect. (In ordinary nebulae where *He* I and *He* II are of nearly equal strength, both are weaker than $H\beta$, $H\gamma$, or $H\delta$.) If the filaments are condensations within or from a higher-temperature gas, their spectra are normal except for the low abundance of *H*. If the filaments are cooled by the greater radiation due to high density, then their density is considerably higher than in most diffuse nebulae, since even in the amorphous inner mass the density is higher than in the Orion nebula. The high density is the explanation of the presence of [*O* I] and [*S* II] lines. The latter seem to be strong in condensations in nebulae and in the T Tauri stars.[4] It seems unnecessary to ascribe their strength to abundance anomalies, as W. H. Ramsey does.[5] (For example, it is certainly incorrect to state that [*N* II] is abnormally strong, since the ratio [*N* II]/[*O* II] is actually less than in many emission nebulae.) We discuss below some expected possible anomalies caused by nuclear processes.

A description of the expected line spectrum at very high temperature is given by K. Wurm.[6] Our interpretation differs from his, in that we feel constrained to adopt a low abundance of hydrogen. He points out that at high T_e, *He* II may exceed *H* emission, even with the normal abundance ratio $He/H = \frac{1}{5}$. However, the lines of *He* I are observed to be relatively strong (Minkowski, *Ap. J.*, **96**, Pl. XIII). At temperatures for which *He* I > *He* II the ionization of *H* cannot be sufficiently high to make it weaker than both *He* I and *He* II, as is observed.

LEVEL OF IONIZATION AND SPECTRAL FEATURES

High electron temperatures require a brief investigation of the spectral features to be expected in the amorphous central mass of the nebula. The electron density is similar to, and the volume greater than, that of typical high-excitation planetary nebulae. In addition, since the dilution is very great, electron-impact ionization (as in the solar corona) plays an important role. Although the properties of the central star are relatively uncertain, we may estimate the minimum level of ionization as that maintained by electron-impact ionization alone. The stellar ultraviolet will serve only to increase the ionization level. Several investigators have made rough estimates of the collisional ionization of the corona (Woolley and Allen, F. Hoyle, S. Miyamoto), and a discussion based on Kramers' law has been recently made by G. Elwert.[7] Corrections for the Fermi-Thomas model and for recaptures on higher levels have been included, together with a factor to enforce agreement between Kramers' law and the laboratory data. Omitting some refinements, the level of collisional ionization of an element with ionization potential χ is given by Elwert as

$$\frac{x}{1-x} = 8.3 \times 10^5 \, \frac{f_2}{f_1} \, \frac{\zeta_n}{g_n} \left(\frac{\chi_H}{\chi}\right)^2 \frac{e^{-\chi/kT_e}}{\chi/kT_e} \, . \tag{7}$$

Such an expression, involving a Coulomb approximation, is relatively poor for a low level of ionization and more reliable for nearly stripped ions. The quantities f_1 and f_2 include empirical corrections whose range of uncertainty is a factor 2 in f_2/f_1; ζ_n gives the electrons left in the nth shell, and g measures the effect of recombinations in upper levels. Since values of $f_2/f_1\, g$ are near unity, equation (7) is used to give in Table 2 the mean ionization potential, $\bar{\chi}$, at which $x = 1 - x$. Table 2 also contains the results of more detailed computations using plausible values of f, ζ_n, g, n, and the observed χ for important

---

[4] Greenstein and Struve, *Pub. A.S.P.*, **58**, 370, 1946; A. H. Joy, *Mt. W. Contr.*, No. 709; *Ap. J.*, **102**, 185, 1945.

[5] *Observatory*, **72**, 12, 1952.

[6] *Mitt. d. Hamburger Sternw. in Bergedorf*, Vol. **9**, No. 81, 1951.

[7] *Zs. f. Naturforsch.*, **7a**, 432, 1952.

TABLE 2

EXPECTED IONS FOR COLLISIONAL IONIZATION

T_e (° K)	$\bar{\chi}$	Possible Ions
2×10^5..........	125	*H*, *He* II,* *Li* III, *C* IV,* *C* V, *N* IV, *N* V, *N* VI, *O* IV, *O* V, *O* VI, *Ne* IV, *Ne* V,* *Fe* VI, *Fe* VII*
10^5.............	71	*H*, *He* II,* *Li* II, *C* III,* *C* IV,* *C* V, *N* III,* *N* IV, *N* V, *O* III,* *O* IV, *Ne* III,* *Ne* IV, *Fe* IV, *Fe* V, *Fe* VI
5×10^4..........	40	*H*, *He* I,* *He* II,* *C* II,* *C* III,* *N* II,* *N* III,* *O* II,* *O* III,* *Ne* II, *Ne* III,* *Fe* III,* *Fe* IV

TABLE 3

LEVEL OF COLLISIONAL IONIZATION AT 200,000° K

Element	$\log_{10} N_i$	Element	$\log_{10} N_i$	Element	$\log_{10} N_i$	Element	$\log_{10} N_i$
H.........	−5.53	*C* IV.......	−1.61	*O* III.......	−4.39	*Ne* V......	−0.21
He I.......	−7.35	*C* V........	−0.01	*O* IV.......	−1.75	*Fe* III......	−9.77
He II......	−2.60	*N* II.......	−8.73	*O* V........	−0.27	*Fe* IV......	−5.48
Li II.......	−2.52	*N* III......	−4.61	*Ne* II......	−7.14	*Fe* V.......	−2.73
Li III......	−0.44	*N* IV.......	−1.72	*Ne* III......	−3.49	*Fe* VI......	−1.07
C II.......	−8.72	*N* V.......	−0.40	*Ne* IV......	−1.11	*Fe* VII.....	−0.25
C III.......	−4.31	*O* II.......	−8.23				

NOTES TO TABLES 2 AND 3

The symbols used require discussion. For example, *C* III means doubly ionized carbon, C^{++}. If emission is excited by collision, the *C* III spectrum would dominate; if recombination occurs, *C* II lines would be emitted.

The coexistence of several stages of ionization is one reason for caution in our previous statement that no stellar source was needed for the luminosity of the nebula. We computed L_{ff} in eq. (6) and noted that bound-free emission was relatively small for hydrogenic ions. This is true enough, but, as Lyman Spitzer has pointed out, loss of energy by collisional excitation might occur for some of the ions considered here. If it does, it may greatly exceed the free-free emission by producing forbidden lines in unobservable regions of the spectrum. Collisional excitation of levels higher than about $4kT$ is rather inefficient. We have examined the dominant ions in Table 3 that have lower levels capable of producing forbidden lines of energy less than $4kT$ (69 volts), with the following results. The elements *Li* II, *C* IV, *N* IV, *N* V, *O* IV, *O* V, *Ne* III, *Ne* IV, *Ne* V, *Fe* V, *Fe* VI, and *Fe* VII all have such levels and are capable of producing both permitted and forbidden lines. In so far as they are hydrogenic, the permitted lines probably can be neglected. But if the collisional cross-sections and the transition probabilities are large, the forbidden lines in the far ultraviolet could provide a radiation leak which would deplete the energy stored in the nebula. Only positive observations of lines of highly ionized elements will prove that the electron temperature is high; if T_e is high, the ultraviolet leak due to forbidden lines is small, or a very hot star still exists.

Elements marked with an asterisk in Table 2 have been observed in emission nebulae.

ions. Table 2 gives the dominant ion (or ions) of an element without regard for the existence of permitted or forbidden lines from low excitation potentials. The elements marked with an asterisk in the table exist in planetary nebulae (or symbiotic stars) and might conceivably be found on better spectra of the amorphous mass of the Crab nebula. The observation of any such emission lines will be very difficult. The velocity-broadened lines of the filaments interfere, and the available spectra show that *H*, *He* I, and even *He* II in the filaments will mask possible similar lines in the amorphous mass.

It is instructive to obtain the detailed equilibria for a high electron temperature; we give the results obtained at $T_e = 200{,}000°$ K for a few critical elements. Simultaneous equations of ionization equilibrium must then be computed to obtain the data presented in Table 3. We give the logarithm of N_i, the fraction of an element present in the particular stage of ionization.

Elwert's discussion of collisional ionization differs somewhat from that of other investigators. It is therefore interesting to compare the results from equation (7) (as given in Table 3) with an earlier computation we have made on the basis of a derivation given by F. Hoyle.[8] The agreement is moderately good, with a general tendency for a lower level of ionization to be computed from Elwert's. Differences by a factor of 2 are common, and exceed 10 for a few cases, where the quantity ζ_n/gn changes abruptly, from one ion to the next, at the beginning of a new shell.

The importance of radiative ionizations is difficult to estimate. Let us assume that the star radiates like a black body of temperature $T_s \gg h\nu/k$. Then the number of stellar ultraviolet quanta reaching a point in a transparent nebula with frequencies between ν_1 and ν_2 is

$$\frac{\pi k T_s W}{h c^2} (\nu_2^2 - \nu_1^2) \,, \tag{8}$$

where W is the dilution. Assume a radiative ionization cross-section of 10^{-17} cm^2. The number of ionizations per second per particle can be estimated for hydrogen by setting $\nu_2 = 2\nu_1 = 2R$ (R = Rydberg constant). Then for a star of radius 0.02 $R_\odot$ and $T_s = 4.6 \times 10^5$, with $W = 5 \times 10^{-19}$, the number of radiative ionizations per second is $5 \times 10^{-9}\, n_H$. On the other hand, the collisional ionization rate from the ground state can be computed from Elwert's equation (25). For $n_e = 10^3$ and $T_e = 2 \times 10^5$, the rate is $1.2 \times 10^{-5}\, n_H$, i.e., about 1000 times larger. We can thus apparently neglect radiative ionizations in computing the equilibrium of elements of ionization potential less than $\bar{\chi}$. It is clear that equation (8) will not apply to energies near the stellar energy maximum (about 40 volts for $T_s = 4.6 \times 10^5$). Under the assumptions of Zanstra's solution for the properties of the stellar nucleus of a gaseous nebula, a star is the source of ultraviolet radiation sufficient to maintain the nebular luminosity. On that assumption, for energies $\chi > kT$, the radiative ionization rate must surpass that of collisional ionization. We may therefore expect that the level of ionization for ions like *Li* III, *C* IV, *N* V, *O* IV, and *Fe* VII is higher than given in Table 3. If no stellar source remains, we can, of course, neglect such corrections to the collisional ionization equilibrium.

Lines of *Li* III and *Li* II have never been observed in stellar sources; the former is hydrogenic, and some lines of the series cascading from $n' > 5$ down to $n = 5$ would be in the observable region (e.g., 7 → 5 is at λ 5160). The transition probability would be high. Lines of *O* III, *N* III, *C* III, and *C* IV are observed in some planetaries and Wolf-Rayet stars and would be best suited to measure the level of ionization in the Crab nebula. The Bowen fluorescence mechanism could operate, since the strength of *He* II in the filaments presumably indicates high abundance of helium in the whole mass.

In Tables 2 and 3 we have paid special attention to the possible detection of the elements *Li* and *C*. Two important differences in elemental abundances have been suggested as occurring in collapsed stellar configurations assumed to exist before a supernova outburst. Borst[9] has suggested the endothermic formation of beryllium from

$$He^4 + He^4 + 19\ \mathrm{MeV} \rightarrow Be^7 + n \,. \tag{9}$$

---

[8] *Some Recent Researches in Solar Physics* (Cambridge: At the University Press, 1949), p. 24.

[9] *Phys. Rev.*, **78**, 807, 1950.

This is followed by K-electron capture with a half-life of 53 days, if the beryllium is neutral. (It can, in fact, be very highly ionized, even in the early stages of the supernova outburst, so an argument based on the apparent coincidence of the decay rate of Be^7 with the light-curve decay time loses much of its force.) Nevertheless, if it occurred, lithium would be produced from

$$Be^7 + e^- \rightarrow Li^7 + \gamma \, . \tag{10}$$

Detection of Li in the nebula would strongly favor Borst's mechanism. Another exothermic reaction which can occur at high densities and pressures is proposed by E. Salpeter.[10] This reaction,

$$He^4 + He^4 + 95 \text{ KeV} \rightarrow Be^8 \, , \tag{11}$$

$$He^4 + Be^8 \rightarrow C^{12} + 7.4 \text{ MeV} \, , \tag{12}$$

leads to conversion of helium into carbon and will occur at lower temperatures than the beryllium formation (eq. [9]). It will produce an excess carbon abundance. Since the Crab nebula is apparently hydrogen-poor, particular search should be made for emission lines of carbon. Several stages of ionization may be present, according to Table 2. Salpeter's mechanism (12) could be followed by further exothermic (α, γ) reactions, producing O^{16} and Ne^{20} from C^{12}. Thermonuclear reaction with any residual H produces N^{14}.

While the present spectra do not show any emission lines in the high-temperature mass, spectra of the filaments resemble closely, except for the weakness of hydrogen, spectra of other filaments in normal diffuse nebulae and of planetary nebulae of low excitation. The unusual strength of [S II] in certain patches is correlated with that of [O I], representing an unusually low level of excitation; [S II] is apparently greatly enhanced in nebulous envelopes at low T_e and high density. Thus abnormal abundances have not yet been proved, except for the probable weakness of hydrogen.

FREE-FREE EMISSION AT RADIO FREQUENCIES

Some of the discrete sources of radio emission have been recently identified with filamentary emission nebulae by Baade and by Minkowski.[11] As examples we may cite the filaments with extraordinarily high velocity dispersion in the Cassiopeia A source, or with smaller dispersion in Puppis A. Other radio sources seem to be collision regions in extragalactic nebulae, for example, Cygnus A. These identifications suggest that radio noise may be generated in interstellar gas masses by collision of ionized, and possibly magnetized, clouds or by the disruption of magnetized filaments. The noise generation is then similar to, but on a larger scale than, the processes occurring in the disturbed solar corona. Attempts to explain galactic radio noise as free-free emission in H II regions failed because of the relatively low T_e in such regions. We will inquire whether the high density and T_e in the Crab nebula might produce such thermal emission. The spectra of most radio sources[12,13] have a flux, F_ν, which varies about as $\nu^{-1.3}$. On the other hand, the Taurus A source agrees very well in position with the Crab nebula and was thought[12] to have F_ν nearly constant from 40 to 1210 Mc. An optically thin, free-free source has constant F_ν, so the possibility of thermal emission requires detailed study. Recent unpublished measures at the Radiophysics Laboratory, Sydney, communicated by Bolton, indicate that the flux from Taurus A drops slowly from 50 to 300 Mc, roughly as $\nu^{-0.7}$, while the normal radio source has $F_\nu \propto \nu^{-2.0}$. Thus considerable uncertainty exists as to the actual spectral-energy distribution of Taurus A, but little doubt as to it being flatter than that of other sources.

---

[10] *Ap. J.*, **115**, 326, 1952.

[11] *Ap. J.*, in press.

[12] Stanley and Slee, *Australian J. Sci. Res.*, *A*, **3**, 234, 1950.

[13] Piddington and Minnett, *Australian J. Sci. Res.*, *A*, **4**, 473, 1951.

Along an outward normal, a spherical mass of gas emits intensity I_ν given by

$$I_\nu = \int_0^{\tau_\nu} \frac{j_\nu}{k_\nu} e^{-t_\nu} dt_\nu . \tag{13}$$

The emissivity is j_ν, and τ_ν is the optical thickness through the nebula, corrected for stimulated emission. Assume the following conditions to hold: $h\nu \ll kT$ in both visual and radio frequencies; $\tau_\nu < 1$; $j_\nu = k_\nu B_\nu(T)$, where k_ν is the free-free absorption coefficient. Then

$$I_\nu d\nu d\omega = [-38.53]\, n_i n_e l T_e^{-1/2} \frac{\pi}{3^{1/2}} g_{III} \Sigma a_Z Z^2 d\nu d\omega , \tag{14}$$

where l is the diameter. It can be shown that the bound-free contribution is negligible at radio frequencies and small at optical frequencies when T_e is high. Equation (14) involves the frequency only through the Gaunt factor, g_{III} (defined in eq. [17]), so the *radio-frequency and optical energies cannot differ in order of magnitude* if both originate from hyperbolic transitions. The opacity in the optical frequencies is very small. We will show $\tau_\nu > 1$ in part of the radio region, so that the radio emission becomes less than that given by equation (14). The g_{III} factor is logarithmic and proves to vary only slightly. Stanley and Slee[12] find that the flux from Taurus A is 2×10^{-23} watt/square meter cycle/sec at the earth at 100 Mc, equivalent to 1.9×10^{-20} erg/sec cm^2/$d\nu$. If the Crab nebula, at a distance of 1100 psc, is the source, then the total emission into 4π solid angle at 100 Mc, $J_\nu = 2.8 \times 10^{24}$ erg/sec/$d\nu$. Minkowski,[1] however, finds $J_\nu(\lambda\, 4250) = 3.4 \times 10^{21}$ erg/sec/$d\nu$, i.e., 800 times smaller. Unless g_{III} varies by a factor of 800, free-free emission cannot be the source of the radio noise. The uncertainty of the intensity of the photographic continuum is not greater than a factor of 2 or 3.

There has been considerable discussion of the value of the g_{III} factor at radio frequencies. An approximation by A. W. Maue[14] has been used, which involves a factor $3^{1/2}/\pi \ln (4kT/h\nu)$; Townes, Shklovsky, and others have derived expressions on classical theory. The best recent development of the theory, by G. E. Elwert[15] (discussed by Burkhardt, Elwert, and Unsöld[16]), is applicable for the entire radio range, and even in the optical range. The conditions are as follows: two-body collisions, classical and nonrelativistic. Two approximation forms exist, distinguished by the ratio of the collision frequency to the frequency of the radiation. The absorption per centimeter, corrected for stimulated emission, is

$$k_\nu = \frac{8\pi n_i n_e Z^2 e^6}{3(6\pi)^{1/2} c\,(m kT_e)^{3/2} \nu^2} \times \begin{cases} \dfrac{3^{1/2}}{\pi} \ln \dfrac{kT_e}{1.44 Z e^2 n_i^{1/3}}, & \text{if } d < 1 , \quad \text{or} \quad (15a) \\ \dfrac{3^{1/2}}{\pi} \ln \dfrac{(2kT_e)^{3/2}}{4.22 m^{1/2} Z e^2 \nu}, & \text{if } d > 1 . \quad (15b) \end{cases}$$

The discriminant d, at frequency f, in megacycles per second, is

$$d = \frac{\pi \nu m^{1/2}}{(kT_e)^{1/2} n_i^{1/3}} = [+0.91]\, f T_e^{-1/2} n_i^{-1/3} . \tag{16}$$

We denote the term following the bracket in equations (15) as g_{III}. The ratio of the two factors following the logarithm is nearly equal to d. For all probable T_e, $d \leq 1$ at radio frequencies, and even for $d = 1$ the error is zero if we use equation (15*a*). Only at 3000 Mc must we use equation (15*b*). The value of the logarithmic term of equation (15*a*) is

[14] *Ann. Phys.*, **13**, 161, 1932.

[15] *Zs. f. Naturforsch.*, **3a**, 477, 1948.

[16] *Zs. f. Ap.*, **25**, 310, 1948.

of the order of $3^{1/2}/\pi \ln(420T_e/Zn_i^{1/3})$. At $T_e = 10^6$, $n_i = 770$ (Table 1) and $Z = 2$, g_{III} is about 9.4. Let us take $g_{III} = 1.0$ in the optical region. Then from equation (14) we predict that the radio emission can be, at most, 9 times the emission in the optical region as against the observed ratio of 800. The radio emission exceeds the predicted value by a factor of about 90. In computation of the optical free-free spectrum, Minkowski set $g_{III} = 1$, as we have done in equation (3). If $d > 1$, g_{III} is of the order of $3^{1/2}/\pi \ln(5 \times 10^7 T_e^{3/2}/Z\nu)$; at $T_e = 10^6$, $Z = 2$ and $\nu = 7 \times 10^{14}$, $g_{III} = 3.5$, which would further *increase* the discrepancy. But it is improper to extend equation (15*b*) to such high frequencies, since it becomes zero and then negative. The correct value for g_{III} is near unity at optical frequencies. Thus we must conclude that the hypothesis of thermal emission must be abandoned. A similar conclusion, based on less precise discussion, has been reached by Unsöld and van de Hulst.

RADIO-FREQUENCY OPACITY OF THE CRAB NEBULA

From equation (15*a*) applied to an isothermal homogeneous nebula we obtain the optical thickness along the diameter, l; we can use a mean charge, Z, in the g_{III} factor, and will assume $d < 1$. Then from equation (13)

$$I_\nu = \frac{2kT_e\nu^2}{c^2}\left(1 - e^{-\tau_\nu}\right) , \tag{17}$$

$$I_\nu = \frac{16\pi n_i n_e l e^6 \Sigma a_Z Z^2 g_{III}}{3m^{3/2}c^3(6\pi k)^{1/2}T_e^{1/2}} , \qquad \text{if } \tau_\nu < 1 ; \tag{18}$$

and equation (18) leads to equation (14). If $\tau_\nu \approx 1$, then equation (17) should be used. Computations based on equation (15*a*) show that, for all models of the amorphous mass given in Table 1, $\tau_\nu > 1$ at some observable radio frequency. Table 1 gives the computed[17] absorption, τ_0, at 100 Mc. At another frequency, f, in megacycles, $\tau_f = \tau_0(100/f)^2$. Equation (14) should not be applied if $\tau_f > 0.2$; the Crab nebula absorbs radio waves for $f < 100$ Mc, especially at electron temperatures below 2×10^{5}° K.

The flux, F, through the surface of a nebula of finite optical thickness involves an integration of $I(0, \mu)$ over a disk which may be appreciably darkened. Such refinements do not seem necessary. From an undarkened solution, $F = \pi I(0,1)$; complete darkening gives $F = \frac{2}{3}\pi I(0,1)$. No substantial error will be made if we compute the flux at the earth (denoted by F' to distinguish it from its value at the nebula, F) from the relation

$$F'_\nu = \frac{\pi}{4}\left(\frac{l}{r}\right)^2 \frac{2kT_e\nu^2}{c^2}\left(1 - e^{-\tau_\nu}\right) , \tag{19}$$

where r is the distance to the nebula, 1100 psc. Table 4 shows the computed values of F'_ν; the changes from equation (15*a*) to (15*b*) and from (17) to (18) have all been included. The observed flux from Taurus A is $\log_{10} F'_\nu = -19.78$ at 100 Mc. Thus the optically thin free-free source in the Crab nebula fails to account for the observed flux by a factor of at least 90 even at 2×10^{6}° K. Recent unpublished Australian measures only slightly reduce the discrepancy. Further, the model with $T_e = 10^{5}$° K shows a pronounced drop at low frequencies; e.g., at 40 Mc the flux is down by a factor of 10 from that at 160 Mc. Even neglecting the discrepancy in the absolute value of the flux, the energy distribution at low T_e differs strongly from that found by Stanley and Slee.[12] We might make a radical change in the total intensity of the visual continuum by assuming a very large interstellar absorption, increasing $n_i n_e l$ greatly. But the increase would result in a larger τ_0, and therefore a predicted $F_\nu \propto \nu^2$, in disagreement with the observations.

---

[17] The foregoing is based on Minkowski's estimate of the occupied volume, 10^{55} cm^3, for the amorphous mass. He has allowed for incomplete filling of the inner region. The amorphous mass has an apparent mean radius of 0.64 psc, which is equivalent to 3×10^{55} cm^3; in the computation of τ_0 we have used a diameter, $l = 3^{-1/2} \times 0.64$ psc.

NONTHERMAL EMISSION FROM AN ABSORBING MEDIUM

All our models of the Crab nebula have appreciable opacity at 100 Mc. (The index of refraction, however, is near unity.) The unexpected situation of a discrete source in an absorbing cloud may explain the unusual spectral-energy distribution of the Taurus A source. All known nonthermal discrete sources, as well as the galaxy and the disturbed sun, generate radiation with large fluxes at low frequencies. If such a spectrum is viewed through an absorbing medium with $\tau_\nu \propto \nu^{-2}$, the emergent flux may have a flat maximum.

We lack any theory of the original emissivity of the generation mechanism for insertion in equation (13). We may assume it is similar to that in the sun or in the filamentary emission nebulae identified by Baade and Minkowski[18] with other discrete radio sources.

TABLE 4

FREE-FREE EMISSION FROM THE CRAB NEBULA

(F'_ν in Erg/Cm² Sec/$d\nu$)

f_{mc}	$T_e = 10^5$ ° K		$T_e = 2 \times 10^6$ ° K	
	τ_ν	$\log_{10} F'_\nu$	τ_ν	$\log_{10} F'_\nu$
30	23.0	−23.14	1.3	−21.97
50	8.4	−22.69	0.47	−21.82
70	4.3	−22.40	0.24	−21.77
100	2.1	−22.15	0.12	−21.75
160	0.82	−21.94	0.05	−21.73
250	0.33	−21.84	0.02	−21.72
400	0.14	−21.78	0.01	−21.72
1000	0.02	−21.77	0.00	−21.72
1600	0.01	−21.79	0.00	−21.72
3000	0.00	−21.81	0.00	−21.74

We can use the observed spectrum of other discrete sources to obtain the shape of the emissivity-curve but cannot predict any absolute values. Geometrically possible arrangements include (1) the outer filaments of the Crab nebula may be the source, or (2) the amorphous mass may contain one or more radio-generating sources, or (3) the amorphous mass may contain many distributed radio sources. The geometrical arrangement has great importance. If the absorption τ_i in front of the ith source is a fluctuating quantity about a mean, $\bar{\tau}$, the emergent flux depends on a summation of $a_i e^{-\tau_i}$. This sum is quite unstable and is greatly affected by terms for which τ_i is small. For example, we can exclude from consideration hypothesis (1) above, since, if the filaments are the source, half of them would be essentially unaffected by the absorption in the amorphous mass; the total emitted energy would be that of these front filaments, i.e., that of a typical discrete source. Hypothesis (2), a few nonthermal "point" sources inside the amorphous mass, is illustrated by cases A1 through C4 in Table 5; hypothesis (3), distributed sources, is illustrated by cases D1–D5.

The original generated radio-frequency spectrum will be taken to be the average of the discrete sources studied by the Australian observers.[12, 13] With reasonable accuracy, we can write

$$\epsilon_f = \epsilon_0 f^{-1.3} . \qquad (20)$$

---

[18] *Ap. J.*, in press.

Then we can compute the flux at the earth from a single source, except for arbitrary multiplying constants, as

$$F_i'(f) = \epsilon_i f^{-1.3} \exp\left[-\tau_{0,i}\left(\frac{100}{f}\right)^2\right]. \tag{21}$$

The summed flux from n sources can be written as

$$F'(f) = \bar{\epsilon} f^{-1.3} \sum_1^n a_i \exp\left[-\tau_{0,i}\left(\frac{100}{f}\right)^2\right], \tag{22}$$

where a_i represents the weight of the ith source. We will take $a_i = 1$ in all cases, for simplicity. Computations based on equation (22) were carried through for a variety of models, since the sources could be seen through a $\tau_{0,i}$ having any value less than the total optical thickness of the nebula (τ_0 of Table 1). The value of τ_0 is somewhat uncertain (probably being less than 3), so that we make rather arbitrary choices of $\tau_{0,i}$ in Table 5. The results of these computations are shown in Figure 1. Note that the behavior at low frequency is completely dominated by the presence of a source near the front of the nebula. Cases C2–C4 differ mainly in moving the nearest one of the four sources from $\tau_{0,1} = 0.75$ to $\tau_{0,1} = 0.0$; the total emission changes by a factor of 20 at 50 Mc! Thus fluctuation or sampling theory might have interesting applications to equation (22). Note how flat C3 is with a source very near the front.

TABLE 5

ASSUMED PROPERTIES OF THE MODELS

Model	Optical Thickness at 100 Mc	Remarks
A1	$\tau_{0,1}=0.5$	One source; eq. (22)
A2	$\tau_{0,1}=1.5$	One source; eq. (22)
B	$\tau_{0,i}=0.75, 2.25$	Two sources; eq. (22)
C1	$\tau_{0,i}=0.75, 1.5, 2.25, 3.0$	Four sources; eq. (22)
C2	$\tau_{0,i}=0.2, 1, 2, 3$	Same, one nearer front
C3	$\tau_{0,i}=0.05, 1, 2, 3$	Same, one very near front
C4	$\tau_{0,i}=0, 1, 2, 3$	Same, one at front
D1	$\tau_0 = 0.5$	Uniformly distributed sources; eq. (24)
D2	$\tau_0 = 1$	Same
D3	$\tau_0 = 3$	Same
D4	$\tau_0 = 10$	Same
D5	$\tau_0 = 0.5, 10$	Same, but half of the surface area is optically thin

To avoid the fluctuation inherent in the above models we propose models D1–D5 in which many nonthermal sources are distributed uniformly throughout the amorphous absorbing mass. Such a model produces a flux

$$F'(f) = \int_0^{\tau_f} \frac{\epsilon_f}{k_f} e^{-t_f} dt_f, \tag{23}$$

$$F'(f) = \frac{\epsilon_0}{k_0} f^{0.7} \left\{1 - \exp\left[-\tau_0\left(\frac{100}{f}\right)^2\right]\right\}. \tag{24}$$

We neglect the variation of g_{III}. Models D1–D4 differ only in the value of τ_0 at 100 Mc (taken to be 0.5, 1.0, 3, or 10). They are characterized by a pseudo-Kirchhoff law expressing the proportionality of the absorption and radio-noise generation; while no physical reason exists for such proportionality, it should represent distributed sources fairly well. If no source exists near the front of the nebula, integration of equation (23) would begin at a nonzero value of t. (No results are plotted, but computation shows that such models tend to have a sharp drop at low frequencies resembling that in A1, A2, B, and C1.) All models based on equation (24) have moderately flat energy-curves, especially if τ_0 is large; these curves fall rapidly, above 1000 Mc, since no model of the Crab nebula gives a large τ_0 at very high frequencies. (The frequency of maximum energy is 74 $\tau_0^{1/2}$ Mc.) Model D5 shows the effect of possible difference of the optical thickness across the nebula. In this model, based on equation (24), half the surface of the nebula is assumed to have a small $\tau_0 = 0.5$; the other half has a large $\tau_0 = 10$. The resulting distribution is extremely flat, even though the frequency varies by a factor of nearly 100. It appears that the presence of many nonthermal radio sources within the absorbing amorphous mass of the Crab nebula may explain its flat spectral-energy distribution.

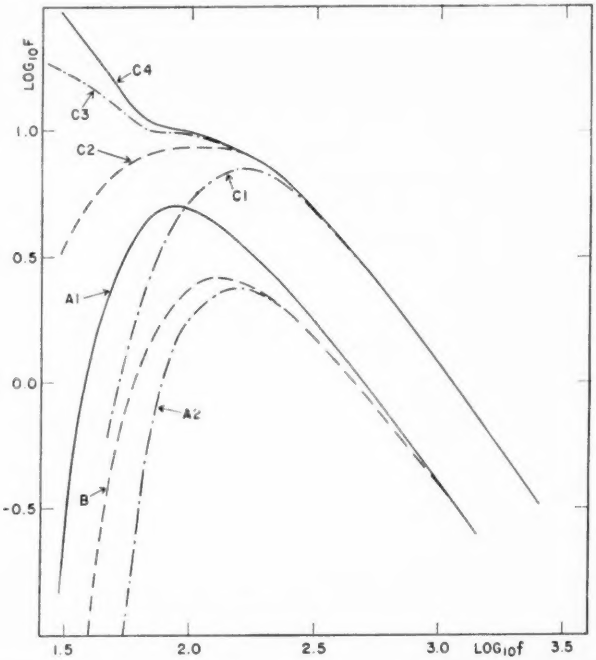

FIG. 1.—Radio-frequency energy distributions based on equation (22) for discrete nonthermal sources surrounded by absorbing material. Model data in Table 5. Ordinates on an arbitrary scale; abscissa is $\log_{10}$ frequency in megacycles. Note that curves *C2–C3–C4* differ only in the optical depth through which a single source (out of four) is observed.

We have shown that no model with purely thermal sources is adequate. The Taurus A source is about 10^{12} times stronger as a radio generator than is the sun, even during intense noise storms. Let us assume that the energy emitted by a radio-generation mechanism is proportional to the volume, to the density squared, and to the magnetic field energy (or possibly its rate of change). In an intense noise storm[19] occurring 0.3 solar radii above the disk, a volume of about 10^{30} cm^3 may be involved; the coronal electron density at that height is $n_e \approx 3 \times 10^7$ cm^{-3}. The required magnetic energy density in the Crab nebula (assuming the same mechanism as in the sun) would be only about 10^{-4} that required in the solar corona during a noise storm. The enormous volume involved, 10^{55} cm^3, is responsible for this favorable ratio. In case the rate of change of the field or merely relative motion of clouds of ionized gas (plasma) generates radio noise, the scaling factor between the sun and the Crab nebula is also reasonable. Velocities of internal motion in the identified radio sources (Puppis and Cassiopeia) are large and exceed those found in sources traveling through the solar corona.

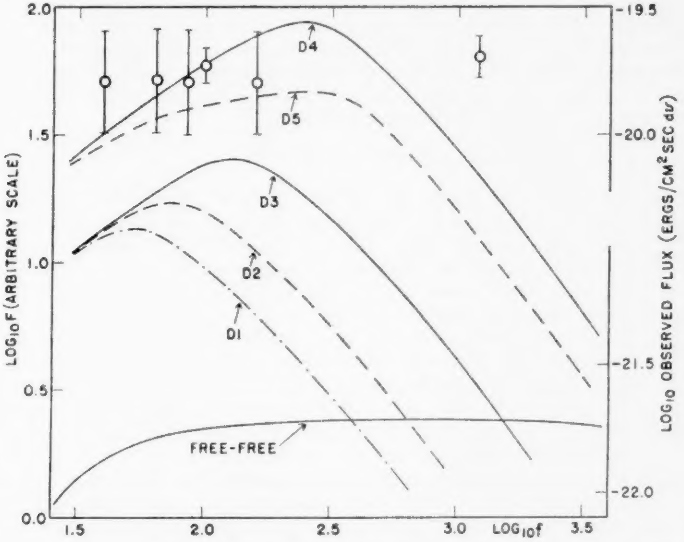

FIG. 2.—Radio-frequency energy distributions based on equation (24) for continuous distribution of sources in an absorbing medium, on left-hand arbitrary scale. Right-hand scale of ordinates for the observed flux (*top*) and the predicted flux of thermal origin (*bottom*). The published fluxes are flat at a value of [−19.78], but unpublished revisions suggest a downward trend with increasing frequency.

RADIO-FREQUENCY OPACITY OF OTHER *H* II REGIONS

The opacity of an ionized gas cloud is given by equation (15*b*) as a function of the "emission measure," *EM*, of the *H* II region. If we define

$$EM = n_i n_e l_{\text{psc}} \approx n_e^2 l_{\text{psc}} , \tag{25}$$

the optical depth at the frequency of *f* megacycles is

$$\tau_f = \frac{0.39EM}{f^2} . \tag{26}$$

---

[19] Payne-Scott and Little, *Australian J. Sci. Res.*, *A*, **4**, 508, 1951.

Equation (26) is derived for ionized hydrogen, at $T_e = 10{,}000°$, and with an approximate mean value of $g_{III} = 7.2$ from equation (15*b*); it agrees well with the computation by Westerhout and Oort.[20]

With radio observations extending down to 40 Mc, where τ_f is relatively large, absorption by an *H* II region will be detectable if *EM* exceeds 2000. B. Strömgren[21] has found that the faintest detectable *H* II regions have *EM* near 400, the average have $EM = 800$, and strong regions $EM = 2000$. Typical diffuse nebulae have $EM = 6400$, and the center of the Orion nebula $EM = 8 \times 10^6$. We therefore see that most observed emission nebulosities are capable of some absorption at radio frequencies. Any considerable path through *H* II regions, for example, along a spiral arm, will have a marked effect on the low-frequency spectrum of the point sources. The latter, when near the sun, show a steeply increasing intensity toward low frequencies; this will be flattened by the absorption. If the original intensity distribution is proportional to $f^{-1.3}$, as in equation (20), the absorption produces a maximum at frequency

$$f_0 = 0.77\,(EM)^{1/2}\,. \tag{27}$$

Thus absorption in a strong *H* II region produces a maximum flux at 34 Mc, while in a typical emission nebula it shifts to 62 Mc. Such effects should be observable, especially since some of the "point" sources prove to be diffuse nebulae. The radio-frequency spectrum should be flattened, at low frequencies, compared to similar sources not seen through *H* II regions. (For a power law, f^{-n}, the maximum is at $f_0^2 = 0.78\,EM/n$.) The *EM* can be derived from the surface brightness in $H\alpha$.

Several applications of this possibility of *absorption* of radio frequencies from point sources can already be seen. Piddington and Minnett[22] suggest tentatively that the large source, Cygnus X, has a relatively flat energy distribution. Cygnus X is behind the heavy dust absorption in the rift near γ Cygni. Patches of filamentary emission nebulosity of rather high surface brightness are visible on 48-inch Schmidt photographs at the least obscured, preceding, end of Cygnus X. The radio source may be a very large (more than 50 psc) filamentary object of the same type as Cassiopeia A and Puppis A. The combination of self-absorption in the filaments and absorption by intervening *H* II regions in Cygnus may produce the observed flattening of the spectrum. It has also been suggested[23] that the radiation from the galactic center has a flatter energy distribution than that of the near-by point sources. Absorption in the intervening spiral arms is very probable. The *EM* of the *H* II regions belonging to inner spiral arms will probably be large because of the higher gas density.

An independent confirmation of this hypothesis would be observation at high frequencies (above 500 Mc) of the thermal flat spectrum of free-free emission at very low galactic latitudes. For this optically thin case, the expected *intensity*, I_ν per unit solid angle, is obtained from equation (14):

$$I_\nu d\omega = [-22.09]\,\Sigma EM d\omega\,. \tag{28}$$

The summation is over all *H* II regions in a line of sight. The galactic-latitude range of the emission would be about ±3°, and, according to Westerhout and Oort,[19] about 0.8 of an *H* II region is encountered per kiloparsec. Thus a ΣEM of 10^4 might be encountered, even without an increase of the gas density toward the galactic center. Whether the resultant small antenna-temperature rise can be measured depends on the antenna acceptance cone and on technical advances only, and we understand it may already have been detected by Ryle and Scheuer.

---

[20] *B.A.N.*, **11**, 323, 1951.

[21] *Problems of Cosmical Aerodynamics* (Dayton, Ohio: Central Air Documents Office, 1951), chap. ii.

[22] *Australian J. Sci. Res.*, *A*, **5**, 17, 1952.

[23] Piddington and Minnett, *ibid.*, **4**, 459, 1951.

In this connection, we should point out a possible test of the hypothesis of thermal emission and a measurement of the electron temperature in the high-frequency radio spectrum of the Orion nebula, a remarkably dense H II region. With the *EM* (8×10^6) found by Strömgren at the center, τ (100 Mc) = 320. The *EM* normally adopted, about 10^5, presumably is an average through the nebula.[24] Even an *EM* of 10^5 gives τ(100 Mc) = 4. The expected energy distribution is that of a black body, at 10,000°, i.e., $\propto f^2$ when $f < 200$ Mc. The expected flux at the earth is 3.5×10^{-22} erg/cm^2 sec/$d\nu$, i.e., 3.5×10^{-25} watt/square meter, for $f > 300$ Mc, about at the lowest limit of detectability. With Strömgren's value of *EM*, of course, the flux is much higher.

The values of *EM* for the brighter planetary nebulae range between 10^5 and 10^6; they are optically thick to very high radio frequencies but subtend too small a solid angle to have been detected so far. The radio detection of the Crab nebula results from its nonthermal character.

We would like to express our appreciation for valuable private communications from workers in this rapidly changing field, especially to John Bolton, J. H. Piddington, F. C. Smith, and R. Hanbury Brown.

---

[24] J. L. Greenstein, *Ap. J.*, **104,** 414, 1946. This *EM* may be obtained from Ambarzumian's surface-brightness determinations of NGC 6572, NGC 7027, and the Orion nebula (*Zs. f. Ap.*, **6,** 107, 1933), together with the known densities and sizes of these planetaries.

RAPID VARIABLES IN THE ORION NEBULA

Guillermo Haro and W. W. Morgan
Observatorios de Tonantzintla y Tacubaya, México, and
Yerkes Observatory, Williams Bay, Wisconsin

Received April 1, 1953

ABSTRACT

Three stars in the Orion Nebula have been found to undergo rapid variations in light in times ranging from 20 to 60 minutes. The variations consist of sudden outbursts of 0.5–1.0 mag. from approximately constant minima.

There are some similarities to the dM "flare stars"; however, the rapid variables in the Orion Nebula have luminosities (uncorrected for absorption) of $M_{pg} = +8$ to $M_{pg} = +9$. These are minimum values in luminosity, since there are certainly appreciable corrections for absorption for the stars described.

A large number of direct exposures of the region of the Orion Nebula have been obtained by Haro during the past three years; these were taken in connection with a general program of study of the nature and distribution of the stars in the region of the nebula. On January 30, 1952, a series of seven plates was obtained with the Schmidt camera of the Tonantzintla Observatory for the purpose of looking for rapid variables. Two exposures of 10 minutes' duration each were made on each plate; there was an interval of 10 minutes between each exposure; and Eastman II*a*-O emulsion was used.

TABLE 1

RAPID VARIABLES

Brun No.	α (1900)	δ (1900)	Mag. (Brun)	Mag. (97)	Range
868	5^h30^m9	$-5°45'$	16.8 (pg)	17.5	0^m5
886	5 30.9	-5 18	15.2 (pg)	16.2	1.0
905 (OX Ori)	5 31.0	-5 31	15.6 (v)	16.9	0.8

On this series, three stars have been observed to undergo rapid variations in light: they are Nos. 868, 886, and 905 in Brun's catalogue.[1] Data for the three stars are given in Table 1.

The fifth column gives approximate photographic magnitudes at minimum light from a comparison with Mount Wilson Selected Area 97; the determinations are uncertain because of the influence of the nebula. The value of the range in light for Brun 905 (OX Ori) was estimated from a plate obtained by Enrique Chavira with the Carte du Ciel camera of the Tacubaya Observatory on December 21, 1952; the greatest increase in light was observed between two exposures whose centers were 30 minutes apart.

Figure 1 (top) gives a reproduction of the Carte du Ciel plate; the mid-exposure was at 7^h58^m U.T. The variable stars T Orionis and AQ Orionis are in the lower left-hand part of the reproduction. The star just to the right of Brun 905 is No. 120 in Haro's catalogue[2] of emission-line stars and is No. 904 (OW Ori) in Brun's list. It is a very interesting variable star having a range of the order of 2 mag. and changes in light in a few days' time.

The two lower reproductions in Figure 1 illustrate a sudden increase in light of Brun 868. The star is invisible on the middle reproduction; the lowest section shows two well-

---

[1] *Lyon Bull.*, **3**, 149, 1934.

[2] *Ap. J.*, **117**, 73, 1953.

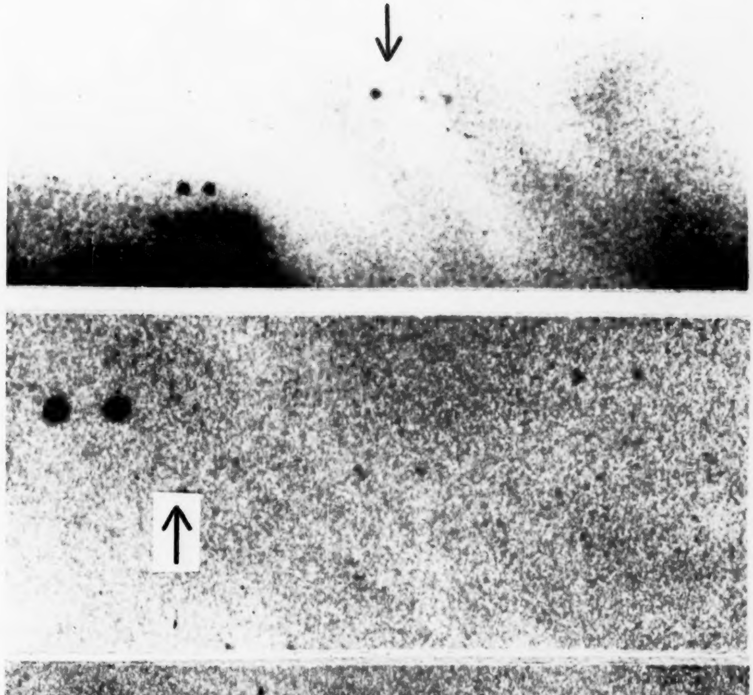

FIG. 1.—*Upper:* Plate of Brun 905 obtained with the Carte du Ciel camera on December 21, 1952. The distance between the images on the two exposures is 15″. North is to the right; east is at the top. The very strong image on the lower left is T Orionis. The interval in time between the mid-points of the two exposures is 30 minutes. Eastman 103*a*-O emulsion.

Lower: Two plates of the field of Brun 868 obtained with the Schmidt camera on January 30, 1952. The mid-point of the two exposures on the middle reproduction was at 2^h25^m U.T.; the mid-point of the two exposures on the lowest plate was at 3^h4^m. The distance between the images of the two exposures on each plate is 31″. North is up; east is to the left. Eastman II*a*-O.

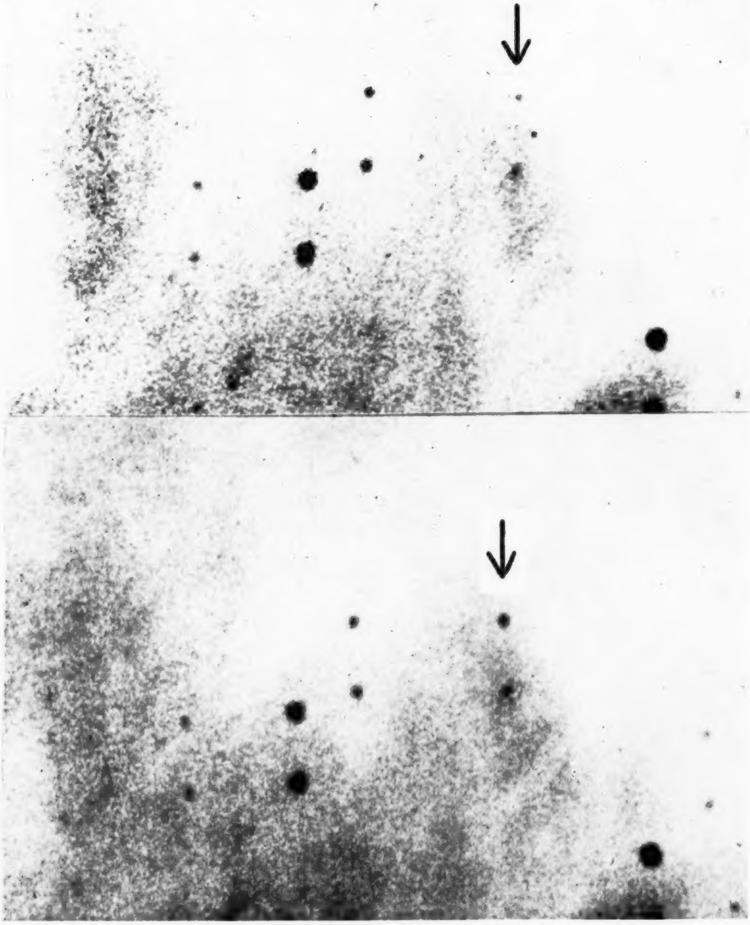

FIG. 2.—Two plates of the field of Brun 886 obtained with the Schmidt camera on January 30, 1952. The mid-point of the two exposures on the upper reproduction was at $4^{h}24^{m}$ U.T.; that of the lower reproduction was at $5^{h}44^{m}$. The distance between the images of the two exposures on each plate is 34″. North is to the right; east is at top. Eastman IIa-O emulsion.

defined images. The interval of time between successive mid-exposures in which the light of the star brightened is 20 minutes. The bright star at the left and above Brun 868 is Brun 885; the first star to the right is Brun 801.

Figure 2 illustrates the increase in light of Brun 886. The lower image of the star in each plate of Figure 2 is affected by a nebulous patch. A comparison of the upper images of Brun 886 with neighboring stars indicates an increase in light of the order of a magnitude in 60 minutes. An intermediate exposure (not illustrated) shows the variable in increasing light. An exposure 15 minutes later than the maximum shows that the variable is decreasing in light. The brightest star in the left-hand part of the field is Brun 870; the star above and to the right of the latter is Brun variable No. 889 (OT Ori); it is No. 104 in Haro's catalogue of emission-line stars.

We may summarize the behavior of the three variables as follows:

They are, for the great majority of the time, at minimum light. The outbursts in brightness occur in a matter of minutes; fading from maximum may be slower but is also rapid. The light-curves are probably similar to those of novae and dM "flare stars."

The nature of the rapid variables in Orion must be different from the dM "flare stars"; the latter have absolute magnitudes considerably fainter than the Orion variables described above. There is certain to be a sensible correction for absorption for the three variables. With a distance modulus of 8.5 for the Orion Nebula, the photographic absolute magnitudes of the three stars are probably brighter than +8 to +9.

The three variables described above showed rapid increases in light in the series of plates covering 4 hours and 30 minutes on a single night. Other objects were suspected of varying in the same period of time. In addition, Haro has found definite cases of variation in time ranging from 3 hours to 19 hours. It therefore seems likely that such rapid variations may be very common among the stars of the Orion Nebula cluster.

INTERCOMPARISON OF SHELL SPECTRA

PAUL W. MERRILL AND A. LOUISE LOWEN
MOUNT WILSON AND PALOMAR OBSERVATORIES
CARNEGIE INSTITUTION OF WASHINGTON
CALIFORNIA INSTITUTE OF TECHNOLOGY

Received February 12,1953

ABSTRACT

Estimates of the intensities of lines of the following elements are recorded for 21 shell stars and 2 c stars; *H*($m = 6$ and $m = 30$), *Mg* I, *Ca* II, *Sc* II, *Ti* II, *Cr* II, *Fe* II, *Ni* II. Correlation plots show that lines of *Mg* I, *Ti* II, and *Cr* II behave about alike. Lines of *Sc* II and *Ni* II show an inverse correlation, although with much scatter; neither element shows a close correlation with other elements. Atomic data offer a partial explanation of these facts. Photometric measurements on the diffuse line λ 4026 *He* I are recorded for 9 stars. The central absorption ranges from 3 to 12 per cent; the actual width, from 5 to 12 A.

Data concerning motions in shells are summarized. In most shells the velocity varies slowly through a large range, and the line structure shows small changes during the velocity-cycle, wings appearing on the side toward which the lines are moving. In stable shells the lines are symmetrical and sharp. Atoms that form a shell probably leave the photosphere very slowly; sometimes they are subject to an outward acceleration. The nature of the outward force is briefly discussed.

About forty examples of stellar shell spectra are now known, exclusive of those "P Cygni" spectra whose dark lines exhibit abnormal shortward displacements. Although these forty form a definite group easily distinguished from normal spectra, they are by no means identical in line intensities or general behavior. The differences are, in fact, of considerable interest in the physical interpretation of the extended stellar atmospheres which give rise to shell spectra.

Twenty-one stars (Table 1), chosen for detailed intercomparison, have well-developed shell spectra showing at least a few lines of ionized metals. Two c stars of spectral type A, η Leonis and α Cygni, were included because, except for lines of *Mg* II and *Si* II, their spectra resemble that of a shell star. Spectrograms of dispersion 10 A/mm were used throughout this study.

The intensities of various groups of lines recorded in Table 2 were based on visual estimates of pairs of spectrograms seen side by side in the Hartmann comparator. The chief lines used for various elements are listed in Table 3. Some difficulty was experienced in estimating intensities of widened lines relative to very sharp lines. To make the results reasonably homogeneous, we did considerable intercomparing of plates with similar lines. A grouping of stars and plates according to line widths is shown in Table 4. As early-type stellar spectra go, all the metallic lines would be called narrow.

Correlation plots of the intensities of lines of various elements on the plates included in Table 2 show that lines of *Mg* I, *Ti* II, and *Cr* II behave in much the same fashion in various stars. Lines of *Fe* II have a strong correlation with lines of *Ca* II and a fair correlation with lines of *Ti* II and *Mg* I. Other combinations, especially those including *Ni* II and *Sc* II, exhibit much scatter. Sample correlation plots are in Figure 1.

In the spectrum of HD 44351, all the elements listed have lines of outstanding strength except *Sc* II, whose lines are surprisingly weak. Another star with weak *Sc* II lines is Pleione, plate Ce 5487. Stars with relatively strong lines of *Sc* II are 17 Leporis; Pleione, Ce 4381; and MWC 985. Stars with relatively strong lines of *Ni* II are β Monocerotis, HD 54858, 48 Librae, HD 183656, and HD 217050. Lines of *Ni* II are relatively weak in 17 Leporis. Lines of *Ca* II are relatively strong in Pleione, Ce 4381 and Ce 5487.

Scandium is a rare element, but λ 4247 *Sc* II attains considerable strength in a few shell stars. This is probably because of the low excitation potential, 0.3 volts, the fairly

TABLE 1

SHELL STARS INTERCOMPARED

Star	MWC	1900 R.A.	1900 Decl.	Mag.	Ref.
Pleione	75	3h 43m3	+23° 51′	5.2	1
HD 33232	100	5 3.7	+40 53	8.1	2
17 Lep	519	6 0.5	−16 29	5.0	3
HD 44351	803	6 16.3	+14 21	8.5	4
HD 45677	142	6 23.7	−13 0	7.5	4
β Mon A	143	6 24.0	− 6 58	4.7	4, 5
HD 45910	145	6 25.2	+ 5 57	6.7	6
HD 50138	158	6 46.7	− 6 51	6.6	4
HD 54858	838	7 5.4	− 9 11	8.4	4
η Leo*	......	10 1.9	+17 15	3.6	......
48 Lib	239	15 52.6	−13 59	4.7	7
T CrB	413	15 55.3	+26 13	Var.	8
HD 179343	978	19 17.1	+ 2 27	6.8	9
BD+30°3526	985	19 17.8	+30 58	9.2	4
HD 183656	988	19 25.5	+ 3 14	6.3	4
HD 192954	335	20 12.6	+15 33	7.3	10
HD 193182	632	20 13.8	+39 16	6.6	11
1 Del	1019	20 25.5	+10 34	5.9	11
α Cyg†	351	20 38.0	+44 55	1.3	......
BD+47°3487	374	21 32.2	+47 28	9.1	4, 12
HD 217050	394	22 52.7	+48 9	5.2	9, 13, 14, 15
HD 218393	397	23 2.6	+49 40	6.8	16
Z And	416	23 28.8	+48 16	Var.	17, 18

* η Leo. Type cA0; not a shell star.

† α Cyg. Type cA2eα; not a shell star.

NOTES TO TABLE 1

1. P. W. Merrill, *Ap. J.*, **115**, 145, 1952.
2. *Ibid.*, **116**, 516, 1952.
3. Burke Smith and Otto Struve, *Ap. J.*, **95**, 468, 1942.
4. P. W. Merrill, *Ap. J.*, **116**, 501, 1952.
5. D. B. McLaughlin, *A.J.*, **56**, 44, 1951.
6. P. W. Merrill, *Ap. J.*, **108**, 481, 1948.
7. *Ibid.*, **117**, 7, 1953.
8. R. F. Sanford, *Ap. J.*, **109**, 81, 1949.
9. P. W. Merrill, *Ap. J.*, **110**, 387, 1949.
10. A. A. Broyles, *Ap. J.*, **97**, 234, 1943.
11. P. W. Merrill, *Ap. J.*, **115**, 42, 1952.
12. C. S. Beals, *Pub. Dom. Ap. Obs. Victoria*, **9**, 1, 1951.
13. R. B. Baldwin, *Ap. J.*, **97**, 388, 1943.
14. O. Struve, *Ap. J.*, **99**, 206, 1944.
15. E. Margaret Burbidge and G. R. Burbidge, *Ap. J.*, **113**, 703, 1951.
16. P. W. Merrill, *Ap. J.*, **110**, 420, 1949.
17. *Ibid.*, **105**, 120, 1947.
18. *Ibid.*, **107**, 317, 1948.

TABLE 2

RELATIVE INTENSITIES OF ABSORPTION LINES OF VARIOUS ELEMENTS

Object	Plate	*H* 10	*H*δ	*Mg* I	*Ca* II	*Sc* II	*Ti* II	*Cr* II	*Fe* II	*Ni* II
Pleione	Ce 3211	6	60	3	7	2	8	7	5	3
	4381	5	60	6	20	6	12	10	8	4
	5487	2	85	2	15	1	12	3	9	3
	6029	Tr	50	Tr	4	Tr	3	2	3	3
	6957	0	10	0	0	0	0	0	0	0
HD 33232	3290	2	120	Tr	5	0	Tr	0	2	2
	3991	6	80	0	8*	0	Tr	0	3	3
	6032	Tr	40	0	Tr	0	0	Tr	(Tr)	1
17 Lep	4106	0	70	2	70	6	30	5	5	(2)
HD 44351	Pc 260	15	140	8	35	1	14	10	12	8
HD 45677	Ce 3291	1	60	Tr	7	0	1	2	Tr	(0)
β Mon A	4923	2	70	0	2	0	0	0	1	3
HD 45910	3629	2	(60)	3	20	Tr	4	3	6	3
HD 50138	3630	2	100	2	30*	Tr	6	2	2	1
	4551	Tr	30	0	7*	0	2	0	Tr	0
HD 54858	Pc 259	2	45	Tr	3	0	1	1	2	2
48 Lib	Ce 1931	1	15	1	2	0	1	1	1	2
	3420	10	130	4	12	Tr	4	3	8	10
	5137	3	60	1	2	0	2	2	2	3
	6441	6	90	2	3	Tr	2	2	4	5
T CrB	4348	4	E	4	3*	3	15	6	3	(2)
HD 179343	5271	Tr	20	Tr	4*	0	1	1	2	1
MWC 985	Pc 122	10	60	4	10	4	7	10	5	6
HD 183656	Ce 6023	2	80	(0)	5*	0	Tr	Tr	2	3
	7222	3	90	1	5	0	2	2	4	4
HD 192954	4953	2	60	1	2	Tr	1	2	2	2
HD 193182	3572	6	60	2	7	1	5	6	5	3
1 Del	5749	1	40	1	4	1	3	4	3	2
MWC 374	5752	Tr	60	0	7	0	0	0	1	(2)
HD 217050	4424	4	60	Tr	4*	0	Tr	0	1	3
HD 218393	3184	Tr	25	0	10*	0	0	0	Tr	Tr
	3607	Tr	25	2	12*	0	3	1	4	(Tr)
Z And	4460	8	E	5	(9)	4	8	6	E	3
η Leo	4520	0	18	2	12	Tr	3	2	4	1
α Cyg	3019	0	35	3	28	1	8	6	8	3

* Blend of stellar and interstellar components.

NOTES TO TABLE 2

Pleione.—Ce 3221 and especially Ce 4381: Lines of high E.P. are relatively strong. Thus lines of *Ti* II λλ 3900, 3913, 4290, 4294, 4300, 4337, with E.P. of lower level 1.1 volts, are relatively strong compared to λλ 3685, 3759, 3761, E.P. 0.6 volts; also *Ni* II λ 4067, E.P. 4.0 volts, is relatively strong compared to λ 3769, E.P. 3.1 volts. Ce 4381: Lines of *Fe* I are relatively strong.

17 Leporis.—The metallic lines are asymmetrical, being sharper on the longward edge. Lines of *Ti* II λ 3900 and λ 3913, E.P. 1.1 volts, are surprisingly weak compared to λλ 3685, 3759, 3761, E.P. 0.6 volts. Lines of *Fe* I are present in moderate strength.

HD 44351.—Lines are slightly sharper on their longward edges. λ 3869, *Ni* II, is decidedly wider than other metallic lines.

HD 45677.—Lines of *Fe* II show traces of narrow minima within wider emission components.

HD 45910.—Absorption lines of *Fe* II have emission on both edges.

48 Librae.—The estimated intensities of the *Ca* II lines are probably not affected appreciably by the faint interstellar components.

T Coronae.—Many lines have emission components. The dark cores of *Ca* II and *Fe* II lie within broader emission lines; dark lines of *Mg* I, *Sc* II, and *Ni* II also have emission edges. The *Ti* II lines λ 3859 and λ 3761 are greatly weakened by emission; the estimate in the table is based on λ 3685.

HD 179343.—Although the lines of *Ca* II are sharp, they may nevertheless possibly be blends of stellar and interstellar components.

MWC 985.—Estimates are difficult because of the narrow spectrum. Lines of *Fe* I are unusually strong.

MWC 374.—The *Fe* II lines have weak emission on their longward edges.

Z Andromedae.—The metallic lines (including lines of *Fe* I) have emission on their shortward edges.

low ionization potential, 6.7 volts, and the fact that the complete spectrum includes only a few strong lines. The strong metastability of the lower level is, of course, an important factor.

Nickel is a cosmically abundant element, its atoms outnumbering those of scandium by a factor of several thousand. Nevertheless, the lines of *Ni* II do not develop great intensity in shell spectra. This is probably because of the high excitation potential of the observable lines (3.1 volts for λ 3769), the rather high ionization potential, 7.6 volts, and the fact that the complete spectrum includes a large number of strong lines.

TABLE 3

WAVE LENGTHS OF CHIEF LINES USED FOR ESTIMATES IN TABLE 2

Element	Wave Lengths	Element	Wave Lengths	Element	Wave Lengths
*H*30	*H*31, 3661; *H*30, 3662; *H*29, 3663	*Mg* I	3829, 3832, 3838	*Cr* II	3677, 3713
		Ca II	3933, 3968	*Fe* II	4233, 4352
*H*6	*H*ε 3970; *H*δ 4101; *H*γ 4340	*Sc* II	4247	*Ni* II	3514, 3769, 4067
		Ti II	3685, 3759, 3761		

TABLE 4

WIDTHS OF LINES

VERY SHARP		SHARP		WIDENED	
Object	Plate No.	Object	Plate No.	Object	Plate No.
HD 33232	Ce 3991 6032	Pleione	Ce 3221 4381 6029	Pleione	Ce 5487 (6957)
HD 45677	3291	HD 33232	3290	17 Lep	4106
β Mon A	4923	HD 44351	Pc 260	HD 45910	3629
HD 54858	Pc 259	48 Lib	Ce 5137	HD 50138	3630 4551
48 Lib	Ce 1931	MWC 985	Pc 122	48 Lib	3420 6441
HD 179343	5271	HD 183656	Ce 6023 7222	T CrB	4348
HD 193182	3572	HD 192954	4953	HD 218393	(3184) 3607
1 Del	5749	MWC 374	5752	α Cyg	3019
HD 217050	4424	η Leo	4520		
Z And	4460				

The correlation in various shell spectra of intensities of *Sc* II lines with intensities of *Ni* II lines, while having much scatter, tends, as might be expected, to be inverse rather than direct.

In the c stars α Cygni and η Leonis the intensities of most of the metallic lines are about the same as in typical shell stars. Lines of *Ni* II and *Sc* II, however, are relatively weak. The lines of *Si* II and *Mg* II are, of course, much stronger than in shell spectra. In α Cygni the actual intensities are considerably greater than in η Leonis, but the relative intensities of various lines are nearly the same in both stars.

Lines of *He* I in shell spectra are so shallow and diffuse that eye estimates of their intensities are not reliable. Because some record of their behavior is desirable, we have made partial photometric tracings of the plates listed in Table 5 and have measured the width and central absorption of the *He* I line λ 4026. The behavior of the helium lines in shell spectra deserves more extensive investigation.

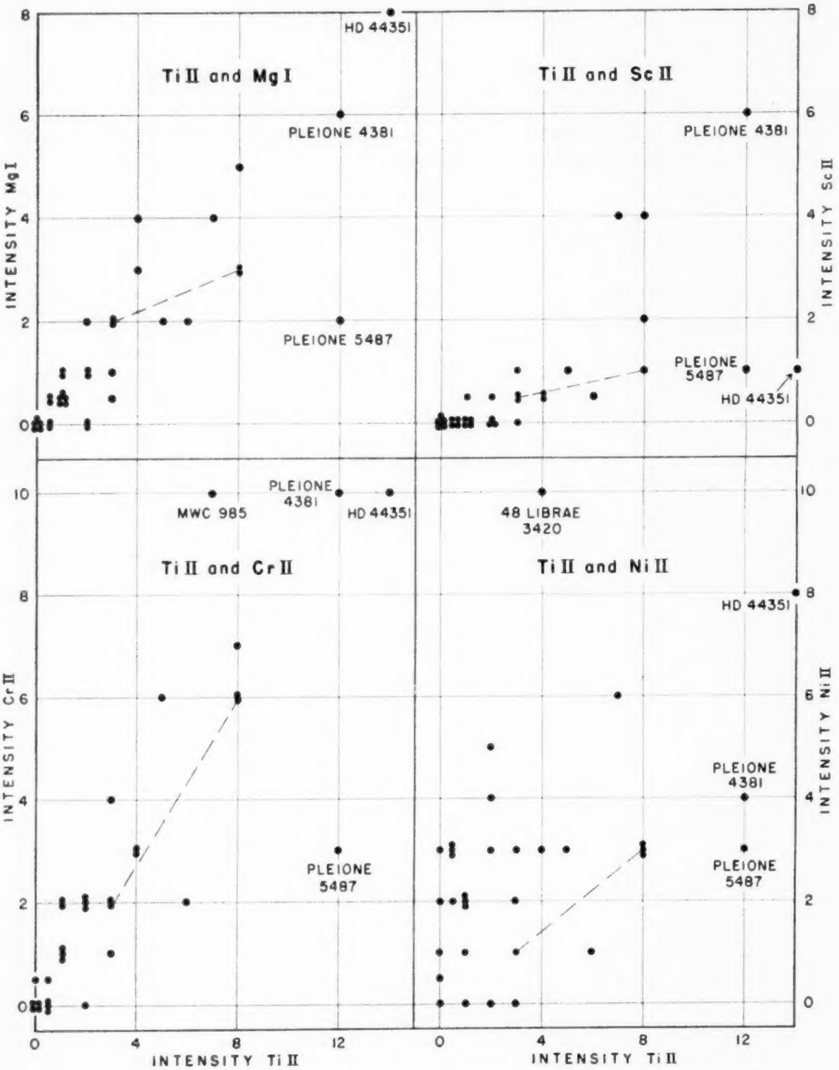

FIG. 1.—Correlation plots of intensities of *Ti* II lines with those of *Mg* I, *Sc* II, *Cr* II, *Ni* II. The stars T Coronae Borealis and 17 Leporis are omitted; their *Ti* II lines are exceptionally intense. Points for η Leonis and α Cygni are connected by dashed lines; in each diagram the point at the upper right-hand end of the line represents α Cygni.

Structure and displacements of lines.—A review of the radial-velocity observations of various shells (Tables 6 and 7) leads to the following tentative generalizations.

I. (*a*) In most shells the velocity varies slowly through a large range in cycles of several years, but the velocity-curves do not repeat themselves closely. Two or three well-observed stars suggest that the following behavior is typical: (*b*) The dark lines are symmetrical for a short time near maximum velocity and for a longer time near minimum velocity. They are winged longward (i.e., are sharper on the shortward edge) preceding maximum, and are winged shortward after maximum during a part of the descending branch of the curve. (*c*) At maximum velocity, lines of the Balmer series show a positive progression in velocity (i.e., lines near $H30$ yield higher velocities than lines near $H\gamma$); at minimum velocity, they show a negative progression; at some intermediate velocity, all lines yield the same velocity. (*d*) The varying displacements of the metallic lines approximate those of the Balmer lines near $H30$.

II. In typical *stable* shells, the dark lines are symmetrical and very sharp. All dark lines yield a velocity which is probably the same as that of the star as a whole.

TABLE 5

PHOTOMETRIC MEASUREMENTS OF λ 4026 *He* I

Star	Plate Ce	Central Absorption (Per Cent)	Actual Width (A)
Pleione	2955	(6)	8
	5487	3	8
	6029	3	8
	6431	3	9
	7227	7	9
HD 33232	3290	14	9
	3991	10	8
	6032	11	9
β Mon A	4923	10	10
HD 50138	4551	(11)	5
48 Lib	3420	12	(12)
	4200	10	10
	5137	10	11
HD 179343	5271	7	9
HD 183656	6023	13	10
	7222	12	10
	7223	10	10
HD 217050	4424	10	12

TABLE 6

SHELLS WITH CONSTANT VELOCITIES

Star	Ref.	Remarks
HD 45677	1	Not a typical shell; the structure of the *H* lines changes but the velocity of the shell may be constant
HD 54858	1	Stable from 1945 to 1952
MWC 985	1	Only 2 spectrograms; possibly stable
HD 187399	2	Apparently a binary, but the *H* lines have a component which yields a constant velocity
HD 193182	3	Well observed
1 Delphini	3	Well observed
HD 195407	4	Helium shell; the spectral details change but the velocity of the shell may be constant

NOTES TO TABLE 6

1. *Ap. J.*, **116**, 501, 1952.
2. *Ibid.*, **110**, 59, 1949.
3. *Ibid.*, **115**, 42, 1952.
4. *Ibid.*, p. 47.

Motions.—Changes in the structure of the lines, described in **1***b* in a preceding paragraph, are represented schematically in Figure 2. The lines are most unsymmetrical not at times of maximum or minimum velocity but rather at intermediate velocities, when the atoms are subject to acceleration. Moreover, the lines are winged on the side toward which they are moving. This means that during both outward and inward motions part of the atoms reach a certain velocity before the others, either because the force on them is stronger or because it is applied somewhat earlier in the cycle. With time the velocities tend to equalize. Curiously enough, as the atoms proceed to take on different velocities, they maintain a sharp limit to the old values.

TABLE 7

SHELLS WITH VARIABLE VELOCITIES

Star	Ref.	Remarks	Star	Ref.	Remarks
Pleione	1	A shell lasted about ten years, then blew away	HD 172694	8	A helium shell; the velocity-curve has an amplitude of about 50 km/sec, but it is peculiar and difficult to interpret
HD 33232	2	The velocity-cycle has lengthened from 3710 days to more than 4000 days	HD 183656	3	The variation in velocity is large, but the observations do not define the curve satisfactorily; if the variation is periodic, the cycle covers 4 years or more, possibly 6.5 years
HD 44351	3	The velocity had a maximum in 1948; the cycle is 8 years or longer, the amplitude large	HD 184279	8	A helium shell; the velocity appears to have changed about 8 km/sec from 1926 to 1945
HD 45910	4, 5	Changes in the structure of the lines and in the displacements of components are rapid and striking; the object may be a binary with a period of 232 days	HD 351123	3	Probably an unstable shell; two spectrograms a year apart yield velocities differing by 25 km/sec
β Mon A	3, 6	The velocity-cycle is about 12.5 years; Dr. Dean B. McLaughlin is making a comprehensive study of this star	HD 218393	9	The structure of the lines is complex and variable; rapid changes sometimes occur
HD 50138	3	Not a typical shell; there are quick changes in the atmospheric motions	HD 220300	3	The variation in velocity is large; the cycle may be a few years
48 Librae	7	A remarkable atmospheric oscillation began in 1935; the cycle is about 9 years; the amplitude appears to be decreasing			

NOTES TO TABLE 7

1. P. W. Merrill, *Ap. J.*, **115**, 145, 1952.
2. *Ibid.*, **116**, 516, 1952.
3. *Ibid.*, p. 501.
4. *Ibid.*, **108**, 481, 1948.
5. *Ibid.*, **116**, 498, 1952.
6. D. B. McLaughlin, *A.J.*, **56**, 44, 1951.
7. P. W. Merrill, *Ap. J.*, **117**, 7, 1953.
8. *Ibid.*, **115**, 47, 1952.
9. *Ibid.*, **110**, 420, 1949.

These facts indicate some type of stratification of effects in the extended atmospheres of shell stars, but the exact interpretation does not appear simple. The present clues could be greatly developed by observing the line profiles at various phases of the velocity-cycles with a dispersion of 3–5 A/mm.

If a shell star has twelve times the mass of the sun and if the radius is five times that of the sun, then the acceleration of gravity at the photosphere would be 0.13 km/sec. This force would control a rotational velocity of 670 km/sec, which corresponds to a rotation period of 9 hours. Of course, if any outward force partially counteracts gravity, then a slower rotation would be required for equilibrium. Under gravity alone, the velocity of escape would be 960 km/sec. A particle projected radially outward from the photosphere with a velocity of 670 km/sec would in a few hours rise to a height of 1 radius above the photosphere.

In novae, atoms are expelled from the star with very high velocities; sometimes the velocity of escape is exceeded, and a gaseous shell expands indefinitely. In P Cygni stars the outward velocity is not so great, and, unless there is a continuing outward force, gravity would halt the atoms at comparatively small distances above the photosphere and would then bring them back. We do not observe this process, probably because in the enlarging sphere of the expanding atomosphere too few atoms remain in the cylinder through which we observe the star, namely, the cylinder whose diameter equals that of the photosphere. Whether the atoms actually return to the star we do not know.

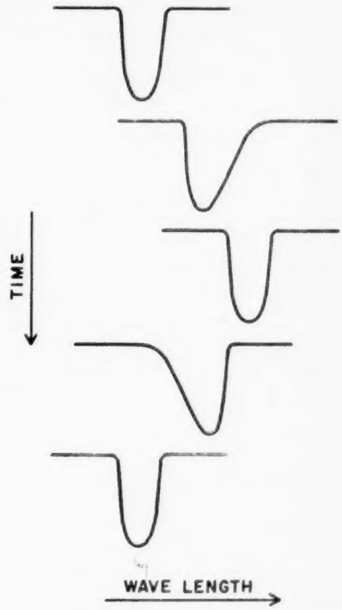

FIG. 2.—Schematic representation of changes in structure of lines in several shell spectra

In shell stars there is every indication that atoms are not expelled from the photosphere with high velocities but drift away very slowly. In certain stars there is little acceleration, and the shell appears stable, its measured velocity being sensibly the same as that of the star as a whole. In other stars the atoms are at times accelerated outward by some force very slightly greater than gravity until the outward velocities are appreciable, sometimes reaching 50–100 km/sec. This outward force, however, may not continue to act on the atoms indefinitely; after a time, or perhaps beyond a certain distance, it may drop off somewhat, allowing gravity to draw the atoms slowly back. In other words, the outward force fluctuates slowly between values slightly greater and slightly less than that of gravity. If the force is a steady one, not variable with time, the circumstances indicate that it drops off more rapidly than gravity as the distance from the star increases. This might be true of a dipolar field or of an electric or magnetic force having its origin near the star's surface. If the outward acceleration has any connection with light-pressure, the star might be slightly brighter on the falling branch of the velocity-curve (motion outward from the photosphere) than on the rising branch; the difference cannot be large but might possibly be within the range of accurate photoelectric measures.

THE RED CORONAL LINE IN THE SPECTRA OF NOVAE

DEAN B. McLAUGHLIN
University of Michigan Observatory

Received December 22, 1952; revised, January 23, 1953

ABSTRACT

A systematic search was made for coronal lines, which have been strong in the spectra of some recurrent novae. The green line, λ 5303 [*Fe* XIV], was neither identified nor suspected in any of the spectra examined. The emission band about λ 6364, commonly attributed chiefly to [*O* I], was composite in the spectra of several novae. Measurements of edges and maxima revealed features that find no satisfactory identification other than λ 6374 [*Fe* X]. The line emerged nearly concurrently with the nebular lines of [*O* III] and reached maximum strength a few months after light-maximum. The identification is considered certain in Nova CP Puppis 1942 and Nova Aquilae 1918: very probable in CP Lacertae 1936 and Nova Geminorum 1912; uncertain in three others.

INTRODUCTION

The occurrence of the red and green coronal lines in the spectra of recurrent novae is well known. They were first recognized, with other coronal lines, by Adams and Joy[1] in the spectrum of RS Ophiuchi near the end of its decline from the maximum of 1933. In T Pyxidis, fading from its maximum of 1944, Joy[2] found the lines in a spectrum that otherwise appeared like that of a typical nova in the nebular stage. Several observers[3] independently identified these lines in T Coronae Borealis during its decline in 1946.

In the spectrum of Nova CP Puppis 1942, Sanford[4] indicated the red line of [*Fe* X] as a possible contributor to a composite band that included λ 6364 [*O* I], but made no remark on its intensity or on the certainty of identification.

The red line was identified in Nova Serpentis 1948 by Wellmann[5] and by Mlle Bloch.[6] The latter indicated that it was approximately equal in strength to λ 6364 [*O* I], which it overlapped. The red line was also identified by Swings and Struve[7] in the spectra of the "symbiotic" stars AX Persei and CI Cygni.

During a visit to Mount Wilson and Palomar Observatories and to Lick Observatory in 1951, the writer made a systematic search for the coronal lines in the spectra of novae. The green line of [*Fe* XIV] was not found in any of the spectra examined, nor was it even suspected. The red line of [*Fe* X], however, was clearly present in Nova Puppis, and in several other novae the band near λ 6364 was obviously composite. In following sections the occurrence and circumstances of identification of the red line will be discussed for each nova separately. In view of the possibly controversial character of some of the identifications, it seems desirable to present the evidence in considerable detail.

SPECTROGRAMS AND MEASUREMENTS

The majority of the spectrograms used in this study were taken at the Lick Observatory with the one-prism spectrograph and 16-inch camera (for the visual region) attached to the 36-inch refractor. The dispersion at λ 6364 is 155 A/mm. The plates of Nova Puppis were taken with the grating spectrograph on the 100-inch reflector of the Mount Wilson Observatory. Their dispersion is 66 A/mm. Several Lowell Observatory prism spectrograms of Nova Geminorum were used; the dispersion is 140 A/mm at λ 6364. Michigan spectrograms of DK Lacertae were obtained with the two-prism spectrograph and 6-inch camera on the 37-inch reflector. These have a dispersion of 320 A/mm at λ 6364.

---

[1] *Pub. A.S.P.*, **45,** 301, 1933.

[2] *Pub. A.S.P.*, **57,** 172, 1945.

[3] Sanford, *Pub. A.S.P.*, **58,** 158, 1946; McLaughlin, *Pub. A.S.P.*, **58,** 160, 1946; Herbig and Neubauer, *Pub. A.S.P.*, **58,** 201, 1946.

[4] *Ap. J.*, **102,** 360, 1945.

[5] *I.A.U. Circ.*, No. 1153, 1948.

[6] *C.R.*, **227,** 333, 1948; *Ann. d'ap.*, **13,** 406, 1950.

[7] *Ap. J.*, **91,** 613, 1940.

Identification of the red line depends on analysis of measures made on all visible edges and maxima in the structure of the composite band that includes λ 6364 [*O* I]. No attempt was made to determine the identification of features during the actual measurement. The line λ 6300 [*O* I] was measured as a control on all plates, and on many of them λ 5755 [*N* II] was measured as an additional control. Both these radiations are believed to be only negligibly affected by blends.

In each of the tables of wave lengths (for example, Tables 2, 4, and 7), the first column gives the name of the feature measured (violet edge, red edge, maximum, etc.). The second column contains the measured wave length reduced to the sun. Following each wave length a number in parentheses indicates the number of plates on which the feature was measured. The third column gives the velocity obtained when the feature is considered as due to λ 6364 [*O* I]. The fourth and fifth columns contain the suggested identifications and the resulting velocities. In general, the latter have been rounded off to the nearest 5 km/sec.

TABLE 1

NOVA PUPPIS—VELOCITIES FOR λ 5755 AND λ 6300

Feature	λ 5755 (Km/Sec)	λ 6300 (Km/Sec)	Feature	λ 5755 (Km/Sec)	λ 6300 (Km/Sec)
Outer violet edge	−929 (4)	....	Minimum	− 79 (1)	− 53 (3)
Violet edge	−712 (2)	−616 (6)	Red edge	+696 (3),	+706 (6)
Maximum	−564 (2)	−444 (2)	Outer red edge	+962 (4)	+994 (1)

TABLE 2

NOVA PUPPIS—WAVE LENGTHS IN COMPOSITE BAND λλ 6364–6380

Feature	λ	[*O* I] Velocity (Km/Sec)	Identification	Velocity (Km/Sec)
Violet edge	6351.6 (6)	− 580	6363.9 [*O* I]	−580
Maximum	6353.9 (2)	− 470	6363.9 [*O* I]	−470
Minimum	6363.3 (2)	− 30	6363.9 [*O* I]	− 30
Maximum	6365.3 (5)	+ 65	6374.5 [*Fe* X]	−430
Red edge	6378.4 (3)	+ 685	6363.9 [*O* I]	+685
Red edge	6388.4 (6)	+1155	6374.5 [*Fe* X]	+655
Red edge	6392.5 (2)	+1350	6379.6 *N* II	+605

The novae will be discussed in order of the reliability of the identification, with the most conclusive case first.

NOVA CP PUPPIS 1942

Six Mount Wilson spectrograms were measured. They cover the interval from November 30, 1942, to March 19, 1943, or 18–127 days after light-maximum. Velocities of edges and maxima of the control bands are listed in Table 1. Measures on the composite band are summarized in Table 2. The probable error of a mean based on six measures is 0.2–0.3 A.

The velocities that result from interpretation of certain features as due to [*Fe* x] agree well enough with those of the control bands to warrant the statement that the identification is conclusive. The coronal line was weaker than λ 6364 on the first date and exceeded it by a factor of about 2 on the last. The increase of strength was steady, so far as the record goes.

NOVA AQUILAE 1918

In all, 32 plates were measured. All were taken at Lick Observatory in the interval June 27 to September 19, or 18–102 days after light-maximum. The band edges were fairly well defined and yielded rather accordant measures. A preliminary plot showed a systematic change about August 1. Accordingly, the measures are discussed in two groups, which will be designated the "July" and "August" observations. Table 3 contains the velocities of the control bands. Measures on the composite band are summarized in Table 4. During July the violet edge oscillated in a manner that correlated significantly with the secondary variations of light. The measures of this feature were therefore separated into two groups, corresponding to maxima and minima of light. The probable error of a mean of 10 measures is approximately 0.2 A.

TABLE 3

NOVA AQUILAE 1918—VELOCITIES FOR λ 5755 AND λ 6300

Feature	λ 5755 (Km/Sec)	λ 6300 (Km/Sec)	Feature	λ 5755 (Km/Sec)	λ 6300 (Km/Sec)
July:			*August:*		
Violet edge. . .	−1746 (18)	−1743 (21)	Violet edge. . .	−1774 (11)	−1726 (11)
Red edge.	+1529 (18)	+1539 (21)	Inner red edge	+1106 (3)	+1158 (3)
			Red edge.	+1526 (11)	+1453 (11)

TABLE 4

NOVA AQUILAE 1918—WAVE LENGTHS IN COMPOSITE BAND λλ 6364–6380

Feature	λ	[*O* I] Velocity (Km/Sec)	Identification	Velocity (Km/Sec
July:				
Violet edge (min.). . .	6338.4 (13)	−1195	6374.5 [*Fe* X]	−1700
Violet edge (max.) . .	6342.0 (7)	−1030	6379.6 *N* II	−1770
Red edge.	6395.3 (8)	+1480	6363.9 [*O* I]	+1480
Red edge.	6402.0 (6)	+1795	6371.4 *Si* II (6369.5 *Fe* II)	+1440 +1530
Red edge.	6406.7 (8)	+2015	6374.5 [*Fe* X]	+1515
August:				
Violet edge.	6337.4 (11)	−1250	6374.5 [*Fe* X]	−1750
Red edge.	6389.5 (2)	+1205	6363.9 [*O* I]	+1205
Red edge.	6402.4 (2)	+1815	6371.4 *Si* II?	+1460
Red edge.	6407.0 (11)	+2030	6374.5 [*Fe* X]	+1530

The innermost red edge is the only one that yields an accordant velocity when interpreted as due to [*O* I]. During July it agreed roughly with the outer red edges of the control bands; during August with the inner. Both edges of the coronal line are well represented during both July and August. However, they were not measurable at maxima of light during July. At the maxima a violet edge due to λ 6380 *N* II was dominant, and the red edge at that time was probably due chiefly to *Si* II. At the minima the most conspicuous edges were due to [*Fe* x]. This behavior is consistent with that of lines of high excitation as compared with those of low excitation during secondary fluctuations. At the minima, lines of high excitation are strengthened relatively.

The identification of the red coronal line in this nova is regarded as conclusive. In this connection, it is of interest to note that Wyse[8] measured a plate taken on August 3 and obtained a violet edge at λ 6337.4 and a red edge at λ 6407, in agreement with the present results.

When the [*O* I] lines λ 6300 and λ 6364 are fairly unblended, the estimated ratio λ 6300 : λ 6364 is approximately 2. Table 5 gives means of estimates of this ratio on the Lick plates of Nova Aquilae. The steady decrease of the ratio indicates the increasing relative intensity of the [*Fe* x] component of the blend.

TABLE 5

NOVA AQUILAE 1918—EYE ESTIMATES OF EMISSION

Mean Date	Ratio λ 6300 : λ 6364	No. of Plates	Mean Date	Ratio λ 6300 : λ 6364	No. of Plates
July 3	1.4	11	Aug. 15	1.1	6
15	1.3	6	Sept. 8	1.1	3
26	1.2	6			

TABLE 6

CP LACERTAE 1936—VELOCITIES FOR λ 5755 AND λ 6300

Feature	λ 5755 (Km/Sec)	λ 6300 (Km/Sec)	Feature	λ 5755 (Km/Sec)	λ 6300 (Km/Sec)
July:			*August:*		
Violet edge	−1320 (7)	−1416 (20)	Violet edge	−1776 (8)	−1406 (19)
Inner red edge	+ 980 (7)	+ 910 (13)	Inner red edge	......	+ 938 (7)
Red edge		+1260 (15)	Red edge	+1470 (8)	+1234 (17)

NOVA CP LACERTAE 1936

The bands were measured on 39 Lick spectrograms, covering the interval July 7 to September 29, or 16–100 days after light-maximum. The edges were much less definite than those in either of the two preceding spectra, and measures were strongly influenced by different photographic densities. The scatter is therefore rather large. The probable error of a mean of 10 measures of an edge at λ 6364 is about 0.4 A. Velocities of edges of the control bands are given in Table 6. In this case λ 5755 proved unsatisfactory because of its great intensity. Evidently the features measured at the two lines were not comparable, except for the inner red edge and perhaps the violet edge during July. The [*O* I] line λ 6300 is considered the better for comparison with the composite band because its intensity and dispersion are similar to those of λ 6364.

Measures on the composite band are summarized in Table 7. Evidently the same outer edges were measured in July and August. The inner red edge of [*O* I], however, shows an unexplained shift from +880 to +1075 km/sec. It is noteworthy that no feature was found to correspond to the outer red edge of λ 6364 [*O* I]. Evidently the overlapping emissions effectively obliterated that edge. The red edge about λ 6397 is interpreted as a blend of the inner red edges of the coronal line and λ 6380 *N* II. In view of the low dispersion, the difference of 5 A between the wave lengths of these lines is not considered too great, especially as the scatter of the measures slightly exceeded this figure.

---

[8] *Pub. Lick Obs.*, **14**, 210, 1939.

TABLE 7

CP LACERTAE 1936—WAVE LENGTHS IN COMPOSITE BAND λλ 6364–6380

Feature	λ	[*O* I] Velocity (Km/Sec)	Identification	Velocity (Km/Sec)
July:				
Violet edge	6337.1 (20)	−1260	6363.9 [*O* I]	−1260
Red edge	6382.6 (17)	+ 880	6363.9 [*O* I]	+ 880
Red edge	6396.6 (16)	+1540	6374.5 [*Fe* X]	+1040
			6379.6 *N* II	+ 800
Red edge	6405.5 (2)	+1960	6379.6 *N* II	+1220
August:				
Violet edge	6336.7 (19)	−1280	6363.9 [*O* I]	−1280
Red edge	6386.7 (8)	+1075	6363.9 [*O* I]	+1075
Red edge	6397.6 (18)	+1585	6374.5 [*Fe* X]	+1085
			6379.6 *N* II	+ 845
Red edge	6406.0 (3)	+1985	6379.6 *N* II	+1240

TABLE 8

CP LACERTAE—ALTERNATIVE WAVE LENGTHS OF RED EDGES (AUGUST)

Feature	λ	[*O* I] Velocity (Km/Sec)	Identification	Velocity (Km/Sec)
Red edge	6386.7 (8)	+1075	6363.9 [*O* I]	+1075
Red edge	6391.7 (3)	+1310	6363.9 [*O* I]	+1310
Red edge	6396.5 (12)	+1535	6374.5 [*Fe* X]	+1035
Red edge	6401.5 (5)	+1770	6374.5 [*Fe* X]	+1270
			6379.6 *N* II	+1030
Red edge	6406.0 (3)	+1985	6379.6 *N* II	+1240

The large scatter of the red edges of both λ 6300 and the composite band suggests a question as to whether it represents a merging of the scatter of measures on *two or more edges*. A frequency diagram gave some support to this view but was far from convincing. Analysis based upon means formed about the apparent maxima of frequency led to no significant change for the July observations. The measures of the August–September plates gave revised means, which are tabulated in Table 8. With this interpretation, three measures indicate an outer red edge of λ 6364. The strongest red edge still requires identification as the inner red edge of the coronal line, perhaps modified by blending with λ 6380 *N* II.

It is concluded that both λ 6374 [*Fe* X] and λ 6380 *N* II were probably major contributors to the composite band. Table 9 gives means of estimates of the ratio λ 6300 : λ 6364.

The increase in relative intensity of the overlapping coronal and *N* II emissions is indicated by the decrease in the ratio with time. The subsequent increase may be assigned to weakening of λ 6380 *N* II after July, but other emissions may have been involved.

NOVA GEMINORUM 1912

Six Lick and six Lowell plates were measured. These extend from March 30 to May 9, or 16–56 days after light-maximum. Velocities of the edges of the control bands and of the strong part of the band near λ 6364 (when interpreted as [*O* I]) are given in Table 10. On four spectrograms, specifically the Lowell plates taken April 3, 8, and 18, and the Lick plate of May 9, a weaker red edge was measured, with a mean wave length of 6392.7 A. If this is interpreted as λ 6374.5 [*Fe* x], it yields a velocity of +855 km/sec, which is fairly accordant with the red edges of the normal bands. The identification, therefore, is considered fairly probable.

TABLE 9

CP LACERTAE—EYE ESTIMATES OF EMISSIONS

Mean Date	Ratio λ 6300:λ 6364	No. of Plates	Mean Dates	Ratio λ 6300:λ 6364	No. of Plates
July 14	1.7	7	Aug. 11	1.1	7
22	1.3	7	Sept. 4	1.3	7
29	0.9	8			

TABLE 10

NOVA GEMINORUM—VELOCITIES OF BAND EDGES

λ	Violet Edge	Red Edge
5755	−762 (12)	+887 (12)
6300	−646 (12)	+774 (12)
6364	−702 (12)	+796 (12)

TABLE 11

DK LACERTAE—VELOCITIES OF λ 5755 AND λ 6300

Feature	λ 5755 (Km/Sec)	λ 6300 (Km/Sec)
Violet edge	−891	−505
Red edge	+859	+803

NOVA DK LACERTAE 1950

Six Michigan plates were measured. They cover the interval February 18–June 9, or about 21–132 days after light-maximum. Velocities of control bands are given in Table 11. The large discrepancy in the violet edge of λ 6300 is not satisfactorily explained but is believed to be partly due to overlap by the interstellar absorption line at λ 6284.

Measured wave lengths in the composite band are given in Table 12. A mean of 5 measures has a probable error of 0.8 A. The inner violet edge, which is attributed to the coronal line, was a fairly definite feature. The outer red edge was less satisfactory, and its discrepancy is large enough to cast some doubt on the identification. It would be fairly accordant if identified as λ 6371 *Si* II, but it seems unlikely that this line was strong enough to appear on any but the first of the four plates on which the edge was measured.

On the last plate, taken June 9, the composite band is much stronger than λ 6300. Its strong violet edge gives the very accordant velocity of −925 km/sec if it is identified as λ 6374 [*Fe* X]. The strong red edge requires identification as λ 6364 [*O* I], and no emission whatever can be seen extending to longer wave lengths, to correspond to the redward part of the coronal line. This curious result raises a suspicion that some unidentified radiation may coincide rather closely with λ 6364 and that an intensity anomaly alone cannot be taken as prima facie evidence of the presence of the coronal line.

NOVA V368 AQUILAE 1936

The only plate of the visual region is a slitless spectrogram taken with the quartz spectrograph on the Crossley reflector on November 6, about 53 days after light-maximum. It shows a striking intensity anomaly, the line about λ 6364 being much stronger than λ 6300. However, the measured wave length is 6362.9 A. The lack of a positive displacement, in spite of suspected overlap of a line of longer wave length, is similar to the situation just noted in DK Lacertae. Velocity half-widths of the two lines are as follows: λ 6300, 1085 km/sec; λ 6363, 1250 km/sec. The difference in width is much less than we should expect if the second line were a blend of two lines that differed in wave length by 10 A. The identification (other than [*O* I]) and the cause of the intensity anomaly remain in doubt.

TABLE 12

DK LACERTAE—WAVE LENGTHS IN COMPOSITE BAND λλ 6364–6380

Feature	λ	[*O* I] Velocity (Km/Sec)	Identification	Velocity (Km/Sec)
Violet edge	6344.0 (5)	− 935	6363.9 [*O* I]	−935
Inner violet edge	6357.8 (5)	− 290	6374.5 [*Fe* X]	−790
Inner red edge	6371* (6)	+ 330:	?	?
	6382*	+ 850:	6363.9 [*O* I]	+850
Outer red edge	6388.4 (4)	+1155	6374.5 [*Fe* X]	+655

* These measures represent limits of the range of red edges of very poor quality and doubtful value.

NOVA CYGNI 1920

Five Lick plates of Nova Cygni 1920 were measured. They were taken August 31–September 4, or 8–22 days after light-maximum. On all the plates the [*O* I] line is much stronger than any other possible component of the band near λ 6364, but weaker than λ 6300. On four plates a faint outer red edge was measured. Its velocity is accordant with that of the red edges of the [*O* I] lines if it is identified as λ 6379.6 *N* II. If the red coronal line was present at all, it was completely masked by this line of *N* II. The stage of the nova was hardly advanced enough for the coronal lines to be strong and their presence at some later stage is not ruled out.

CONCLUSION

To summarize, the search for the red coronal line gave the results shown in the accompanying tabulation. Apparently the red coronal line can be regarded as a normal constituent of spectra of typical novae in the early nebular stage. So far as the evidence goes, its general behavior in recurrent and nonrecurrent novae is similar, but it reaches a greater maximum strength in the recurrent stars and, for that reason, is detectable at an earlier stage. The line emerges simultaneously with others of high excitation during the transition stage, 3–5 mag. below maximum, and remains strong for at least a few months. There is insufficient data concerning its later behavior.

Nova Puppis 1942	Certainly present
Nova Aquilae 1918	Certainly present
Nova Lacertae 1936	Very probably present
Nova Geminorum 1912	Probably present, but few measures
Nova Lacertae 1950	Possibly present
Nova v368 Aquilae 1936	Doubtful
Nova Cygni 1920	Insufficient evidence

An attempt at physical interpretation will not be made here. In this connection, reference may be made to a very suggestive discussion by Bowen and Swings[9] on the significance of the occurrence, in a single peculiar stellar spectrum, of emission lines of ions with widely different ionization potentials.

That the red coronal line escaped recognition in typical novae for so long a time was clearly due to a combination of two main causes: (1) the low dispersion commonly employed in the visual region of nova spectra and (2) the serious overlapping of λ 6364 [*O* I] on plates of any dispersion. The earlier recognition in recurrent novae was aided by the relative narrowness of the bright lines and the higher excitation in the spectra of two of those stars.

I am happy to record here my gratitude to the director of the Lick Observatory for the privilege of using the fine series of spectrograms of several novae. To the director of Mount Wilson and Palomar Observatories I am greatly indebted for the opportunity to measure the plates of Nova Puppis. I am grateful to Dr. V. M. Slipher, director of the Lowell Observatory, for the use of spectrograms of Nova Geminorum. It is also a pleasure to acknowledge support of this work by a grant from Faculty Research Funds of the Horace H. Rackham School of Graduate Studies of the University of Michigan.

---

[9] *Ap. J.*, **105**, 92, 1947.

THE ORBIT OF BOSS 1074

ROSCOE F. SANFORD

MOUNT WILSON AND PALOMAR OBSERVATORIES
CARNEGIE INSTITUTION OF WASHINGTON
CALIFORNIA INSTITUTE OF TECHNOLOGY

Received January 6, 1953, revised January 30, 1953

ABSTRACT

The spectroscopic binary orbit of Boss 1074 has been derived from radial velocities extending over nearly a half-century. This orbit is noteworthy for its very long period, 10,470 days, and its very large eccentricity, 0.65. Its mass factor is $1.01\odot$ and a sin i of the primary star is 1400×10^6 km.

The interstellar H and K lines are present, superposed on the broad stellar H and K of strongly exposed spectrograms. Interstellar D lines appear beside the stellar D lines on high-dispersion spectrograms at the time of minimum stellar velocity. The interstellar velocity is +5.2 km/sec. Interstellar K has an equivalent width of 0.08 A.

Micrometer observations at the last apastron failed to show duplicity. It is hoped that still more careful observations can again test this at the next apastron (1964).

The velocity residuals from the long-period curve seem too large for errors of observations. There may be a shorter period involved, but present observations have not revealed this.

The radial velocities of Boss 1074[1] have now been obtained over nearly a half-century, during which interval the velocities have passed twice through rapid minima and through one complete broad maximum. The long-period velocity variation can now be fairly accurately determined.

High-dispersion spectrograms (about 10 A/mm) have been obtained as follows: five at the Lick Observatory,[2] three at the Bonn Observatory,[3] and thirty-four at the Mount Wilson Observatory (1942–1952). These forty-two velocities are given in Table 1. Between 1918 and 1942 about 100 other velocities were derived from spectrograms of considerably lower dispersion (35 A/mm at $H\gamma$). These latter lower-dispersion velocities have been combined into normal places that are concisely described in Table 2. The period that was judged best for assembling the velocities of Tables 1 and 2 is 10,470 days. Numerous trials and adjustments of the five other orbital elements led to the data in Table 3.

Figure 1 has the velocity-curve defined by the elements of Table 3, together with the velocities plotted from Tables 1 and 2. It is evident that the individual high-dispersion velocities of Table 1 do not fit the velocity-curve as precisely as might be expected if these velocities are solely the effect of motion in the orbit with a period of 10,470 days. The residuals given for the normal places in Table 2 and the spread found among the velocities forming a normal likewise point to excessive scatter about the long-period variation. However, no short-period variation has been found to fit these residuals. Therefore, these observations suffice only to provide the elements in Table 3, and these elements have been tentatively adopted, since greater refinement of them seems unjustified if the residuals are affected by a short-period oscillation. The elements previously obtained[4] from insufficient observations have been found to be wrong.

The classification of Boss 1074 as K0, A3 quite possibly rests upon the fact that strongly exposed objective-prism spectrograms appear to have stellar H stronger than

---

[1] 58 Persei e, HD 29094–95; (1900) $\alpha = 4^h29^m8$, $\delta = +41°4'$; 4.5 mag.; K0, A3.

[2] *Pub. Lick Obs.*, **16**, 59, 1928.

[3] F. Küstner, *A.N.*, **198**, 419, 1914.

[4] R. F. Sanford, *Pub. A.S.P.*, **43**, 268, 1931.

TABLE 1

HIGH-DISPERSION SPECTROGRAMS OF BOSS 1074

PLATE NO.	JD	PHASE (DAYS)	STELL. VEL. (KM/SEC)	Δv (KM/SEC)	INTERSTELLAR VEL. (KM/SEC)
	Lick Observatory				
	2417535	5237	+10.0	−0.3	....
	7949	5651	+ 9.1	−0.8	....
	8252	5954	+ 9.6	−0.2	....
	8627	6329	+10.5	+1.1	....
	2422955	187	−10.4	−0.6	....
	Bonn Observatory*				
	2419077	6779	+10.3	+1.4	....
	9106	6808	+ 9.0	+0.2	....
	9816	7518	+ 6.7	−0.8	....
	Mount Wilson Observatory				
Ce 1139......	2428416	5648	+ 9.0	−1.0	....
1455......	8771	6003	+ 9.1	−0.6	+3.8
1462......	8772	6004	+11.4	+1.6	+2.6
1467......	8773	6005	+ 9.8	0.0	....
1803......	9179	6411	+ 8.9	−0.3	....
2880......	2430657	7889	+ 6.5	−0.4	....
3154......	0955	8187	+ 5.5	−0.6	+7.5
3416......	1196	8428	+ 4.2	−1.0	....
3580......	1363	8595	+ 6.3	+1.4	+7.4
4022......	1749	8981	+ 3.5	+0.7	+4.9
4192......	1897	9129	+ 4.0	+2.0	+6.4
4397......	2071	9303	+ 1.4	+0.8	+4.0
4588......	2224	9456	− 1.2	0.0	+5.2
4855......	2433	9665	− 3.3	0.0	....
5060......	2571	9803	− 4.5	+0.6	+6.6
5109......	2611	9843	− 6.9	−1.2	+3.0
5156......	2660	9892	− 6.1	+0.6	....
5288......	2782	10014	− 8.5	+0.3	+5.3
5410......	2850	10082	−10.6	−0.4	+5.4
5454......	2879	10111	−11.1	−0.3	+5.2
5515......	2924	10156	−11.2	+0.5	....
5561......	2968	10200	−12.1	+0.5	+6.6
5615......	3014	10246	−13.0	+0.4	....
5744......	3109	10341	−14.6	−0.1	....
5856......	3144	10376	−15.0	−0.2	+4.3
5946......	3172	10404	−14.8	−0.1	+4.8
5995......	3202	10434	−14.9	−0.3	....
6030......	3234	10466	−13.2	+1.1	....
6125......	3330	92	−12.1	+0.3	+4.5
6205......	3376	138	−12.8	−1.6	....
6555......	3550	312	− 6.5	−0.8	+5.2
6815......	3668	430	− 3.7	−1.3	+6.3
7429......	3907	669	+ 2.3	+0.1	+5.3
8494......	4326	1088	+ 7.7	+1.1	....

* Velocities corrected for systematic error of + 2.7 km/sec: *Pub. Lick Obs.*, **16,** xxxi, 1928.

stellar K and the other stellar lines more blurred and shallower than usual for class K0. This could be the result of an A3 spectrum with little else than hydrogen lines combined with a K0 spectrum. The line taken for H would, in fact, be a combination of H belonging to the K0 star and of $H\epsilon$ belonging to the A3 star, so that H would seem to be stronger than K. Although heavy exposure also produces a similar effect upon high-dispersion spectrograms, such exposure also reveals sharp absorption lines superposed on the centers of the broad stellar H and K lines (Fig. 2). The velocities given by these sharp H and K components are in the sixth column of Table 1 for those spectrograms which are strongly enough exposed to show both of these sharp components clearly. These velocities evidently are not sharing in the variation shown by the stellar velocities (fourth column, Table 1). Their mean value is +5.2 ± 0.2 km/sec. Two spectrograms, Ce 6044 and Ce 6045 (dispersion 6.7 A/mm), which were obtained on December 3, 1949, at phase 12 days, resolve the D lines into shortward diffuse components and longward

TABLE 2

NORMAL PLACES FROM LOWER-DISPERSION SPECTROGRAMS OF BOSS 1074

JD	Phase (Days)	Vel. (Km/Sec)	Δv (Km/Sec)	No.	Vel. Range (Km/Sec)	Interval (JD)
2421916	9618	+ 1.7	+4.5	2	0.8	2421913–1916
1966	9668	− 3.6	0.0	2	1.6	1941–1971
2018	9720	− 2.4	+1.6	2	5.7	2010–2027
2060	9762	− 5.0	−0.4	1	....	....
2301	10003	− 7.4	+1.3	1	....	....
2740	10442	−12.5	+2.0	1	....	....
2766	10468	−15.2	−1.0	....	....	....
3032	264	− 8.5	−1.1	3	4.5	3031–3034
3066	298	− 7.5	−1.6	3	4.4	3060–3070
3107	339	− 4.6	+0.2	3	1.6	3100–3120
3147	379	− 2.8	+1.2	2	2.5	3131–3163
3375	607	+ 4.5	+3.1	2	0.5	3302–3393
3729	961	+ 4.0	−1.6	6	3.8	3664–3863
4131	1363	+ 7.7	−0.5	2	2.6	4076–4158
4567	1799	+10.8	+1.4	2	1.1	4514–4776
5735	2967	+11.9	+1.2	6	7.8	5163–5995
6882	4114	+12.9	+2.9	9	5.4	6262–7168
7441	4673	+10.7	+0.2	8	5.3	7329–7517
7795	5027	+ 9.3	−1.1	8	3.6	7706–7916
8116	5348	+ 7.5	−2.7	9	4.6	7999–8261
8514	5746	+ 9.8	−0.1	8	5.1	8379–8613
8853	6085	+ 9.4	−0.3	10	6.5	8774–8972
9361	6593	+ 8.0	−1.0	7	7.3	9179–9300
2430195	7427	+ 6.3	−1.5	4	7.8	9897–0394

TABLE 3

ORBITAL ELEMENTS OF BOSS 1074

$P = 10{,}470$ days

$K_1 = 12.8$ km/sec

$T =$ JD 2422768

$\gamma = +5.9$ km/sec

$\omega = 197\overset{\circ}{.}0$

$$\frac{m_2^3 \sin^3 i}{(m_1 + m_2)^2} = 1.01\odot$$

$e = 0.65$

$a_1 \sin i = 1400 \times 10^6$ km

sharp ones. They give -14.2 km/sec and $+5.4$ km/sec, thus agreeing with the orbital velocity and the velocity from the sharp H and K lines, respectively. These sharp H, K, and D lines are, therefore, assumed to be of interstellar origin. The equivalent widths of the K line as measured on three spectrograms gave a mean of 0.08 A.

The measured trigonometric parallax,[5] 0″.020, gives the distance of Boss 1074 as 50 parsecs, and its spectroscopically determined visual magnitude,[6] -1.3 corresponds to a distance of 160 parsecs. The interstellar lines seem to favor the larger distance, but the mass function seems to favor the smaller. Since both criteria give distances of little weight, there is no basis for judgment between the two distances, 50 and 160 parsecs.

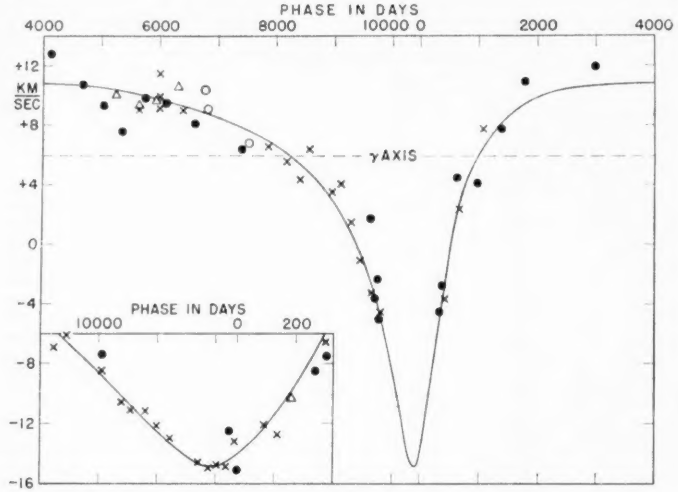

FIG. 1.—Radial velocity-curve of Boss 1074; velocities are represented by triangles, circles, and crosses for Lick, Bonn, and Mount Wilson, respectively (Table 1) and by solid circles (Table 2). The curve in the box shows the lower part of the velocity-curve with its scale of abscissae five times expanded.

A spectroscopic binary whose primary has a major semiaxis of no less than 1400×10^6 km and a distance of not more than 160 parsecs should be examined for evidence of duplicity by a skilled double-star observer at the time of the greatest separation of primary and secondary. The most powerful equipment available and the best of seeing conditions are additional requirements. Dr. H. M. Jeffers has examined this star with the 36-inch refractor of the Lick Observatory and found no certain evidence that it was a double star. However, he was not favored with the best seeing conditions. Apastron will again occur in 1964, around which time it is hoped that careful observations under the best conditions may again test whether this spectroscopic binary is also a visual binary.

---

[5] Louise F. Jenkins, *Yale Catalogue of Trigonometric Parallaxes* (1952).

[6] Adams, Joy, Humason, and Brayton, *Mt. W. Contr.*, No. 511; *Ap. J.*, **81**, 187, 1935.

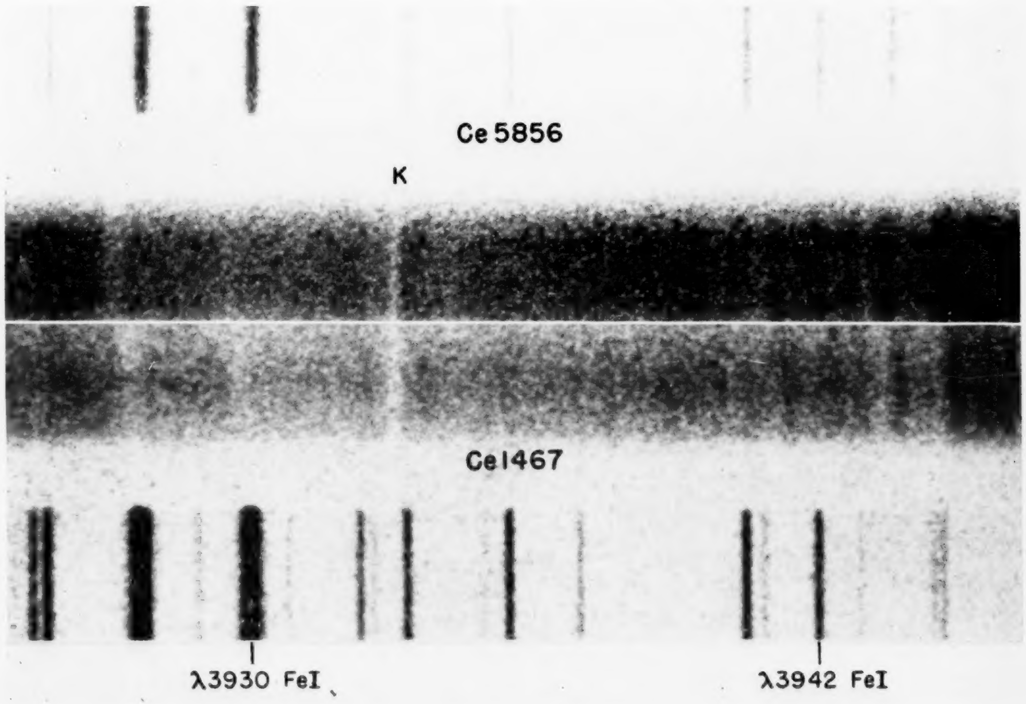

FIG. 2.—The K-line region of spectrograms Ce1467 and Ce5856 which have very closely the same reduction to the sun but greatly different orbital velocities (Table 1). By lining up their *Fe* comparison spectra their sharp absorption K-lines are seen to coincide but all other absorption lines are offset. The constant-velocity K-line is assumed to be of interstellar origin.

BETA CEPHEI*

O. STRUVE, D. H. MCNAMARA, S. M. KUNG, AND C. BEYMER
Berkeley Astronomical Department, University of California

Received December 16, 1952; revised January 1, 1953

ABSTRACT

The measurements of 713 spectrograms, taken in 1950–1952, were used to study the gradual increase in the 4-hour period of this star. The values of K show appreciable differences in different cycles, but no beat period was discovered. The variation in radial velocity corresponds to the period P_1, there being no discernible change in the line profiles. The variation in K is probably irregular in character (but the observations do not completely exclude a beat period of less than a day).

The star β Cephei has long been recognized as a pulsating variable whose period of $4\frac{1}{2}$ hours is shared by its radial velocity and its brightness. It differs from β Canis Majoris in several respects:

a) β Cep has only one period, P_1, and shows no periodic variation in line profiles; β CMa has two interfering periods, P_1 and P_2, the second of which is associated with a variation in the line profiles.

TABLE 1

LIST OF STAR LINES

Wave Length	Element	Plate*	Wave Length	Element	Plate*	Wave Length	Element	Plate*
3933.66......	*Ca* II	γ	4075.88......	*O* II	γ	4471.84......	*He* I	γ, L
3964.73......	*He* I	γ	4101.74......	$H\delta$	γ	4481.23......	*Mg* II	γ, L
3995.00......	*N* II	γ	4120.81......	*He* I	γ	4552.65......	*Si* III	L
4009.27......	*He* I	γ	4143.76......	*He* I	γ	4567.87......	*Si* III	L
4026.19......	*He* I	γ	4267.17......	*C* II	γ	4574.78......	*Si* III	L
4069.79......	*O* II	γ	4340.47......	$H\gamma$	γ	4590.97......	*O* II	L
4072.16......	*O* II	γ	4387.93......	*He* I	γ	4596.18......	*O* II	L

* γ = Mt. Wilson cassegrain on the 60-inch telescope; L = Lick three-prism spectrograph on the 36-inch refractor.

b) The spectral type of β Cep resembles that of β CMa, but the luminosity criteria indicate a lower luminosity for the former.

c) There occurred, approximately in 1914, a sudden change in the period P_1, and the question has arisen whether any later changes in the period—gradual or sudden—can now be definitely established. No such changes in the period P_1 have been observed in β CMa. Instead, there has been a gradual change in P_2 only.

The earlier literature on β Cep is listed in recent papers by Burke Smith[1] and N. Roman.[2] The purpose of the present investigation was to study the individual cycles of the radial-velocity-curve in order to determine (1) whether the values of K and γ undergo regular or irregular variations and (2) whether the value of the period P_1 has changed since the epoch of the last previous (Yerkes Observatory) determination.[1] The discussion is based upon the best of the earlier determinations of the velocity-curve of β Cep and upon our measurements of 460 new Mount Wilson spectrograms, having a linear dispersion of 32 A/mm at $H\delta$ and 253 Lick spectrograms with a dispersion of 12 A/mm at λ 4565.

Table 1 gives the star lines used in this work, while Table 2 records the individual radial velocities.

---

* The new observational data used in this paper were obtained by Mr. Struve as guest investigator at the Mount Wilson Observatory, and by Mr. McNamara at the Lick Observatory. Most of the measurements and the discussion are the work of Mr. Kung.

[1] *Ap. J.*, **98**, 82, 1943. [2] *Ap. J.*, **106**, 311, 1947; see also M. Rudkjöbing, *Ap. J.*, **109**, 331, 1949.

TABLE 2
RADIAL VELOCITIES

JD 2433+	Radial Velocity (Km/Sec)	JD 2433+	Radial Velocity (Km/Sec)	JD 2433+	Radial Velocity (Km/Sec)	JD 2433+	Radial Velocity (Km/Sec)
549.633	−15.5 γ	551.616	+ 8.2 γ	552.907	− 8.1 γ	590.595	−14.9 L
.645	−18.9 γ	.624	+10.6 γ	.917	− 2.2 γ	.606	−16.9 L
.654	− 8.3 γ	.632	+10.9 γ	.927	+ 0.2 γ	.625	− 6.2 L
.662	−10.4 γ	.640	+12.4 γ	553.604	− 9.4 γ	.634	− 3.6 L
.672	− 4.7 γ	.649	+ 9.5 γ	.618	−16.6 γ	.643	− 2.0 L
.682	−20.6 γ	.656	+ 6.4 γ	.626	−14.4 γ	.651	+ 1.5 L
.694	− 4.3 γ	.664	+ 2.0 γ	.637	−17.5 γ	.660	+ 6.9 L
.703	− 1.5 γ	.672	+ 0.2 γ	.647	−19.9 γ	.676	+ 3.8 L
.711	+ 5.9 γ	.680	− 6.2 γ	.656	−12.7 γ	.690	+ 5.5 L
.719	+ 8.3 γ	.690	− 5.0 γ	.664	−10.0 γ	.699	+ 6.5 L
.727	+ 8.9 γ	.699	−13.6 γ	.674	− 8.5 γ	.708	+ 5.1 L
.735	+ 6.2 γ	.707	−14.7 γ	.683	− 5.6 γ	.717	− 0.9 L
.751	+ 2.7 γ	.717	−16.8 γ	.692	− 1.7 γ	.725	− 2.8 L
.759	+ 4.6 γ	.726	−14.1 γ	.701	+ 4.6 γ	.734	− 6.0 L
.767	− 3.5 γ	.733	−19.8 γ	.711	+ 7.9 γ	.744	−11.6 L
.775	− 1.4 γ	.740	−12.0 γ	.719	+ 7.9 γ	.753	−12.6 L
.783	−11.1 γ	.748	− 8.9 γ	.730	+ 7.7 γ	.763	−20.4 L
.797	− 9.3 γ	.756	− 8.9 γ	.740	+ 7.8 γ	.772	−20.0 L
.808	−14.1 γ	.763	− 6.9 γ	.750	+ 5.1 γ	.789	−17.7 L
.819	−12.0 γ	.771	− 5.0 γ	.759	+ 0.1 γ	.801	−14.0 L
.831	−15.0 γ	.779	− 5.5 γ	.768	− 2.0 γ	597.594	−10.8 L
.851	−13.5 γ	.787	+ 2.9 γ	.778	− 6.9 γ	.603	−16.7 L
.863	− 8.9 γ	.794	+ 0.5 γ	.788	−10.2 γ	.612	−17.7 L
.868	− 8.3 γ	.804	+ 1.8 γ	.797	−16.4 γ	.621	−19.3 L
.878	− 4.6 γ	.812	+ 6.7 γ	.807	−14.3 γ	.630	−17.2 L
.890	+ 0.7 γ	.819	+ 9.0 γ	.817	−16.8 γ	.639	−16.8 L
.900	+ 4.6 γ	.829	+ 9.0 γ	.827	−17.0 γ	.647	−13.6 L
.909	+ 9.6 γ	.838	+ 9.6 γ	.837	−18.8 γ	.656	−13.1 L
.918	+ 5.0 γ	.847	+ 4.2 γ	562.677	+ 7.8 L	.665	− 9.0 L
.927	+ 4.1 γ	.857	+ 2.1 γ	.686	+ 7.7 L	.674	− 3.2 L
.936	+ 3.7 γ	.867	− 6.8 γ	.705	+ 0.7 L	.683	− 0.9 L
.945	+ 2.6 γ	.876	−10.3 γ	.731	− 7.8 L	.692	+ 1.7 L
.955	+ 0.4 γ	.885	−12.8 γ	.740	− 9.6 L	.710	+ 8.7 L
550.601	−13.5 γ	.895	−12.7 γ	.749	−13.8 L	.719	+10.8 L
.609	−12.1 γ	.905	−14.3 γ	.766	−20.4 L	.728	+12.0 L
.618	− 8.0 γ	.916	−18.1 γ	.773	−18.2 L	.737	+ 6.9 L
.627	− 4.0 γ	.925	−22.5 γ	.785	−14.7 L	.747	+ 8.0 L
.635	− 1.9 γ	.935	−17.5 γ	.798	−12.5 L	.756	+ 5.4 L
.647	+ 0.3 γ	552.597	+12.3 γ	.811	− 6.7 L	.765	+ 0.4 L
.655	+ 6.6 γ	.605	+ 8.8 γ	.825	− 1.8 L	.773	− 4.0 L
.662	+ 6.5 γ	.613	+ 8.2 γ	.836	+ 4.8 L	.782	− 6.4 L
.671	+13.2 γ	.622	+ 3.6 γ	.847	+ 5.9 L	.791	−11.4 L
.679	+ 9.2 γ	.629	+ 1.9 γ	.858	+ 8.9 L	.803	−14.3 L
.688	+11.4 γ	.638	− 0.4 γ	.868	+ 9.3 L	.820	−14.8 L
.696	+11.8 γ	.646	− 6.8 γ	.878	+11.9 L	924.631	0.0 L
.708	+ 5.3 γ	.653	− 9.6 γ	.890	+ 5.8 L	.641	+ 1.8 L
.718	− 1.3 γ	.660	−10.7 γ	.903	− 0.6 L	.658	− 7.0 L
.738	− 4.5 γ	.669	−14.7 γ	.913	− 2.9 L	.670	−14.7 L
.748	− 8.4 γ	.677	−19.5 γ	.924	− 8.2 L	.679	−14.0 L
.758	− 8.9 γ	.685	−16.8 γ	.938	−13.5 L	.689	−14.5 L
.769	−11.9 γ	.692	−12.3 γ	569.715	+10.9 L	.708	−16.3 L
.781	−12.9 γ	.700	− 9.8 γ	.726	+12.3 L	.719	−14.8 L
.792	−10.9 γ	.708	−11.2 γ	.738	+ 9.1 L	.728	−12.5 L
.802	− 7.7 γ	.716	− 8.0 γ	.748	+ 1.9 L	.738	− 7.8 L
.811	− 7.5 γ	.724	− 2.4 γ	.758	− 0.9 L	.749	− 4.5 L
.821	− 4.9 γ	.732	− 3.3 γ	.779	− 4.9 L	.758	− 0.2 L
.831	+ 2.4 γ	.742	+ 2.1 γ	.790	− 7.8 L	.775	+ 8.3 L
.842	+ 0.6 γ	.748	+ 0.6 γ	.803	−14.0 L	.785	+ 4.9 L
.851	+ 4.2 γ	.757	+ 6.5 γ	.826	−13.7 L	.798	+ 9.4 L
.861	+ 3.8 γ	.775	− 1.4 γ	.839	−13.8 L	.806	+ 9.9 L
.872	+ 4.4 γ	.784	+11.5 γ	.851	− 7.0 L	.819	+ 4.2 L
.897	+ 4.4 γ	.793	+12.6 γ	.863	− 3.2 L	.826	+ 3.4 L
.918	− 2.0 γ	.802	+ 7.4 γ	.888	+ 1.3 L	.834	− 2.6 L
.929	− 8.6 γ	.811	+ 2.0 γ	.899	+ 6.6 L		
551.599	− 1.5 γ	.820	− 1.4 γ	.912	+ 9.1 L		
.608	− 1.5 γ	.898	−17.6 γ	.924	+ 8.3 L		

TABLE 2—*Continued*

JD 2434+	Radial Velocity (Km/Sec)	JD 2434+	Radial Velocity (Km/Sec)	JD 2434+	Radial Velocity (Km/Sec)	JD 2434+	Radial Velocity (Km/Sec)
161.803	− 3.8 L	165.829	−11.1 γ	167.953	−12.9 γ	196.803	+ 5.0 γ
.817	−11.3 L	.839	−12.4 γ	.961	−14.0 γ	.807	+ 9.5 γ
.830	−16.8 L	.848	−17.4 γ	.970	−11.8 γ	.811	+ 6.0 γ
.844	−16.9 L	.857	−19.9 γ	.978	− 9.0 γ	.815	+11.8 γ
.856	−17.2 L	.867	−12.2 γ	.986	− 5.6 γ	.820	+ 7.5 γ
.869	−19.7 L	.876	− 8.6 γ	.994	− 3.2 γ	.825	+ 5.4 γ
.883	−17.4 L	.886	− 8.7 γ	169.753	+ 9.6 L	.831	+ 3.9 γ
.898	− 9.2 L	.905	− 0.3 γ	.787	+ 5.6 L	.835	+ 3.2 γ
.911	− 3.2 L	.915	+ 1.8 γ	.800	+ 2.4 L	.840	+ 3.7 γ
.928	+ 5.0 L	.925	+ 6.9 γ	.812	− 6.5 L	.844	+ 5.7 γ
.942	+ 6.9 L	.934	+11.5 γ	.827	−11.1 L	.848	+ 2.5 γ
.953	+ 8.1 L	.944	+16.4 γ	.842	−17.7 L	.852	+ 3.7 γ
.964	+ 7.2 L	.953	+12.9 γ	.854	−19.7 L	.883	− 4.2 γ
.972	+ 7.3 L	.962	+ 8.1 γ	.872	−18.8 L	.899	− 9.1 γ
.983	+ 5.0 L	.974	+11.2 γ	.884	−17.4 L	.906	−10.1 γ
.990	+ 0.2 L	.983	+ 5.1 γ	.899	− 8.3 L	.910	−13.0 γ
.997	− 3.8 L	.992	+ 1.8 γ	.906	− 4.9 L	.919	−14.1 γ
163.798	− 7.6 γ	166.796	− 6.5 γ	.929	− 5.7 L	.924	−12.9 γ
.808	− 6.9 γ	.804	−11.5 γ	.940	+ 1.6 L	.928	− 9.1 γ
.817	+ 5.0 γ	.814	−12.0 γ	177.749	+ 8.7 L	.932	− 7.3 γ
.826	− 0.8 γ	.821	−12.4 γ	.761	+ 9.5 L	.935	− 5.9 γ
.837	+ 8.2 γ	.830	−12.2 γ	.776	+ 6.4 L	.939	− 5.4 γ
.850	+12.9 γ	.839	− 9.8 γ	.790	+ 1.6 L	.942	− 6.4 γ
.860	+10.2 γ	.847	−11.8 γ	.801	− 3.0 L	.947	− 2.5 γ
.881	+ 0.8 γ	.857	− 6.2 γ	.812	− 7.6 L	.951	− 1.8 γ
.891	+ 4.0 γ	.865	− 4.0 γ	.824	−15.1 L	.956	− 0.6 γ
.901	− 4.5 γ	.874	− 2.0 γ	.838	−22.8 L	.960	− 0.3 γ
.911	− 6.6 γ	.883	+ 3.5 γ	184.762	− 7.3 L	.965	+ 3.1 γ
.921	−10.8 γ	.892	+ 6.2 γ	.772	+ 0.4 L	.969	+ 3.4 γ
.931	−14.8 γ	.900	+ 7.3 γ	.783	+ 4.0 L	.972	+ 4.6 γ
.941	−12.9 γ	.910	− 0.3 γ	.794	+ 7.0 L	.976	+ 5.6 γ
.951	−16.0 γ	.918	+ 3.2 γ	.806	+ 8.4 L	.980	+ 5.1 γ
.963	−13.4 γ	.927	+ 4.8 γ	.817	+ 9.3 L	.983	+ 3.0 γ
.972	−13.1 γ	.936	+ 2.6 γ	.831	+ 5.3 L	.987	+ 7.0 γ
.981	− 9.5 γ	.944	+ 0.9 γ	.846	− 0.3 L	.990	+ 8.0 γ
.990	− 5.8 γ	.952	+ 4.1 γ	.862	− 6.0 L	197.719	+ 0.6 γ
164.803	+ 7.7 γ	.966	+ 2.2 γ	.874	−12.7 L	.724	+ 2.7 γ
.812	+ 8.0 γ	.978	− 3.2 γ	.885	−17.6 L	.730	+ 6.0 γ
.821	+ 5.9 γ	.986	− 1.2 γ	.897	−21.2 L	.735	+ 8.6 γ
.831	− 0.1 γ	167.001	− 4.0 γ	.915	−19.0 L	.741	+ 4.2 γ
.840	− 3.7 γ	.785	−10.0 γ	.925	−17.7 L	.747	+ 8.3 γ
.851	− 1.0 γ	.794	− 9.7 γ	.935	−16.2 L	.752	+11.8 γ
.859	− 4.2 γ	.802	− 2.2 γ	.944	−12.3 L	.762	+14.5 γ
.869	− 6.4 γ	.810	− 1.1 γ	.955	− 6.8 L	.768	+12.2 γ
.878	−10.6 γ	.818	− 1.1 γ	196.722	−10.7 γ	.774	+11.3 γ
.888	−13.4 γ	.826	+ 1.6 γ	.725	−13.3 γ	.778	+13.4 γ
.899	−16.2 γ	.835	+ 5.9 γ	.729	−12.3 γ	.785	+ 9.3 γ
.908	−10.0 γ	.843	+ 7.4 γ	.733	−13.7 γ	.790	+11.4 γ
.917	−13.2 γ	.851	+ 7.8 γ	.738	− 7.5 γ	.797	+ 5.2 γ
.927	− 5.0 γ	.860	+ 5.3 γ	.742	− 6.0 γ	.803	+ 3.7 γ
.935	− 1.1 γ	.868	+ 4.7 γ	.748	− 8.0 γ	.810	+ 0.4 γ
.946	+ 4.7 γ	.878	− 1.4 γ	.752	− 6.2 γ	.817	− 5.4 γ
.955	+ 5.8 γ	.887	− 1.7 γ	.757	− 3.5 γ	.824	− 3.7 γ
.965	+ 5.6 γ	.895	− 0.3 γ	.761	− 5.6 γ	.833	− 6.0 γ
.975	+ 9.1 γ	.903	− 1.4 γ	.765	− 0.6 γ	.840	− 9.2 γ
.984	+ 9.9 γ	.911	− 3.4 γ	.769	+ 1.2 γ	.847	−10.5 γ
.993	+12.3 γ	.919	−13.2 γ	.773	+ 1.6 γ	.854	− 9.9 γ
165.801	+ 3.0 γ	.928	− 6.0 γ	.788	+ 6.8 γ	.859	− 6.7 γ
.810	+ 1.6 γ	.935	−11.5 γ	.792	+ 7.2 γ	.865	− 7.9 γ
.819	− 4.9 γ	.944	−10.9 γ	.797	+ 5.3 γ	.871	− 6.9 γ

TABLE 2—*Continued*

JD 2434+	Radial Velocity (Km/Sec)	JD 2434+	Radial Velocity (Km/Sec)	JD 2434+	Radial Velocity (Km/Sec)	JD 2434+	Radial Velocity (Km/Sec)
197.877	−10.1 γ	198.912	+12.5 γ	199.944	+ 1.0 γ	217.934	+ 7.1 L
.883	− 5.8 γ	.917	+15.0 γ	.950	+ 4.2 γ	.956	+10.6 L
.888	− 0.7 γ	.927	+10.4 γ	.956	− 0.8 γ	225.699	−13.4 L
.896	− 0.5 γ	.933	+10.9 γ	.961	+ 0.2 γ	.712	− 7.0 L
.901	+ 5.9 γ	.938	+ 6.9 γ	.967	+ 2.0 γ	.730	+ 0.3 L
.907	+ 6.3 γ	.942	+11.0 γ	.973	+ 1.7 γ	.741	+ 6.9 L
.913	+ 7.3 γ	.947	+ 8.8 γ	.978	− 2.2 γ	.754	+10.4 L
.919	+ 0.8 γ	.953	+ 5.9 γ	.984	+ 0.2 γ	.777	+ 3.5 L
.925	+ 6.9 γ	.958	+ 2.8 γ	.990	− 0.6 γ	.792	− 0.6 L
.931	+10.9 γ	.965	− 0.1 γ	210.694	+ 8.3 L	.820	−10.1 L
.938	+13.9 γ	.970	− 2.4 γ	.715	+10.0 L	.830	−14.4 L
.942	+12.4 γ	.976	−10.3 γ	.727	+ 7.1 L	.843	−19.4 L
.948	+11.8 γ	.981	− 6.8 γ	.738	+ 8.1 L	.851	−19.7 L
.953	+ 7.5 γ	.986	−11.7 γ	.746	+ 5.4 L	.862	−18.6 L
.959	+10.0 γ	.991	− 5.7 γ	.764	+ 2.9 L	.880	−13.1 L
.964	+11.3 γ	199.717	− 2.8 γ	.772	+ 3.5 L	.896	− 8.7 L
.969	+11.5 γ	.724	− 6.2 γ	.793	+ 0.3 L	.902	− 4.3 L
.976	+ 6.9 γ	.728	− 7.5 γ	.803	− 8.8 L	.911	− 1.5 L
.982	+ 9.7 γ	.733	− 5.6 γ	.816	− 7.4 L	238.651	−14.3 L
.988	+ 5.0 γ	.742	− 7.1 γ	.827	− 6.6 L	.662	− 9.8 L
198.722	+14.4 γ	.748	−10.3 γ	.838	− 7.4 L	.672	− 3.7 L
.728	+17.3 γ	.753	−10.1 γ	.847	− 6.1 L	.683	+ 0.9 L
.733	+ 7.0 γ	.760	− 4.8 γ	.855	− 3.2 L	.695	+ 7.9 L
.738	+ 7.7 γ	.765	− 1.8 γ	.872	− 1.8 L	.706	+ 9.8 L
.744	+ 8.3 γ	.771	− 4.4 γ	.880	+ 2.4 L	.716	+13.7 L
.749	+ 6.8 γ	.776	− 9.5 γ	.888	+ 5.8 L	.728	+ 5.1 L
.756	+ 7.2 γ	.781	− 2.1 γ	.896	+ 4.5 L	.740	+ 8.0 L
.762	0.0 γ	.786	− 0.4 γ	.905	+ 5.8 L	.752	+ 0.9 L
.768	+ 4.6 γ	.797	− 1.3 γ	.926	+ 5.8 L	.765	− 0.5 L
.773	− 1.8 γ	.802	− 0.9 γ	.935	+ 4.5 L	.776	− 9.7 L
.778	−10.1 γ	.808	− 0.3 γ	.955	+ 2.8 L	.792	−16.9 L
.784	− 9.1 γ	.813	+ 5.3 γ	.964	− 3.1 L	.806	−16.9 L
.790	− 8.8 γ	.819	+ 7.4 γ	.979	− 3.8 L	.817	−15.3 L
.796	− 8.1 γ	.824	+ 3.8 γ	217.712	− 7.9 L	.829	−16.1 L
.805	−13.3 γ	.831	+ 5.7 γ	.726	− 1.5 L	.846	−12.7 L
.810	−10.4 γ	.836	+ 8.3 γ	.747	+ 7.8 L	.854	− 4.9 L
.816	−11.4 γ	.844	+10.7 γ	.755	+10.7 L	247.760	−17.0 L
.822	−12.2 γ	.849	+12.6 γ	.762	+ 9.6 L	.771	−17.5 L
.826	−11.8 γ	.855	+12.3 γ	.769	+ 9.3 L	.782	−16.4 L
.832	− 9.8 γ	.860	+13.4 γ	.778	+10.2 L	.793	−13.0 L
.838	− 2.0 γ	.865	+14.3 γ	.786	+ 5.1 L	.804	− 8.0 L
.845	+ 0.5 γ	.872	+12.4 γ	.796	− 1.0 L	.825	+ 0.7 L
.851	− 5.4 γ	.878	+12.8 γ	.803	− 0.2 L	.836	+ 5.1 L
.856	+ 2.4 γ	.886	+12.2 γ	.814	− 5.5 L	.848	+ 7.6 L
.861	+ 2.2 γ	.892	+10.0 γ	.825	−12.3 L	.859	+10.5 L
.866	+ 5.0 γ	.897	+12.0 γ	.838	−17.2 L	.872	+ 6.9 L
.872	+ 5.8 γ	.902	+10.0 γ	.847	−20.3 L	.888	+ 1.9 L
.878	+11.5 γ	.907	+10.7 γ	.860	−17.7 L	.900	− 1.6 L
.885	+13.1 γ	.913	+ 7.8 γ	.872	−16.9 L	.915	−10.9 L
.891	+18.4 γ	.919	+ 7.7 γ	.885	−16.3 L	.926	−11.6 L
.896	+17.1 γ	.928	+ 3.6 γ	.904	− 3.9 L	.940	−17.5 L
.901	+14.4 γ	.933	+ 6.6 γ	.914	− 1.6 L	.948	−17.2 L
.906	+13.0 γ	.939	+ 0.3 γ	.924	+ 3.1 L	.957	−16.8 L

There are 88 complete cycles of the radial velocity, with well-defined values of K, γ, and the times of the maximum radial velocity in each cycle, covering a span of 46 years, from May 28, 1906, to August 23, 1952. Although the values of $2K$ and γ vary from cycle to cycle (see Table 3), there is no drastic change between two successive cycles. Four nights in 1950–1952, each have two successive well-defined values of maximum radial velocity. As is shown in Figure 1, the two maxima on September 25, 1950, and July 4, 1952, are almost equal. Those of September 27, 1950, and July 17, 1952, show a difference of about 2 km/sec. In the old observations the two successive maxima of March 8, 1923, observed by Henroteau[3] show a difference of 3 or 4 km/sec. Some of his other radial-velocity-curves show successive maxima with differences of 5 or 6 or even with 10 km/sec, but they are quite uncertain.

Between two successive days the change of $2K$ is usually about 2 km/sec and that of γ about 1 km/sec. However, there are quite a few exceptions. The largest change of $2K$ is 13 km/sec, between September 21 and 22, 1940;[1] the next is one of 12 km/sec, between June 2 and 3, 1952. Other large changes of $2K$ are 8 km/sec, between September 22 and 23, 1940;[1] 6 km/sec between June 1 and 2 and July 5 and 6, 1952. In all these cases the corresponding changes of γ are normal, about 1 km/sec. The largest change in γ is 11 km/sec, between March 2 and 3, 1922,[3] while the corresponding change of $2K$ is also abnormal, about 6 km/sec.

The largest observed value of $2K$ falls on May 13, 1912,[4] and September 22, 1940,[1] both of 46 km/sec; the next largest is 44 km/sec on October 1, 1912,[4] and February 3, 1920.[5] The smallest value of $2K$ is 18 km/sec on July 17, 1952, and the next is 19 km/sec on February 20, 1922.[3]

The largest observed value of γ, $+4$ km/sec, occurred on September 1, 1919,[4] and the next was $+3$ km/sec on July 6, 1952. The smallest value of γ was -21 km/sec on June 1, 1914,[4] and the next was -20 km/sec on March 24, 1922.[3]

On the basis of a preliminary period of 0.190479 day, Crump[6] improved the value to 0.1904795 day in a range of about 10 years, from 1902 to 1912. Van Arnam[7] derived a period of 0.1904843 day in order to bring the 1922 observations into coincidence with those of 1919. Duncan and Mitchell[8] made observations of β Cephei on August 21, 1928. If Crump's period of 0.1904795 day is employed, the number of cycles between the time of the maximum radial velocity of their observations and those of Mendenhall, on November 6, 1921, turns out to be 13,020.39.[9]

Kohl[10] compiled a table containing the observed times of maximum radial velocity for most of the existing data up to 1931, together with the calculated times of maximum radial velocities. His work shows that the calculated values with $P = 0.1904795$ day agree very well with the observed ones from July 6, 1906, to October 9, 1914, the difference being less than one-tenth of the period. The differences, however, increase later, amounting to three-tenths of the period after 1923 and to over half the period in 1931. He employed a new period of 0.1904851 day and illustrated the good agreement between the observed and the calculated times of maximum velocity from May 15, 1918, up to 1931.

---

[3] *Pub. Dom. Obs., Ottawa*, **9**, 36, 1925.

[4] C. C. Crump, *Ap. J.*, **79**, 246, 1934.

[5] Henroteau, *Pub. Dom. Obs., Ottawa*, **5**, 77, 1922.

[6] *Pub. Detroit Obs., U. of Michigan*, **2**, 144, 1916.

[7] *Pub. Dom. Ap. Obs., Victoria*, **4**, 171, 1928.

[8] *Ap. J.*, **70**, 127, 1929.

[9] The authors erroneously give the number of cycles elapsed between the two observations as 16,390.4.

[10] *A.N.*, **248**, No. 5950, 398, 1933.

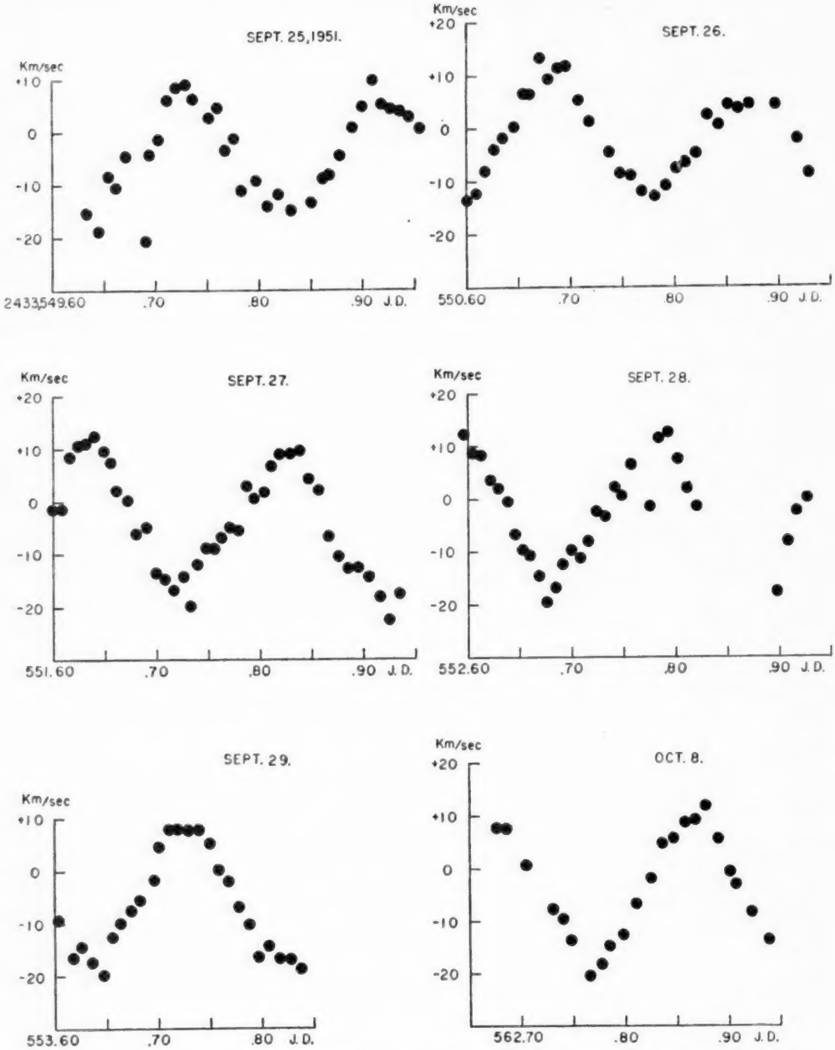

FIG. 1*a*.—Radial velocities of β cephei

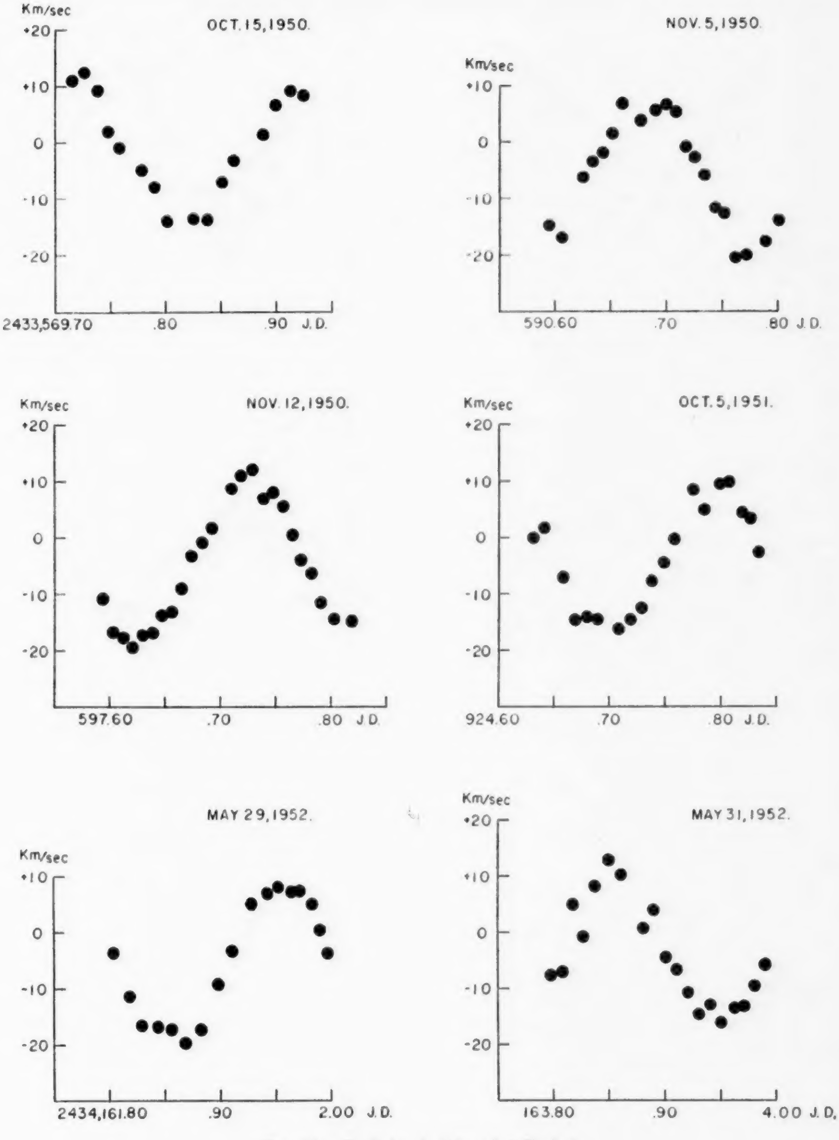

FIG. 1*b*.—Radial velocities of β Cephei

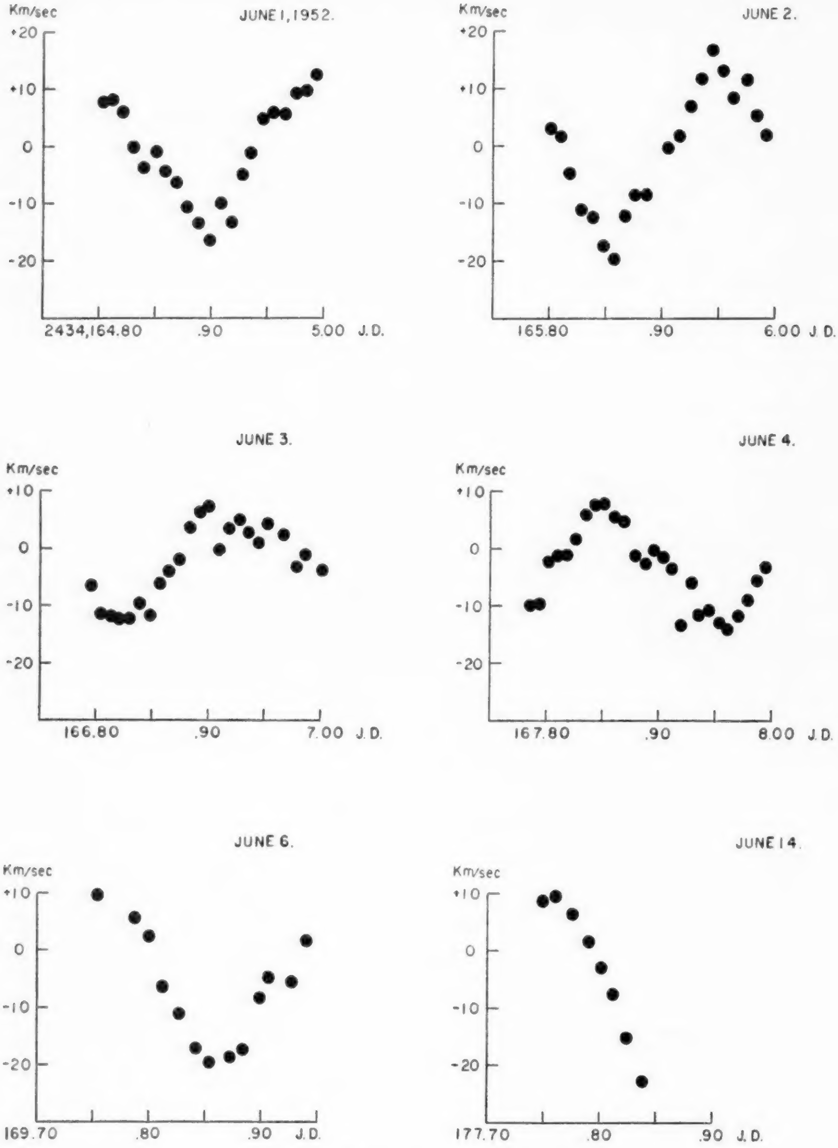

FIG. 1*c*.—Radial velocities of β Cephei

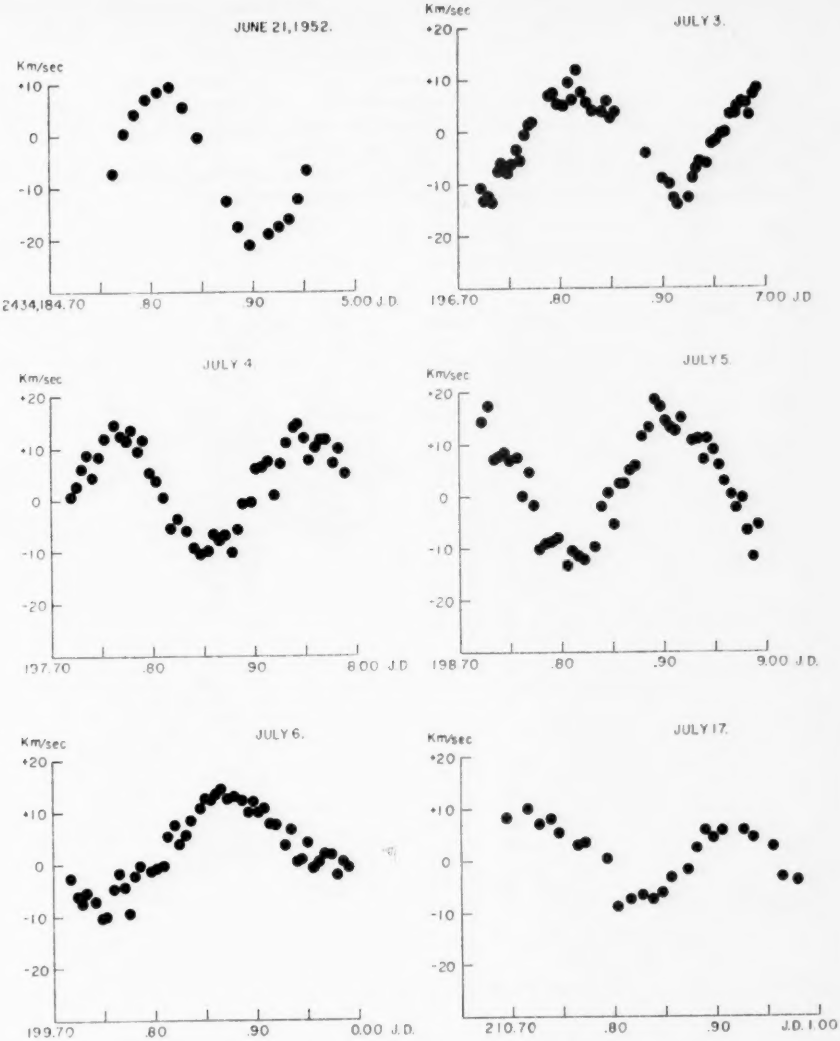

FIG. 1*d*.—Radial velocities of β Cephei

Smith[1] made a study of the radial velocity of β Cephei, based upon 91 Yerkes plates taken in 1940–1942, and presented a review of all published radial-velocity measurements of this star. One of his tables shows the departures of the observed times of maximum radial velocities from those computed with $P = 0.1904795$ day, extending over the interval from 1906 to 1942. He noticed that there was an abrupt change in period during the years 1914–1916. He suggested that the departure from $P = 0.1904795$ day was 0.0000041 day in 1917 and 0.0000091 day in 1942.

About half the data on the times of the observed maximum velocities listed in Kohl's table are mean values obtained from separate observations which were made on different nights. Some of the data listed in Smith's table were taken over from Kohl's table and are thus also mean values. If an abrupt change of the period took place in the interval covered by these observations, it will not be shown precisely. Some of the values of K and γ listed in Smith's table are also mean values from different cycles. Hence we have included in Table 3 only those values of K, γ, and the time of maximum velocity which could be accurately determined[11] in a single cycle.

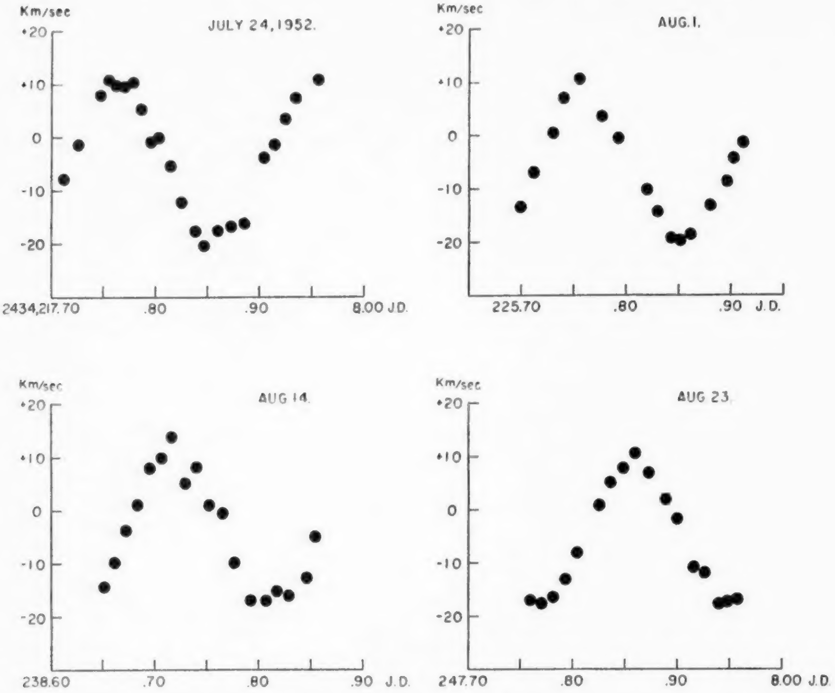

FIG. 1c.—Radial velocities of β Cephei

---

[11] In compiling Table 3 an error in Smith's table was discovered. Crump's values (see n. 4) of the Julian days for the observations in the interval from October 27, 1929, to September 5, 1932, are (except on October 27, 1929) all half a day greater than the actual values. Smith corrected them accordingly. However, on October 27 (October 26 in Smith's table) the value of the Julian day given by Crump is 1½ days greater than the actual value. Smith also corrected these data by half a day. This error accounts for the discordance shown conspicuously in Fig. 2 of Smith's paper, in which two points are located too high above the dotted average curve.

TABLE 3

TIME OF MAXIMUM RADIAL VELOCITY, AMPLITUDE K, AND VELOCITY OF CENTER MASS γ

(Calculated Time Based on Period, $P = 0.1904795$ Day)

Date	Observed Time of Max. Radial Velocity JD	E	O−C (Day)	$2K$ (Km/Sec)	γ (Km/Sec)	Authority	Reference*
1906 May 28	2417359.715	0	0.000	30	− 6	Crump	4
June 22	384.865	132	+ .007	38	− 9	Crump	4
July 6	398.765	205	+ .002	33	− 9	Crump	4
Aug. 27	450.767	478	+ .003	43	−13	Crump	4
1907 May 20	716.868	1875	+ .004	36	−10	Crump	4
July 29	786.776	2242	+ .006	33	− 9	Crump	4
Aug. 2	790.771	2263	+ .001	39	−10	Crump	4
Nov. 11	891.730	2793	+ .006	37	−11	Crump	4
1908 June 15	2418108.683	3932	+ .003	30	−10	Crump	4
29	122.781	4006	+ .005	40	− 6	Crump	4
1912 Apr. 29	2419522.815	11356	+ .015	38	−12	Crump	6
May 13	536.904	11430	+ .008	46	−12	Crump	6
Aug. 29	644.709	11996	+ .002	27	−14	Crump	6
Oct. 1	677.667	12196	+ .007	44	−12	Crump	6
15	691.565	12242	.000	36	−15	Crump	6
24	700.710	12290	+ .002	32	−13	Crump	6
Nov. 7	714.610	12363	− .003	34	−15	Crump	6
21	728.715	12437	+ .007	25	−13	Crump	6
1914 June 1	2420285.867	15362	+ .006	41	−21	Crump	6
1919 Sept. 1	2422203.790	25431	− .009	34	+ 4	Crump	6
17	219.790	25515	− .009	28	− 9	Van Arnam	7
20	222.837	25531	− .010	28	− 9	Van Arnam	7
1920 Jan. 19	343.795	26166	− .007	28	− 8	Henroteau	5
21	345.722	26176	+ .016	36	−16	Henroteau	5
28	352.760	26213	+ .006	38	− 9	Henroteau	5
30	354.842	26224	− .007	35	− 9	Henroteau	5
Feb. 3	358.660	26244	+ .001	44	− 6	Henroteau	5
1921 Nov. 6	2423000.779	29615	+ .014	30	− 3	Hobe, Mendenhall	14
1922 Feb. 16	102.887	30151	+ .025	30	−18	Henroteau	3
20	106.883	30172	+ .021	19	− 8	Henroteau	3
Mar. 2	116.600	30223	+ .023	37	− 7	Henroteau	3
3	117.735	30229	+ .015	31	−18	Henroteau	3
5	119.650	30239	+ .025	38	−14	Henroteau	3
8	122.700	30255	+ .028	40	−15	Henroteau	3
24	138.700	30339	+ .028	30	−20	Henroteau	3
Aug. 26	293.930	31154	+ .017	25	−10	Van Arnam	7
1923 Mar. 5	484.800	32156	+ .006	22	− 7	Henroteau	3
8	487.663	32171	+ .032	26	− 8	Henroteau	3
14	493.762	32203	+ .036	26	− 9	Henroteau	3
16	495.844	32214	+ .022	25	0	Henroteau	3
26	505.560	32265	+ .024	36	−11	Henroteau	3
1926 June 23	2424690.952	38448	+ .062	30	− 7	Mendenhall	14
July 12	709.990	38588	+ .052	34	− 6	Mendenhall	14
Aug. 8	736.855	38729	+ .059	26	− 6	Mendenhall	14
11	739.900	38745	+ .057	30	− 6	Mendenhall	14
14	742.955	38761	+ .064	27	− 7	Mendenhall	14
Oct. 7	796.860	39044	+ .063	35	− 5	Mendenhall	14
24	813.620	39132	+ .061	35	− 4	Mendenhall	14
1928 Aug. 22	2425480.894	42635	+ .086	38	− 1	Duncan, Mitchell	8
Sept. 10	500.870	42740	+ .061	34	− 4	Mendenhall	14
1929 Oct. 27	911.585	44896	+ .102	34	− 5	Crump	4
Nov. 16	931.583	45001	+ .100	39	− 2	Crump	4
1930 Oct. 19	2426268.554	46770	+ .113	34	− 3	Crump	4
1931 Aug. 26	580.575	48408	+ .128	36	− 2.5	Kohl	10
Sept. 11	595.611	48487	+ .116	38	0	Crump	4
Nov. 4	650.285	48774	+0.123	34	− 4	Kohl	10

* The numbers below refer to the same references numbered in the footnotes.

TABLE 3—*Continued*

Date	Observed Time of Max. Radial Velocity JD	*E*	O−C (Day)	2*K* (Km/Sec)	γ (Km/Sec)	Authority	Reference*
1932 Sept. 5	2426956.134	50377	+0.133	42	+ 1	Crump	4
1940 Sept. 21	2429893.702	65801	+ .245	33	− 1	Smith	1
22	894.658	65806	+ .249	46	− 2	Smith	1
23	895.603	65811	+ .241	38	− 3	Smith	1
Oct. 2	904.564	65858	+ .250	32	− 5	Smith	1
1941 July 18	2430193.915	67377	+ .263	34	− 2	Roman, Struve	2
26	201.730	67418	+ .268	38	− 4	Smith	1
1950 Sept. 25	2433549.727	84994	+ .398	22	− 3	Present paper	
26	550.680	84999	+ .398	25	0	Present paper	
27	551.635	85004	+ .401	27	− 2.5	Present paper	
28	552.785	85010	+ .408	30	− 3	Present paper	
29	553.730	85015	+ .400	26	− 4	Present paper	
Oct. 8	562.875	85063	+ .402	30	− 5	Present paper	
15	569.725	85099	+ .395	26	− 1	Present paper	
Nov. 5	590.685	85209	+ .402	26	− 7	Present paper	
12	597.728	85246	+ .398	30	− 3	Present paper	
1951 Oct. 5	924.799	86963	+ .415	26	− 3.5	Present apper	
1952 May 29	2434161.955	88208	+ .424	27	− 5.5	Present paper	
31	163.850	88218	+ .424	28	− 2	Present paper	
June 2	165.950	88229	+ .419	32	− 2	Present paper	
3	166.905	88234	+ .422	20	− 2	Present paper	
4	167.850	88239	+ .414	22	− 3	Present paper	
21	184.810	88328	+ .422	30	− 6	Present paper	
July 3	196.810	88391	+ .422	22	− 3	Present paper	
4	197.765	88396	+ .424	24	+ 2	Present paper	
5	198.905	88402	+ .421	28	+ 2	Present paper	
6	199.865	88407	+ .429	22	+ 3	Present paper	
17	210.715	88464	+ .422	18	0	Present paper	
24	217.763	88501	+ .422	30	− 4	Present paper	
Aug. 1	225.755	88543	+ .414	30	− 5	Present paper	
14	238.715	88611	+ .421	30	− 2	Present paper	
23	247.860	88659	+0.423	28	− 4	Present paper	

The old data were examined by re-estimating the values of $2K$, γ, and the times of the maximum radial velocities. Table 3 also lists our recent results for 1950–1952. Successive columns give the times of maximum radial velocities, the number of cycles elapsed, the differences between the observed and calculated times of maximum velocity, based upon $P = 0.1904795$ day, the values of $2K$ and γ.

The differences between the observed and calculated times of maximum velocity are plotted against the time of maximum velocity in Figure 2. A change of period certainly occurred in the interval between 1914 and 1919. The only observation in this interval is on May 15, 1918, by Henroteau.[5] Its time of maximum velocity is not precise enough to give significant information concerning the variation of the period. After 1919 the trend of the points in Figure 2 follows a smooth curve upward. The slope of this curve increases slowly with time. Thus there seems to have been no abrupt change of the period after 1919, but, instead, the period slowly increased.

We have tried to express ΔT, the difference of the time of maximum velocity, as a polynomial of the third degree in T. Six points were chosen, each representing a weighted mean of one of the six groups of observations, along the entire curve; then a least-squares solution was made to determine the coefficients of the polynomial. Thus the difference of the times of maxima, in the sense observed *minus* calculated, is given by

$$\Delta T = -0.2372 - 3.0550 \times 10^{-6} T + 4.9651 \times 10^{-10} T^2 + 4.7274 \times 10^{-15} T^3 \,, \quad (1)$$

where T, expressed in days, is counted from JD 2400000. The residuals of ΔT (C−O) at the selected six points are shown in the accompanying tabulation. The foregoing

Date	JD 2422200	24700	26600	30000	33500	34000
Year	1920	1927	1932	1941	1950	1952
Difference of ΔT (C−O)	+0.001	+0.001	0.000	−0.004	−0.002	+0.004

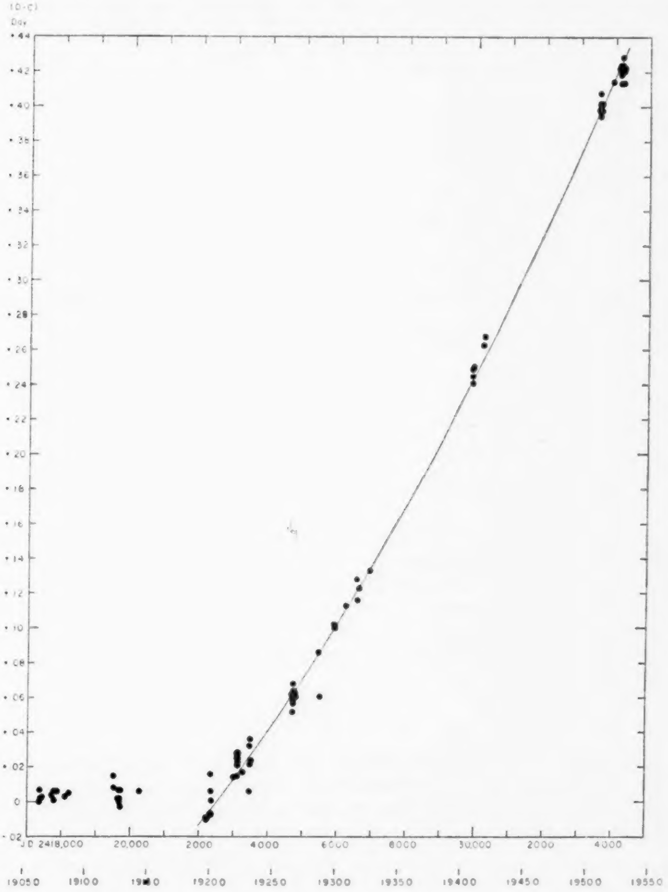

FIG. 2.—Differences in the times of maximum radial velocity in the sense *observed* minus *calculated*. The calculated times are based on $P = 0.1904795$ day. The curve represents equation (1), a third-degree polynomial in time, T.

polynomial (1) represents the observations very well. The curve representing the polynomial is plotted in Figure 2.

With the epoch at JD 2422203.790 (the time of maximum radial velocity on September 1, 1919), the observed times of maximum velocity are well represented by

$$T(\text{max.}) = \text{JD } 2422203.790 + 0.1904844E + 2.9440 \times 10^{-11}E^2 + 3.2671 \times 10^{-17}E^3 , \tag{2}$$

and the period of the radial velocity is given by

$$P = +0.1904844 + 5.8880 \times 10^{-11}E + 9.8013 \times 10^{-17}E^2 \text{ day} , \tag{3}$$

where E is the number of cycles which elapsed after the foregoing epoch.

Henroteau,[3] from his 1922 observations, derived a beat period for K of 28 days. This period does not fit the other observations; for example, the time interval between maximum values of $2K$—43 km/sec on August 27, 1906, and 44 km/sec on October 1, 1912—would be equal to 79.53 P, when $P = 28$ days.

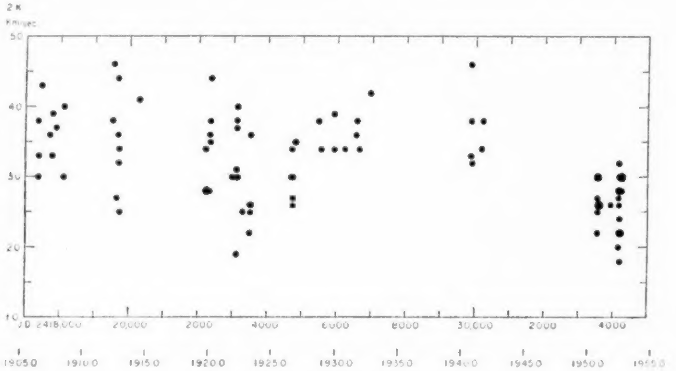

FIG. 3.—The variation of $2K$, twice the amplitudes of the radial-velocity-curves

We have plotted in Figure 3 the values of $2K$ against the time for all the existing data from 1906 to 1952. There are fifteen cycles, observed over an interval of 3 months in 1952, June 1 to August 23. The data for 1952 are shown on a larger scale in Figure 5. We are unable to find a period of the variation of K to represent all observations. This is actually what we ought to expect if we take into account the following consideration: According to Struve's designation,[12] the periodicity of K, if it exists, is given by the beat period P_3:

$$\frac{1}{P_3} = \mp \frac{1}{P_2} \pm \frac{1}{P_1} , \tag{4}$$

where P_1 is the period of the radial velocity, say, 0.1904795 in the present case, and P_2 is the period of variation of the line profiles of the stellar spectra. There is no change in the line profile of β Cephei,[2] but its change may be too small to be observed. Suppose P_2 does exist and is constant, then from equation (1) we have

$$\delta P_3 = \pm \left(\frac{P_3}{P_1}\right)^2 \delta P_1 . \tag{5}$$

---

[12] *Ap. J.*, 112, 520, 1950.

In general, (P_3/P_1^2) is a very large quantity of the order of magnitude of 10^4 in the case of 16 Lacertae, β Canis Majoris, and ν Eridani.[13] In view of the increasing nature of P_1 after 1919, P_3 will show large changes according to formula (5). Thus any possible value of P_3 would be correct for only one season or so. But even during such limited intervals of time we were unable to detect any real periodicity in K. The changes in the amplitudes of the velocity-curves are too large to be attributed to errors in the observations. We

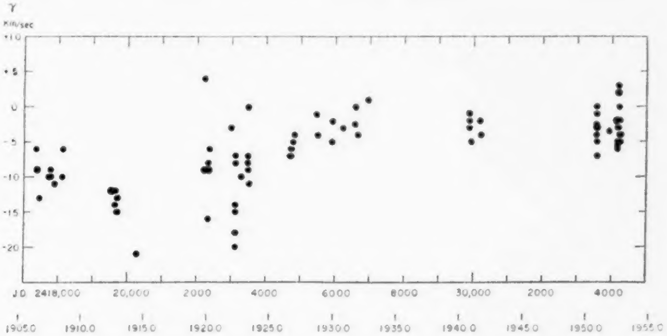

FIG. 4.—The variation of γ, the velocities of the center of mass

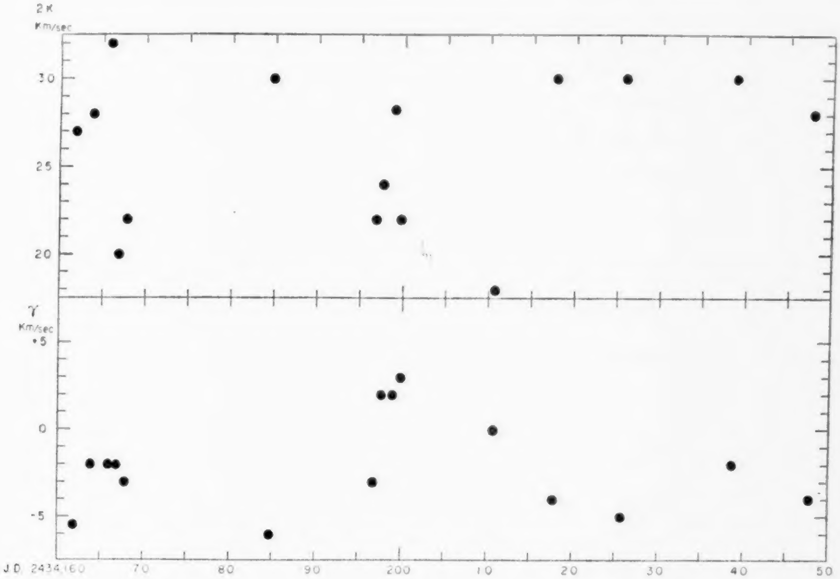

FIG. 5.—Variations of $2K$, twice the amplitudes of the radial-velocity-curves and of γ, the velocities of the center of mass in 1952, from June 1 to August 23.

---

[13] Struve, *Ann. d'ap.*, **15**, 157, 1952.

conclude that in β Cephei only one oscillation, with period P_1, is present but that there are, in addition, irregular variations in the velocity. This star is thus the opposite of σ Scorpii,[14] where only P_2 is present. But both types of oscillations are associated with irregular changes.

Although the material does not completely rule out a beat period of less than a day, there is no reason, at present, to believe that such a period really exists.

Mendenhall[15] estimated a period of 20 years for the variation of γ, and Smith[2] later suggested a period of 50 years. These periods are not very convincing, as may be inferred from their illustrations.

We have plotted in Figure 4 the values of γ against the time for all the existing data from 1906 to 1952 and on a larger scale, in Figure 5, for 1952. We are unable to find a period of the variation of γ to represent the observations. In general, the values of γ before 1919 are low, all smaller than -8 km/sec, except for two for values at -6 km/sec. After 1925 all γ's are greater than -8 km/sec.

The line *Ca* II 3933.6 was measured on 189 spectrograms. The average radial velocity is -8.3 km/sec.

To date, six stars of the β CMa–β Cep class have been investigated in detail (β CMa,[16] 12 Lac,[17] σ Sco,[14] 16 Lac,[18] ν Eri,[19] and β Cep). All belong to a narrow region in the HR diagram, between spectral classes B1 and B3 and between luminosity classes II and IV. But apparently not all stars within this region are members of the group. Three of the six show conspicuous beat effects of the periods P_1 and P_2 in the radial velocities and sometimes also in the brightnesses (β CMa, 16 Lac, ν Eri). Two stars show only the variation, P_2, associated with a change in line profile (12 Lac, σ Sco), and one shows only a variation, P_1, without change in line profile (β Cep). All six stars show irregular changes in radial velocity which are superposed over the periodic changes. These changes are relatively small in β CMa, where they seem to affect only the P_2-variation. They are very large in 12 Lac and σ Sco, where they distort the P_2-variation, but they are quite conspicuous also in β Cep, where they affect the P_1-variation.

[14] R. D. Levee, *Ap. J.*, **115**, 402, 1952.

[15] *Lick Obs. Bull.*, **14**, 133, 1930.

[16] *Ap. J.*, **112**, 471, 1950.

[17] *Ibid.*, **113**, 589, 1951.

[18] *Ibid.*, **116**, 81, 1952.

[19] *Ibid.*, in press.

THE SYSTEM OF ALPHA CORONAE BOREALIS*

GERALD E. KRON AND KATHERINE C. GORDON
Lick Observatory, University of California

Received August 25, 1952; revised March 6, 1953

ABSTRACT

A photoelectric light-curve at λ 7230 has been obtained for α Coronae Borealis. The secondary minimum was located, and its depth, width, and phase have been measured. Orbital and physical elements have been derived, both relative and absolute. The light-curve was analyzed after correction of it for the distorting effect of the rotation of the primary component; likewise, an assumption that the secondary component also has appreciable axial rotation was found to be necessary. The absolute elements were derived by means of a special application of the mass-luminosity law, and an attempt was made to estimate the uncertainty of the absolute elements. It is concluded that observationally determined darkening coefficients in red light may be significantly smaller than predicted by theory and that α Coronae Borealis is appreciably brighter for its mass than Sirius.

INTRODUCTION

The star α Coronae Borealis is one of several interesting eclipsing variables discovered by means of photoelectric methods and studied by Joel Stebbins in a survey of promising spectroscopic binaries.[1] At the time of discovery, in 1912, two radial-velocity-curves and corresponding elements were available, one by Cannon,[2] the other by Jordan.[3] Stebbins' light-curve, in combination with Jordan's spectrographic elements, yielded a considerable amount of information regarding the star. The most important was that the primary minimum (resulting from an annular eclipse) showed continuous variation, which indicates the presence of limb darkening on the star that is eclipsed. Stebbins was able to estimate the degree of limb darkening from his light-curve, the first such information for this star. The chief remaining properties of the system were the luminosity of the fainter component and the orbital inclination. Stebbins used light of effective wave length λ 4500, and he was unable to detect the secondary minimum. His observations of the primary minimum were such that he found it expedient to assume a 90° inclination. Clearly, a precise solution for the orbital elements, including the darkening coefficient, would be greatly aided by knowledge of the luminosity of the secondary component and by a value of the inclination determined analytically from the light-curve itself.

McLaughlin's spectrographic work on α Coronae Borealis[4] also indicated the desirability of more extensive photometric measures. He confirmed the accuracy of Jordan's elements and, more important, demonstrated that the primary component is in rapid rotation, with a rotational speed far in excess of the orbital speed. The high rotational speed, which is partly responsible for the extremely broad spectral lines, was confirmed by Struve and Elvey,[5] who employed the width of the λ 4481 line as an indication of rotational velocity. They obtained a rotational velocity in agreement with McLaughlin's, which was derived from measurements of the rotational distortion of the velocity-curve. The high rotational speed of the primary component makes α Coronae Borealis a particularly rare type of eclipsing system. It is important to know the orbital inclination in order to interpret with confidence McLaughlin's rotational data. The inclination can

---

* *Contributions from the Lick Observatory*, Ser. II, No. 46.

[1] *Pub. Washburn Obs.*, **15**, chaps. ii, iii, viii, ix, and x, 1928.

[2] *J.R.A.S. Canada*, **3**, 421, 1909.

[3] *Pub. Allegheny Obs.*, **1**, 85, 1909.

[4] *Pub. Obs. U. Michigan*, **5**, 91, 1933.

[5] *Ap. J.*, **71**, 221, 1930.

be derived from the primary minimum alone, provided observations of a very high precision are available.

The secondary minimum can be observed by employing a spectral region in the red, which will enhance the brightness of the companion, relatively red compared to the A0-type primary star. Observations were made in this region with a red-sensitive photoelectric photometer that could be used without refrigeration[6] on bright stars. Details of the observations are to be found in the Appendix.

SOLUTION FOR ORBITAL ELEMENTS

Because α Coronae Borealis contains at least one component that is distorted (by the flattening due to rotation), the solution for elements became an iterative process, with the start made by a simple determination of circular elements based upon the assumption that both components are spherical. Throughout the treatment in this paper, the axes of rotation of the stars are assumed to be perpendicular to the orbital plane, and the stars are assumed to rotate like solid bodies with complete central concentration.

TABLE 1

CIRCULAR ELEMENTS FROM PRIMARY MINIMUM

ELEMENT	SOLUTION		
	I	II	III
u_1	0.200 ± 0.056	0.200	0.200
$\cos^2 i'$	0.002008 ± 0.00009	0.001819	0.002177
r_1'	0.0842 ± 0.0005	0.0834	0.0847
r_2'	0.02530 ± 0.00018	0.02493	0.02551
$(1-\lambda_1)$	$0\overset{\mathrm{m}}{.}0811$	$0\overset{\mathrm{m}}{.}0740$	$0\overset{\mathrm{m}}{.}0886$
k_s/k_d	1.042	1.082	1.000
$v_1^{\prime 2}$	0.0	0.148	0.148
$v_2^{(2)}$	0.0	0.0	0.28
$\Sigma(O-C)^2$	1270	1353	1074

NOTE.—The subscript 1 refers to the larger star; the subscript 2, to the smaller star. The values for radii are the semimajor axes of the ellipsoids; k_s/k_d is the ratio of the "shape" k to the "depth" k, where k is the ratio of the radii. The residuals from which the sums of the squares were derived were in units of 10^{-4} of the total light of the system.

A preliminary solution by Russell's method was first made for the primary minimum, with the assumption of a circular orbit.[7] Since the depth of even the primary minimum is so small—less than 0.1 mag.—elements derived from this minimum may be of low weight. Also, since elements of low determinacy would make the star of little further interest astrophysically, a least-squares solution (solution I) was decided upon to correct these elements and to derive their weights in order to test the determinacy. To reduce the labor of making the least-squares corrections, only the four most critical elements were carried as unknowns: the darkening coefficient of the larger star, u_1; the radii of the two stars, r_1' and r_2', in terms of the radius of the fictitious circular orbit; and the inclination of the fictitious orbit, i'. The only unknown of much consequence not included was the depth of the primary minimum. Since this quantity can be determined with precision by trial, its exclusion from the formal solution did not have an important effect on the weights of the unknowns. Irwin's tables[8] were used for computation of the differential coefficients. The least-squares solution for α Coronae Borealis converges very slowly unless preliminary elements of unusually high precision are available. The corrections therefore add little to the value of the investigation as far as improvement of the elements is concerned. The solution did show, however, that the orbital elements based upon the present light-curve are remarkably determinate, a fact that encouraged further analysis of the data. The circular elements based upon the hypothesis of spherical stars are given in Table 1, along with the probable errors, which demonstrate the determinacy of the elements. The residuals yielded by solution I are given in the fourth column of Table 2. The probable error of a single normal point is ±0.0007 mag.

---

[6] G. E. Kron, *Pub. A.S.P.*, **59**, 190, 1947.

[7] We are indebted to Dr. Henry Norris Russell for aid with this solution during his tenure as Morrison Research Associate at the Lick Observatory.

TABLE 2

PRIMARY MINIMUM: NORMAL POINTS, RESIDUALS, AND RECTIFICATION

No.	Phase (Day)	Normal	(O−C)			h^*	
			I	II	III	II	III
1	0.2643	$0^{m}9982$	$+0^{m}0007$	$+0^{m}0007$	$+0^{m}0003$	$+0^{m}0005$	$-0^{m}0005$
2	.2433	.9890	− .0005	− .0006	− .0007	+ .0010	− .0010
3	.2198	.9781	+ .0009	+ .0008	+ .0006	+ .0017	− .0018
4	.1914	.9594	− .0007	− .0009	− .0009	+ .0027	− .0028
5	.1658	.9458	+ .0013	+ .0011	+ .0009	+ .0038	− .0038
6	.1443	.9315	− .0013	− .0015	− .0012	+ .0044	− .0045
7	.1286	.9273	+ .0017	+ .0019	+ .0015	+ .0054	− .0055
8	.1154	.9200	− .0011	− .0008	− .0009	+ .0060	− .0059
9	.1041	.9188	.0000	+ .0001	− .0004	+ .0071	− .0073
10	.0930	.9171	− .0011	− .0009	− .0012	+ .0071	− .0074
11	.0814	.9183	+ .0006	+ .0007	+ .0006	+ .0071	− .0073
12	.0697	.9180	+ .0006	+ .0008	+ .0008	+ .0071	− .0074
13	.0540	.9171	+ .0002	+ .0003	+ .0004	+ .0071	− .0074
14	.0346	.9154	− .0011	− .0012	− .0010	+ .0070	− .0073
15	0.0115	0.9163	0.0000	−0.0002	−0.0002	+0.0069	−0.0073

THE MEASUREMENT OF ROTATION

The fit to the observed light-curve obtained by solution I is good indeed; however, it is unreasonable to suppose that the elements so obtained are the best possible, because the effects of the rotation of the primary body have been neglected. McLaughlin obtained a rotational velocity "in excess of 100 km/sec,"[4] while Struve and Elvey found 130 and 125 km/sec, respectively.[5] In all three cases the authors give minimum values, McLaughlin because he assumed a 90° inclination and neglected gravity darkening (which gave weighting factors that were low) and Struve and Elvey because they neglected the effects of limb darkening and gravity darkening. In order to make a more precise estimate of the rotational velocity from McLaughlin's data, we have recomputed it from his measurements and from our value for the orbital inclination, applying the modern theory of Kopal[9] for the general computation of the weighting factors. Our redetermination results in a value of 190 km/sec for the rotational velocity, and, in view of the Struve-Elvey results, we have decided to adopt 150 km/sec. The weighting factors are given in the Appendix.

---

[8] *Ap. J.*, **106**, 380, 1947.

[9] *Proc. Nat. Acad. Sci.*, **28**, 133, 1942.

THE EFFECTS OF ROTATION

The modification of the computed orbital elements to take into account the effects of rotation of the components is made practicable by recent publications of Kopal. In the present case the work has been facilitated by following his analysis in *The Computation of the Elements of Eclipsing Binary Systems.*[10] Reference to this fine book of Kopal's will hereafter be made by the term "*Manual.*"

The present case represents a simplification of Kopal's general treatment of the perturbations of distorted binary systems. All terms of Kopal's general equations (*Manual*, eqs. [6.55] and [6.56]) vanish, with the exception of those accounting for the effects of the difference in polar flattening between the two stars, and of the terms in gravity darkening of the star eclipsed. It was, however, necessary to use the complete expansion in the significant terms. Because of the small darkening coefficient, only equation (6.55) for the undarkened case was needed. It was found that the chief contributing factor to the perturbations was the flattening term, the gravity-darkening term being relative small, though not negligible. This state of affairs is caused partly by the long wave length in which the observations were made and partly by the particular value of the inclination, which tends to minimize the effect of gravity brightening. In addition to some of the data given later in Table 10, the following data were used in the computation of the perturbations:

$$\begin{aligned} \text{Effective wave length} &= 7230 \text{ A}, \\ T &= 11{,}000^\circ \text{ K}, \\ V_r &= 150 \text{ km/sec}, \\ v_1^{(2)} &= 0.148, \end{aligned}$$

where $v_1^{(2)}$ is the coefficient of the flattening term due to axial rotation of the primary star. The computations were carried out first by approximate formulae given by Kopal,[11] and they were then repeated according to the complete analysis in chapter vi of the *Manual* when it became available. Values of the I-integrals were taken from *Harvard Circular* No. 450. The derived perturbations (seventh column of Table 2), when applied, with opposite sign, to the observed values of l, the fractional light of the system, yielded points on a light-curve which, when fitted, would be represented by the desired elements. The most conspicuous change effected by the application of the perturbations is that the depth of primary minimum, $1 - \lambda_1$, was reduced. New elements were derived first by improving the elements of solution I by trial and error and then, as a completing formality, by subjecting the elements to a least-squares correction. The resulting elements, solution II, are given in Table 1 and the residuals in the fifth column of Table 2. Clearly, the only really important change occurred in the value of $1 - \lambda_1$. Actually, the change in the depth of minimum may be estimated at the start to be about 0^l0070 by calculating the figure of the ellipsoid of revolution corresponding to $v_1^{(2)} = 0.148$ and by computing from this value the effect on the depth of minimum of the substitution of an elliptical area for a circlar area of radius equal to the semimajor axis. The only additional information yielded by the elaboration of Kopal's equation (6.55) is in the small change in the *shape* of the light-curve, caused by substitution of the elliptical edge for the circular edge and, of course, by the hypothetical presence of gravity darkening.

When a solution is made in the case of an annular eclipse, there are always two independent ways of computing the value for k, the ratio of the radii. One value of k results as a matter of course from the solution that fits the observed points of the light-curve; since this value of k depends upon the shape of the curve, it is called the "shape" k. A second value of k can be derived from the light-elements; this value of k is often called the "depth" k, because the depths of both the primary and the secondary minima enter into its evaluation. The two values of k should, of course, check within the expected degree of determinacy of the solution. Agreement between the two values is an excellent over-all check of the accuracy of the computations and of the validity of the physical assumptions on which the solution was based. The test has been applied to α Coronae Borealis, and the results are shown in Table 1. It is apparent that the two values of k are irreconcilable on the basis of observational error for solution I, and especially for the physically more complete solution II. The shape k cannot be varied by more than 1 per cent without very obviously violating the shape of the computed minimum. The value of λ_1 cannot be changed by more than 0.5 per cent, whereas the value of λ_2 would have to go to such a high value that the secondary minimum would be deeper than the primary. We have here a genuine case in which the shape and depth values of k are not in agreement, and we must therefore search for some reasonable physical cause.

---

[10] *Harvard Obs. Mono.*, No. 8 (Cambridge, 1950).

[11] *Ap. J.*, **94**, 159, 1941; **96**, 20, 1942.

THE THIRD-BODY HYPOTHESIS

The discrepancy between the two k-values can be removed by assuming that an extra source of light exists in the system. The most logical source of extra light would be a third body. The introduction into the solution of the effects of extra light from a third body is very simple (*Manual,* pp. 81–83) when the eclipses are total and annular. We know from the depth of the secondary minimum that the light of the orbital companion, L_2, is $0.0195 = 1 - \lambda_2$. By substituting the observed value of $1 - \lambda_1$, 0.0740, in equation (3.27) of the *Manual*, we find that λ_2 must equal 0.8410 to yield $k = 0.299$. Inasmuch as the observed value of λ_2 is 0.9805, where $1 - L_2 = L_1 + L_3$, we find $L_3 = 0.1395$. A third body, therefore, would have to have eight times the light of the orbital companion and nearly 14 per cent of the total light of the system. The magnitude difference between the third body and the rest of the system would be 2.2 mag. in the red and slightly more in the visual. The star α Coronae Borealis has been scrutinized many times by observers, and it is unlikely that a visually resolvable companion of this brightness would have escaped notice. High-dispersion infrared spectrograms, taken, respectively, at the McDonald and Mount Wilson Observatories through the courtesy of W. A. Hiltner[12] and R. F. Sanford,[13] failed to show evidence of a low-temperature companion star; furthermore, the velocity of the system of α Coronae Borealis is believed to be constant. Stebbins' accurate six-color photometry of α Coronae Borealis, presented later in this paper, shows that the light-distribution is that of a normal A0 star. These considerations eliminate all but the unlikely possibility that the third body is a very close optical companion, approximately of the same spectral type as the primary component.

ROTATION OF THE COMPANION

The perturbations caused by the oblateness of the primary component were of such a nature that they enhanced the k-discrepancy of α Coronae Borealis. Therefore, if rotation is assumed for the companion as well, the k-discrepancy will be reduced and, in theory, at least, may be made to vanish. Computation of the perturbations for rotation of the secondary component introduces a value for $v_2^{(2)}$ in the oblateness terms in equation (6.55) of the *Manual*. The sign of the difference term, $v_1^{(2)} - v_2^{(2)}$, in the oblateness expression becomes reversed, but the gravity-darkening expression is unchanged. If a value of $v_2^{(2)} = 0.28$ is assumed, the rectification constants become as given in the last column of Table 2. We find that if the elements of solution I are used experimentally to represent this new light-curve, the value for $1 - \lambda_1$ becomes 0.0884. If this value is now substituted in equation (3.27) of the *Manual*, we get 0.300 for the depth k, in agreement with the shape k for solution I. From the data in Table 10 and the expression for $v_n^{(2)}$ (*Manual*, eq. [6.60′]) we derive an equatorial velocity of 197 km/sec for the secondary star, equivalent to one rotation in $5\frac{1}{2}$ hours. The ratio of the minor axis to the major axis of the projected ellipse (*Manual*, eq. [6.69]) is 0.85. It is clear that while a rather rapid rotation is required for the secondary component, this rotation is still far from the disruption point and not much faster than the orbital angular speed of some rapidly rotating eclipsing variable stars. Thus the hypothesis of a rapidly rotating secondary component is a possible one, at least physically, and further analysis is justified. New elements were determined on the hypothesis that both components rotate; these are given in Table 1 under solution III, and the residuals are given in the sixth column of Table 2. An examination of the residuals shows that solution III fits the observations as well as solutions I and II. While not much weight should be given to the decrease in residuals, since a chance decrease of a large residual can affect the sum of the squares by a considerable amount, nevertheless the results of solution III do not weaken the case for rotation of the secondary body. It is unfortunate that the secondary minimum is so shallow that its observed shape is indeterminate, for, if this were not so, the shape would serve as an independent test of the validity of the rotation hypothesis.

---

[12] *Ap. J.*, **105**, 214, 1947.

[13] Private communication.

DERIVATION OF TRUE ELEMENTS FROM SECONDARY MINIMUM

The analysis of the secondary minimum, resulting in the derivation of the physically most plausible or "real" elements, was carried out from the circular elements of solution III. However, the differences between the elements of the three solutions are so small that, for astrophysical use of the absolute elements, it matters little which of the three circular solutions is used to obtain the final elements.

TABLE 3

CIRCULAR ELEMENTS DERIVED FROM SECONDARY MINIMUM

ELEMENT	SOLUTION		
	A	B	C
r_1''	0.0505	0.0530	0.0553
e	0.347	0.331	0.319
ω	314°	316°	318°
$\cot i''$	0.0166	0.0183	0.0199
$(O-C)^2/(n-1)$	0.0000959	0.0000544	0.0000605

The restriction placed on the circular elements for the secondary minimum by equation (5.49) of the *Manual* allows only one significant element to be arbitrarily selected. The influence of the darkening coefficient of the smaller star, u_2, is obviously insignificant for such a shallow minimum, and it has been assumed to be 0.4. The most convenient element to pick as an independent variable in fitting the secondary minimum is the fictitious radius of the larger star, r_1''. The value of k was, of course, set equal to 0.301 as derived from solution III. Three representations were made for the secondary minimum for three values of r_1''. The three sets of elements are given in Table 3. The best value of r_1'' could be determined by plotting the sums of the squares of the residuals (Table 4), by fitting a parabola through the points, and by selecting the value of r_1'' that gave the minimum sum. In the present case, however, any refinement beyond simply using solution B (Tables 3 and 4) seems pointless. The dependence of e and ω on r_1'' may be estimated from the data in Table 3; obviously these quantities are not seriously affected by the inherent indeterminacy of the selection of the best value of r_1''. However, e and ω depend upon the observed times of minima, t_1 and t_2, and the ratio of the widths of the two minima in such a complex way that a reliable estimate of their precision is practically hopeless without resorting to a prohibitively laborious least-squares adjustment.

The final, real, relative elements can now be derived by proper combination of the circular elements from solutions III and B. (See *Manual*, p. 112.) After a small correction, given on page 145 of the *Manual*, for the effect of polar flattening on the inclination, the resulting real, relative elements are as presented in Table 5. The normal points and the computed light-curve based on solution III B are given in Figure 1 for the minima. Normal points for the complete light-curve are shown in Figure 2.

TABLE 4

SECONDARY MINIMUM: NORMAL POINTS AND RESIDUALS FROM SOLUTIONS

No.	Phase (Day)	Normal	(O−C)		
			A	B	C
1	0.234	$0\overset{l}{.}9994$	…	…	…
2	.209	0.9995	…	…	…
3	.198	1.0022	…	…	…
4	.190	0.9994	…	…	$+0\overset{l}{.}0005$
5	.178	0.9995	…	$-0\overset{l}{.}0001$	+ .0008
6	.167	0.9994	$+0\overset{l}{.}0002$	+ .0014	+ .0027
7	.159	0.9958	− .0021	− .0006	+ .0009
8	.148	0.9976	+ .0022	+ .0039	+ .0055
9	.134	0.9857	− .0057	− .0041	− .0028
10	.123	0.9848	− .0040	− .0021	− .0008
11	.112	0.9839	− .0013	− .0002	+ .0008
12	.102	0.9812	− .0015	− .0009	−0.0002
13	.091	0.9785	−0.0023	−0.0020	…
14	.079	0.9830	…	…	…
15	.056	0.9794	…	…	…
16	.036	0.9812	…	…	…
17	.022	0.9767	…	…	…
18	0.007	0.9839	…	…	…

TABLE 5

REAL, RELATIVE GEOMETRICAL ELEMENTS

Element	Larger Star	Smaller Star
Equatorial radius*	0.069 ± 0.001	0.0208 ± 0.0002
Polar radius*	0.064	0.0177
Inclination, *i*	88°30 ± 0°07	
Eccentricity, *e*	0.331	
Longitude of periastron, ω	316°	

* In terms of the semimajor axis of the orbit.

The geometrical elements of α Coronae Borealis are commonplace enough in themselves; the only novel aspect of the analysis is the assumption of rotation of the secondary component. Rapid axial rotation is rare, if indeed not unknown, in late-type main-sequence stars, unless they are members of close binary systems, such as the W Ursae

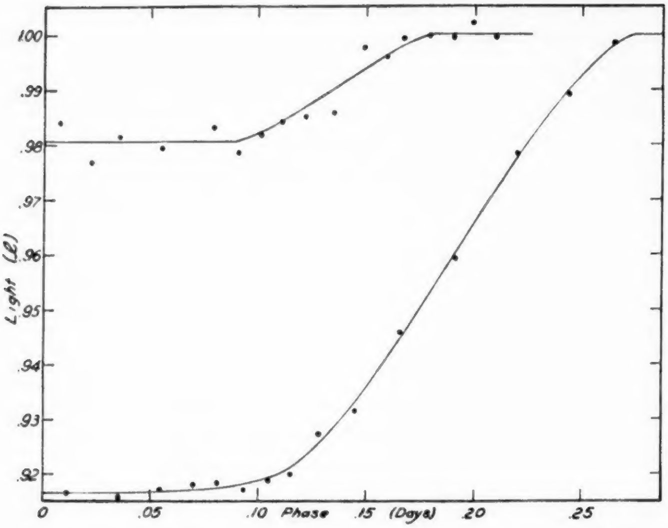

FIG. 1.—Minima of α Coronae Borealis. The normal points are plotted, and the heavy line is the light-curve computed from solution III B.

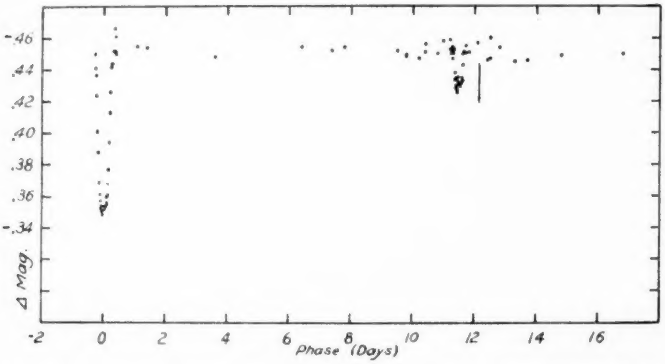

FIG. 2.—Normal points for the complete light-curve for α Coronae Borealis. The minima are plotted from the unreflected normal points mentioned, but not tabulated, in the text. The observations between minima are given in Table 12. The short vertical line represents the position of secondary minimum predicted on the basis of McLaughlin's spectrographic elements. The large scatter of the points between minima (uncorrected for night-to-night variation) probably is real and indicates variation between α and γ Coronae Borealis.

Majoris stars. However, very little is known about the properties of companion stars in a system such as α Coronae Borealis, so there is no precedent to serve as a guide to the validity of the rotation hypothesis.

PHYSICAL CONSTANTS AND ABSOLUTE DIMENSIONS

The spectrographic data for α Coronae Borealis can be combined with the photometric results in the usual way to determine absolute properties for the system. The fact that α Coronae Borealis is a single-lined spectroscopic binary prevents a straightforward derivation, but its known parallax can be used to overcome, in part, this inherent difficulty. In favor of the single-lined binary, in any event, is the freedom from a systematic error in the velocity amplitude caused by a tendency for the person measuring the plates to set too close to the neighboring line.

The most important datum yielded by the spectrographic work is the value for the semiamplitude, K_1:

$$34.93 \pm 0.52 \text{ (p.e.) km/sec (Jordan)},$$

$$34.83 \pm 0.52 \text{ (p.e.) km/sec (McLaughlin)},$$

$$\text{Mean } K_1 = 34.88 \pm 0.36 \text{ (p.e.) km/sec.}$$

The probable errors quoted resulted from least-squares solutions by Jordan and by McLaughlin.

We also have the following orbital eccentricities, e:

$$0.387 \pm 0.014 \text{ (p.e.) (Jordan)},$$

$$0.377 \pm 0.012 \text{ (p.e.) (McLaughlin)},$$

$$0.331 \pm 0.009 \text{ (p.e.) (present)},$$

$$\text{Mean } e = 0.356 \pm 0.020 \text{ (p.e. from external agreement)}.$$

The probable error of the eccentricity derived in the present work was arbitrarily set to give it approximately double the weight of the eccentricities determined by the spectrographic method. Calling $\sin i = 1.000$, we now derive

$$a_1 = (7.78 \pm 0.16) \times 10^6 \text{ km}$$

and

$$\frac{\mathfrak{M}_2^3}{(\mathfrak{M}_1 + \mathfrak{M}_2)^2} = 0.0629 \pm 0.0033 \text{ (p.e.)}.$$

Because the parallax and therefore the luminosity of the system are known, we may most reasonably determine the absolute elements from values for the masses. By means of the mass function given above, we prepare for later use the following table of masses

TABLE 6

COMPONENT MASSES AND RATIOS
(Unit = 1.0☉)

	Assumed $\mathfrak{M}_2$						Percentage P.E.
	0.80	0.85	0.90	0.95	1.00	1.05	
$\mathfrak{M}_1$	2.05	2.28	2.51	2.74	2.99	3.28	±4
$\mathfrak{M}_1/\mathfrak{M}_2$	2.57	2.69	2.79	2.88	2.99	3.12	±4

for component 1, $\mathfrak{M}_1$, and the mass ratio, $\mathfrak{M}_1/\mathfrak{M}_2$, computed from reasonable assumed values of the mass of component 2, $\mathfrak{M}_2$.

The percentage probable errors in $\mathfrak{M}_1$ and in $\mathfrak{M}_1/\mathfrak{M}_2$ result from the probable error in the mass function. The table also shows that the range in the values assumed for $\mathfrak{M}_2$, $0.25\odot$, gives a range in $\mathfrak{M}_1$ of $1.23\odot$. Hence if $\mathfrak{M}_1$ is computed from $\mathfrak{M}_2$, the former will have 4.9 times the probable error of the latter.

Several determinations of the apparent magnitude of α Coronae Borealis are available. The values have been converted to the International System by the formulae of Seares[14] and of Seares and Joyner.[15] Using the **P**, **V** convention of notation,[16] we have the apparent magnitudes shown in the accompanying tabulation. Because the "Harvard Mimeogram" value differs considerably from the others, it was omitted in forming the mean for **P**. Eggen gives a color which, when converted to the **P**, **V** system by means of a formula given by Kron and Smith,[16] becomes $(P - V) = -0\overset{\mathrm{m}}{.}16$. The value for $(P - V)$ from the mean values of **P** and **V** above, −0.155 mag., is in excellent agreement. An indirect check on Eggen's color is that he finds $(P - V) = -0\overset{\mathrm{m}}{.}16$ for β Ursae Majoris, and unpublished six-color results kindly furnished by Dr. Stebbins show that α Coronae Borealis and β Ursae Majoris are of the same color.

P (Mag.)	Authority	**V** (Mag.)	Authority
2.24	Hogg*	2.40	HR
2.25	De Vaucouleurs†	(2.25)	"Harvard Mimeogram"
2.23	Oosterhoff‡	2.38	PDM
2.26	Eggen§	2.42	Eggen§
Mean = $2\overset{\mathrm{m}}{.}245 \pm 0\overset{\mathrm{m}}{.}004$ (p.e.)		Mean = $2\overset{\mathrm{m}}{.}400 \pm 0\overset{\mathrm{m}}{.}007$ (p.e.)	

* Unpublished. Monochromatic, photoelectric magnitude, converted to the **P** system.

† *Ann. d'ap.*, **10**, 123, 1947.

‡ *B.A.N.*, **10**, 45, 1944.

§ *Ap. J.*, **112**, 141, 1950. Eggen's Pg_p magnitude system can be converted to the **P** system for a limited color range simply by adding 0.14 mag.

The distance of α Coronae Borealis is about 20 parsecs, and its galactic co-ordinates are $l = 8\overset{\circ}{.}5$ and $b = +52\overset{\circ}{.}5$. Thus α Coronae Borealis is too far from the galactic plane and too near for its light to suffer any large amount of space absorption. Support for this general conclusion is given by the six-color measures that show a normal A-type distribution of radiation. We therefore make small corrections of −0.020 and −0.016 mag. for absorption, based upon 1.0 magnitude per kiloparsec for the **P** magnitude and 0.8 magnitude per kiloparsec for the **V** magnitude, respectively. The final apparent magnitudes, corrected for absorption, are

$$
\begin{aligned}
P &= +2\overset{\mathrm{m}}{.}225 \pm 0\overset{\mathrm{m}}{.}004 \text{ (p.e.)},\\
V &= +2\overset{\mathrm{m}}{.}384 \pm 0\overset{\mathrm{m}}{.}007 \text{ (p.e.)},\\
(P - V) &= -0\overset{\mathrm{m}}{.}159 \pm 0\overset{\mathrm{m}}{.}008 \text{ (p.e.)}.
\end{aligned}
$$

---

[14] *Ap. J.*, **78**, 141, 1933.

[15] *Ap. J.*, **79**, 203, 1934.

[16] The symbols **P** and **V** denote apparent photographic and photovisual magnitudes determined photoelectrically on a system based on magnitudes of nine particular stars in the North Polar Sequence. See Kron and Smith, *Ap. J.*, **113**, 324, 1951. The **P**, **V** magnitude system is made as nearly as possible similar to the International System.

The mean trigonometric parallax on the Yale system, according to Louise F. Jenkins' *General Catalog of Trigonometric Stellar Parallaxes* (available to us at the time of writing only on punched cards; later published by Yale University Observatory, 1952) is

$$\pi = 0''.043 \pm 0''.006 \text{ (p.e.)} .$$

Eggen obtained $0''.049$ as a photometric parallax and $0''.047$ as a cluster parallax if α Coronae Borealis is a member of the Ursa Major cluster.[17] We adopt arbitrarily a mean of these three values, giving the trigonometric parallax double weight. The resulting value of the adopted mean parallax is

$$\pi = 0''.046 \pm 0''.002 \text{ (p.e. from external agreement)} .$$

The uncertainty in π is responsible for most of the uncertainty in the mass determination of the primary, component 1. The corresponding distance modulus is $m - M = +1^{\mathrm{m}}.68 \pm 0^{\mathrm{m}}.10$.

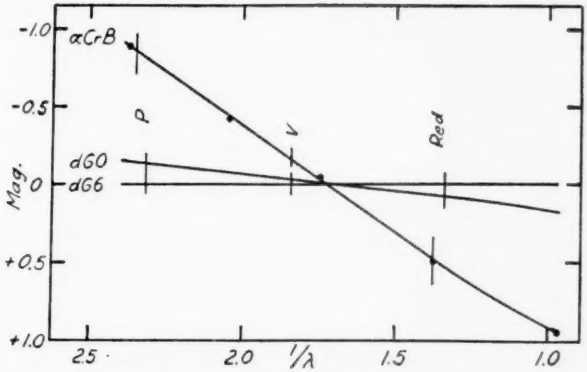

FIG. 3.—Relative spectral-energy distribution in five colors (from Stebbins' six-color photometry) of stars considered in the text. The abscissae of the short vertical lines indicate effective wave lengths. The plotted points are Stebbins' results for α Coronae Borealis, corrected for the presence of the G-type companion.

To reduce the apparent magnitude of the system to the magnitude of the primary component alone, a correction of +0.01 mag. must be applied to both the P and V magnitudes. We therefore find the absolute magnitudes of the primary component to be

$$\text{Abs. pg. mag.: } M_{P_1} = +0^{\mathrm{m}}.54 \pm 0^{\mathrm{m}}.10 ,$$
$$\text{Abs. vis. mag.: } M_{V_1} = +0^{\mathrm{m}}.70 \pm 0^{\mathrm{m}}.10 .$$

The magnitude of the secondary component can be determined by an iterative process from the known wave length of the observations, the six-color results, and the information from Eggen's published work. The spectral-energy distribution in five colors (ultraviolet omitted) of α Coronae Borealis, along with those for a dG0 and a dG6 star, are plotted as a function of $1/\lambda$ in Figure 3.[18] In this figure, the abscissae of the short vertical lines are the reciprocals of the wave lengths of the ***P*** and ***V*** systems for each of the two components and the reciprocals of the wave lengths in which the two components were observed in the present study.

---

[17] *Ap. J.* **112**, 141, 1950.

[18] We are indebted to Joel Stebbins for making the six-color observations and for allowing us to use them in advance of publication. The results for α CrB are based on five separate determinations; those for the G0 star are the mean values for β Comae and β Canum Venaticorum from Stebbins and Whitford, *Ap. J.*, **102**, 318, 1945, Table 3. The six-color system is standardized on dG6, so for this spectral type the spectral-energy distribution is represented by a horizontal line.

The observed light-ratio in the red is $l_2/l_1 = 0.0195/0.9805 = 0.0199 \pm 0.0009$. The probable error of this ratio was computed from the probable error of a single normal of the secondary minimum, ±0.0015 mag., with account taken of the fact that the depth of the secondary minimum is determined by the difference between two group means, each having five normal points: Nos. 1–5 and 14–18 of Table 4. The light-ratio yields a magnitude difference in the red equal to 4.25 ± 0.05 mag. The ordinates at the appropriate wave lengths in Figure 3 can now be used to derive magnitude differences which, when added to 4.25, will give the difference in magnitude between the two components in any other color, specifically, in the present case, at the effective wave lengths of the two colors of the ***P***, ***V*** system. These magnitude differences, when added to the absolute magnitude of the primary component, will give the absolute magnitude of component 2 and, of course, its color. These absolute-magnitude and color data are collected in Table 7 for component 2 for several assumptions of its spectral type. It is perhaps worth pointing out that, in the derivation of these data, the spectral type is the only quantity that does not result from direct observation. The probable error of the absolute magnitude is large because of the large probable errors of the distance modulus and of the red magnitude difference. The probable error of the color is smaller because of the absence of the distance modulus as a direct factor in its determination. The spectral-type criterion indicates that component 2 is a G3 star, whereas the color criterion favors a spectral type of later than G9. We shall call the companion "G6" and use the data in the fourth column of Table 7, noting that the uncertainties in color and magnitude will allow G6 to satisfy both criteria within the limits of error.

TABLE 7

ABSOLUTE MAGNITUDE AND COLOR OF COMPONENT 2

	ASSUMED SPECTRAL TYPE				P.E.
	G0	G3	G6	G9	
M_{P_2}	$+5\overset{\mathrm{M}}{.}91$	$+6\overset{\mathrm{M}}{.}01$	$+6\overset{\mathrm{M}}{.}12$	$+6\overset{\mathrm{M}}{.}24$	$\pm 0\overset{\mathrm{M}}{.}12$
M_{V_2}	+5.46	+5.51	+5.56	+5.61	±0.12
Color, $(P-V)_2$	$+0\overset{\mathrm{m}}{.}45$	$+0\overset{\mathrm{m}}{.}50$	$+0\overset{\mathrm{m}}{.}56$	$+0\overset{\mathrm{m}}{.}63$	$\pm 0\overset{\mathrm{m}}{.}05$
Derived $(P-V)_2$*	+0.61	+0.62	+0.65	+0.66	....
Derived spectral type*	G1	G3	G5	G7	....

* The derived spectral types are obtained by entering Fig. 3 of Eggen's Paper IV with the color converted to C_P. The derived colors are obtained similarly but by entering Table 6 or the same paper with the absolute magnitude converted to Pg_p.

The physical properties of the companion are favorable data with which to enter a mass-luminosity relationship, because the star is nearly a solar type and because its type is bracketed by the two components of α Centauri whose mass and luminosity are among the best determined of all the binary stars. It is true that the magnitude data of the primary component of α Coronae Borealis are more accurate than those of its companion; however, we are reasonably certain that the companion is a main-sequence star, a kind of star for which reliable mass comparisons may be made.

Kuiper's adopted values of mass and luminosity for the sun[19] and for α Centauri[20] are given in Table 8. These data are plotted as dots in Figure 4, along with Kuiper's values for Sirius[20] and with the derived values for the two components of α Coronae Borealis (shown as rectangles). The mass of component 2 was derived directly from the mass-luminosity curve; the mass of component 1 was obtained by entering Table 6 with the mass of component 2. The masses are

---

[19] *Ap. J.*, **88**, 438, 1938.

[20] *Ibid.*, p. 472.

$$\mathfrak{M}_1 = (2.46 \pm 0.12),$$
$$\mathfrak{M}_2 = (0.89 \pm 0.015)\,.$$

The probable errors were obtained from the probable errors in Table 6, combined with the effects of the probable error of the luminosity of component 2, Table 7. The contribution of any error in the mass-luminosity curve to the uncertainties of the physical properties of α Coronae Borealis is assumed to be negligible. Absolute geometrical elements can now be derived; these are given in Table 9, and the system is shown schematically in Figure 5.

TABLE 8

MASS-LUMINOSITY DATA

Star	Mass	M_V
α Centauri B	0.87	$+5^{\mathrm{M}}83$
Sun	1.00	+4.73
α Centauri A	1.08	+4.46

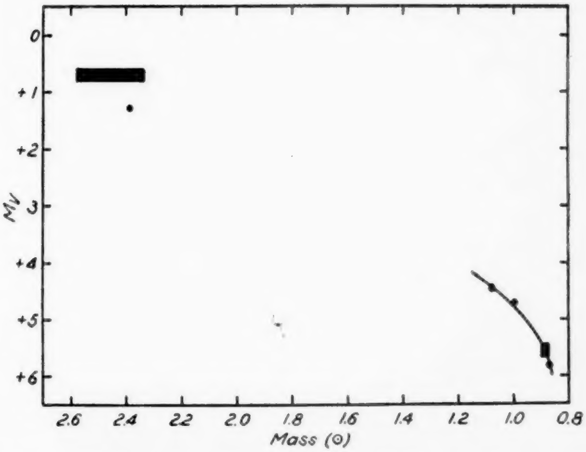

FIG. 4.—Mass-luminosity data for stars considered in the text. The two rectangles represent the two components of α Coronae Borealis, and their dimensions are twice their probable errors. The dots represent, from left to right, respectively, Sirius A, α Centauri A, the sun, and α Centauri B.

The derived absolute radii agree with generally accepted values for the corresponding spectral types. This result is a good independent check of the basic hypothesis that the companion star is a normal main-sequence object.

COMPARISON WITH STEBBINS' RESULTS

Stebbins' analysis of his light-curve did not show the *k*-discrepancy found in the present study. The agreement between the shape *k* and the depth *k* in the earlier work is caused by the small value of the shape *k*, which, in turn, is caused partly by the assumption of 90° orbital inclination and partly by the shape of the primary minimum, which is narrower and steeper than that of the present light-curve. The depth *k*'s are almost identical from Stebbins' and from the present analysis. When Stebbins' normal points are examined, it is apparent that the width of his primary minimum and the steepness of the curve are determined by only four points (one of which indicates a wide minimum), and all four were assigned low weight. It may therefore be possible to reconcile the two light-curves on this basis. It is unlikely that the differences between the two can be explained on the basis of a physical effect that is a function of the wave length in which the two sets of observations were made. No such effect was found in the two-color work on the similar eclipsing binary, YZ Cassiopeiae.[21] However, the differences in the light-curves of α Coronae Borealis could be explained on the basis of the improbable assumption that a rapid apsidal rotation fortuitously escaped being found by the determinations of longitude of periastron in 1907, 1929, and 1947.

TABLE 9

ABSOLUTE GEOMETRICAL ELEMENTS, WITH PROBABLE ERRORS

Orbital semimajor axis, component 1, a_1	$(7.78 \pm 0.16) \times 10^6$ km
Orbital semimajor axis, component 2, a_2	$(21.5 \pm 0.43) \times 10^6$ km
Semimajor axis, relative orbit, a	$(29.3 \pm 2.1) \times 10^6$ km
Equatorial radius, component 1, r_1	(2.9 ± 0.2)
Equatorial radius, component 2, r_2	(0.88 ± 0.06)

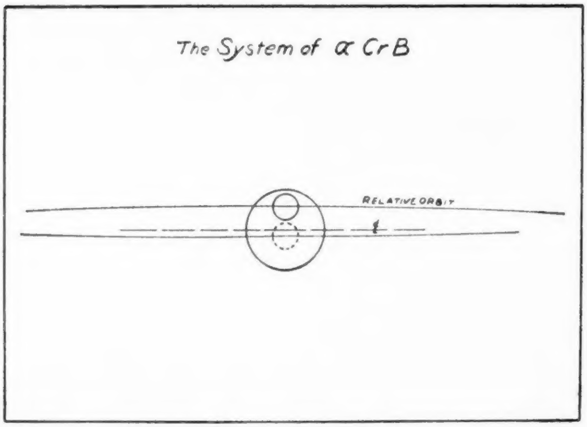

FIG. 5.—Schematic diagram of the system of α Coronae Borealis

---

[21] G. E. Kron, *Lick Obs. Bull.*, **19**, 59, 1939; *Ap. J.*, **96**, 173, 1942.

DISCUSSION

The final physical data of the system of α Coronae Borealis are collected in Table 10. The limb-darkening coefficient of component 1, 0.20, is well determined and may be compared with the limb-darkening coefficient derived at λ 6700 for the A-type component of YZ Cassiopeiae. For this A3 star, the value found was 0.33 ± 0.03. Because YZ Cassiopeiae was observed in two colors, an estimate of the limb-darkening coefficient at λ 7230 can be made by extrapolation; this value is about 0.31 ± 0.03, and it becomes 0.27 if transferred from A3 to A0 according to the dependence upon spectral type theoretically derived by G. Münch and S. Chandrasekhar.[22] The agreement is satisfactory in view of the difficulties of determining these coefficients. The mean value is about 0.23, compared with the theoretical value of 0.34 for an A0 star derived by Münch and Chandrasekhar. The disagreement between these two is much larger than the disagreement between the two independently observed values. We seem to have a case for a smaller observed value of limb darkening in red light than is theoretically predicted. It should perhaps be mentioned that neither series of observations in the red could have been affected by hydrogen absorption as represented by the Paschen series.

TABLE 10

PHYSICAL CONSTANTS OF α CORONAE BOREALIS

	Larger Star	Smaller Star
Spectral type	dA0	dG6*
Absolute visual magnitude, M_V	$+0^{M}.70 \pm 0^{M}.10$	$+5^{M}.56 \pm 0^{M}.12$
Color index, $(P-V)$	$-0^{m}.16$	$+0^{m}.56 \pm 0^{m}.05$
Mass†	2.46‡ ±0.12	0.89‡ ±0.015
Equatorial radius†	2.9 ±0.2	0.88 ±0.06
Mean density†	0.101	1.31
Equatorial velocity	150 km/sec	195 km/sec
Limb-darkening coefficient	0.200±0.056	....

Orbital period	17.359907 days
t_2-t_1	11.454 days
Orbital eccentricity	0.36±0.02
Longitude of periastron	316°
Inclination	$88^{\circ}.30 \pm 0^{\circ}.07$
Semimajor axis of orbit	$(29.3 \pm 2.3) \times 10^{6}$ km

* Derived.

† ⊙ = 1.

‡ From a mass-luminosity relationship.

In Figure 4 the mass and luminosity of Sirius may be compared with those of the A0 component of α Coronae Borealis. The diagram shows that here we probably are dealing with a real difference in mass-luminosity properties; α Coronae Borealis is about 0.5 mag. brighter than Sirius, although its mass is the same within observational error. Eggen classifies α Coronae Borealis as a "bright blue-dwarf" and Sirius as a "blue-dwarf," which may imply a difference in physical properties between these two stars of almost similar spectral type. The difference in mass may be indicative of a physical cause for the separation of the upper part of the main sequence into several similar, but not identical, sequences, as suggested by Eggen's work. The rotational velocity of α Coronae Borealis is too low for any unusual distribution of surface brightness that might explain the difference in luminosity between it and Sirius.

---

[22] *Harvard Circ.*, No. 453, 3, 1949.

APPENDIX

OBSERVATIONS

The first photoelectric observations in the red, made by A. B. Wyse at the Lick Observatory in 1941, are not included in our study because of color incompatibility. The brightness of α Coronae Borealis permitted observations to be made with the 12-inch refractor, which was used from May 6, 1946, to August 29, 1948. The principal comparison star was γ Coronae Borealis, with β Coronae Borealis as a check star. Data on the variable and comparison stars are given in Table 11. The comparison star γ Coronae Borealis is multiple, and consists of a long-period visual pair and a spectroscopic binary of small velocity variation. The principal star, of spectral type A0, radiates most of the energy. It is unlikely that any property of the multiplicity of γ Coronae Borealis will make the light of the system vary by more than that to be expected of a comparable single star. The three stars are rather widely separated for the most precise relative photometry, but observing in red light, with its relatively low atmospheric extinction, goes far toward reducing the effects of variable differential extinction. The check star was employed on ten nights, always in addition to the principal comparison star. The night-to-night check between γ and β Coronae Borealis is too poor to be explained on the basis of observational error alone, and there is indication of the presence of appreciable intrinsic variation between the two stars. Similarly, the night-to-night variation between α Coronae Borealis outside eclipse, and the comparison stars, showed the presence of relative variability. Magnitude differences between the two comparison stars, and between the variable and γ Coronae Borealis, are given in Table 12. The sixth and eighth columns contain the number of sets, of 5 meter-deflections each, contained in each mean magnitude difference, and the fifth column contains the internal probable error of the mean magnitude difference in the fourth column. The other columns are self-explanatory.

TABLE 11

DATA ON STARS

STAR	1900		SPECTRAL TYPE	MAG.
	R.A.	Dec.		
α Coronae Borealis..........	$15^{h}30^{m}.5$	+27° 03′	A0	$2^{m}.31$
γ Coronae Borealis..........	15 38.5	+26 37	A0	3.93
β Coronae Borealis..........	15 23.7	+29 27	F0p	3.72

From May 6, 1946, until February 19, 1947, the filters used were one piece of Schott RG1 2 mm thick on the comparison star, and a second piece of RG1 from the same stock with 2 mm of Schott NG5 on the variable. Since only one filter slide was available, two red filters were required in order to change conveniently from the simple red filter to the compound red and neutral filter necessary for the brighter star. On February 19, 1947, one of the red filters was moved to a fixed position over the window of the light-receiver, which allowed the same red filter to be used for both stars. This change in filters did not have an appreciable effect on the observations. The RG1 filter transmits from λ 6000 redward to the threshold sensitivity of the two photocells used, which was at about λ 10500 in both cases. The sensitivity of the filter-cell combination to equi-energy light was determined with a monochromator calibrated by means of a thermopile. The ordinates of the resulting sensitivity-curve were multiplied by the light-distribution in a 11,000° K and a 5300° K black body to obtain the two curves in Figure 4, which are assumed to represent the sensitivity of the photometer to the light of the two components of α Coronae Borealis. The vertical lines of Figure 6 divide the respective curves into two equal areas, and they are positioned at λ 7320 and λ 7460—wave lengths that are assumed to represent the effective wave lengths in which each of the two components was observed.

The photocell used from May 6, 1946, through September 16, 1946, was a type CE-23 operated at 54 volts on the cathode. On April 12, 1947, because of its superior properties, we changed to a CE-25 with 90 volts on the cathode. The color sensitivities of the two cells redward of λ 6000 are almost identical. A systematic correction of −0.060 mag. has been applied in all tabulations in this paper to the magnitude differences obtained with the CE-23 to make them homogeneous with the more numerous CE-25 observations.

From May 6, 1946, until June 13, 1947, the photocell was used with a 2 × 10^{11}-ohm load resistor and a VX-41 low-grid-current amplifying tube in a conventional circuit, employed with a power d.c. amplifier driving a Weston Model 430 0-1 milliammeter. On June 13 we changed to a 10^{12}-ohm grid resistor and a direct-feed-back capacity-neutralization circuit.[23] The changes in circuits and load resistors had no apparent effect on observations made on bright stars.

TABLE 12

OBSERVATIONS BETWEEN MINIMA

No.	Mean JD 2432000+	Mean Phase (Days)	Δ Mag. ($\alpha-\gamma$) (Mag.)	P.E. (Mag.)	No.	Δ Mag. ($\beta-\gamma$) (Mag.)	No.
1	7.765	7.8	−0.454	±0.0012	8	....	.....
2	9.734	9.8	− .449	± .0012	9	....	.....
3	10.774	10.8	− .450	± .0015	16	−0.315	4
4	11.750	11.8	− .451	± .0018	16	− .321	8
5	12.758	12.8	− .454	± .0015	16	− .319	8
6	14.782	14.8	− .449	± .0015	6	− .325	4
7	16.794	16.8	− .450	± .0013	8	− .331	6
8	17.722	0.4	− .461	± .0013	8	− .330	4
9	18.716	1.4	− .454	± .0020	8	− .324	4
10	23.722	6.4	− .454	± .0022	8	− .326	4
11	24.784	7.5	− .452	± .0016	8	....	.....
12	28.783	11.5	− .476	± .0025	4	− .324	4
13	45.691	11.0	− .458	± .0006	8	−0.337	4
14	80.653	11.3	− .447	± .0033	10	....	.....
15	288.943	11.2	− .459	± .0011	21	....	.....
16	289.828	12.1	− .457	± .0033	4	....	.....
17	308.756	13.7	− .446	± .0017	5	....	.....
18	312.783	0.3	− .445	± .0013	13	....	.....
19	323.700	11.2	− .454	± .0013	6	....	.....
20	325.771	13.3	− .445	± .0008	4	....	.....
21	350.794	3.6	− .448	± .0018	4	....	.....
22	358.813	11.6	− .455	± .0009	17	....	.....
23	364.836	0.3	− .466	± .0009	9	....	.....
24	409.680	10.4	− .456	± .0026	4	....	.....
25	411.673	12.4	− .446	± .0020	4	....	.....
26	417.672	1.1	− .455	± .0011	4	....	.....
27	654.819	12.5	− .447	± .0012	7	....	.....
28	704.770	10.4	− .451	± .0017	6	....	.....
29	790.662	9.5	− .452	± .0007	4	....	.....
30	793.658	12.5	−0.460	±0.0016	4	....	.....

An "observation" on each star consists of five 10-second meter-deflections. There are 245 observations between minima, 510 in or near primary minimum, and 270 in or near secondary minimum. The first observations of the secondary minimum on July 26, 1946, are included in Table 12 (under JD 2432028.783) to show how easily even such a shallow minimum can be recognized by photoelectric methods.

---

[23] G. E. Kron, *Pub. A.S.P.*, **59**, 190, 1947.

A mean zenith extinction of 0.12 mag., derived from the observational data, was used to correct all observations for differential extinction. The maximum differential extinction correction was 0.010 mag. at an hour angle of 4^h50^m west. An error in the zenith extinction of 10 per cent will cause an error in this largest correction of only 0.001 mag. Inasmuch as the average differential extinction correction was only 0.0025 mag., the systematic errors caused by night-to-night fluctuations in zenith extinction must have been small. The sky background brightness was measured as a routine operation, but it was negligible except during the brightest moon. A focal-plane aperture having a diameter of 60″ was used; the size is ample to clear the color aberration of the objective lens.

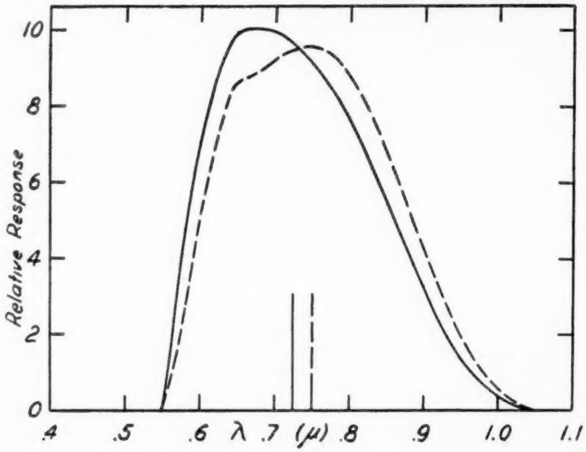

FIG. 6.—Distribution of radiation in which each of the two components of α Coronae Borealis was observed. The solid line represents the radiation distribution for the A-type component, the dashed line that for the G-type component. The vertical lines, if extended, divide the respective curves into two equal areas. These lines, at λ 7230 and λ 7460, are assumed to represent the effective wave lengths in which the photometric observations were made.

TABLE 13

NIGHT-TO-NIGHT CORRECTIONS

JD 2430000+	Correction (Mag.)	JD 2430000+	Correction (Mag.)	JD 2430000+	Correction (Mag.)
1947	0.000	2288	+0.007	2381	+0.007
1999	+ .004	2294	+ .005	2410	+ .023
2028	.000	2312	− .007	2416	+ .023
2034	.000	2323	+ .002	2653	− .018
2069	.000	2329	.000	2676	− .006
2080	− .005	2346	− .005	2757	− .010
2236	− .020	2358	+ .003	2792	−0.006
2277	−0.002	2364	+0.010		

Owing to the long period of α Coronae Borealis, only the minima were covered with overlapping observations. These were used to derive the night-to-night systematic corrections tabulated in Table 13. We believe that these corrections represent real variations in the light of α or γ Coronae Borealis or both, although the corrections on JD 2432653 and later may contain a systematic effect due to rehousing of the photocell.

Table 14 contains the original observations, corrected for differential extinction, in a con-

TABLE 14

OBSERVATIONS DURING MINIMA

Heliocentric JD 2430000+	Helioc. Phase (Days)	Δm $(a-\gamma)$ (Mag.)	Heliocentric JD 2430000+	Helioc. Phase (Days)	Δm $(a-\gamma)$ (Mag.)
1947.774	− 0.108	−0.352	2277.801	+ 0.080	−0.363
.791	− 0.091	− .350	.811	+ 0.090	− .344
.809	− 0.073	− .356	.821	+ 0.100	− .347
.831	− 0.051	− .354	.832	+ 0.111	− .340
.857	− 0.025	− .359	.843	+ 0.122	− .362
1999.706	− 0.256	− .441	.853	+ 0.132	− .374
.720	− 0.242	− .438	.866	+ 0.145	− .363
.735	− 0.227	− .433	.875	+ 0.154	− .376
.751	− 0.211	− .417	.885	+ 0.164	− .386
.777	− 0.185	− .399	.895	+ 0.174	− .388
.793	− 0.169	− .395	.907	+ 0.186	− .393
.817	− 0.145	− .377	.916	+ 0.195	− .396
.832	− 0.130	− .361	.927	+ 0.206	− .411
.846	− 0.116	− .364	.937	+ 0.216	− .420
.865	− 0.097	− .356	.947	+ 0.226	− .420
.886	− 0.076	− .350	.957	+ 0.236	− .418
.898	− 0.064	− .366	.976	+ 0.255	− .436
2028.749	+11.427	− .431	2288.911	+11.190	− .462
.760	+11.438	− .425	.922	+11.201	− .460
.769	+11.447	− .430	.932	+11.211	− .457
.779	+11.457	− .446	.943	+11.222	− .460
.787	+11.465	− .436	.961	+11.240	− .460
2034.682	0.000	− .350	.972	+11.251	− .459
.694	+ 0.012	− .355	.983	+11.262	− .458
.705	+ 0.023	− .352	.995	+11.274	− .462
.714	+ 0.032	− .348	2289.006	+11.285	− .457
.725	+ 0.043	− .349	.016	+11.295	− .454
.737	+ 0.055	− .355	2294.794	− 0.287	− .453
.749	+ 0.067	− .350	.805	− 0.276	− .451
.763	+ 0.081	− .350	.815	− 0.266	− .454
.774	+ 0.092	− .354	.825	− 0.256	− .452
.786	+ 0.104	− .354	.835	− 0.246	− .446
.798	+ 0.116	− .351	.847	− 0.234	− .434
.809	+ 0.127	− .368	.857	− 0.224	− .431
2069.661	+ 0.259	− .445	.869	− 0.212	− .418
.671	+ 0.269	− .446	.880	− 0.201	− .408
.681	+ 0.279	− .439	.894	− 0.187	− .402
.691	+ 0.289	− .433	.906	− 0.175	− .392
2080.636	+11.234	− .439	.917	− 0.164	− .392
.648	+11.246	− .446	.932	− 0.149	− .377
.658	+11.256	− .446	.945	− 0.136	− .376
.664	+11.262	− .460	.956	− 0.125	− .359
2236.935	+11.294	− .421	.967	− 0.114	− .361
.948	+11.307	− .431	.977	− 0.104	− .356
.973	+11.332	− .415	.988	− 0.093	− .351
.991	+11.350	− .409	2295.001	− 0.080	− .359
2237.009	+11.368	− .404	.009	− 0.072	− .357
.044	+11.403	− .415	2312.731	+ 0.290	− .446
.054	+11.413	− .406	.743	+ 0.302	− .443
.064	+11.423	−0.411	.753	+ 0.312	−0.438

TABLE 14—*Continued*

Heliocentric JD 2430000+	Helioc. Phase (Days)	Δm (α−γ) (Mag.)
2312.764	+ 0.323	−0.444
.776	+ 0.335	− .448
.786	+ 0.345	− .446
.795	+ 0.354	− .446
.801	+ 0.360	− .437
2323.694	+11.253	− .455
.704	+11.263	− .454
.714	+11.273	− .459
.724	+11.283	− .453
.734	+11.293	− .461
.746	+11.305	− .459
.758	+11.317	− .434
.769	+11.328	− .432
.779	+11.338	− .437
.789	+11.348	− .433
.799	+11.358	− .428
.810	+11.369	− .432
.821	+11.380	− .437
.832	+11.391	− .429
.842	+11.401	− .431
.867	+11.426	− .427
2329.687	− 0.114	− .354
.698	− 0.103	− .349
.709	− 0.092	− .347
.718	− 0.083	− .350
.728	− 0.073	− .354
.740	− 0.061	− .352
.751	− 0.050	− .357
.760	− 0.041	− .340
.771	− 0.030	− .342
.780	− 0.021	− .351
.791	− 0.010	− .354
.801	0.000	− .351
.812	+ 0.011	− .358
.821	+ 0.020	− .356
.841	+ 0.040	− .350
.851	+ 0.050	− .355
.862	+ 0.061	− .356
.873	+ 0.072	− .350
.883	+ 0.082	− .357
.895	+ 0.094	− .358
.904	+ 0.103	− .361
.914	+ 0.113	− .361
.924	+ 0.123	− .357
.938	+ 0.137	− .376
.948	+ 0.147	− .372
.958	+ 0.157	− .374
.968	+ 0.167	− .387
2346.854	− 0.307	− .450
.865	− 0.296	−0.443
2346.875	− 0.286	−0.448
.886	− 0.275	− .442
.897	− 0.264	− .435
.906	− 0.255	− .427
.916	− 0.245	− .440
.925	− 0.236	− .432
.935	− 0.226	− .435
.945	− 0.216	− .409
2358.701	+11.540	− .428
.711	+11.550	− .431
.721	+11.560	− .438
.732	+11.571	− .436
.741	+11.580	− .435
.747	+11.586	− .431
.768	+11.607	− .450
.778	+11.617	− .452
.790	+11.629	− .457
.800	+11.639	− .455
.810	+11.649	− .457
.820	+11.659	− .451
.831	+11.670	− .458
.839	+11.678	− .456
2364.701	+ 0.180	− .405
.711	+ 0.180	− .412
.721	+ 0.200	− .415
.735	+ 0.214	− .426
.747	+ 0.226	− .435
.758	+ 0.237	− .441
.768	+ 0.247	− .444
.777	+ 0.256	− .453
.787	+ 0.266	− .450
.798	+ 0.277	− .450
.808	+ 0.287	− .463
.818	+ 0.297	− .463
.827	+ 0.306	− .463
.836	+ 0.315	− .467
.845	+ 0.324	− .466
2381.697	+ 0.184	− .404
.707	+ 0.174	− .394
.719	+ 0.162	− .393
.729	+ 0.152	− .382
.739	+ 0.142	− .378
.749	+ 0.132	− .368
.760	+ 0.121	− .363
.771	+ 0.110	− .364
.780	+ 0.101	− .360
.790	+ 0.091	− .359
.800	+ 0.081	− .358
.809	+ 0.072	− .355
.819	+ 0.062	−0.353

TABLE 14—*Continued*

Heliocentric JD 2430000+	Helioc. Phase (Days)	Δm $(\alpha-\gamma)$ (Mag.)	Heliocentric JD 2430000+	Helioc. Phase (Days)	Δm $(\alpha-\gamma)$ (Mag.)
2381.828	− 0.053	−0.357	2676.881	− 0.119	−0.355
.835	− 0.046	− .356	.891	− 0.109	− .347
.841	− 0.040	− .359	.900	− 0.100	− .348
2410.678	+11.437	− .443	.910	− 0.090	− .345
.688	+11.447	− .462	.919	− 0.081	− .334
.697	+11.456	− .450	.929	− 0.071	− .342
.707	+11.466	− .448	.939	− 0.061	− .334
.717	+11.476	− .451	.948	− 0.052	− .344
.725	+11.484	− .454	.959	− 0.041	− .347
.731	+11.490	− .458	.969	− 0.031	− .347
2416.671	+ 0.071	− .379	.978	− 0.022	− .344
.680	+ 0.080	− .392	.987	− 0.013	− .335
.690	+ 0.090	− .386	.994	− 0.006	− .342
.700	+ 0.100	− .386	2757.691	+11.252	− .444
.709	+ 0.109	− .382	.701	+11.262	− .441
.720	+ 0.120	− .380	.711	+11.272	− .439
.730	+ 0.130	− .387	.722	+11.283	− .437
.739	+ 0.139	− .384	.732	+11.293	− .438
.749	+ 0.149	− .396	.742	+11.303	− .437
2653.835	+11.555	− .416	.753	+11.314	− .430
.844	+11.564	− .417	.763	+11.324	− .433
.855	+11.575	− .423	.773	+11.334	− .425
.866	+11.586	− .421	.782	+11.343	− .425
.875	+11.595	− .427	.796	+11.357	− .421
.885	+11.605	− .428	.809	+11.370	− .426
.894	+11.614	− .428	2792.655	+11.496	− .424
.905	+11.625	− .433	.665	+11.506	− .422
.915	+11.635	− .427	.674	+11.515	− .419
.925	+11.645	− .430	.683	+11.524	− .427
.933	+11.653	− .428	.694	+11.535	− .426
.940	+11.660	− .430	.704	+11.545	− .431
2676.862	− 0.138	− .367	.714	+11.555	− .424
.871	− 0.129	−0.358	.724	+11.565	−0.424

densed form: each tabular entry is the mean of three consecutive observations. The night-to-night corrections of Table 13 have *not* been included. Because of the slow variation in the light of α Coronae Borealis, we feel the condensed presentation of the data does not reduce its value. The heliocentric phase, given in the second column, was computed according to the ephemeris:

$$t_1 = \text{JD } 2423163.770 + 17^{\text{d}}.359907E\,.$$

The last column contains the difference in magnitude between γ Coronae Borealis and α Coronae Borealis plus neutral filter in the sense $(\alpha - \gamma)$.

The present investigation has yielded a more precise determination of the period than the 17.360-day period found by Stebbins, and the revised period represents his observations as well as ours. The observations during minima were assembled according to phase and were grouped into normal points of ten observations each. The primary normals were reflected to test for asymmetry, while those of the secondary minimum were reflected to find the center of the secondary eclipse. Since no asymmetry was apparent in the primary minimum, the observations were reflected about the centers of the respective minima and were re-formed into normal points of thirty observations each for the primary, and fifteen each for the secondary, minimum. These normal points, converted into light-units, are given in Tables 2 and 4.

ROTATIONAL-VELOCITY WEIGHTING FACTORS

The rotational-velocity weighting factors for the reanalysis of McLaughlin's spectrographic observations of rotational velocity were computed from the physical elements given in the body of this paper, and the results are given in Table 15. The first column contains the phase of McLaughlin's velocity observations; the second column gives the observed velocities with a systematic correction of +3.1 km/sec. This correction reduces the tendency of McLaughlin's values to be negative, caused partly by the small shift in the zero phase of the primary minimum, which was already appreciable in 1929. The third column contains the rotational weighting factor computed by Kopal's method, and the fourth column contains the observational weight assigned by McLaughlin. The fifth column gives a weight assigned by us on the basis of an estimated determinacy of the rotational velocity to be derived from the point. In effect, all points with weighting factors less than 0.02 were discarded. The final column contains the product weight times rotational velocity for each significant point. The sum of this column is equal to 12,103; dividing this number by the sum of the multiplied weights, $\Sigma w_1 w_2 = 64$, we find a value of the mean equatorial velocity equal to 190 km/sec.

TABLE 15

ROTATIONAL-VELOCITY WEIGHTING FACTORS

Phase (Day)	Velocity (Km/Sec)	F	w_1	w_2	(Vel/F)× w_1w_2
−0.241	0.0	0.008	5	0	....
− .216	+ 0.8	.023	7.5	1	263
− .188	+ 4.3	.036	4.5	1	540
− .058	+ 6.6	.026	6	1	1500
− .028	+ 5.5	.013	5.5	0	....
+ .001	− 3.8	.000	6	0	....
+ .042	− 2.3	.018	7	0	....
+ .074	− 6.2	.032	10	1	1930
+ .096	−10.4	.043	10	1	2400
+ .117	− 9.1	.047	9	1	1740
+ .136	−12.1	.047	8	1	2060
+ .160	− 8.5	.046	9	1	1670
+0.191	− 3.7	0.035	8.5	0	....

STELLAR SPECTRA AND COLORS IN AN IRREGULAR REGION IN CYGNUS

PAUL R. ANNEAR
Burrell Observatory, Baldwin-Wallace College, Berea, Ohio

Received January 6, 1953; revised February 26, 1953

ABSTRACT

Observations of spectra and photographic magnitudes are given for nearly all stars brighter than photographic magnitude 12.0 within a circular field in Cygnus 4°1 in diameter (excluding some stars in an overlapping region previously published). Red color indices are also presented for 557 of the 1019 stars.

This is part of a Warner and Swasey Observatory program instituted primarily for study of the fluctuations in the stellar luminosity function near the galactic plane. A description of the objectives of this study, with the co-ordinates of the centers of the fields investigated, has been published by McCuskey and Seyfert.[1] The observational material here presented is in the same form as in other similar papers of this series, the first of which was published by McCuskey.[2] The region under consideration here is the one designated as "LF3a" and has co-ordinates of center as follows: R.A. = 20^h04^m; Decl. = +35°4 (1950); or $l = 40°$, $b = +1°$. The manner in which it overlaps LF3 and LF3b has been shown in a published analysis of the latter field by Nassau and MacRae;[3] the reasons for subjecting this interesting region to special study are explained there also. Since the observational material for LF3b has been published by the same authors,[4] those stars in the overlapping region have been omitted from this paper. There are then 1019 stars remaining in the area, which was originally circular, with a diameter of 4°1.

The catalogue (Table 1) follows the pattern previously established, as follows:

The first column shows a number system similar to that in the *BD* catalogue; the numbers refer to the charts which follow this catalogue. Zone boundaries are approximate and are for the epoch of 1950. An asterisk following the number indicates that the star is listed in the *BD* catalogue. The letter "R" indicates that there are some remarks (at the end of this catalogue) concerning the star. A few remarks refer to stars in the overlapping region previously published.[4]

The second column gives the photographic magnitude. The magnitudes of the 25 sequence stars were determined by comparison with the North Polar Sequence and Harvard Region C 10;[5] five double-exposure plates were used for this purpose. These sequence stars were then compared with the 1019 field stars by means of a graduated scale of images. Three plates were used for the field stars, and the probable error of a mean magnitude is ±0.06. Except for a few stars which are either very bright or have overlapping spectra, the catalogue is complete to photographic magnitude 12.0, with a few additional stars somewhat fainter.

The third column gives the red color index. Red magnitudes were determined for all stars of type O through A0 and for a few stars of later type. The red magnitudes were obtained from 103*a*-E plates with a No. 22 Wratten filter in much the same manner as the photographic magnitudes. Five double-exposure plates were used for the same 25 sequence stars. Red magnitudes of the North Polar Sequence stars as determined by Nassau and Burger,[6] and red magnitudes established by the same authors for stars in

---

[1] *Ap. J.*, **106**, 1, 1947.

[2] *Ap. J.*, **109**, 426, 1949.

[3] *Ap. J.*, **110**, 40, 1949.

[4] *Ibid.*, p. 478.

[5] *Harvard Bull.*, No. 781, 1922.

[6] *Ap. J.*, **103**, 25, 1946.

Table 1

Observational Data for Region LF3a

Zone +33°

No.	mpg	R. I.	Sp.	No.	mpg	R. I.	Sp.	No.	mpg	R. I.	Sp.
1*	8.83	- .53	B8	51*R	8.98	- .52	B8	101*	10.85	+ 1.91	K3III
2	11.90	. . . .	A3:	52	11.61	. . . .	F8V	102	11.50	- .50	B8
3	11.62	. . . .	A2:	53	11.89	+ 1.76	K0Vp	103*	10.56	. . . .	F0V
4*	10.21	. . . .	G0V	54	11.88	. . . .	G0:	104	11.81	. . . .	F8V
5	11.24	+ .07	A0	55	11.77	+ .17	B8	105*	10.25	. . . .	G8III
6	11.94	. . . .	G0V	56	12.08	+ .22	B9	106	11.42	. . . .	G0:
7	11.36	- .24	B9	57	11.14	+ .02	A0	107	11.19	. . . .	G5IV
8*	9.92	. . . .	F8V	58	12.09	- .02	A0	108*	10.23	. . . .	F5V
9	11.00	- .23	A0:	59*	9.35	- .47	B8	109*	9.53	+ .21	B9
10	10.81	. . . .	A2	60*	10.32	- .02	B2	110	11.20	+ .42	B9
11	11.36	- .06	B9	61	11.48	. . . .	F8V	111	10.66	. . . .	F2V
12*	10.67	+ 1.07	G8IV	62	11.97	. . . .	F8	112	11.77	+ .38	G2V
13	11.80	. . . .	B8:	63*	7.98	. . . .	G5III	113	11.15	+ .20	B5
14*	9.67	+ 2.07	M5III	64*R	. . . .	. . . .	. . .	114	11.51	. . . .	F8III
15	10.85	. . . .	A5	65*R	10.39	+ .09	B2	115*	9.69	+ .52	G0V
16*	11.60	. . . .	K2III	66*	11.23	+ 2.51	M0III	116	10.00	. . . .	G2V
17	11.06	. . . .	A2	67*	10.13	- .34	B9	117	11.71	. . . .	A2
18	10.25	- .29	B9	68*	10.81	. . . .	G2IV	118*	9.21	- .06	A2
19	11.72	- .27	A0	69*	9.76	- .54	B9	119	10.21	. . . .	A5
20	12.06	. . . .	G0:	70	11.99	. . . .	A2:	120	11.21	. . . .	F8V
21	11.36	. . . .	G0V	71	11.48	- .06	B9	121	10.52	. . . .	G2V
22*	10.96	. . . .	G5IV	72*	9.82	. . . .	A2	122*	10.92	. . . .	F5V
23	10.86	- .09	B9	73	11.74	+ .04	A0	123*	10.51	. . . .	K2III
24	11.15	- .21	B9	74	11.88	. . . .	G8III	124*	10.14	- .16	A0
25*	10.57	+ 2.15	K5III	75*	10.31	- .16	B9	125*	10.81	. . . .	A3
26	10.90	. . . .	F5V	76	11.94	. . . .	A2:	126*	10.14	. . . .	G8III
27	11.51	- .30	B8	77	11.76	. . . .	G8V	127*	10.85	. . . .	A2
28*	10.06	. . . .	K0III	78*	10.36	- .11	B2	128*	9.47	- .16	B9
29*	10.99	. . . .	G0V	79*	10.48	- .17	B9	129*	10.13	- .17	B9
30*	10.34	. . . .	F8Ib	80	11.29	- .07	B8	130	12.00	. . . .	A3
31	. . . .	. . . .	F8:	81	10.89	. . . .	F5V	131	11.82	. . . .	A3
32*	10.57	- .23	A2	82*	10.44	. . . .	F8IV	132	11.01	. . . .	A2
33	12.10	+ .19	B9	83*	9.64	. . . .	A2	133*	8.88	. . . .	K0III
34*	8.91	+ .26	A3	84*	8.35	- .59	B9	134*	7.62	- .38	B5
35*	10.49	+ .37	F8V	85	11.07	- .23	B9	135	11.92	+ .11	A0
36*	8.91	- .61	B8	86*	11.11	+ 1.45	K0III	136	11.65	. . . .	G8III
37*R	10.43	. . . .	G5:	87	11.27	. . . .	F5V	137*	8.41	+ 1.61	K5III
38*	9.86	- .03	A0	88*	10.35	. . . .	G8III	138	10.75	. . . .	A3
39	12.02	+ .21	A0	89	10.78	+ .06	A0	139	11.08	. . . .	A3
40	11.93	. . . .	G5:	90	11.31	. . . .	G0V	140*	9.83	- .29	B9
41	11.22	- .09	A0	91*	10.19	. . . .	A3	141*	9.72	. . . .	A2
42	12.04	- .12	B9:	92*	10.57	- .21	B8	142	10.39	. . . .	K0V
43	11.67	. . . .	A2:	93*	9.59	+ .29	F5V	143*	11.01	. . . .	A2
44	10.86	. . . .	F5V	94	11.15	- .14	B9	144*	9.91	+ .05	B5
45	10.91	. . . .	A3	95*	10.72	. . . .	F2V	145*	9.97	- .30	B9
46	12.02	. . . .	G0	96	11.88	+ .12	B9	146*	10.28	- .17	B9
47*	10.48	. . . .	K0III	97*	11.01	. . . .	G5IV	147	11.56	- .04	A0
48*	8.39	- .33	B2	98	11.03	. . . .	A5	148*	10.09	- .14	A0
49	11.51	. . . .	F5V	99	9.66	- .18	B9	149*	9.07	- .30	B9
50	11.16	- .07	B9	100*	8.15	- .33	B8	150*R	7.80	+ .05	A0

Table 1

Observational Data for Region LF3a

Zone +33° (Cont'd.)

No.	m_{pg}	R. I.	Sp.
151*	8.96	- .36	B9
152*	7.45	- .19	B5
153*R	7.95	- .31	B9
154	10.50	+ .03	B9
155*	9.08	- .41	B9
156	11.23	. . . .	A3
157*	10.68	. . . .	G8III
158*	10.48	. . . .	G8IV
159*	9.99	. . . .	F5V
160	11.87	. . . .	G0
161	11.95	. . . .	A2
162*	8.03	+ .53	F8V
163	11.65	. . . .	G5III
164	10.97	. . . .	F2V
165*	11.42	. . . .	K3III
166*	10.03	. . . .	K0III
167	11.35	. . . .	A3
168	11.38	. . . .	A5

Zone +34°

No.	m_{pg}	R. I.	Sp.
1*R	10.96	. . . .	A2
2*	10.33	. . . .	A2
3	11.57	. . . .	F2:
4*	10.29	. . . .	G8III
5*	10.74	+ 2.26	K3III
6*	7.51	- .45	B9
7	10.86	- .20	B9
8	11.41	. . . .	A5
9*	8.10	- .48	B8
10	11.90	. . . .	G0
11	11.18	. . . .	G8III
12	11.98	. . . .	A3
13	11.38	. . . .	F0V
14*	10.46	. . . .	G2V
15	11.90	. . . .	A2:
16*	8.75	- .40	B9
17	11.49	. . . .	A2
18	11.53	. . . .	A2
19	11.37	. . . .	A5
20	11.29	. . . .	F5
21*	9.74	. . . .	A2
22	10.75	. . . .	F5
23	10.77	+ .83	G5V
24*	10.02	. . . .	G8III
25	11.27	+ .42	F2
26	11.78	. . . .	A2
27	12.03	. . . .	A2
28	11.41	. . . .	K2V
29*	11.75	+ 1.31	G5III
30*	9.48	. . . .	K2III

No.	m_{pg}	R. I.	Sp.
31	11.67	. . . .	A5:
32	11.37	. . . .	A3:
33*	11.60	+ 1.04	G5V
34	11.98	+ .28	B9
35	11.37	- .05	A0
36*	10.65	. . . .	F8V
37*R	9.00	- .36	B9
38	12.10	+ .26	A0
39	10.49	+ .02	A0
40*	10.61	. . . .	G0V
41	11.57	+ 1.44	G8III
42	12.06	. . . .	F8:
43	11.32	. . . .	A3
44*	8.01	- .41	B5
45	10.70	- .25	B9
46	11.01	+ .11	A0
47	10.73	. . . .	G2IV
48	10.70	. . . .	F2V
49	12.02	. . . .	G0V
50	10.85	- .15	A0
51*	10.38	. . . .	G0IV
52*	9.88	+ .25	F5V
53	12.02	. . . .	G2:
54	12.03	. . . .	F5:
55	11.24	. . . .	F8V
56	12.02	+ .21	A0
57*	10.34	- .13	B9
58*	10.00	. . . .	K0III
59*	10.31	. . . .	A3
60	11.64	. . . .	K2III
61	10.77	+ .23	A0
62*	9.65	. . . .	G8III
63	11.85	. . . .	A2
64*	8.50	- .20	B9
65*	9.97	. . . .	A2
66	11.76	. . . .	F5V
67*	10.15	- .21	B9
68	11.52	. . . .	G8V
69	11.96	. . . .	G5
70*	9.91	. . . .	A3
71	11.27	+ .10	B9
72	12.00	. . . .	A3
73	11.70	+ 1.52	G5IV
74*	10.09	. . . .	K2III
75*	9.87	+ .21	A0
76	11.73	. . . .	G5III
77*	9.17	- .35	B8
78	11.01	. . . .	K2III
79	11.97	. . . .	A2
80	11.95	. . . .	G5III

No.	m_{pg}	R. I.	Sp.
81	12.10	. . . .	A2:
82*	9.87	. . . .	G2IV
83*	10.34	- .02	A0
84	11.85	+ .79	A0
85*	10.94	. . . .	F8V
86*	11.26	. . . .	G2IV
87*	10.58	. . . .	A3
88	11.38	. . . .	F5V
89	11.23	- .06	A0
90	11.02	- .10	B8
91	11.39	. . . .	A2:
92*	10.72	. . . .	G8IV
93*	10.90	. . . .	G5IV
94*	8.39	- .03	A0
95*	9.83	. . . .	F8V
96*	10.54	. . . .	G8III
97*	10.37	. . . .	G8III
98*	10.66	- .29	B9
99	11.61	- .04	A0
100	11.71	- .05	B9
101*	8.59	. . . .	G8III
102	11.20	- .03	A0
103	11.05	. . . .	F8V
104*	9.67	- .29	B9
105	11.41	. . . .	G8III
106*	9.62	- .28	B9
107	11.24	- .06	B9
108	11.53	. . . .	G8III
109	12.10	- .01	B9
110	10.92	- .07	A0
111	12.02	. . . .	F5
112	11.14	+ .08	A0
113*	9.78	. . . .	K2III
114	11.70	+ 1.00	K0V
115	10.37	- .10	B8
116	11.22	+ .16	B8
117	11.88	- .06	B9:
118	11.88	. . . .	A5:
119	11.22	- .26	A0
120*	10.29	- .18	B5
121	11.71	. . . .	F8V
122	11.29	. . . .	G8IV
123	11.15	- .19	A0
124	10.83	. . . .	A3:
125	11.71	- .15	A0
126	11.61	+ 1.08	G5IV
127	11.92	. . . .	A3:
128	12.04	. . . .	G8V
129	11.38	. . . .	F5V
130	11.76	. . . .	F0V

Table 1

Observational Data for Region LF3a

Zone +34° (Cont'd.)

No.	m_{pg}	R. I.	Sp.	No.	m_{pg}	R. I.	Sp.	No.	m_{pg}	R. I.	Sp.
131	11.79	....	F8V	181	11.71	....	F8IV	231	11.71	+ 1.43	G5III
132*	8.08	- .30	A0	182	11.49	....	A3	232	11.83	....	A2
133	11.70	+ .10	B8	183	11.12	....	A2	233*	9.14	- .51	B8
134	11.98	+ .34	B9	184	10.88	....	A2	234	11.91	....	G0V
135	11.88	+ .07	A0	185	10.82	- .13	B9	235	12.02	....	F5
136*	9.42	....	A2	186	11.27	- .37	B9	236	11.91	+ .21	B9
137*	8.70	+ .83	F2V	187	10.92	....	G0V	237	11.59	- .04	A0
138	10.90	- .16	B9	188	11.20	....	F8V	238*	10.72	+ .47	B5
139*	10.09	....	F0V	189	10.98	....	K0III	239	11.91	....	G8III
140*	10.00	- .36	B5	190	11.83	+ .13	A0	240	12.06	+ .20	F5
141*	9.89	....	K0III	191	10.56	....	A3	241*	10.75	- .09	B9
142	11.43	....	A5	192*	9.59	+ .33	B2	242	11.96	+ .31	F2
143*	9.79	+ .30	F8V	193	12.04	- .22	A0	243	11.95	....	F5
144	11.16	....	F5V	194*	10.17	....	G2V	244*	10.93	- .08	B9
145	11.74	....	B8:	195	11.44	....	A2	245	11.23	- .19	B9
146	11.33	- .32	B8	196	9.88	- .36	B5	246	11.81	+ 1.45	G5III
147	11.33	- .37	A0	197	11.50	....	F8IV	247*	11.16	....	K0III
148	10.52	- .27	A0	198	10.86	+ .14	B9	248*R	9.64	....	G8IV
149	10.83	....	G0V	199	11.33	- .31	B9	249	11.71	....	A2
150	11.27	+ .04	B9	200	10.80	....	G0V	250*R	7.44	+ .11	A3
151	11.60	+ .11	A0:	201*	11.61	+ 2.40	K3III	251	10.98	....	A3
152	10.82	+ .22	B5	202	12.10	- .06	B9	252*	9.60	- .24	B9
153	11.77	....	K0III	203	11.28	....	G8V	253*	9.19	- .43	B9
154	12.02	+ .16	B8	204	11.50	- .04	A0	254	11.92	....	A3
155	10.59	- .25	B8	205*	9.34	+ 1.44	K2III	255*	9.29	....	K2III
156*	8.69	+ 1.08	G8III	206	11.70	- .11	A0	256	11.38	....	F2V
157	11.39	....	K2III	207*	10.95	....	F8:	257	11.98	....	G0
158	10.57	....	A2	208	11.16	....	K0III	258	11.32	....	G0V
159*R	8.71	+ .23	0B	209	11.01	+ .06	B9	259	12.00	....	F5
160*	8.64	+ .57	G0IV	210*	10.13	....	F0V	260*	9.86	....	K2III
161	10.41	+ .05	A0	211	11.23	....	A3	261	12.07	+ .47	A0
162	11.38	....	K0III	212*	10.45	....	G0V	262*	10.71	....	G8III
163*	10.68	- .28	B8	213	10.89	- .12	B2	263	10.81	- .19	A0
164	11.00	....	A3	214	12.02	- .08	A0	264	11.35	....	F2V
165	11.09	- .21	B8	215	11.44	+ .38	B9	265*	10.08	+ .24	B2
166	11.48	....	F8V	216	11.32	- .10	B5	266*R	8.67	+ .09	B9
167	11.05	+ .21	F5V	217*	9.73	....	G2IV	267*	10.90	....	G5V
168	11.16	....	F8V	218	11.51	....	F8III	268	9.56	....	K5III
169	11.09	....	A2	219	11.82	....	G8III	269*	8.24	- .18	B9
170*	8.36	+ .14	F0V	220	12.02	+ .37	A0	270*	9.15	- .11	B9
171	11.98	+ .22	A0	221	11.44	....	G0V	271	11.70	....	A3
172	11.26	+ .14	B9	222	10.30	....	G0V	272*	8.73	+ .31	0B
173*	....	....	0B	223*	10.89	+ 1.44	G8IV	273	10.93	+ .28	B8
174*	7.83	- .55	B5	224*R	8.21	....	G2V	274*	9.37	+ .54	G0V
175	11.23	....	G2III	225	11.48	....	A2	275	11.98	....	G5
176	10.93	- .02	B5	226*	9.34	....	F8V	276*	10.29	+ .46	B2
177	11.25	- .05	B8	227*	10.45	....	G0V	277*	10.18	....	K2IV
178	11.29	....	G0IV	228*	9.98	....	A3	278*	8.87	....	K0III
179	11.93	+ .39	B9	229	11.29	....	G0V	279	11.28	- .02	A0
180	11.15	....	F8V	230	11.78	+ .08	A0	280	12.07	....	K0:

Table 1

Observational Data for Region LF3a

Zone +34° (Cont'd.)

No.	m_{pg}	R. I.	Sp.
281	11.63	+ .57	B9
282	10.75	+ .33	B5
283	10.63	....	A5
284	11.80	+ .91	B9
285*	10.85	....	G8V
286	11.44	+ .88	G5V
287*	10.71	....	G5IV
288	11.38	....	A3
289	11.34	....	G8III
290*	8.90	....	G8III
291*	8.83	- .27	B8
292*	10.46	+ .10	A0
293	11.74	+ .42	B2
294	11.83	....	G5
295*	10.98	+ .98	G5V
296	10.95	....	A5
297	12.00	+ .40	B8
298*	9.86	....	K5III
299	12.03	....	G0:
300*R	....	....	A0
301	11.98	+ .38	B9
302	11.83	....	G0
303	11.61	+ .01	B5
304	10.53	+ .56	B2
305	11.87	+ .27	B5
306	11.70	....	G0
307*	10.20	+ .49	F5V
308*	10.01	- .29	B9
309*	10.29	- .07	B9
310*	11.55	....	K0III
311	10.86	....	G0V
312	11.83	....	G5
313*	10.11	+ .80	F5V
314	11.71	+ .65	B9
315*	9.85	+ .63	F5V
316*	9.74	....	G8IV

Zone +35°

No.	m_{pg}	R. I.	Sp.
1	10.79	- .21	B5
2	11.80	....	F2
3	10.86	+ .44	F8V
4*	11.66	....	G5III
5*	8.96	- .49	B8
6	11.51	+ .39	A0
7*	10.91	+ .21	A3
8	10.49	+ .13	A0
9*	9.56	- .28	A0
10	10.62	+ .02	B9
11	11.89	....	G5:
12	10.74	+ .27	B9
13*	11.23	....	G0V
14*	10.86	....	K0III
15*	10.33	+ 1.91	K0III
16	11.97	....	A2
17*	7.10	- .03	B9
18	11.98	- .13	B8
19*	10.24	- .18	B9
20	11.42	....	F0:
21*R	10.98	....	A2:
22*	10.29	- .07	B9
23	12.04	+ .34	B8
24*R	7.88	- .08	B9
25	11.71	+ .29	G0V
26*	9.11	- .25	B2
27	11.57	....	A2
28*	9.86	....	A3m
29*R	9.02:	....	K0III
30*	9.56	....	A2
31	11.84	- .16	A0
32*R	10.81	....	F8V
33	10.52	....	F2V
34*	9.66	....	A2
35	11.55	....	F8V
36	12.00	....	A2:
37	11.10	....	F0V
38	10.84	....	A5
39*	9.34	+ .20	0B
40*	9.52	+ 2.54	K5III
41	11.61	....	A5
42	10.51	....	A2
43	10.99	....	A2
44	11.40	....	F5V
45	11.08	....	F8V
46	11.84	- .10	A0
47	11.04	....	A3
48*	10.53	- .07	A0
49*	9.39	....	K2III
50*	11.03	....	G8IV
51*	10.17	- .19	B9
52	11.53	- .07	B8
53	11.22	....	A2
54*	10.49	+ .13	B9
55	11.17	- .19	A0
56	11.56	....	F8V
57*	11.27	....	K0III
58	11.34	....	A2:
59	10.75	....	A3
60	11.88	....	F8V
61*	10.42	+ .24	B2
62	11.51	+ .22	A0
63*	10.92	....	0B
64	11.96	....	A3
65*	11.30	....	G8III
66	12.06	....	F5:
67*	11.12	....	G5IV
68*R	10.96	+ .18	A0
69*	10.86	+ 1.71	K0III
70	11.40	....	G0V
71*	9.34	....	G8III
72*	7.45	- .15	B8
73*	9.94	....	G0IV
74*	10.87	....	K0III
75*	10.44	+ .72	0B
76	11.44	+ .44	A0:
77	11.23	+ .17	B9
78*R	9.58:	+ .43	B5
79	11.07	+ .60	B5
80*	11.44	....	F8III
81	11.60	....	K5III
82*	10.15	....	G0IV
83	11.10	....	G0V
84	11.19	....	A5
85	11.29	+ .17	A0
86	11.71	+ .01	A0:
87	11.47	....	...
88	11.05	....	A2
89	10.54	+ .12	A0
90	11.49	....	F8V
91*	11.06	....	K0III
92*	10.13	- .29	B9
93	11.79	....	F8
94	10.85	- .16	B5
95	11.15	....	F2V
96*	10.83	+ .41	A0
97*	9.73	- .05	B2
98*R	....	....	0B
99	11.19	+ .72	B2
100	11.32	+ .31	B5:
101	11.94	....	G0
102	11.78	+ .04	B9
103	11.14	+ .02	B9
104	11.73	+ 1.24	G5
105*	9.56	+ .26	B2
106*	9.38	+ .18	A2
107*R	11.05	....	F2Vp
108	12.03	....	F8
109	11.00	+ .28	B8
110	11.94	+ .29	B2

Table 1

Observational Data for Region LF3a

Zone +35° (Cont'd.)

No.	m_{pg}	R. I.	Sp.
111*	9.82	. . . .	A3
112	11.33	. . . .	G0V
113	11.69	. . . .	F2V
114	10.71	- .23	B9
115*	9.88	- .21	B8
116	11.79	. . . .	F8:
117	12.10	. . . .	G2
118	11.28	- .02	B9
119	11.92	. . . .	G8
120	11.60	. . . .	F2V
121	12.02	+ .62	B8:
122	12.01	. . . .	A5
123*	9.24	. . . .	A2
124	10.82	. . . .	F8IV
125	11.21	- .09	B8
126*	10.42	. . . .	G0V
127	11.21	. . . .	A5
128	11.66	+ .06	B9
129*R	10.57	- .03	B5
130	11.39	. . . .	G0V
131*	10.67	. . . .	A3
132*	10.83	. . . .	A2
133*	10.15	+ 2.19	K2III
134	12.05	+ .06	B8:
135	11.33	- .15	B5
136	10.96	+ .01	B2
137	11.03	. . . .	A2
138	10.93	- .13	B5
139*	9.69	+ .03	B5
140	10.92	+ .14	B2
141	11.84	+ .42	B8
142*	8.97	- .07	B2
143*R	7.79	+ .04	0B
144	10.93	- .13	B5
145	11.53	- .11	B5
146	11.70	. . . .	F8
147*R	8.88	+ .35	0B
148	11.88	- .11	B5:
149	10.79	. . . .	A5
150	10.41	+ .05	B2
151*	10.10	. . . .	. . .
152*	7.34	+ .04	0B
153*R	. . . .	. . . .	0B
154*R	7.52	+ .04	. . .
155*R	9.01	. . . .	0B
156*R	8.26	- .27	0B
157	11.03	- .03	B8
158	10.25	+ .30	B2
159	11.99	+ .18	B9:
160	11.43	. . . .	F0V
161	11.00	+ .16	B5:
162*	10.36	- .06	B9
163	11.07	- .05	B5
164	11.33	+ .66	G0V
165	11.10	+ .04	B9
166	11.44	. . . .	G0V
167*	8.23	+ .31	0B
168*	10.04	. . . .	K0:III:
169	10.87	+ .03	B2
170*	10.65	. . . .	G0V
171	11.20	. . . .	A3:
172	11.65	+ .28	B9:
173	11.14	- .22	B9
174	10.99	- .07	B8
175	11.61	+ .01	B9:
176	10.31	- .16	B0
177*	. . . .	. . . .	G8IV
178*R	9.58	- .35	B2
179	11.10	. . . .	G0V
180*	10.19	. . . .	G8III
181*	10.36	+ .22	A5p
182	10.73	+ .05	A0
183*	8.27	- .02	B2
184	11.40	. . . .	F8V
185*	8.86	. . . .	A2
186	10.61	+ .60	G0V
187	11.81	+ .27	B8:
188	11.26	. . . .	F2V
189	11.16	- .38	B5
190*	9.56	- .28	B2
191	10.61	- .23	B8
192	11.27	- .31	B9
193	10.37	+ .01	B2
194	11.44	- .10	B5:
195	11.55	- .26	B5
196*	10.45	- .02	B5
197*	9.18	- .22	B9
198	11.29	- .01	A0
199*R	8.53	- .46	B2
200	10.00	- .13	B2
201	10.69	- .26	B5
202*R	7.15	+ .03	0B
203	11.29	+ .23	B9:
204	10.61	- .09	B5
205	11.78	+ .24	B8
206*	9.44	+ 1.50	K2III
207*	9.29	- .30	B9
208*	9.43	- .35	B8
209	11.50	. . . .	F0V
210	10.96	. . . .	F8V
211	10.99	. . . .	F2V
212	11.16	+ .04	B8
213	10.71	- .07	B2
214	10.52	.00	B2
215	11.83	. . . .	F8
216	11.28	- .01	A0
217	11.50	+ .02	B8
218*	9.24	- .14	A0
219	11.40	- .14	B9
220	11.04	- .19	A2
221	11.29	. . . .	A2
222*	10.47	+ .05	B9
223	11.95	. . . .	A3
224	11.45	. . . .	G2V
225*	9.49	- .25	B5
226	11.80	+ .26	B9
227	11.16	+ .21	B8
228*	11.08	. . . .	A3
229*R	8.70	. . . .	0B
230	11.67	. . . .	G0III
231	10.26	- .05	B2
232	11.88	+ .25	G0
233	10.39	- .08	B2
234	10.94	+ .07	A2
235*	8.73	+ 1.97	M2III
236	11.26	+ .08	A0
237	11.57	+ .03	B5:
238	11.30	+ .70	A5:
239	10.75	. . . .	B2:
240*R	8.22	- .29	B2
241*	8.69	- .41	B9
242*	9.33	- .19	B8
243	11.91	+ .15	A0
244	10.89	. . . .	F5V
245	11.16	+ .10	B5
246	11.30	. . . .	G0V
247	10.97	- .20	B0
248*	9.34	+ .15	A3
249	11.57	. . . .	F8IV
250	11.67	+ 1.31	G5III
251*	10.50	+ .25	B2
252*	9.64	- .26	B2
253*	9.44	- .22	B5
254*	. . . .	. . . .	B2
255*	10.23	. . . .	G0IV
256	11.16	+ .21	A0
257	11.64	.00	B2
258	11.85	+ .26	B9:
259	11.67	. . . .	G5
260*	10.01	.00	B2

Table 1

Observational Data for Region LF3a

Zone +35° (Cont'd.)

No.	m_{pg}	R. I.	Sp.	No.	m_{pg}	R. I.	Sp.	No.	m_{pg}	R. I.	Sp.
261*	7.86	+ .14	0B	311*R	10.29	....	A2	361	10.50	- .10	B9
262	11.33	+ .81	G5III	312	11.90	....	A2:	362*	10.88	....	K0IV
263*	10.58	+ .11	B2	313	11.07	+ .01	B2	363	11.02	+ .12	A0
264*	10.07	- .18	B2	314	11.33	....	A2	364	11.48	+ .42	B8
265*	11.23	....	G2V	315	10.95	....	F8III	365	10.44	....	A3
266	11.54	.00	B8	316	10.10	....	B8	366	11.33	+ .38	B5
267	10.66	+ .19	B9	317	11.02	....	A2	367	10.93	....	F0V
268	11.60	....	A3:	318	11.42	....	F8V	368*	10.44	....	G5:IV:p
269	10.71	- .19	B8	319*	9.56	- .09	B8	369*	10.36	+ .69	B5
270	11.26	- .10	B2	320*	9.60	+ .60	F8V	370	11.83	+ .23	B8
271	10.24	- .12	B2	321	11.91	+ .21	B9	371	11.77	+ 1.93	K0III
272*R	9.24	+ .09	0B	322	10.76	....	A3	372	11.35	+ .40	B5
273*	10.67	....	F8V	323	10.89	- .01	B9	373	11.23	+ .17	A0
274*	10.75	....	F5V	324	12.10	- .10	B8	374	12.10	- .17	B5
275	11.58	+ .52	B5	325*	11.04	+ .09	B2	375*R	7.95	....	F8V
276	11.00	....	F0V	326	11.35	+ .29	B5	376	10.89	+ .53	B2
277	11.12	....	F2V	327	11.71	+ .11	B9	377	11.44	+ .38	B8
278	12.00	- .16	A0	328*	10.76	- .14	B2	378*	9.04	- .17	B9
279	11.02	....	F8V	329	10.76	+ .04	B9	379	11.89	....	F8:
280*R	....	....	...	330	10.88	+ .46	F5V	380*	8.66	- .14	B8
281*	10.90	....	K0III	331	11.44	....	A2	381	11.33	....	F8V
282*	11.23	....	G2V	332	10.93	....	F0V	382*R	8.50	- .03	B9
283*R	8.67	+ .05	0B	333	10.33	- .03	B2	383	11.77	+ .54	B2
284*	10.76	- .08	B5	334R	11.58	+ .06	...	384*	10.06	....	G8III
285	10.55	- .35	B5	335*	9.80	- .16	B5	385	10.97	+ .02	B5
286	10.80	- .15	B5	336	11.67	....	F2V	386	11.23	....	F5V
287	12.05	- .11	B5	337*	8.61	....	K0III	387	11.49	+ .65	F5V
288	11.15	- .08	B5	338	11.84	....	F5	388	11.87	+ .70	B8
289*	11.16	....	G2V	339	11.20	+ .20	B5	389	11.40	+ .45	B5
290	11.91	+ .31	A2	340	11.38	....	A3	390*	10.16	- .20	B8
291*	7.64	- .28	B2	341*	11.04	....	K2III	391	12.02	....	G5:
292	11.20	+ .20	B8	342*	9.54	- .24	B9	392	11.55	+ .37	B5
293	11.45	- .09	B8	343	10.78	- .06	B9	393*	10.14	....	A5
294	11.84	....	K5III	344	11.98	....	G5:	394*	10.83	....	G0V
295	11.64	- .22	B5	345	10.84	....	A2	395	11.78	+ .18	B8
296*R	9.31	- .21	B5	346*	10.21	+ .91	B2	396	12.10	....	F8:
297*	9.88	- .32	B8	347*	9.84	- .36	B8	397	12.02	....	A2:
298	11.73	....	A3	348	12.02	....	K2	398*	9.62	+ .58	G0V
299	11.09	....	G0V	349	10.93	....	A5	399*	11.57	....	A2
300	10.72	+ .07	B5	350	11.30	- .06	B5	400	11.23	....	A2
301	10.86	- .11	B5	351	11.50	....	F5V	401	11.50	+ .14	B8
302*	9.76	+ .04	A0	352	11.43	....	F5	402	11.86	....	G5III
303	11.05	....	F8V	353*	8.04	+ 1.33	K0III	403*	8.56	+ .81:	G0V
304	11.91	- .03	B5	354	11.55	+ .43	A0	404	11.34	+ .34	A0
305	11.05	+ .21	B8	355*	10.23	....	A2	405*	9.14	- .07	B9
306	10.64	+ .14	B2	356	11.30	+ .35	B8	406	12.10	+ .78	G0V
307	11.05	+ .29	A0	357	10.48	....	K2III	407	11.23	+ .58	F8V
308	11.27	+ .21	B5	358	10.59	....	A3	408	11.23	+ .22	B8
309*	10.88	....	F5	359*	10.57	+ .21	B8	409	12.06	....	B9
310	10.89	....	A3	360	10.84	+ .37	B5	410	11.88	+ .28	B8

Table 1

Observational Data for Region LF3a

Zone +35° (Cont'd.)

No.	m_{pg}	R. I.	Sp.
411*	10.69	. . . .	G0V
412*	11.67	. . . .	K2III
413*	11.28	. . . .	K2III
414	11.83	+ 2.29	K2III
415*	9.82	. . . .	G0V
416	11.54	+ .69	G2V
417	11.15	+ .20	A0
418*	9.92	+ .14	A0
419*	7.06	- .12	B8

Zone +36°

No.	m_{pg}	R. I.	Sp.
1	11.29	. . . .	A3
2	11.55	. . . .	A3
3	11.95	+ .14	B9
4	11.68	- .08	B9
5	11.20	+ .14	B9
6	10.96	. . . .	F8V
7	11.16	+ .10	B2
8*	11.61	+ 2.62	K2III
9	11.73	. . . .	A2
10	11.16	+ .10	A0
11	11.80	- .01	B9
12	11.09	+ .09	B5
13*	10.94	- .01	B5
14*	8.83	+ .29	0B
15	11.85	- .03	B8
16	11.34	- .26	B5
17	11.20	. . . .	A5
18	11.45	. . . .	A2
19	10.90	. . . .	B5
20*	9.70	. . . .	A2
21*	11.20	. . . .	K5III
22*	9.11	+ .39	0B
23*	10.55	. . . .	K2III
24*	8.38	- .44	B8
25*	7.86	- .16	. . .
26*R	9.44	- .28	B9
27*	9.32	- .28	B8
28	10.84	- .22	B5
29	11.33	- .09	B2
30	11.13	+ .13	B9
31	11.13	+ .07	B8
32	11.37	- .11	B8
33	11.16	. . . .	F8V
34	12.05	- .17	B8
35	11.13	- .10	B9
36	11.90	- .20	B8
37	10.59	- .06	B8
38	11.02	- .04	B5
39	10.97	+ .02	B8
40	10.84	.00	B2
41*	10.21	- .04	B9
42*	10.59	+ .12	B9
43	11.20	+ .14	B5
44	11.08	+ .02	B9
45*	10.63	. . . .	K0III
46	11.05	- .07	B2
47	12.02	+ .16	A0
48	11.30	. . . .	F2V
49	11.05	. . . .	G5:III:
50	11.95	+ .09	B5:
51*	10.58	+ .11	B9
52	9.78	. . . .	G8III
53*	9.18	- .34	B2
54	11.91	+ .26	B5:
55	11.74	+ .14	B5
56	11.26	. . . .	A2
57	11.28	- .42	B2
58*	7.86	- .16	. . .
59*	10.13	+ .85	G8IV
60	10.81	+ .21	B8
61	11.91	. . . .	A2
62	10.85	+ .20	B9
63	11.51	- .09	B5
64	11.92	+ .09	B8
65	11.51	. . . .	F2
66	10.53	+ .06	B5
67	11.91	+ .26	B2
68	11.25	+ .07	B8
69*R	10.00	- .13	B2
70	11.50	+ .08	B5
71*	8.41	- .01	B9
72	11.23	. . . .	A2
73	10.89	. . . .	A2
74*	9.66	+ .16	B2
75	11.23	+ .17	B5
76	10.89	. . . .	A5
77	11.89	+ .81	B5
78	11.83	. . . .	A2
79	11.13	+ .07	A0
80*R	9.97	. . . .	A3
81	11.50	+ .44	B8
82	10.89	+ .42	B5
83*	8.57	. . . .	A2
84	11.38	. . . .	G5:
85	11.33	+ .49	F8V
86	10.93	+ .39	B5
87	11.54	- .06	B8
88	11.78	+ .13	B9
89*	10.79	+ .37	B5
90	11.60	. . . .	A2
91	12.03	+ .09	B8
92	11.88	. . . .	G8III
93	11.88	+ .34	A0
94*	9.49	. . . .	A3
95*	7.09	- .03	. . .
96	11.39	. . . .	A3
97*	8.45	. . . .	A2
98*R	8.99	+ .35	. . .
99	11.50	+ .49	F5V
100	11.35	+ .23	B2
101*	9.62:	+ .40:	B5:
102	11.25	. . . .	G0:
103*	. . . .	. . . .	A0
104	10.73	. . . .	A3
105	11.83	. . . .	F8:
106*	9.82	. . . .	K2III
107	11.37	. . . .	F5:V:
108	11.91	- .03	A0
109	10.85	+ .01	A0
110*	9.60	+ 2.33	K2III
111	11.98	+ .17	B8
112	11.09	+ .09	B9
113*	8.11	+ .21	. . .
114	10.54	+ .40	B2
115*	10.39	- .03	B9
116*	11.35	+ .34	B5

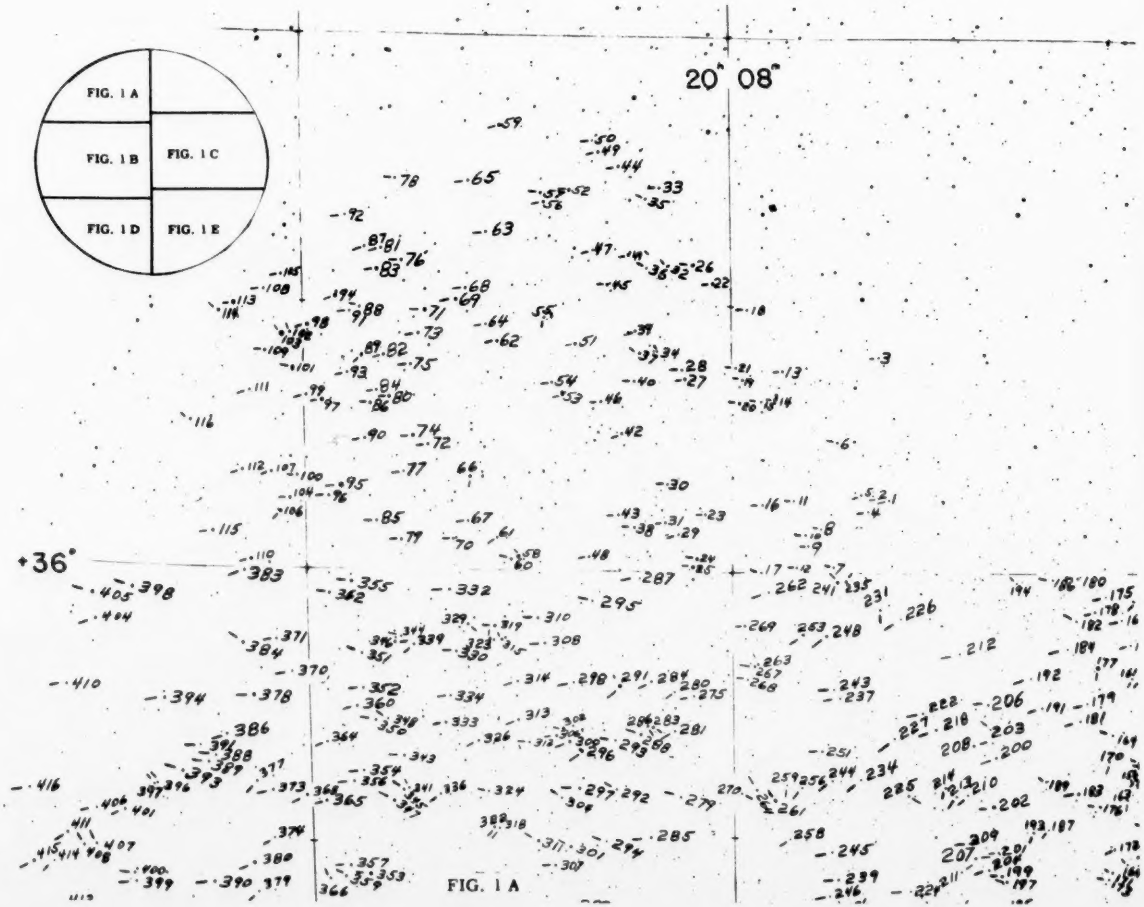
20h 08m
+36°
FIG. 1 A
FIG. 1 B
FIG. 1 C
FIG. 1 D
FIG. 1 E

FIG. 1 A

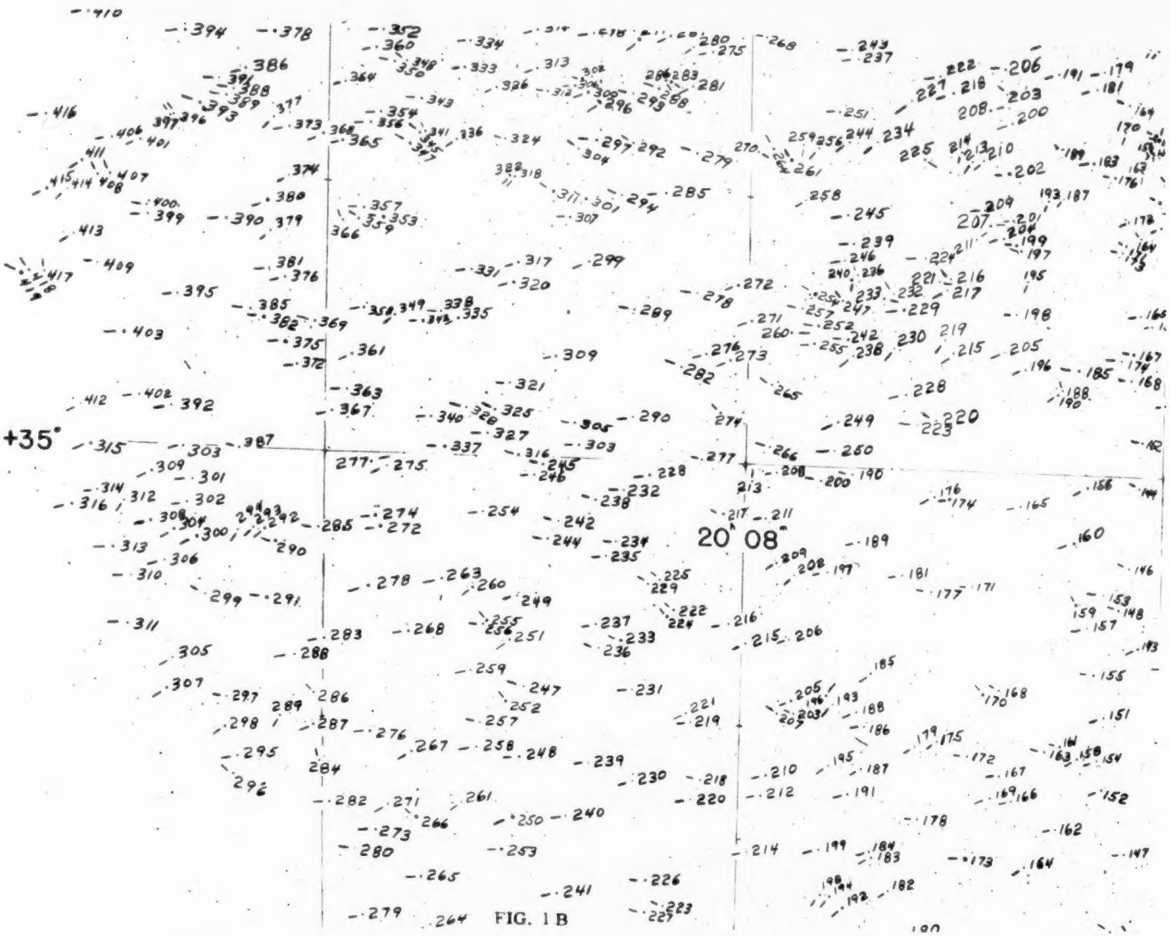

FIG. 1 B

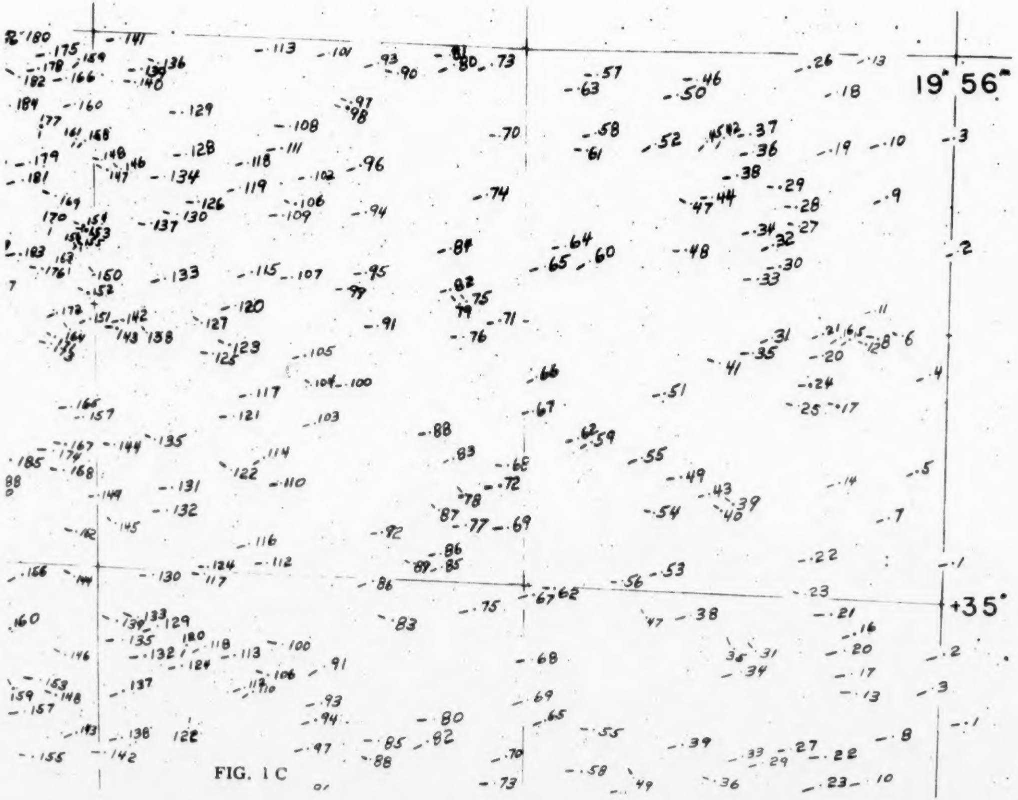

FIG. 1 C

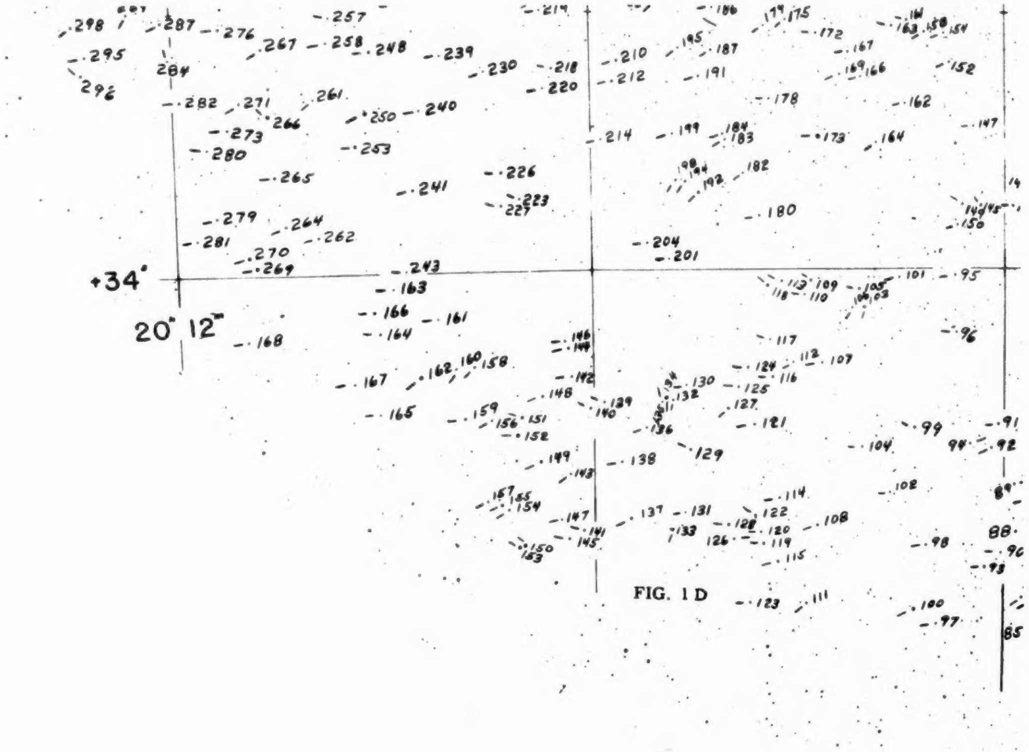

FIG. 1 D

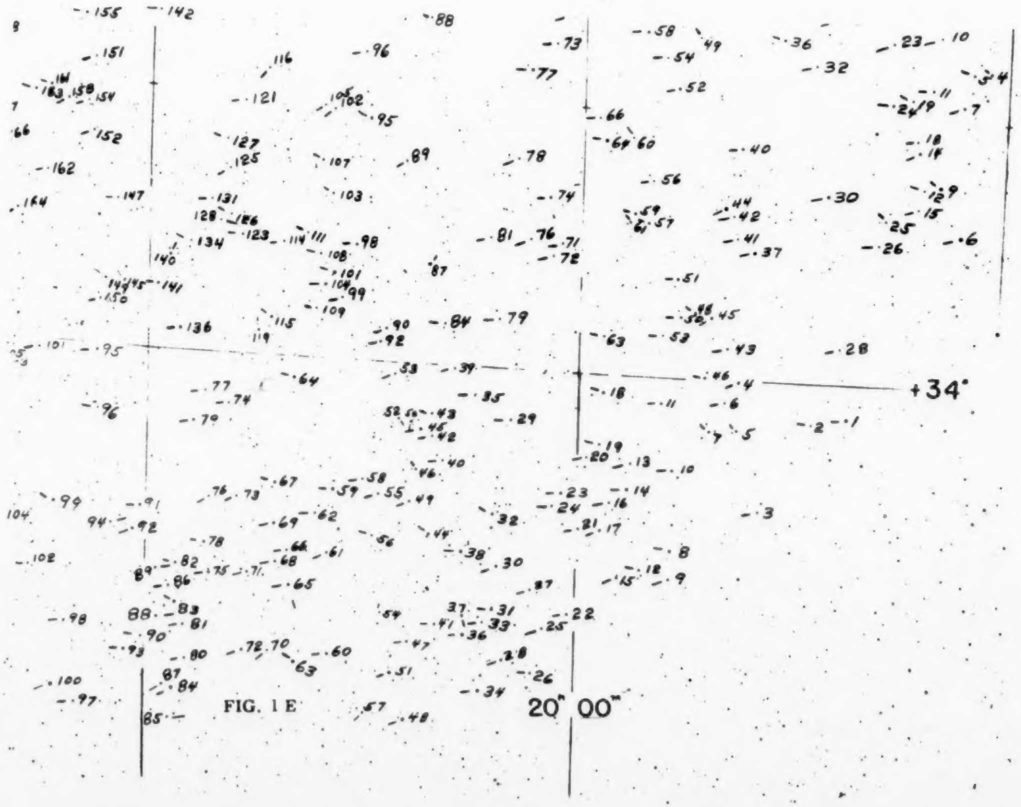

FIG. 1 E

Selected Area 39 were used as standards. I am indebted to the authors for providing the latter magnitudes and also for supplying slight modifications of the former magnitudes. Two plates (in some cases three) were used for the 557 field stars. The probable error of a mean magnitude is again ±0.06.

The fourth column gives the spectral type and luminosity, as in previous papers of this series. The criteria used were those described by Nassau and Seyfert[7] and Nassau and van Albada.[8] Stars designated as OB have been so classified by Nassau and Morgan,[9] or by Nassau and Harris.[10]

The method by which the charts were made has been described in the LF3b observational paper.[4]

Various comparisons with other investigations were made, with regard to magnitudes, colors, and spectra. These comparisons showed good general agreement with those found in LF3b.[3, 4] Therefore, the intercomparisons between LF3b and other sources are generally applicable to LF3a.

After correcting for the absorption, an analysis of the stellar density and luminosity function in this region has been made, and the results have been published in abstract form by the writer.[11] Since the region shows definite heterogeneity in absorption, it is felt that a more detailed density analysis is unwarranted.

I wish to thank Dr. J. J. Nassau for generously making the facilities of the Warner and Swasey Observatory available to me and also for his continuing advice and encouragement. Others who have been very helpful are Dr. S. W. McCuskey and Dr. D. A. MacRae, of the same observatory, and Dr. Freeman D. Miller, of the University of Michigan.

NOTES TO TABLE 1

Zone +33°

37 BD+33°3701, ADS 13300.
51 BD+33°3709, *HDC* lists spectrum as G5, apparently an error in *HDC*.
64 BD+33°3718, CD Cygni.
65 BD+33°3717, *HDC* lists spectrum as F8, apparently an error in *HDC*.
150 BD+33°3778, ADS 13463; the companion is 33°153.
153 BD+33°3780, ADS 13463; the companion is 33°150.

Zone +34°

1 BD+34°3808, ADS 13171.
37 BD+33°3683, ADS 13235.
159 BD+34°3874, ADS 13391.
224 BD+34°3899, ADS 13465.
248 BD+34°3907, ADS 13507.
250 BD+34°3908, ADS 13508.
266 BD+34°3916, ADS 13532.
300 BD+34°3937, ADS 13587.

Zone +35°

21 BD+35°3897, ADS 13203.
24 BD+35°3898, ADS 13204.
29 BD+35°3902, ADS 13218.
32 BD+35°3904, ADS 13219.
68 BD+34°3844, ADS 13283.
78 BD+34°3850, ADS 13292.
98 BD+35°3930, ADS 13312.
107 BD+35°3934, G band diffuse, K line strong.
129 BD+35°3942, *HDE* lists as F0.
143 BD+35°3949, ADS 13361.
147 BD+35°3950, Merrill-Burwell catalogue (*Ap. J.*, **78**, 139, 1933) lists as Be.
153 BD+35°3953, ADS 13374; the companion is 35°154.

---

[7] *Ap. J.*, **103**, 117, 1946.

[8] *Ap. J.*, **106**, 20, 1947.

[9] *Ap. J.*, **113**, 141, 1951.

[10] *Ap. J.*, **115**, 459, 1952.

[11] *A.J.*, **54**, 181, 1949.

154 BD+35°3955, ADS 13374; the companion is 35°153.
155 BD+35°3956, ADS 13376; the companion is 35°156.
156 BD+35°3957, ADS 13376; the companion is 35°155.
178 BD+35°3960, *HDE* lists as A.
199 BD+35°3969, ADS 13402.
202 BD+35°3970, ADS 13405.
229 BD+35°3983, ADS 13423.
240 BD+35°3987, ADS 13429.
272 BD+35°3998, Merrill-Burwell catalogue lists as B3ne.
280 BD+35°4002, RY Cygni.
283 BD+35°4004, Merrill-Burwell catalogue lists as B3ne.
296 BD+35°4008, ADS 13486.
311 BD+35°4012, ADS 13496.
334 Nebulous image, spectral lines weak.
375 BD+34°3930, ADS 13562.
382 BD+34°3934, ADS 13569.

Zone +36°
26 BD+36°3917, ADS 13453.
69 BD+36°3932, *HDE* lists as A5.
80 BD+36°3936, ADS 13537.
98 BD+36°3946, Merrill-Burwell catalogue lists as B0ne.

Sequence stars: The following stars were used as standards for both photographic and photored magnitudes: 33°118. 34°137, 156, 163, 201, 250. 35°152, 167, 177, 178, 181, 183, 192, 197, 206, 220, 225, 232, 234, 240, 291.

STARS IN REGION OVERLAPPING WITH LF*3b*

Zone +36°
109 *Read* A2 *for* B5 in spectral classification.
120 *Read* Appears to be later than B2 *for* B2 (overlap).
125 *Read* 10.89 *for* 11.89 in m_{pg}.
150 Insert remarks: "Stebbins, Huffer, and Whitford list color C_1 as +0.28 (*Ap. J.*, **91**, 43, 1940). After a check measure, Whitford confirms the LF3b color (also confirmed by LF3a) and suggests that the star had been previously misidentified (private communication)."
196 *Read* B9 *for* F0 in spectral classification.
252, 253 *Read* 253, 252 in LF3b catalogue numbers.
269 *Read* K2 V *for* K2 III in spectral classification.

Zone +37°
272 Insert remarks: "BD+36°3876, ADS 13396."
324 Insert remarks: "BD+36°3902, V402 Cygni."

SOME CHARACTERISTICS OF COLOR SYSTEMS*

W. W. MORGAN, D. L. HARRIS, AND H. L. JOHNSON
Yerkes and McDonald Observatories; Lowell Observatory

Received December 22, 1952; revised February 26, 1953

ABSTRACT

Relations between various color systems are investigated. Systemic reductions are given in terms of interstellar reddening, a normal main sequence, and the yellow giants. As would be expected from the work of W. Becker and the "Six-Color Photometry" of Stebbins and Whitford, different relations are found for the three groups of stars. The ratios of reddening to total visual absorption are found to be:

$$A_{\text{vis}} = 0.96 E_{[V-I]}\ ; \qquad A_{\text{vis}} = 3.0 E_{(B-V)}\ ; \qquad A_{\text{vis}} = 6.1 E_1\ .$$

TERMINOLOGY

(U, B, V) system: The photometric system described by Johnson and Morgan.[1]
$[V - I]$, $[U - B]$, etc.: The colors of Stebbins and Whitford, "Six-Color Photometry."[2]
C_1: The color system of Stebbins, Huffer, and Whitford as defined in "733 B Stars" and "1332 B Stars."[3] The present dicussion does not apply to other investigations utilizing the same symbol.
E_1: Color excesses on the C_1 system as defined above.
$E_{(B-V)}$, $E_{[V-I]}$, etc.: Color excesses on the $(B - V)$ and $[V - I]$ systems.
A_V: Interstellar absorption on the V magnitude system.[1]
MK: The classification system of the Yerkes revised spectral atlas.
"Impartial line": See *Ap. J.*, **102**, 366, 1945. Probable errors are used throughout.

INTRODUCTION

It is possible to note certain general features of the relation between two color systems, one of which is more strongly affected by Balmer-line absorption and continuum than the other. Figure 1 gives a schematic description of two such systems: the one more strongly affected by hydrogen absorption is plotted as the ordinate; the positions of the (unreddened) main sequence and yellow giants are shown, together with the path followed by O stars affected by varying degrees of interstellar reddening. In general, the O reddening path (or O path) is located above the main sequence, and the yellow giants are below. These effects have been described by W. Becker[4] and in Parts I and III of the Stebbins-Whitford "Six-Color Photometry."

For the most accurate determination of the reddening path it is important to include only stars of similar intrinsic color; the O stars are probably the most useful group for the purpose, since their range in intrinsic color is small and they can be classified with ease. The greatest range in reddening, however, has been observed for the early B supergiants of luminosity class I*a;* the group B0 I*a*–B2 I*a* allows the most accurate determination of the reddening path to be made. In general, only a slight zero-point correction is needed to reduce this relation to that for the O stars; when there is an appreciable difference of zero point, the slope is determined from the B0 I*a*–B2 I*a* group.

---

* *Contributions from the McDonald Observatory, University of Texas,* No. 224.

[1] *Ap. J.*, **117**, 313, 1953.

[2] *Ap. J.*, **102**, 318, 1945.

[3] *Pub. Washburn Obs.*, Vol. **15**, Part 5, 1934; *Ap. J.*, **91**, 61, 1940.

[4] For references see *Ap. J.*, **107**, 278, 1948.

THE REDDENING PATHS FOR $(B - V)$ AND VARIOUS COMBINATIONS

Observational data are given in Table 1 for the intercomparison of several color systems. The selection includes the following, which are contained in the investigation of Johnson and Morgan[1] (Table 3) or in the "Six-Color Photometry"[2, 5] of Stebbins and Whitford: (*a*) all unreddened stars of luminosity class V (MK system) earlier than M0; (*b*) stars B0 I*a*–B2 I*a*, inclusive; (*c*) all stars having spectral types earlier than B0 (white dwarfs and subdwarfs have been omitted); (*d*) stars of classes G8 III–K5 III, inclusive. To these have been added values of C_1 for stars in the above-mentioned list.[3]

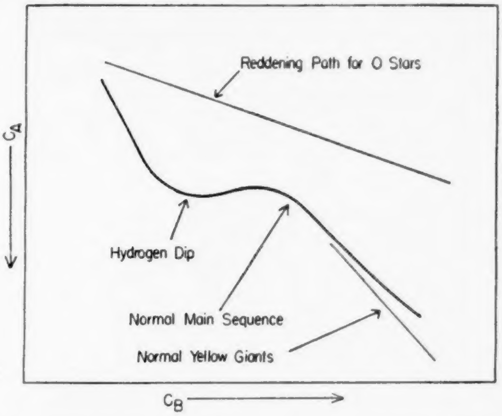

FIG. 1.—Schematic diagram showing two-color relations for unreddened main sequence, unreddened G8 III–K5 III stars and reddening path for O stars. Color C_A is more strongly affected by hydrogen absorption than C_B.

Figure 2 gives the relation between color indices $(B - V)$ and $(U - B)$ for the stars in Table 1. The reddening line for the B0 I*a*–B2 I*a* supergiants is

$$\begin{aligned} U - B &= -0.910 + 0.886(B - V), \\ &\pm 0.006 \pm 0.008 \end{aligned} \tag{1}$$

from a least-squares solution ("impartial line").

The relation between $(B - V)$ and C_1 is shown in Figure 3. The "impartial" reddening line for the O stars and B0 I*a*–B2 I*a* is

$$\begin{aligned} C_1 &= -0.144 + 0.483(B - V). \\ &\pm 0.006 \pm 0.015 \end{aligned} \tag{2}$$

There are no main-sequence stars common to the two series later than A7; for the range B1–A7 a linear relation represents the unreddened main sequence satisfactorily:

$$\begin{aligned} C_1 &= -0.103 + 0.568(B - V). \\ &\pm 0.005 \pm 0.027 \end{aligned} \tag{3}$$

---

[5] We are greatly indebted to Dr. Stebbins for permission to use and publish a number of six-color observations not included in "Six-Color Photometry." These have strengthened the weight of the reductions greatly.

TABLE 1

COLORS FROM (U, B, V), SIX-COLOR, AND C_1 SYSTEMS

HD	Name	MK	$B-V$	$U-B$	No. of Obs.*	$[B-R]$	$[U-B]$	$[V-G]$	$[V-I]$	C_1†
116658‡	α Vir	B1 V	−0.26	−0.94	4	−1.12	−1.56	−1.13	−2.49	−0.23
120315	η UMa	B3 V	− .20	− .68	6	−1.10	−1.28	−1.06	−2.40	− .23
74280	η Hya	B3 V	− .20	− .74	Stand.	......	......	......	......	− .23
160762	ι Her	B3 V	− .18	− .69	5	......	......	......	......	− .20
32630	η Aur	B3 V	− .17	− .68	3	......	......	......	......	− .20
4727	ν And	B5 V	− .15	− .57	1	−1.05	−1.13	−1.02	−2.23	− .18
87901	α Leo	B7 V	− .12	− .38	2	......	......	......	......	......
135742	β Lib	B8 V	− .11	− .37	Stand.	......	......	......	......	......
196867	α Del	B9 V	− .06	− .23	4	......	......	......	......	......
222661	ω^2 Aqr	B9.5 V	......	......	......	−0.95	−0.49	−0.83	−1.88	......
139006	α CrB	A0 V	− .02	− .02	6	......	......	......	......	......
130109	109 Vir	A0 V	− .01	− .03	2	......	......	......	......	......
71155	HR 3314	A0 V	− .01	.00	2	......	......	......	......	......
172167	α Lyr	A0 V	.00	− .01	8	−0.93	−0.37	−0.88	−1.85	......
103287	γ UMa	A0 V	.00	+ .01	4	......	......	......	......	......
161868	γ Oph	A0 V	+ .04	+ .06	3	......	......	......	......	......
95418	β UMa	A1 V	− .02	.00	H4	......	......	......	......	......
48915	α CMa	A1 V	+ .01	− .08	2	......	......	......	......	......
198001	ε Aqr	A1 V	+ .02	+ .06	3	......	......	......	......	......
140159	ι Ser	A1 V	+ .04	+ .04	2	......	......	......	......	......
21447	HR 1046	A1 V	+ .05	+ .04	2	......	......	......	......	......
18331	HR 875	A1 V	+ .09	+ .05	Stand.	......	......	......	......	......
116656	ζ UMa (br)	A2 V	+ .02	+ .01	H3	......	......	......	......	......
1280	θ And	A2 V	+ .06	+ .02	2	......	......	......	......	......
40183‡	β Aur	A2 V	......	......	......	−0.88	−0.32	−0.79	−1.77	......
106591	δ UMa	A3 V	+ .08	+ .07	2	......	......	......	......	......
102647	β Leo	A3 V	+ .09	+ .04	2	......	......	......	......	......
56537	λ Gem	A3 V	+ .10	+ .09	2	......	......	......	......	......
8538‡	δ Cas	A5 V	+ .14	+ .10	2	−0.70	−0.17	−0.63	−1.45	......
11636	β Ari	A5 V	+ .14	+ .10	2	......	......	......	......	− .03
116842	80 UMa	A5 V	+ .16	+ .08	5	......	......	......	......	......
87696	21 LMi	A7 V	+ .16	+ .07	2	......	......	......	......	0.00
6961	θ Cas	A7 V	+ .17	+ .11	2	......	......	......	......	......
76644	ι UMa	A7 V	+ .18	+ .06	2	......	......	......	......	......
187642	α Aql	A7 IV, V	+ .23	+ .07	5	−0.61	−0.24	−0.61	−1.30	......
203280	α Cep	A7 IV, V	+ .23	+ .10	2	−0.62	−0.21	−0.58	−1.24	......
58946	ρ Gem	F0 V	+ .31	− .04	2	......	......	......	......	......
110379	γ Vir (AB)	F0 V	+ .34	− .05	H6	......	......	......	......	......
112412	α CVn (ft)	F0 V	+ .34	− .03	2	......	......	......	......	......
91480	37 UMa	F1 V	+ .32	− .01	H4	......	......	......	......	......
113139	78 UMa	F2 V	+ .37	.00	5	−0.35	−0.30	−0.40	−0.86	......
124674	κ Boo (B)	F2 V	+ .39	− .04	2	......	......	......	......	......
129798	....	F2 V	+ .39	.00	H5	......	......	......	......	......
164259	ζ Ser	F3 V	+ .38	.00	3	......	......	......	......	......
76943	10 UMa	F5 V	+ .43	+ .06	2	......	......	......	......	......
210027	ι Peg	F5 V	+ .44	− .05	7	......	......	......	......	......
111456	....	F5 V	+ .46	− .03	H5	......	......	......	......	......
187013	17 Cyg (A)	F5 V	+ .46	.00	2	......	......	......	......	......
30652	π^3 Ori	F6 V	+ .46	.00	3	......	......	......	......	......
173667	110 Her	F6 V	+0.46	0.00	3	......	......	......	......	......

---

* When no letter precedes the number, the observer is Johnson; the prefix "H" refers to Harris.

† The C_1 colors are from *Ap. J.*, **91**, 20, 1940, and *Pub. Washburn Obs.*, Vol. **15**, Part 5, 1934.

‡ Unpublished six-color observations, kindly communicated by Dr. Stebbins.

TABLE 1—*Continued*

HD	Name	MK	$B-V$	$U-B$	No. of Obs.*	$[B-R]$	$[U-B]$	$[V-G]$	$[V-I]$	C_1†
142860...	γ Ser	F6 V	+0.48	−0.02	3	......	......	......	......	......
184960...	....	F7 V	+0.47	−0.03	H5	......	......	......	......	......
16895...	θ Per	F7 V	+0.48	−0.01	2	......	......	......	......	......
120136...	τ Boo	F7 V	+0.48	+0.04	2	......	......	......	......	......
126660...	θ Boo	F7 V	+0.50	+0.01	3	......	......	......	......	......
170153...	χ Dra	F7 V	+0.50	−0.07	2	......	......	......	......	......
222368...	ι Psc	F7 V	+0.51	−0.01	3	......	......	......	......	......
165908...	99 Her	F7 V	+0.52	−0.10	4	......	......	......	......	......
90839...	36 UMa	F8 V	+0.51	0.00	2	......	......	......	......	......
9826...	50 And	F8 V	+0.54	+0.06	3	......	......	......	......	......
102870...	β Vir	F8 V	+0.54	+0.10	7	......	......	......	......	......
142373...	χ Her	F9 V	+0.56	+0.01	3	−0.08	−0.28	−0.18	−0.31	......
114710...	β Com	G0 V	+0.56	+0.05	5	−0.14	−0.20	−0.14	−0.37	......
4614...	η Cas	G0 V	+0.58	0.00	2	......	......	......	......	......
109358...	β CVn	G0 V	+0.59	+0.05	3	−0.09	−0.21	−0.13	−0.30	......
JM 144§..	....	G0 V	+0.59	+0.01	2	......	......	......	......	......
19373...	ι Per	G0 V	+0.60	+0.10	2	......	......	......	......	......
141004...	λ Ser	G0 V	+0.60	+0.11	4	......	......	......	......	......
13974...	δ Tri	G0 V	+0.61	+0.02	4	......	......	......	......	......
157214...	72 Her	G0 V	+0.62	+0.07	3	......	......	......	......	......
34411...	λ Aur	G0 V	+0.67	+0.10	1	......	......	......	......	......
115043...	....	G1 V	+0.60	+0.10	H5	......	......	......	......	......
160269...	26 Dra	G1 V	+0.61	+0.10	3	......	......	......	......	......
10307...	HR 483	G2 V	+0.63	+0.12	3	−0.07	−0.18	−0.12	−0.24	......
186408...	16 Cyg (A)	G2 V	+0.64	+0.19	2	......	......	......	......	......
224930...	85 Peg	G2 V	+0.66	+0.04	1	......	......	......	......	......
186427...	16 Cyg (B)	G5 V	+0.66	+0.20	2	......	......	......	......	......
20630...	κ Cet	G5 V	+0.68	+0.18	5	......	......	......	......	......
6582...	μ Cas	G5 Vp	+0.69	+0.09	2	......	......	......	......	......
117176...	70 Vir	G5 V	+0.71	+0.24	2	......	......	......	......	......
115617...	61 Vir	G6 V	+0.70	+0.26	2	......	......	......	......	......
111395...	....	G7 V	......	......	......	0.00	−0.04	−0.02	−0.06	......
101501...	61 UMa	G8 V	+0.69	+0.27	2	......	......	......	......	......
152391...	....	G8 V	......	......	......	0.00	+0.04	+0.07	+0.15	......
10700...	τ Cet	G8 Vp	+0.72	+0.18	2	......	......	......	......	......
154345...	....	G8 V	......	......	......	+0.04	+0.03	+0.01	0.00	......
103095...	Gr 1830	G8 Vp	+0.75	+0.17	3	......	......	......	......	......
185144...	σ Dra	K0 V	+0.79	+0.39	3	......	......	......	......	......
10780...	HR 511	K0 V	+0.81	+0.40	3	......	......	......	......	......
124752...	....	K0 V	+0.83	+0.52	H5	......	......	......	......	......
3651...	54 Psc	K0 V	+0.86	+0.56	2	+0.09	+0.32	+0.19	+0.32	......
10476...	....	K1 V	+0.84	+0.48	2	......	......	......	......	......
166620...	HR 6806	K2 V	+0.87	+0.59	4	+0.23	+0.41	+0.21	+0.43	......
3765...	....	K2 V	......	......	......	+0.22	+0.55	+0.34	+0.63	......
109011...	....	K2 V	+0.94	+0.63	H5	......	......	......	......	......
110463...	....	K3 V	+0.94	+0.73	H5	......	......	......	......	......
219134...	HR 8832	K3 V	+1.01	+0.89	Stand.	......	......	......	......	......
128165...	....	K3 V	......	......	......	+0.43	+0.78	+0.51	+0.98	......
154363...	....	K5 V	+1.16	+1.05	3	......	......	......	......	......
201091‡..	61 Cyg (A)	K5 V	+1.19	+1.10	4	+0.74	+1.14	+0.62	+1.36	......
JM 104§.	....	K7 V	+1.36	+1.26	2	......	......	......	......	......
157881...	....	K7 V	+1.36	+1.27	3	......	......	......	......	......
151288...	....	K7 V	+1.37	+1.29	3	+1.03	......	+0.86	+1.88	......
201092‡..	61 Cyg (B)	K7 V	+1.38	+1.23	4	+1.02	+1.30	+0.93	+2.01:	......
37128...	ε Ori	B0 I*a*	−0.20	−1.06	2	−1.04	−1.62	−1.06	−2.37	−0.20

§ Serial number from Table 3 of Johnson and Morgan, "Fundamental Stellar Photometry."

TABLE 1—*Continued*

HD	Name	MK	*B−V*	*U−B*	No. of Obs.*	[*B−R*]	[*U−B*]	[*V−G*]	[*V−I*]	C_1†
38771	κ Ori	B0.5 I*a*	−0.18	−1.06	2	......	......	......	......	−0.16
2905	κ Cas	B1 I*a*	+0.15	−0.80	2	−0.65	−1.34	−0.73	−1.50	− .09
41117	χ^2 Ori	B2 I*a*	+0.27	−0.70	2	......	......	......	......	− .02
216411	......	B1 I*a*	......	......	......	−0.02	−0.69	−0.21	−0.09	+ .15
229239	......	B0.5 I	+0.85	−0.15	H3	......	......	......	......	......
169454	......	B1 I*a*	......	......	......	+0.61	−0.27	+0.26	+1.04	+ .29
194839	......	B0.5 I*a*	+0.96	−0.06	H3	+0.61	−0.21	+0.33	+1.14	+ .34
194279	......	B1.5 I*a*	+1.01	−0.02	H3	+0.71	−0.14	+0.33	+1.28	+ .33
229059	......	B1.5 I*a*p	+1.50	+0.43	H4	......	......	......	......	......
37043	ι Ori	O9 III	−0.25	−1.11	2	......	......	......	......	− .23
14633	......	O8	−0.21	−1.09	3	−1.10	−1.74	−1.14	−2.55	− .30
36486	δ Ori	O9.5 II	......	......	......	−1.11	−1.69	−1.10	−2.52	− .23
214680	10 Lac	O9 V	−0.20	−1.04	Stand.	−1.11	−1.73	−1.11	−2.49	− .23
57061	τ CMa	O9 III	−0.14	−0.99	6	......	......	......	......	− .25
37742	ζ Ori	O9.5 I*b*	......	......	......	−1.07	−1.67	−1.07	−2.43	− .22
1337‡	......	O9 III	......	......	......	−0.97	−1.64	−1.01	−2.24	− .20
188209	......	O9.5 III	......	......	......	−0.92	−1.58	−0.94	−2.08	− .17
203064	68 Cyg	O8	......	......	......	−0.76	−1.57	−0.87	−1.82	− .16
24912	ξ Per	O7	......	......	......	−0.76	−1.49	−0.86	−1.80	− .14
149757	ζ Oph	O9.5 V	+0.01	−0.86	H5	......	......	......	......	− .13
199579	......	O6	......	......	......	−0.73	−1.42	−0.81	−1.70	− .12
209975	19 Cep	O9.5 I*b*	......	......	......	−0.71	−1.39	−0.77	−1.62	− .12
193322	......	O8	......	......	......	−0.66	−1.33	−0.71	−1.57	− .07
37022	θ^1 Ori‖	(O9)	......	......	......	−0.56	−1.35	−0.76	−1.30	− .02
46150	......	O6	+0.12	−0.85	2	......	......	......	......	− .04
46149	......	O8	+0.16	−0.80	2	......	......	......	......	− .09
46202	......	O9 V	+0.17	−0.76	2	......	......	......	......	− .10
46223	......	O5	+0.21	−0.78	3	......	......	......	......	− .04
210839	λ Cep	O6 f	+0.26	−0.73	2	−0.47	−1.25	−0.60	−1.17	− .04
207198	......	O9 II	......	......	......	−0.38	−1.13	−0.53	−1.03	+ .03
192639	......	O8 f	......	......	......	−0.34	−1.07	−0.47	−0.87	+ .03
192281	......	O5 f	......	......	......	−0.22	−1.06	−0.42	−0.80	+ .07
193443	......	O9 III	+0.38	−0.53	H3	−0.28	−0.99	−0.43	−0.78	+ .03
193514	......	O7 f	+0.43	−0.50	H3	−0.12	−0.88	−0.36	−0.48	+ .10
195592	......	O9.5 I*a*	......	......	......	+0.39	−0.32	+0.09	+0.75	+ .30
229234	......	O9.5 III	+0.76	−0.20	H3	......	......	......	......	......
166734	......	O8 f:	......	......	......	+0.81	−0.29	+0.35	+1.46	+ .39
216131‡	μ Peg	G8 III	......	......	......	+0.22	+0.60	+0.33	+0.56	......
21120	ο Tau	G8 III	+0.89	+0.64	2	......	......	......	......	......
148387‡	η Dra	G8 III	+0.91	+0.64	H4	+0.24	+0.58	+0.29	+0.47	......
148856	β Her	G8 III	+0.91	+0.66	H4	......	......	......	......	......
62345	κ Gem	G8 III	+0.92	+0.68	3; H1	......	......	......	......	+ .49
133208	β Boo	G8 III	+0.95	+0.72	H5	+0.29	+0.65	+0.36	+0.56	......
135722	δ Boo	G8 III	+0.96	+0.68	2; H2	+0.32	+0.61	+0.37	+0.65	......
9270	η Psc	G8 III	+0.98	+0.79	2	+0.16	+0.54	+0.27	+0.51	......
180711‡	δ Dra	G9 III	+1.00	+0.78	H2	+0.34	+0.75	+0.44	+0.74	......
181276	κ Cyg	K0 III	+0.95	+0.74	H2	......	......	......	......	......
27697‡	δ Tau	K0 III	+0.98	+0.84	2	+0.26	+0.80	+0.41	+0.63	......
27371	γ Tau	K0 III	+0.99	+0.84	2	......	......	......	......	......
40035	δ Aur	K0 III	+0.99	+0.86	2	......	......	......	......	......
62509	β Gem	K0 III	+1.00	+0.84	5	......	......	......	......	+0.52
145328	τ CrB	K0 III	+1.02	+0.85	H4	+0.38	+0.83	+0.43	+0.77	......
28305‡	ε Tau	K0 III	+1.03	+0.87	2	+0.30	+0.91	+0.45	+0.70	......
197989	ε Cyg	K0 III	+1.03	+0.87	5	......	......	......	......	......
95689	α UMa	K0 III	+1.06	+0.90	3; H1	......	......	......	......	......

‖ The MK types of the Trapezium stars, in order of decreasing brightness, are: O6 p, B0.5 p, B0.5 p, and B3 p. The mean type weighted by magnitude is near O9.

TABLE 1—*Continued*

HD	Name	MK	$B-V$	$U-B$	No. of Obs.*	$[B-R]$	$[U-B]$	$[V-G]$	$[V-I]$	C_1†
203504...	1 Peg	K1 III	+1.10	+1.05	2	......	......	......	......	......
96833...	ψ UMa	K1 III	+1.13	+1.11	3; H1	......	......	......	......	......
153210...	κ Oph	K2 III	+1.14	+1.18	H5	......	......	......	......	......
12929‡..	α Ari	K2 III	+1.15	+1.12	Stand.	+0.48	+1.21	+0.64	+1.16	......
140573...	α Ser	K2 III	+1.16	+1.24	Stand.	......	......	......	......	......
161096...	β Oph	K2 III	+1.16	+1.24	3; H2	......	......	......	......	......
137759...	ι Dra	K2 III	+1.17	+1.22	3; H2	......	......	......	......	......
163588...	ξ Dra	K2 III	+1.18	+1.23	H5	......	......	......	......	......
143107...	ε CrB	K3 III	+1.23	+1.28	Stand.	......	......	......	......	......
127665...	ρ Boo	K3 III	+1.28	+1.44	2; H2	......	......	......	......	......
216446‡..	....	K3 III	......	......	......	+0.69	+1.47	+0.79	+1.46	......
9927...	51 And	K3 III	+1.28	+1.46	2	......	......	......	......	+0.74
98262...	ν UMa	K3 III	+1.38	+1.57	2; H3	......	......	......	......	+ .81
131873‡..	β UMi	K4 III	+1.46	+1.75	H4	+0.93	+2.00	+1.03	+1.91	......
69267...	β Cnc	K4 III	+1.48	+1.77	Stand.	......	......	......	......	+0.89
29139...	α Tau	K5 III	+1.51	+1.81	2	+1.10	+2.09	+1.18	+2.38	......
164058‡..	γ Dra	K5 III	+1.52	+1.87	3; H2	+1.03	+2.16	+1.13	+2.18	......

The five yellow giants in common have a markedly different relation:

$$C_1 = -0.196 + 0.731(B - V). \qquad (4)$$
$$\pm 0.026 \pm 0.021$$

The relation between $(B - V)$ and the $[B - R]$ index of the "Six-Color Photometry" is shown in Figure 4. Here $(B - V)$ is considered as the ordinate, since the effect of hydrogen absorption on $[B - R]$ is probably slight; *Hα* is within the sensitivity range of the $[R]$-point, and *Hβ*-*Hδ* are included in $[B]$; the higher members of the Paschen series which are within the range of the $[R]$-point[6] would tend toward balancing the hydrogen effect on the two filter combinations. A single reduction formula is not satisfactory; the O reddening path, the main sequence, and the yellow giants all require different relations if an accurate reduction is desired. At $[B - R] \sim +0.7$, there is a difference of the order of 0.3 mag. in $B - V$ between the O reddening path and the yellow giants; the K-type main-sequence stars lie in an intermediate position. There is also a trace of the hydrogen dip in the main sequence.

Figure 5 gives the relation between $(B - V)$ and $[V - G]$. This comparison is of special interest because of the similarity in the effective wave lengths of the two systems. Since $[V]$ includes more ultraviolet light than B, $(B - V)$ is selected as the abscissa.

In spite of the similar instrumentation, traces of some of the systematic effects already noted persist; the stars of classes O and B0 I*a*–B2 I*a* lie systematically above the main sequence by a small amount, and the yellow giants lie slightly below the main sequence. At $(B - V) = +1.0$ the difference between the O reddening path and the yellow giants is around 0.1 mag. in $[V - G]$. While a mean relation for all three kinds of stars might be considered satisfactory for some purposes, an appreciable sacrifice in the accuracy of the observations would result. The relation for the main sequence is not linear; a quadratic interpolation curve computed by least squares is

$$B - V = +0.703 + 0.803[V - G] - 0.044[V - G]^2. \qquad (5)$$
$$\pm 0.005 \pm 0.005 \qquad \pm 0.007$$

---

[6] See transmission curves in *Ap. J.*, **98**, 23, 1943.

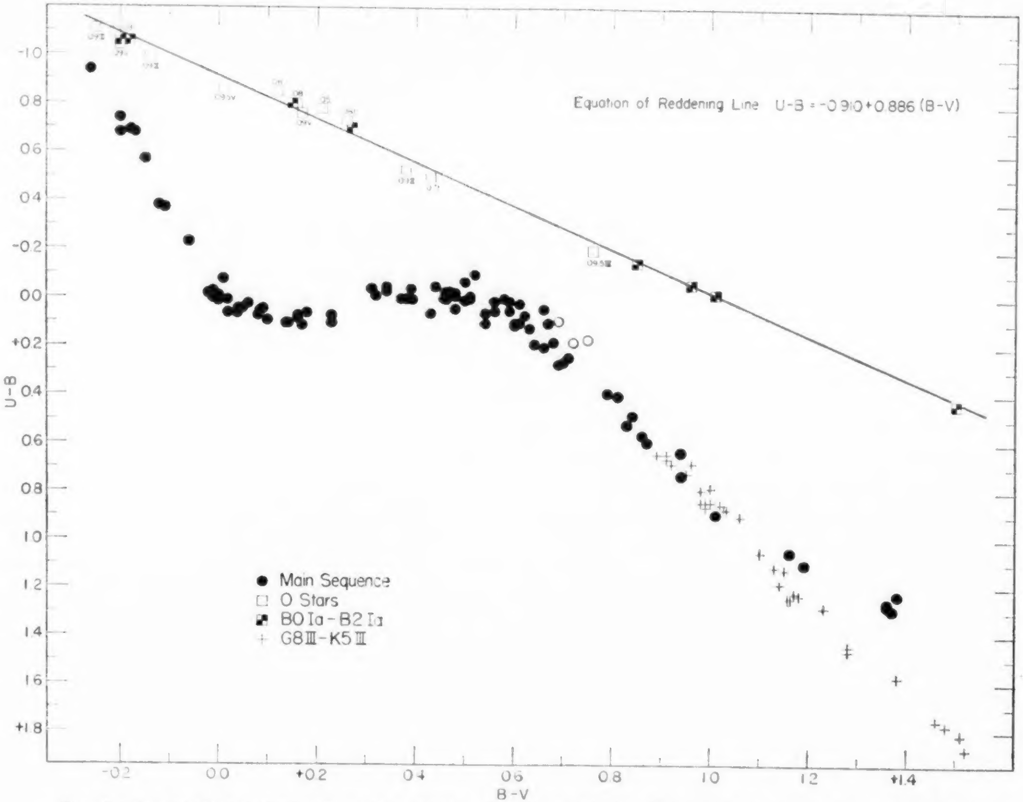

FIG. 2.—The relation between $(B - V)$ and $(U - B)$. The reddening line was determined from the B0 I*a*–B2 I*a* stars. The three open circles refer to μ Cas (G5 Vp), τ Cet (G8 Vp), and Gr 1830 (G8 Vp).

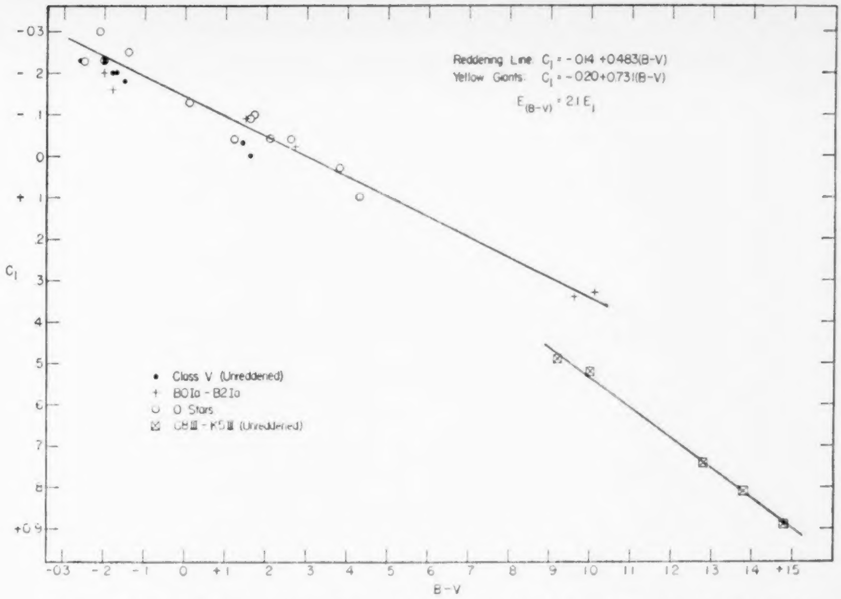

FIG. 3.—The relation between $(B - V)$ and C_1. The reddening line was determined from a combination of O and B0 I*a*–B2 I*a* stars.

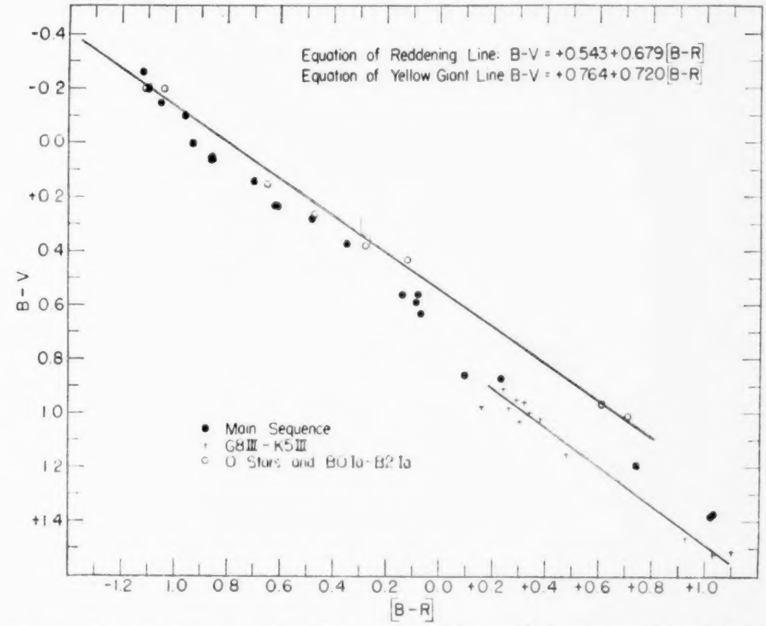

FIG. 4.—The relation between [B − R] and (B − V). The reddening line was determined from the B0 I*a*–B2 I*a* stars.

The reddening path for O and B0 I*a*–B2 I*a* stars can be represented by the line

$$\begin{aligned} B - V &= +0.725 + 0.827[V - G]. \\ &\quad \pm 0.009 \pm 0.013 \end{aligned} \tag{6}$$

The least-squares linear solution for the yellow giants is

$$\begin{aligned} B - V &= +0.697 + 0.716[V - G]. \\ &\quad \pm 0.008 \pm 0.011 \end{aligned} \tag{7}$$

The relation between $(B - V)$ and $[V - I]$ is illustrated in Figure 6. Here a different effect is observed: the O reddening line crosses the main-sequence relation near $B - V =$

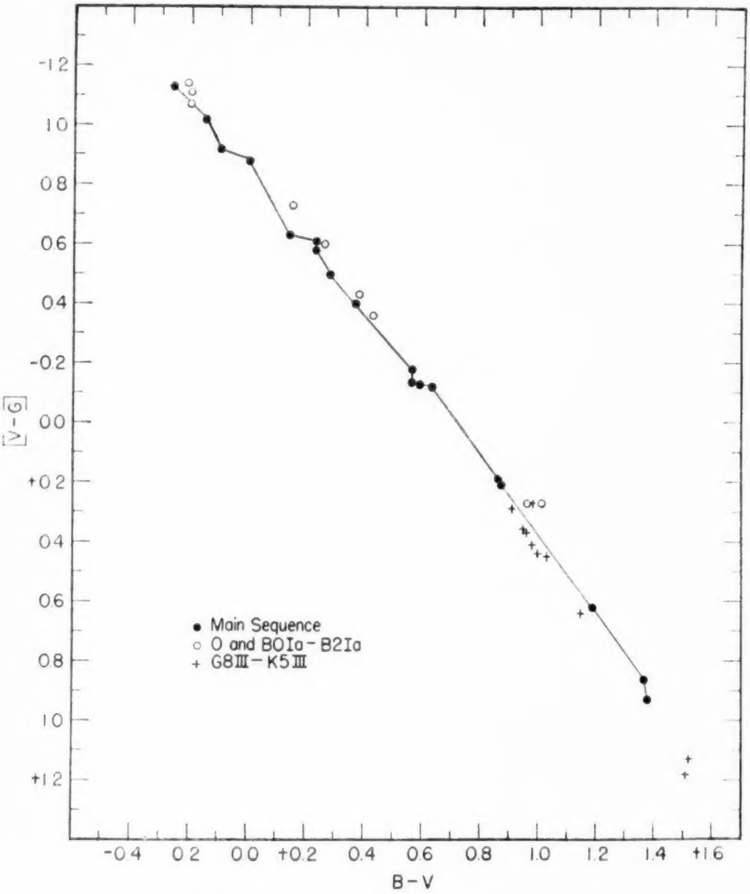

FIG. 5.—The relation between $(B - V)$ and $[V - G]$

$+0.1$. A possible explanation lies in the characteristics of the $[V-I]$ color index: for the redder stars (both intrinsically redder and space-reddened) the Balmer absorption effect is more marked in $B-V$; we thus find the O reddening line above the main sequence and the yellow giants below. For stars bluer than $B-V=0$, however, the effect of the Balmer absorption on the $[V]$-point becomes the dominant factor; the blue part of the diagram should therefore be plotted with $B-V$ as the abscissa, to be consistent in sense with earlier diagrams.

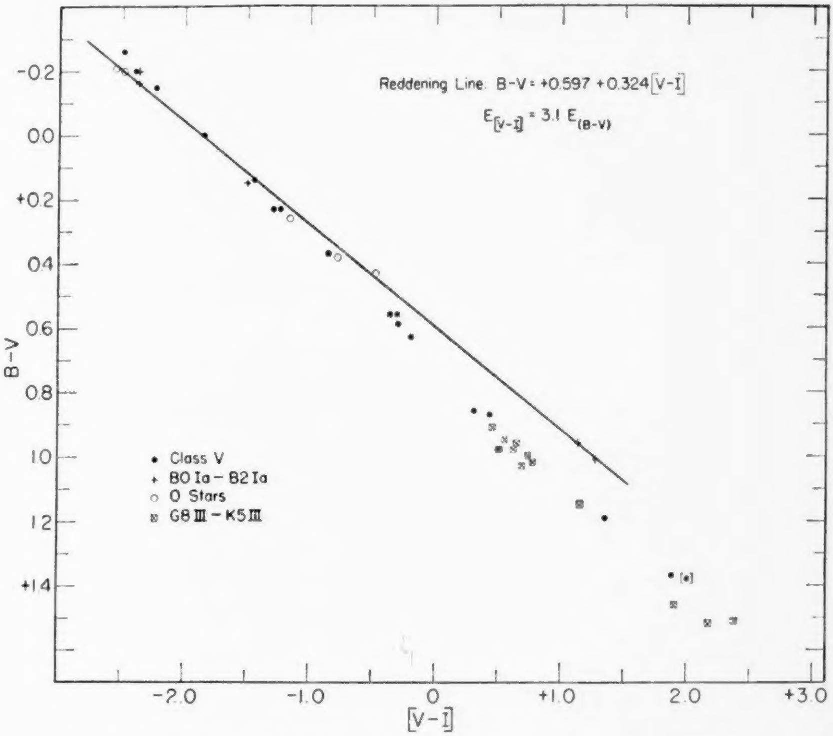

FIG. 6.—The relation between $[V-I]$ and $(B-V)$. The reddening line was determined from the B0 I*a*–B2 I*a* stars.

THE REDDENING PATHS FOR THE SIX-COLOR PHOTOMETRY

We shall now consider certain combinations from the "Six-Color Photometry," together with C_1.

Figure 7 illustrates the relation between $[V-I]$ and $[U-B]$. There is a qualitative similarity to Figure 2. The reddening line for B0 I*a*–B2 I*a* is

$$\begin{gathered}[U-B] = -0.678 + 0.410[V-I]. \\ \pm 0.009 \pm 0.006\end{gathered} \tag{8}$$

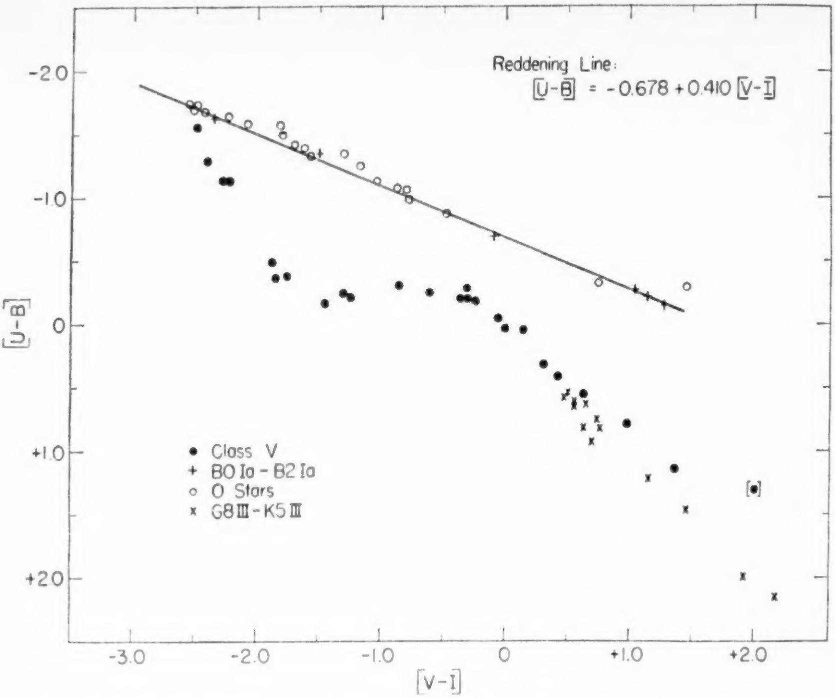

FIG. 7.—The relation between $[V-I]$ and $[U-B]$. The reddening line was determined from the B0 I*a*–B2 I*a* stars.

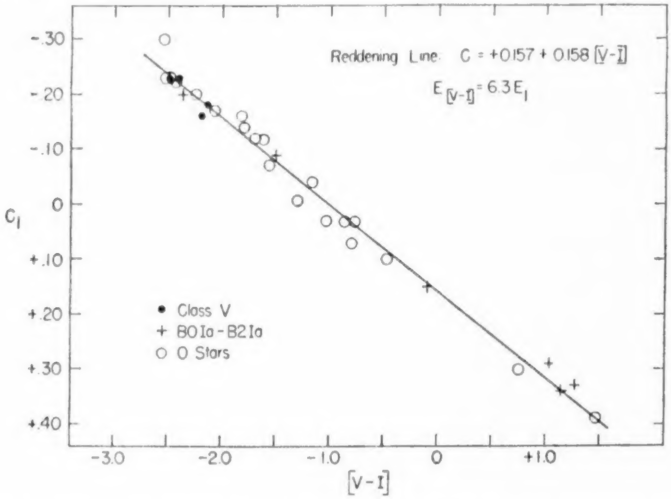

FIG. 8.—The relation between $[V-I]$ and C_1. The reddening line was determined from a combination of the O and B0 I*a*–B2 I*a* stars.

The relation between $[V - I]$ and C_1 is shown in Figure 8. No yellow giants and only four main-sequence stars of Table 1 are common to the two series. However, the reddening path itself is well defined and bears testimony to the good accuracy of the short baseline C_1 colors. The mean relation for O and B0 I*a*–B2 I*a* stars is

$$C_1 = \underset{\pm 0.004}{+0.157} + \underset{\pm 0.003}{0.158}[V - I]. \tag{9}$$

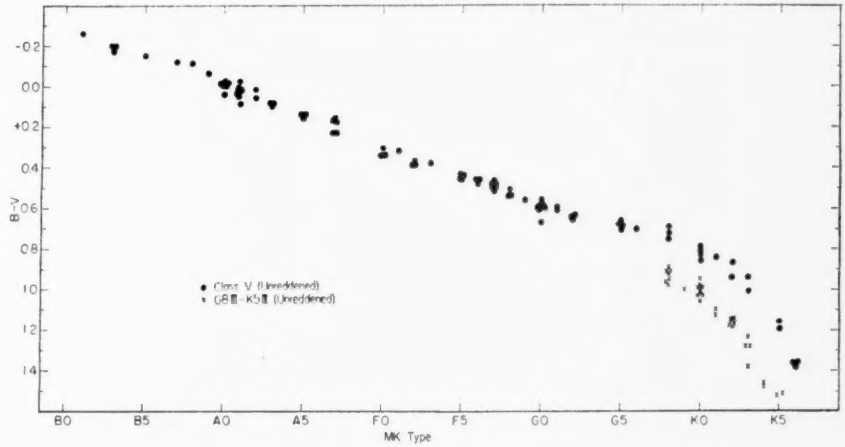

FIG. 9.—The relation between MK spectral type and $(B - V)$

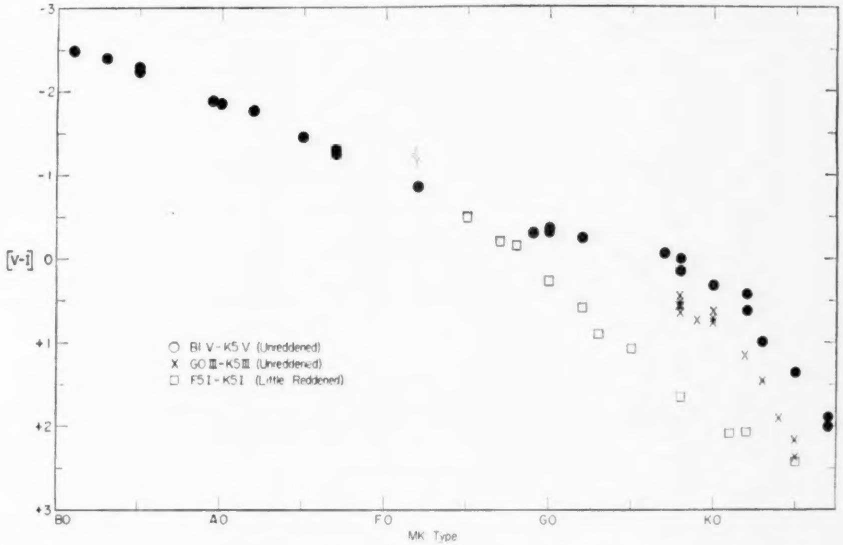

FIG. 10.—The relation between MK type and $[V - I]$

SOME RELATIONS BETWEEN COLOR AND MK TYPE

Figures 9 and 10 illustrate the relations between the normal main-sequence stars and yellow giants, and colors on the $(B - V)$ and $[V - I]$ systems, respectively. In addition, the little-reddened supergiants of classes F5 I–K5 I are shown in Figure 10; the data on the latter are given in Table 2.

TABLE 2

LITTLE-REDDENED F5 I–K5 I STARS

Star	MK	$[V-I]$ (Mag.)	$[U-B]$ (Mag.)	Star	MK	$[V-I]$ (Mag.)	$[U-B]$ (Mag.)
α Per........	F5 I*b*	−0.49	+0.20	α^1 Cap........	G3 I*b*	+0.90	+0.82
45 Dra........	F7 I*b*	− .21	+ .32	9 Peg........	G5 I*b*	+1.08	+1.08
γ Cyg........	F8 I*b*	− .15	+ .40	ε Peg........	K2 I*b*	+2.07	+2.02
β Aqr........	G0 I*b*	+ .27	+ .49	ξ Cyg........	K5 I*b*	+2.43	+2.19
α Aqr........	G2 I*b*	+0.62	+0.78				

TABLE 3

INTRINSIC COLORS

MK	$B-V$ (Mag.)	C_1 (Mag.)	MK	$B-V$ (Mag.)	C_1 (Mag.)
O7........	−0.32	−0.29	B6........	−0.14	−0.18
O8........	− .31	− .28	B7........	− .12	− .16
O9........	− .31	− .27	B8........	− .09	− .15
B0........	− .30	− .26	B9........	− .06	− .14
B0.5........	− .28	− .25	B9.5........	− .03	− .13
B1........	− .26	− .24	A0........	.00	− .12
B2........	− .24	− .23	A1........	+ .03	− .10
B3........	− .20	− .22	A2........	+0.06	−0.08
B5........	−0.16	−0.19			

THE INTRINSIC COLORS

One of the most difficult problems in the assignment of intrinsic colors is that of the O stars. Even in clusters containing O stars, the differential determination of intrinsic colors of the latter is not easy, because of the tendency of reddening material to be concentrated in the immediate neighborhood of the O stars.

Preliminary intrinsic colors for $(B - V)$ and C_1 are listed in Table 3. The values have been smoothed. Some of the stars on which the calibration of the C_1 intrinsic colors was based are listed in Table 4. To the class V stars have been added four F stars of class IV.

SUMMARY OF REDDENING RATIOS AND CONVERSION TO TOTAL ABSORPTION

In a note published separately,[7] D. L. Harris and H. L. Johnson have reinvestigated the problem of the ratio of total to selective absorption, and find:

$$A_V = 0.96 E_{[V-I]} . \\ \pm 0.05 \tag{10}$$

---

[7] *Ap. J.*, in press.

This fundamental quantity allows the reduction of the relative values determined earlier. The various fundamental ratios are collected below:

$$E_{[V-I]} = \underset{\pm\,0.06}{3.08}E_{(B-V)}, \tag{11}$$

$$E_{[V-I]} = \underset{\pm\,0.1}{6.3}E_1, \tag{12}$$

$$A_V = \underset{\pm\,0.2}{3.0}E_{(B-V)}, \tag{13}$$

$$A_V = \underset{\pm\,0.4}{6.1}E_1. \tag{14}$$

TABLE 4

STANDARD STARS FOR C_1 COLORS

Star	MK	C_1 (Mag.)	Star	MK	C_1 (Mag.)
α Vir	B1 V	−0.23	ο Peg	A1 V	−0.14
η Hya	B3 V	− .23	υ Psc	A2 V	− .10
η UMa	B3 V	− .23	26 UMa	A2 V	− .08
ι Her	B3 V	− .20	θ Peg	A2 V	− .08
η Aur	B3 V	− .20	ε Ari	A2 V	− .07
ν And	B5 V	− .18	β Ari	A5 V	− .03
κ Hya	B5 V	− .18	21 LMi	A7 V	.00
ζ Peg	B8 V	− .14	λ Psc	A7 V	.00
θ Hya	B9.5 V	− .14	ρ Psc	F2 V:	+0.10
ρ Peg	B9.5 Vp*	−0.12			

F IV STARS

Star	MK	C_1 (Mag.)	Star	MK	C_1 (Mag.)
δ Gem	F0 IV	+0.07	ι Leo	F2 IV	+0.11
23 UMa	F0 IV	+0.07	40 Leo	F6 IV	+0.18

* The K line is stronger than in α CMa (A1 V); *He* I is as strong as in α Del (B9 V).

From these relations precise corrections for interstellar absorption can be made in investigations of galactic structure—so long as the ratio of total to selective absorption is found not to vary.

THE POSSIBLE INFLUENCE OF INTERSTELLAR CLOUDS ON STELLAR VELOCITIES. II*

LYMAN SPITZER, JR., AND MARTIN SCHWARZSCHILD
Princeton University Observatory

Received February 26, 1953

ABSTRACT

The increase with time of random stellar velocities, as a result of gravitational encounters with interstellar cloud complexes, has been recomputed, taking into account the presence of differential galactic rotation. As a result of such nonuniform rotation, the clouds will have velocities relative to one another even if their random velocities are zero; the gravitational potential of these clouds will be a fluctuating function of time; and the stars will gain kinetic energy from the clouds.

To explain the increase of velocity dispersion with advancing spectral type along the main sequence, the mass of a typical cloud complex must be in the neighborhood of $10^6 m_\odot$, the value found previously; but the random velocity of a cloud complex, as a whole, is irrelevant and may be vanishingly small. Since inhomogeneities of density with the required scale of some 300 parsecs or more seem indicated by the extinction observations, it seems not unlikely that star-cloud encounters are, in fact, responsible for the greater velocity dispersion of the later-type, older stars of population type I.

I. INTRODUCTION

In a previous paper[1] (subsequently referred to as "Paper I"), it was suggested that gravitational encounters between stars and interstellar clouds might increase the velocity dispersion of the stars. Such a cause would naturally produce a greater effect on the older stars. The early-type stars, presumably formed recently from interstellar matter,[2] would not have had time to change appreciably their root-mean-square velocities, which would therefore equal more closely the velocities of the clouds from which they had formed. This mechanism provides a natural qualitative explanation of the fact, known for many years, that the root-mean-square random velocity for stars of each spectral type along the main sequence increases systematically with advancing spectral type, ranging from 10 km/sec for the O and early B stars to some 20 km/sec for the F stars.

The discussion in Paper I showed that small clouds, with radii of some 5 parsecs and masses of about $100 m_\odot$, would not produce any measurable effect on the velocities of the stars in times less than 10^{11} years. The same conclusion follows from the analysis by D. Osterbrock.[3] The larger complexes, of the type considered by Greenstein[4] and Bok,[5] have much greater masses, and it is these that must be primarily responsible for the effect in question. The detailed analysis in Paper I was based on conditions in an infinite homogeneous medium, and neglected galactic rotation. The results indicated that star-cloud encounters could, in fact, produce the results envisaged if:

a) Most of interstellar matter is gathered into cloud complexes with masses of the order of $10^6 m_\odot$.

b) The velocity dispersion of these massive cloud complexes is about 10 km/sec.

---

* This work was supported in part by funds of the Eugene Higgins Trust allocated to Princeton University.

[1] L. Spitzer, Jr., and M. Schwarzschild, *Ap. J.*, **114**, 385, 1951.

[2] For a survey of this theory see L. Spitzer, Jr., *J. Washington Acad. Sci.*, **41**, 309, 1951.

[3] *Ap. J.*, **116**, 164, 1952; *ibid.*, in press.

[4] *Harvard Ann.*, **105**, 359, 1937.

[5] *Centennial Symposia* (Cambridge, Mass.: Harvard College Obs., 1948).

The first of these requirements might seem rather difficult to meet, since the mass of a typical large cloud of the type observed seems to be more nearly $10^5 m_{\odot}$. However, the total mass of the Orion nebula may well exceed $10^6 m_{\odot}$, and such large masses cannot be excluded. Requirement *b* is even more difficult to meet. Although no extensive measurements are available on the systematic motion of very large clouds or groups of clouds, it would seem likely that the mean random velocity of such a very massive cloud complex would be substantially less than the velocity of the smaller clouds observed by Adams.[6]

In the present paper the analysis is extended to take into account the presence of differential galactic rotation. The results indicate that in this more realistic case requirement *b* is eliminated entirely, and the random motion of the clouds may be arbitrarily small; i.e., the star-cloud encounters will increase the stellar velocity dispersion even if each cloud is assumed to be moving with the circular velocity around the galactic center. Requirement *a* is formally not much changed—in fact, it becomes easier to meet, once requirement *b* is removed. Regions of excess density extending over several hundred parsecs and comprising masses of $10^6 m_{\odot}$ seem much more plausible than the relatively coherent dynamic units of this mass which were originally envisaged.

One may readily see why requirement *b* can be eliminated if differential galactic rotation is present. Let us suppose that the random motions of the clouds are rigorously zero. Then, if no differential rotation is present, the position of each cloud with respect to every other cloud is fixed in time. The potential energy of a star is then a simple function of position only, the sum of the potential and kinetic energies remains constant, and the velocity dispersion is unchanged by encounters. In the presence of differential rotation, the clouds nearer the galactic center have greater angular velocities than those farther out, the distances between different clouds will vary, and the potential energy of a star is no longer a simple function of position. In such a case, the stars form a nonconservative system, and their velocity dispersion will tend to increase as a result of the encounters.

To illustrate these effects by a specific example, let us consider a star in the neighborhood of the sun whose velocity relative to the local standard of rest is initially directed toward the galactic center and is numerically equal to 10 km/sec, a relatively low value. Such a star will move in an ellipse, with major and minor axes equal to 1400 and 700 parsecs, respectively, and with the minor axis pointing toward the galactic center. Over this range of distances from the galactic center the circular velocity of galactic rotation will change by some 30 km/sec. If the interstellar clouds are assumed to be moving with the local circular velocity, with no random velocities, the effective velocity spread of the clouds encountered by the star along its path will be ± 15 km/sec. While the detailed situation is somewhat more complicated than this simple example implies, this large effective spread of velocities greatly facilitates the transfer of energy from the inhomogeneous interstellar medium to the stars.

The energy gained by the stars must come, of course, from the interstellar matter, which will fall inward toward the galactic center by an inappreciable amount.

II. STATISTICS OF ENCOUNTERS IN A ROTATING SYSTEM

First, we shall consider the orbit of a single star, neglecting encounters. Then the effect of encounters can be considered, assuming that the clouds have negligible random velocities and utilizing in each segment of the star's orbit the results obtained in a uniform medium in the absence of external forces. An average over the orbit may next be taken, to find the mean change of the stellar velocity. Finally, an average over all stars in a particular group may be taken, to yield the rate of change of the velocity dispersion.

---

[6] *Ap. J.*, **109**, 354, 1949.

We write the equations of motion for a single star in the smoothed gravitational field of the Galaxy. Let x and y be the co-ordinates of a star relative to some point, P, which is at a fixed distance, R_p, from the galactic center but which is moving about the center at the angular velocity ω. The direction of positive x is taken to be the direction of increasing R, while y is taken to be positive in the direction of galactic rotation. Motions in the z direction, perpendicular to the galactic plane, do not affect motions in the xy plane, to a first approximation, and will be ignored. If $\Phi(R)$ is the gravitational potential per unit mass, then the familiar equations of motion in a frame of reference rotating with angular velocity ω become

$$\frac{d v_x}{dt} - 2\omega v_y = 4A\omega x \,, \tag{1}$$

$$\frac{d v_y}{dt} + 2\omega v_x = 0 \,, \tag{2}$$

where A, the familiar Oort constant, may be written

$$A = \frac{\omega}{4}\left[1 - R_p\left(\frac{d^2\Phi/dR^2}{d\Phi/dR}\right)\right], \tag{3}$$

with the derivatives evaluated for R equal to R_p. In equations (1) and (2) terms of the order $(x/R)^2$ and $(y/R)^2$ have been ignored.

These equations yield the solution:

$$v_x = K \sin 2(-B\omega)^{1/2} t \,, \tag{4}$$

$$v_y = K\left(-\frac{\omega}{B}\right)^{1/2} \cos 2(-B\omega)^{1/2} t - 2A\bar{x} \,, \tag{5}$$

where K is a constant of integration and B is the second Oort constant, given by

$$B = A - \omega \,. \tag{6}$$

The term $\bar{x}$ in equation (5) will be ignored, since this term may be eliminated by a simple change of co-ordinate system, i.e., by a change of the point P about which the expansion is made. The values of x and y as functions of time are readily obtained by direct integration of equations (4) and (5).

Before the theory of encounters can be applied, we must know u_x and u_y, the components of the star's velocity at each point relative to the local standard of rest. Since the circular velocity, in this co-ordinate system, is $-2Ax$, parallel to the y axis, we have

$$u_x = v_x \,, \tag{7}$$

$$u_y = v_y + 2Ax \,. \tag{8}$$

If we insert in equation (8) the value of x found by integration of equation (4), and substitute equation (5) for v_y, we find

$$u_y = K\left(-\frac{B}{\omega}\right)^{1/2} \cos 2(-B\omega)^{1/2} t \,. \tag{9}$$

It may be remarked that in an inverse-square field of force, B equals $-\omega/4$. Then v_y at its greatest is twice as great as the maximum value of v_x, while u_y at maximum is only half the greatest value of u_x.

We now assume that the star encounters clouds in its orbit. The problem will be treated on the assumption that each encounter takes place in a region small compared to the size of the stellar orbit about the point P. Thus the effect of the encounter may be computed as though the star were moving in a straight line. Each cloud will be assumed motionless relative to the local standard of rest. All deflections will be assumed small, a legitimate approximation for inverse-square encounters in general, and particularly appropriate in the present case, where the finite radius of the clouds reduces the deflections produced by the closer encounters. Under these assumptions, the effect of each encounter is to deflect the star by some angle $\Delta\theta$ in the xy plane, without changing its local velocity u. Thus the changes of u_x and u_y are given, to the first order, by

$$\Delta u_x = -u_y \Delta\theta \ , \qquad \Delta u_y = u_x \Delta\theta \ . \tag{10}$$

It is readily verified that the mean square local velocity $u_x^2 + u_y^2$ is unchanged by this transformation.

Such a deflection will, in general, change the velocity v, measured relative to the point P. Equations (4), (7), and (9) may be combined to determine K in terms of u_x and u_y, yielding

$$K^2 = u_x^2 - \frac{\omega}{B} u_y^2 \, . \tag{11}$$

If transformation (10) is now used to find the change of K resulting from a deflection $\Delta\theta$, we have

$$K\Delta K = -\frac{A}{B} u_x u_y \Delta\theta \, . \tag{12}$$

To relate our results to observable quantities, we express K in terms of V^2, defined as half the mean square value of u, averaged around the star's orbit. Evidently

$$V^2 = \tfrac{1}{2}\left(\overline{u_x^2} + \overline{u_y^2}\right) = \tfrac{1}{4} K^2 \left(1 - \frac{B}{\omega}\right). \tag{13}$$

Hence

$$V\Delta V = \frac{A}{4B}\left(1 - \frac{B}{\omega}\right) u_x u_y \Delta\theta \, . \tag{14}$$

The mean value of ΔV in one revolution about the point P is zero. However, the mean square value of ΔV is not zero. If we let V_n be the value of V after n deflections, then

$$\overline{V_n^2} = \overline{\left(V_0 + \Delta V_1 + \Delta V_2 + \ldots + \Delta V_n\right)^2} \, , \tag{15}$$

$$= V_0^2 + \sum_{i=1}^{n} \overline{(\Delta V_i)^2} \, , \tag{16}$$

since the terms not involving squares of ΔV cancel out on averaging. If we denote by $\langle (\Delta V)^2 \rangle$ the mean sum of all the separate values $(\Delta V)^2$ within a unit time, then

$$\frac{d\overline{V^2}}{dt} = \langle (\Delta V)^2 \rangle \, . \tag{17}$$

The quantity $\langle (\Delta V)^2 \rangle$, a diffusion coefficient for the change in velocity, is equal to

$$\langle (\Delta V)^2 \rangle = \frac{1}{16 V^2}\left[\frac{A}{B}\left(1 - \frac{B}{\omega}\right)\right]^2 \overline{u_x^2 u_y^2 \langle (\Delta\theta)^2 \rangle} \, , \tag{18}$$

where the horizontal bar denotes an average around the star's orbit. The quantity $\langle(\Delta\theta)^2\rangle$, the sum of all the mean square deflections per second, may be taken from Chandrasekhar,[7] and we have

$$\langle(\Delta\theta)^2\rangle = \frac{4\pi G^2 n_c m_c^2 \ln a}{u^3}, \tag{19}$$

where n_c and m_c are, respectively, the number of clouds per unit volume and the mass of each cloud.

The quantity u^2 is again the local velocity, equal to $u_x^2 + u_y^2$, while, as in Paper I, the term $\ln a$ may be set equal to 3. We may substitute from equations (4), (7), and (9) for u_x and u_y, and express K in terms of V by means of equation (13). If we also assume that, for all the stars in a group, V has a Maxwellian distribution, with root-mean-square value V_m (neglecting u_z again), we obtain

$$\langle(\Delta V_m)^2\rangle = \frac{\pi^{3/2} G^2 n_c m_c^2 \ln a}{2V_m} F\left(\frac{B}{\omega}\right), \tag{20}$$

where

$$F\left(\frac{B}{\omega}\right) = -\frac{\omega}{B}\left(1-\frac{B^2}{\omega^2}\right)^2\left(1-\frac{B}{\omega}\right)^{-1/2} \times \frac{2}{\pi}\int_0^{\pi/2} \frac{\sin^2\theta\cos^2\theta\, d\theta}{(\sin^2\theta - B\cos^2\theta/\omega)^{3/2}}. \tag{21}$$

The integral in equation (21) may be evaluated directly, if the denominator is expanded as a series in $1 + B/\omega$, and we obtain

$$F\left(\frac{B}{\omega}\right) = -\frac{\omega}{8B}\left(1-\frac{B^2}{\omega^2}\right)^2\left(1-\frac{B}{\omega}\right)^{-1/2} G\left(1+\frac{B}{\omega}\right), \tag{22}$$

where

$$G(x) = 1 + \frac{3}{4}x + \frac{75}{128}x^2 + \frac{245}{512}x^3 + \frac{6615}{16{,}384}x^4 + \dots . \tag{23}$$

In the extreme case of an inverse-square force field, $1 + B/\omega$ is 0.75, and the series in equation (23) converges very slowly. A numerical integration in this case gives

$$G(0.75) = 2.48 . \tag{24}$$

If equation (20) is now substituted in equation (17), averaged over all stars in the group, we may integrate at once. If $V_m(0)$ denotes the value of V_m at time zero, we have

$$V_m = V_m(0)\left(1+\frac{t}{t_E}\right)^{1/3}, \tag{25}$$

where

$$t_E = \frac{4V_m^3(0)}{3\pi^{3/2}G^2 n_c m_c^2 \ln a\, F(B/\omega)}. \tag{26}$$

Equation (25) is clearly only approximate, since the distribution of stellar velocities will not remain exactly Maxwellian even if it is so initially; more accurately, one should compute the distribution function $f(V)$ as in Paper I. However, the results of Paper I indicate that results obtained on the assumption of a Maxwellian distribution are remarkably close to the truth.

---

[7] *Principles of Stellar Dynamics* (Chicago: University of Chicago Press, 1942), eq. (5.724). This equation must be divided by 2, since deflections in the z direction are not considered here. The quantity $H(x_0)$ is unity, since the clouds are stationary and both j and x_0 are, therefore, infinite.

III. APPLICATION TO OBSERVED VELOCITIES

The observations of V for stars near the sun are summarized in Table 4 of Paper I. We discuss the extent to which the theory in the preceding section may be used to explain these observations.

In the neighborhood of the sun, the values of A and B are[8] about 0.021 km/sec psc, and -0.007 km/sec psc. Thus ω is about 0.028 km/sec psc, or 0.9×10^{-15} sec^{-1}, while $-B/\omega$ is 0.25, the value corresponding to an inverse-square field of force. Combining equations (22) and (24), we see that the corresponding value of $F(B/\omega)$ is 0.98.

We have seen in Paper I that, if the increase of velocity along the main sequence is to be explained as an age effect, the value of V for the F stars—about 20 km/sec—must be attained in half the age of the universe, or about 1.5×10^9 years. If $V_m(0)$ is assumed to be 10 km/sec, we compute from equation (25) that t_E must equal about 2×10^8 years. If this value of t_E is inserted in equation (26) and the product $n_c m_c$ is set equal to 3×10^{-24} gm/cm^3, we find

$$m_c = 4.9 \times 10^5 m_{\odot}\,, \tag{27}$$

or about one-half the value found in Paper I. If we assume that only half the interstellar medium is concentrated in such clouds, with the rest distributed somewhat more uniformly, m_c will increase to $9.8 \times 10^5 m_{\odot}$. Evidently, m_c must be about $10^6 m_{\odot}$ if star-cloud encounters are to have an appreciable effect. If the density in such a massive cloud, or cloud complex, corresponds to 15 H atoms/cm^3, the radius[9] of such a cloud will be about 100 parsecs. The mean distance between centers of neighboring clouds, if the interstellar medium were infinite and homogeneous, would be about 350 parsecs.

It is evident that with such large cloud complexes the analysis in Section II is not exactly applicable for two reasons. In the first place, the spacing between the clouds is about equal to the thickness of the Galaxy. In the second place, the size of the clouds and the spacing between them are not so very much smaller than the size of the star orbits. As we have already seen, if K is 10 km/sec, corresponding to a value of 5.6 km/sec for V, then the major and minor axes of the orbit, given by $-K/B$ and $K/(-B\omega)^{1/2}$, are equal to 1400 and 700 parsecs, respectively. We investigate in a rough way the modifications required by these two effects.

One may readily compute $(\Delta\theta)^2$ for a star moving in a plane, encountering clouds which are all situated in the same plane. If n_c' is the density of such clouds per unit area and a is the radius of a cloud, then, if we ignore encounters in which the star passes through the cloud (for which the distance of closest approach is less than a), we find

$$\langle (\Delta\theta)^2 \rangle = \frac{8G^2 n_c' m_c^2}{a u^3}\,. \tag{28}$$

The ratio of equation (28) to equation (19) is simply $2n_c'/\pi a n_c \ln \alpha$. Since $n_c'/a n_c$ is somewhere between 2 and 5, this ratio is not far from unity. Hence the difference between equations (28) and (19) does not have a major effect on the increase of stellar velocity in the galactic plane, although this difference must be considered in a more precise analysis.

If deflections perpendicular to the plane are considered, a quite different result is found. In the idealized two-dimensional picture, all deflections are in the galactic plane, and the velocities in the z direction, perpendicular to the galactic plane, are not affected by the star-cloud encounters. A more realistic analysis would yield some increase of these z velocities, but certainly less than is found in the simple three-dimensional picture, where velocities parallel and perpendicular to the plane are affected equally. Hence we see that the theory yields a simple qualitative explanation of the persistence of low z velocities in the older stars.

---

[8] J. H. Oort, *Ap. J.*, **116**, 233, 1952.

[9] Paper I incorrectly gives 100 parsecs for the diameter, instead of the radius, of a cloud complex with a mass of $10^6 m_{\odot}$.

The second effect to be considered is the large size of the cloud complexes relative to the stellar orbits. If the minimum distance of closest approach to be considered is 100 parsecs, the curvature of the star's orbit is certainly not negligible during an encounter. A detailed analysis, taking into account the motion of the star in an elliptical orbit, would be complicated. It would seem that such a more realistic analysis would give a somewhat more rapid rate of deflection of a star. This result follows, in part, from the fact that for clouds outside the star's orbit the differential galactic rotation will reduce the relative velocity between star and cloud, in the y direction, and thus lengthen the time during which the star is accelerated by a single cloud. However, it seems unlikely that these effects would decrease m_c to much less than half the value in equation (27), and we shall neglect this change.

IV. CONCLUSION

The results in Paper I were somewhat speculative, since it was uncertain whether such massive cloud complexes could behave as single dynamical entities, with the assumed root-mean-square velocity of some 10 km/sec. The present analysis indicates that the presence of differential galactic rotation makes the random velocities of the cloud complexes irrelevant. Acceleration of type I stars during times of 3×10^9 years will be important if density fluctuations exist in the interstellar medium with a scale of not less than about 300 parsecs and with an amplitude of fluctuation equal to an appreciable fraction of the mean density. Such density fluctuations need have no coherent structure and need not even be stable.

The large fluctuations of obscuration observed in the Milky Way over relatively large regions strongly suggest that inhomogeneities of the type required by the present theory are, in fact, present. The authors have taken as a working hypothesis the picture that type I stars, or "cloud stars," are forming continuously from interstellar matter and that the mean age of all type I stars later than spectral type F is about 1.5×10^9 years. Even if this hypothesis should not be substantiated in detail, it now appears likely that large-scale fluctuations in density of the interstellar medium are responsible, at least in part, for the increase of velocity dispersion with advancing spectral type along the main sequence.

MAGNETIC FIELDS IN SPIRAL ARMS

S. Chandrasekhar and E. Fermi
University of Chicago

Received March 23, 1953

ABSTRACT

In this paper two independent methods are described for estimating the magnetic field in the spiral arm in which we are located. The first method is based on an interpretation of the dispersion (of the order of 10°) in the observed planes of polarization of the light of the distant stars; it leads to an estimate of $H = 7.2 \times 10^{-6}$ gauss. The second method is based on the requirement of equilibrium of the spiral arm with respect to lateral expansion and contraction: it leads to an estimate of $H = 6 \times 10^{-6}$ gauss.

The hypothesis of the existence of a magnetic field in galactic space[1] has received some confirmation by Hiltner's[2] observation of the polarization of the light of the distant stars. It seems plausible that this polarization is due to a magnetic orientation of the interstellar dust particles;[3] for such an orientation would lead to different amounts of absorption of light polarized parallel and perpendicular to the magnetic field and, therefore, to a polarization of the light reaching us. On this interpretation of the interstellar polarization we should expect to observe no polarization in the general direction of the magnetic lines of force and a maximum polarization in a direction normal to the lines of force. And if we interpret from this point of view the maps[4] of the polarization effect as a function of the direction of observation, it appears that the direction of the galactic magnetic field is roughly parallel to the direction of the spiral arm in which we are located. In this paper we shall discuss some further consequences of this interpretation of interstellar polarization, in an attempt to arrive at an estimate of the strength of the interstellar magnetic field.

As we observe distant stars in a direction approximately perpendicular to the spiral arm, it appears that the direction of polarization is only approximately parallel to the arm. There are indeed quite appreciable and apparently irregular fluctuations in the direction of polarization of the distant stars.[4] This would indicate that the magnetic lines of force are not strictly straight and that they may be better described as "wavy" lines. The mean angular deviation of the plane of polarization from the direction of the spiral arm appears to be about $\alpha = 0.2$ radians.[4] There must clearly be a relation between this angle, α, and the strength of the magnetic field, H. For, if the magnetic field were sufficiently strong, the lines of force would be quite straight and α would be very small; on the other hand, if the magnetic field were sufficiently weak, the lines of force would be dragged around in various directions by the turbulent motions of the gas masses in the spiral arm and α would be large. To obtain the general relation between α and H, we proceed as follows:

The velocity of the transverse magneto-hydrodynamic wave is given by

$$V = \frac{H}{\sqrt{(4\pi\rho)}}, \tag{1}$$

---

[1] E. Fermi, *Phys. Rev.*, **75**, 1169, 1949.

[2] W. A. Hiltner, *Ap. J.*, **109**, 471, 1949.

[3] Of the two theories which have been proposed (L. Spitzer and J. W. Tukey, *Ap. J.*, **114**, 187, 1951, and L. Davis and J. L. Greenstein, *Ap. J.*, **114**, 206, 1951), that by Davis and Greenstein appears to be in better accord with the facts.

[4] W. A. Hiltner, *Ap. J.*, **114**, 241, 1951.

where ρ is the density of the diffused matter. In computing the velocity, V, we should not include in ρ the average density due to the stars, since the stars may be presumed to move across the lines of force without appreciable interaction with them, whereas the diffused matter in the form of both gas and dust has a sufficiently high electrical conductivity to be effectively attached to the magnetic lines of force in such a way that only longitudinal relative displacements are possible.

According to equation (1), the transverse oscillations of a particular line of force can be described by an equation of the form

$$y = a \cos k\,(x - Vt)\,, \tag{2}$$

where x is a longitudinal co-ordinate and y represents the lateral displacement. We take the derivatives of y with respect to x and t and obtain

$$y' = -\,ak \sin k\,(x - Vt)$$

and

$$\dot{y} = -\,akV \sin k\,(x - Vt)\,. \tag{3}$$

From these equations it follows that

$$V^2\overline{y'^2} = \overline{\dot{y}^2}\,. \tag{4}$$

The lateral velocity of the lines of force must be equal to the lateral velocity of the turbulent gas. If v denotes the root-mean-square velocity of the turbulent motion, we should have

$$\overline{\dot{y}^2} = \tfrac{1}{3}\,v^2\,. \tag{5}$$

The factor $\frac{1}{3}$ arises from the fact that only one component of the velocity is effective in shifting the lines of force in the y-direction. The quantity y', on the other hand, represents the deviation of the line of force from a straight line projected on the plane of view. Hence,

$$\overline{y'^2} = \alpha^2\,. \tag{6}$$

Now, combining equations (1), (4), (5), and (6), we obtain

$$H = (\tfrac{4}{3}\pi\rho)^{1/2}\,\frac{v}{\alpha}\,. \tag{7}$$

In equation (7) we shall substitute the following numerical values, which appear to describe approximately the conditions prevailing in the spiral arm in which we are located:[5]

$$\rho = 2 \times 10^{-24}\ \mathrm{gm/cm^3},\quad v = 5 \times 10^5\ \mathrm{cm/sec},\ \text{and}\ \alpha = 0.2\ \text{radians}. \tag{8}$$

With these values equation (7) gives

$$H = 7.2 \times 10^{-6}\ \text{gauss}. \tag{9}$$

An alternative procedure for estimating the intensity of the magnetic field is based on the requirement of equilibrium of the spiral arm with respect to lateral expansion and contraction. As an order of magnitude, we may expect to obtain the condition for this equilibrium by equating the gravitational pressure in the spiral arm to the sum of the material pressure and the pressure due to the magnetic field. In computing the gravitational pressure, we should allow for the gravitational force due to all the mass present, i.e., of the stars as well as of the diffused matter. We are interested, however, in computing the gravitational pressure exerted on the diffused matter only. Assuming for simplicity that the spiral arm is a cylinder of radius R with uniform density, one finds for the gravitational pressure:

---

[5] For ρ, the estimate of J. H. Oort (cf. *Ap. J.*, **116**, 233, 1952) from observations of the 21-cm line is used; while the value of v adopted is that of A. Blaauw, *B.A.N.*, **11**, 405, 1952.

$$p_{\mathrm{grav}} = \pi G \rho \rho_t R^2 \,, \tag{10}$$

where G denotes the constant of gravitation, ρ is the density of the diffused matter only, and ρ_t is the total mean density, including the contribution of the stars. The kinetic pressure of the turbulent gas is given by

$$p_{\mathrm{kin}} = \tfrac{1}{3} \rho v^2 \tag{11}$$

while the magnetic pressure is given by

$$p_{\mathrm{mag}} = \frac{H^2}{8\pi} \,. \tag{12}$$

And for the equilibrium we must have

$$p_{\mathrm{grav}} = p_{\mathrm{kin}} + p_{\mathrm{mag}} \,. \tag{13}$$

In computing p_{grav} we shall assume a radius of the spiral arm of 250 parsecs or $R = 7.7 \times 10^{20}$ cm. As before, we shall take $\rho = 2 \times 10^{-24}$ gm/cm^3; and for ρ_t we shall assume[6] 6×10^{-24} gm/cm^3. For these values of R, ρ, and ρ_t equation (9) gives $p_{\mathrm{grav}} = 1.5 \times 10^{-12}$ dynes, while p_{kin} computed with the values already given is 0.2×10^{-12} dynes. We attribute the difference to the magnetic pressure. Hence

$$\frac{H^2}{8\pi} = 1.3 \times 10^{-12} \,, \tag{14}$$

or

$$H = 6 \times 10^{-6} \text{ gauss.} \tag{15}$$

The two independent methods of estimating H therefore agree in giving essentially the same value for the field strength. A field of about 7×10^{-6} gauss indicated by these estimates is ten times smaller than that which Davis and Greenstein[3] have estimated as necessary for producing an adequate orientation of the dust particles to account for the interstellar polarization. If the present estimate of 7×10^{-6} gauss is correct, one should conclude that the mechanism of orientation is somewhat more effective than has been assumed by Davis and Greenstein.

Since this paper was written, our attention has been drawn to the fact that the idea underlying the first of the two methods by which we estimate the magnetic field in the spiral arm is contained in an earlier paper by Leverett Davis, Jr. (*Phys. Rev.*, **81,** 890, 1951). We are sorry that we were not aware of this paper when we wrote ours. However, since with the better estimates of the astronomical parameters now available the value of H derived is a great deal different from Davis' value and since further the value we have derived is in accord with our second independent estimate, we have allowed the paper to stand in its original form.

---

[6] Cf. J. H. Oort, *Ap. J.*, **116,** 233, 1952.

PROBLEMS OF GRAVITATIONAL STABILITY IN THE PRESENCE OF A MAGNETIC FIELD

S. Chandrasekhar and E. Fermi
University of Chicago

Received March 23, 1953

ABSTRACT

In this paper a number of problems are considered which are related to the gravitational stability of cosmical masses of infinite electrical conductivity in which there is a prevalent magnetic field. In Section I the virial theorem is extended to include the magnetic terms in the equations of motion, and it is shown that when the magnetic energy exceeds the numerical value of the gravitational potential energy, the configuration becomes dynamically unstable. It is suggested that the relatively long periods of the magnetic variables may be due to the magnetic energy of these stars approaching the limit set by the virial theorem. In Section II the adiabatic radial pulsations of an infinite cylinder along the axis of which a magnetic field is acting is considered. An explicit expression for the period is obtained. Section III is devoted to an investigation of the stability for transverse oscillations of an infinite cylinder of incompressible fluid when there is a uniform magnetic field acting in the direction of the axis. It is shown that the cylinder is unstable for all periodic deformations of the boundary with wave lengths exceeding a certain critical value, depending on the strength of the field. The wave length of maximum instability is also determined. It is found that the magnetic field has a stabilizing effect both in increasing the wave length of maximum instability and in prolonging the time needed for the instability to manifest itself. For a cylinder of radius $R = 250$ parsecs and $\rho = 2 \times 10^{-24}$ gm/cm^3 a magnetic field in excess of 7×10^{-6} gauss effectively removes the instability. In Section IV it is shown that a fluid sphere with a uniform magnetic field inside and a dipole field outside is not a configuration of equilibrium and that it will tend to become oblate by contracting in the direction of the field. Finally, in Section V the gravitational instability of an infinite homogeneous medium in the presence of a magnetic field is considered, and it is shown that Jeans's condition is unaffected by the presence of the field.

1. *Introduction.*—In this paper we shall consider a number of problems relating to the dynamical and gravitational stability of cosmical masses in which there is a prevalent magnetic field. In the discussion of these problems, the assumption will be made that the medium is effectively of infinite electrical conductivity. This latter assumption implies only that the conductivity is large enough for the magnetic lines of force to be considered as practically attached to the matter during the length of time under consideration; it has been known for some time that this is the case in most astronomical connections.[1]

The abstract gives an adequate summary of the paper.

I. THE VIRIAL THEOREM AND THE CONDITION FOR DYNAMICAL STABILITY

2. *The virial theorem.*—In a subject such as this it is perhaps best that we start by establishing theorems of the widest possible generality. The extension of the virial theorem to include the forces derived from the prevailing magnetic field provides such a starting point. We shall see that under conditions of equilibrium this extension of the virial theorem leads to the relation

$$2T + 3(\gamma - 1)\mathfrak{U} + \mathfrak{M} + \Omega = 0 \tag{1}$$

between the kinetic energy (T) of mass motion, the heat energy ($\mathfrak{U}$) of molecular motion, the magnetic energy ($\mathfrak{M}$) of the prevailing field, and the gravitational potential energy (Ω), where γ denotes the ratio of the specific heats. That a relation of the form (1) should exist is readily understood: For the balance between the pressures p_{kin}, p_{gas}, and p_{mag} due to the visible motions, the molecular motions, and the magnetic field, on the one hand, and the gravitational pressure, p_{grav}, on the other, requires

---

[1] Cf. L. Biermann, *Annual Review of Nuclear Science*, 2 (Stanford: Annual Reviews, Inc., 1953), 349.

$$p_{\mathrm{kin}} + p_{\mathrm{gas}} + p_{\mathrm{mag}} = p_{\mathrm{grav}} \,, \tag{2}$$

while the order of magnitudes of these pressures are given by

$$p_{\mathrm{kin}} = c_1 \frac{T}{V} \,, \qquad p_{\mathrm{gas}} = c_2 \frac{\mathfrak{U}}{V} \,, \qquad p_{\mathrm{mag}} = \frac{H^2}{8\pi} = c_3 \frac{\mathfrak{M}}{V} \,, \tag{3}$$

and

$$p_{\mathrm{grav}} = \text{Density} \times \text{gravity} \times \text{linear dimension} = -\, c_4 \frac{\Omega}{V} \,, \tag{3a}$$

where V denotes the volume of the configuration and c_1, c_2, c_3, and c_4 are numerical constants. A relation of the form (1) is therefore clearly implied. We now proceed to establish the exact relation (1).

With the usual assumptions of hydromagnetics, the equations of motion governing an inviscid fluid can be written in the form

$$\rho \frac{d u_i}{dt} = -\frac{\partial}{\partial x_i}\left(p + \frac{|\boldsymbol{H}|^2}{8\pi}\right) + \rho \frac{\partial V}{\partial x_i} + \frac{1}{4\pi} \frac{\partial}{\partial x_j} H_i H_j \,, \tag{4}$$

where ρ denotes the density, p the pressure, V the gravitational potential, and $\boldsymbol{H}$ the intensity of the magnetic field. (In eq. [1] and in the sequel, summation over repeated indices is to be understood.)

Multiply equation (4) by x_i and integrate over the volume of the configuration. Reducing the left-hand side of the equation in the usual manner, we find

$$\begin{aligned} \iiint \rho x_i \frac{d u_i}{dt}\, dx_1 dx_2 dx_3 &= \int_0^M x_i \frac{d^2 x_i}{dt^2}\, dm \\ &= \frac{1}{2} \frac{d^2}{dt^2} \int_0^M r^2 dm - \int_0^M |\boldsymbol{u}|^2 dm \,, \end{aligned} \tag{5}$$

where $dm = \rho dx_1 dx_2 dx_3$ and the integration is effected over the entire mass, M, of the configuration. Letting

$$I = \int_0^M r^2 dm \qquad \text{and} \qquad T = \frac{1}{2} \int |\boldsymbol{u}|^2 dm \tag{6}$$

denote the moment of inertia and the kinetic energy of mass motion, respectively, we have

$$\begin{aligned} \frac{1}{2} \frac{d^2 I}{dt^2} - 2T = &- \iiint x_i \frac{\partial}{\partial x_i}\left(p + \frac{|\boldsymbol{H}|^2}{8\pi}\right) dx_1 dx_2 dx_3 \\ &+ \frac{1}{4\pi} \iiint x_i \frac{\partial}{\partial x_j} H_i H_j\, dx_1 dx_2 dx_3 + \int_0^M x_i \frac{\partial V}{\partial x_i}\, dm \,. \end{aligned} \tag{7}$$

The last of the three integrals on the right-hand side of this equation represents the gravitational potential energy, Ω, of the configuration. The remaining two volume integrals can be reduced by integration by parts. Thus the first of the two integrals gives

$$\begin{aligned} &- \iiint x_i \frac{\partial}{\partial x_i}\left(p + \frac{|\boldsymbol{H}|^2}{8\pi}\right) dx_1 dx_2 dx_3 \\ &\qquad = -\int \left(p + \frac{|\boldsymbol{H}|^2}{8\pi}\right) \boldsymbol{r} \cdot d\boldsymbol{S} + 3 \iiint \left(p + \frac{|\boldsymbol{H}|^2}{8\pi}\right) dx_1 dx_2 dx_3 \,. \end{aligned} \tag{8}$$

The surface integral (over $d\boldsymbol{S}$) vanishes, since the pressure (including the magnetic pressure $|\boldsymbol{H}|^2/8\pi$) must vanish on the boundary of the configuration; and the volume integral over p and $|\boldsymbol{H}|^2/8\pi$ is readily expressible in terms of the internal energy ($\mathfrak{U}$) and the magnetic energy ($\mathfrak{M}$) of the configuration. Thus we have

$$-\iiint x_i \frac{\partial}{\partial x_i}\left(p+\frac{|\boldsymbol{H}|^2}{8\pi}\right) dx_1 dx_2 dx_3 = 3(\gamma-1)\mathfrak{U}+3\mathfrak{M}\,, \tag{9}$$

where γ denotes the ratio of the specific heats. In the same way the second volume integral in equation (7) gives

$$\frac{1}{4\pi}\iiint x_i \frac{\partial}{\partial x_j} H_i H_j \, dx_1 dx_2 dx_3 = -2\mathfrak{M}\,. \tag{10}$$

Now, combining equations (7), (9), and (10), we have

$$\frac{1}{2}\frac{d^2 I}{dt^2} = 2T + 3(\gamma-1)\mathfrak{U} + \mathfrak{M} + \Omega\,. \tag{11}$$

This is the required generalization of the virial theorem; it differs from the usual one only in the appearance of $\mathfrak{M} + \Omega$ in place of Ω.

3. *The condition for dynamical stability.*—If the configuration is one of equilibrium, then it follows from the virial theorem that

$$3(\gamma-1)\mathfrak{U} + \mathfrak{M} + \Omega = 0\,. \tag{12}$$

On the other hand, the total energy, $\mathfrak{E}$, of the configuration is given by

$$\mathfrak{E} = \mathfrak{U} + \mathfrak{M} + \Omega\,. \tag{13}$$

Eliminating $\mathfrak{U}$ between equations (12) and (13), we obtain

$$\mathfrak{E} = -\frac{3\gamma-4}{3(\gamma-1)}\left(|\Omega| - \mathfrak{M}\right). \tag{14}$$

From this equation for the total energy it follows that *a necessary condition for the dynamical stability of an equilibrium configuration is*

$$(3\gamma-4)(|\Omega| - \mathfrak{M}) > 0\,. \tag{15}$$

Thus, even when $\gamma > \frac{4}{3}$ (the condition for dynamical stability in the absence of a magnetic field) a sufficiently strong internal magnetic field can induce dynamical instability in the configuration. In fact, according to formula (15), the condition for dynamical stability, when $\gamma > \frac{4}{3}$, is

$$\mathfrak{M} = \frac{1}{8\pi}\iiint |\boldsymbol{H}|^2 dx_1 dx_2 dx_3 = \tfrac{1}{6}R^3 (H^2)_{\text{av}} < |\Omega|\,, \tag{16}$$

where $(H^2)_{\text{av}}$ denotes the mean square magnetic field.

For a spherical configuration of uniform density,

$$\Omega = -\frac{3}{5}\frac{GM^2}{R}\,, \tag{17}$$

where M is its mass, R is its radius, and G is the constant of gravitation. We can use this expression for Ω to estimate the limit imposed by the virial theorem on the magnetic fields which can prevail. On expressing M and R in units of the solar mass and the solar radius, we find from equations (16) and (17) that

$$\sqrt{(H^2)_{\mathrm{av}}} < 2.0 \times 10^8 \frac{M}{R^2} \text{ gauss} . \tag{18}$$

For the peculiar A stars for which Babcock has found magnetic fields of the order of 10^4 gauss, we may estimate that

$$M \simeq 4\odot \qquad \text{and} \qquad R \simeq 5R_\odot \qquad \text{(A star)}; \tag{19}$$

and expression (18) gives

$$\sqrt{(H^2)_{\mathrm{av}}} < 3 \times 10^7 \text{ gauss} \qquad \text{(A stars)}. \tag{19a}$$

Of greater interest is the limit set by expression (18) for an S-type star for which Babcock has found a variable magnetic field of the order of 1000 gauss. For an S-type star we can estimate that

$$M \simeq 15\odot \qquad \text{and} \qquad \mathrm{R} \simeq 300R_\odot \qquad \text{(S star)}; \tag{20}$$

and (18) now gives

$$\sqrt{(H^2)_{\mathrm{av}}} < 3 \times 10^4 \text{ gauss} \qquad \text{(S star)}. \tag{20a}$$

Thus the limit set by (18) is seen to be two to three orders of magnitude larger than the surface fields observed by Babcock. However, the fields in the interior may be much stronger than the surface fields; and it is even possible that the actual root-mean-square fields in these stars are near their maximum values. Indeed, from the fact that the periods of the magnetic variables are long compared with the adiabatic pulsation periods they would have if they were nonmagnetic, we may surmise that $\sqrt{(H^2)_{\mathrm{av}}}$ is near the limit set by (18); for, as is well known, we may lengthen the period of the lowest mode of oscillation of a system by approaching the limit of dynamical stability; and we can accomplish this by letting $\mathfrak{M} \rightarrow |\Omega|$.

Note added June 17.—Since we wrote this paper, Dr. Babcock has informed us that he has measured a variable magnetic field (+2000 to −1200 gauss) for the star VV Cephei. It has been estimated that for this star $M = 100\odot$ and $R = 2600R_\odot$. With these values, inequality (18) gives $\sqrt{(H^2)_{\mathrm{av}}} < 3000$ gauss. We may conclude that this star must be on the verge of dynamical stability and, anticipating the result established in Section IV, probably highly oblate.

4. *The virial theorem for an infinite cylindrical distribution of matter.*—Some care is needed in applying the results of §§ 2 and 3 to a distribution of matter which can be idealized as an infinite cylinder (such as, for example, a spiral arm); for the potential energy per unit length of an infinite cylinder is infinite. For this reason it is perhaps best that we consider the problem *de novo.*

We shall consider, then, an infinite cylinder in which the prevailing magnetic field is in the direction of the axis of the cylinder; and we shall suppose that all the variables are functions only of the distance r from the axis of the cylinder. Under these conditions the equations of motion reduce to the single one

$$\rho \frac{d u_r}{d t} = -\frac{\partial}{\partial r}\left(p + \frac{H^2}{8\pi}\right) - \frac{2 G m(r)}{r} \rho , \tag{21}$$

where $m(r)$ is the mass per unit length interior to r.

Multiplying equation (21) by $2\pi r^2 dr$ and integrating over the entire range of r, we find in the usual manner that

$$\frac{1}{2} \frac{d^2}{d t^2} \int_0^M r^2 d m - \int_0^M \left(\frac{d r}{d t}\right)^2 d m = 2(\gamma - 1)\mathfrak{U} + 2\mathfrak{M} - G M^2 , \tag{22}$$

where M denotes the mass per unit length of the cylinder and $\mathfrak{U}$ and $\mathfrak{M}$ are the kinetic and the magnetic energies per unit length of the cylinder, respectively.

From equation (22) it follows that, under equilibrium conditions, we should have

$$2(\gamma-1)\mathfrak{U}+2\mathfrak{M}-GM^2=0\,. \tag{23}$$

A necessary condition for equilibrium to obtain is, therefore,

$$\mathfrak{M}<\tfrac{1}{2}GM^2\,. \tag{24}$$

We can rewrite the condition (24) alternatively in the form

$$\mathfrak{M}=\frac{1}{4}\int_0^R H^2 r\,d r=\tfrac{1}{8}\,(H^2)_{\text{av}}R^2<\tfrac{1}{2}\pi^2R^4\bar{\rho}^2G\,, \tag{25}$$

or

$$\sqrt{(H^2)_{\text{av}}}<2\pi R\bar{\rho}G\,. \tag{25a}$$

This last condition on the root-mean-square field is essentially equivalent to one of the formulae used in the preceding paper[2] (eq. [13]) for estimating the magnetic field in the spiral arm; the difference between the two formulae arises from the fact that in that paper the gravitational attraction was not limited to the interstellar gas only; allowance was also made for the stars contributing to the gravitational force acting on the gas.

II. THE RADIAL PULSATIONS OF AN INFINITE CYLINDER

5. *The pulsation equation.*—In view of the inconclusive nature of the current treatments[3] of the adiabatic pulsations of magnetic stars, it is perhaps of interest to see how the corresponding problem in infinite cylinders can be fully solved. We consider, then, the radial pulsation of an infinite cylinder, along the axis of which there is a prevailing magnetic field.

Choosing the time t and the mass per unit length, $m(r)$, interior to r, as the independent variables, we can write the equations of continuity and motion in the forms

$$\frac{\partial}{\partial m}(\pi r^2)=\frac{1}{\rho} \tag{26}$$

and

$$\frac{\partial^2 r}{\partial t^2}=-2\pi r\frac{\partial P}{\partial m}-\frac{2Gm(r)}{r}\,, \tag{27}$$

where

$$P=p+\frac{H^2}{8\pi} \tag{28}$$

denotes the total pressure. Distinguishing the values of the various parameters for the equilibrium configuration by a subscript zero and writing

$$r=r_0+\delta r,\qquad P=P_0+\delta P,\qquad \rho=\rho_0+\delta\rho,\ \text{etc.} \tag{29}$$

we find that the equations governing radial oscillations of small amplitudes are

$$\frac{\partial}{\partial m}(2\pi r_0\delta r)=-\frac{\delta\rho}{\rho_0^2} \tag{30}$$

and

$$\frac{\partial^2}{\partial t^2}\delta r=-2\pi\delta r\frac{\partial P_0}{\partial m}-2\pi r_0\frac{\partial}{\partial m}\delta P+\frac{2Gm}{r_0^2}\delta r\,. \tag{31}$$

[2] *Ap. J.*, **118**, 113, 1953.

[3] M. Schwarzschild, *Ann. d'ap.*, **12**, 148, 1949; G. Gjellestad, *Rep. No. 1, Inst. Ther. Ap.* (Oslo, 1950), and *Ann. d'ap.*, **15**, 276, 1952; V. C. A. Ferraro and D. J. Memory, *M.N.*, **112**, 361, 1952; T. G. Cowling, *M.N.*, **112**, 527, 1952.

Using the equation

$$2\pi r_0 \frac{\partial P_0}{\partial m} = -\frac{2Gm}{r_0}, \tag{32}$$

which must obtain in equilibrium, we can rewrite equation (31) in the form

$$\frac{\partial^2}{\partial t^2}\,\delta r = -2\pi r_0 \frac{\partial}{\partial m}\,\delta P + \frac{4Gm}{r_0^2}\,\delta r\,. \tag{33}$$

We shall now evaluate δP. For an adiabatic pulsation,

$$\delta P = \delta p + \frac{\boldsymbol{H}_0 \cdot \delta \boldsymbol{H}}{4\pi} = \gamma\,\frac{p_0}{\rho_0}\,\delta\rho + \frac{\boldsymbol{H}_0 \cdot \delta \boldsymbol{H}}{4\pi}\,. \tag{34}$$

Now when the medium is of infinite electrical conductivity, the change, $\Delta \boldsymbol{H}$, *at a given point* in a prevailing magnetic field, $\boldsymbol{H}_0$, caused by a displacement $\delta \boldsymbol{r}$, is given quite generally by

$$\Delta \boldsymbol{H} = \operatorname{curl}\,(\delta \boldsymbol{r} \times \boldsymbol{H}_0)\,. \tag{35}$$

This relation is derived in § 14 below (see eq. [130]); but we may note here that it merely expresses the fact that the changes in the magnetic field are simply a consequence of the lines of force being pushed aside. According to equation (35), the change in the magnetic field, $\delta \boldsymbol{H}$, *as we follow the motion*, is given by

$$\delta \boldsymbol{H} = \operatorname{curl}\,(\delta \boldsymbol{r} \times \boldsymbol{H}_0) + (\delta \boldsymbol{r}\cdot\operatorname{grad})\,\boldsymbol{H}_0\,. \tag{36}$$

When $\boldsymbol{H}_0$ is in the z-direction and $\delta \boldsymbol{r}$ is radial, the only nonvanishing component of $\delta \boldsymbol{H}$ is

$$\delta H_z = -\frac{1}{r}\frac{\partial}{\partial r}(H_0 r\,\delta r) + \delta r\,\frac{\partial H_0}{\partial r} = -\frac{H_0}{r}\frac{\partial}{\partial r}(r\,\delta r)\,, \tag{37}$$

in the z-direction. Hence in the case under consideration

$$\frac{\boldsymbol{H}_0 \cdot \delta \boldsymbol{H}}{4\pi} = -\frac{H_0^2 \rho_0}{4\pi}\frac{\partial}{\partial m}(2\pi r_0\,\delta r)\,, \tag{38}$$

and the expression for δP becomes

$$\delta P = -\left(\gamma p_0 + \frac{H_0^2}{4\pi}\right)\rho_0 \frac{\partial}{\partial m}(2\pi r_0\,\delta r)\,, \tag{39}$$

where we have substituted for $\delta\rho$ in equation (34) in accordance with equation (30).

With δP given by equation (38), equation (33) takes the form

$$\frac{\partial^2}{\partial t^2}\,\delta r = 4\pi^2 r\,\frac{\partial}{\partial m}\left\{\left(\gamma p + \frac{H^2}{4\pi}\right)\rho\,\frac{\partial}{\partial m}(r\,\delta r)\right\} + \frac{4Gm}{r^2}\,\delta r\,. \tag{40}$$

In writing equation (39), we have suppressed the subscripts zero distinguishing the equilibrium configuration, since there is no longer any cause for ambiguity.

When all the physical variables vary with time like $e^{i\sigma t}$, equation (39) reduces to

$$\left(\sigma^2 + \frac{4Gm}{r^2}\right)\delta r = -4\pi^2 r\,\frac{d}{dm}\left\{\left(\gamma p + \frac{H^2}{4\pi}\right)\rho\,\frac{d}{dm}(r\,\delta r)\right\}, \tag{41}$$

where δr has now the meaning of an amplitude.

The boundary conditions,

$$\delta r = 0 \quad \text{at} \quad m = 0 \quad \text{and} \quad \delta P = 0 \quad \text{at} \quad m = M\,, \tag{42}$$

in conjunction with the pulsation equation (40) will determine for σ^2 a sequence of possible characteristic values, σ_k^2. And it can be readily shown that the solutions, δr_k, belonging to the different characteristic values, are orthogonal:

$$\int_0^M \delta r_k \delta r_l d m = 0 \qquad (k \neq l)\,. \tag{43}$$

In view of this orthogonality of the functions δr_k, we should expect that the characteristic values themselves could be determined by a variational method. The basis for this method is developed in the following section.

6. *An integral formula for σ^2 and a variational method for determining it.*—Multiply equation (41) by δr and integrate over the range of m, i.e., from 0 to M. We obtain

$$\sigma^2 \int_0^M (\delta r)^2 d m + 4G \int_0^M \left(\frac{\delta r}{r}\right)^2 d m = -4\pi^2 \int_0^M r\,\delta r \frac{d}{d m}\left\{\left(\gamma p + \frac{H^2}{4\pi}\right)\rho \frac{d}{d m}(r\,\delta r)\right\} d m\,. \tag{44}$$

By integrating by parts the integral on the right-hand side, we obtain

$$\sigma^2 \int_0^M (\delta r)^2 d m + 4G \int_0^M \left(\frac{\delta r}{r}\right)^2 d m = 4\pi^2 \int_0^M \left(\gamma p + \frac{H^2}{4\pi}\right)\rho \left[\frac{d}{d m}(r\,\delta r)\right]^2 d m\,. \tag{45}$$

Writing $p = (P - H^2/8\pi)$ in equation (45), we obtain, after some elementary reductions,

$$\sigma^2 \int_0^M (\delta r)^2 d m = \gamma \int_0^M \frac{P}{\rho}\left[\frac{1}{r}\frac{d}{d r}(r\,\delta r)\right]^2 d m - 4G \int_0^M \left(\frac{\delta r}{r}\right)^2 m\, d m + \frac{1}{8\pi}(2-\gamma)\int_0^M \frac{H^2}{\rho}\left[\frac{1}{r}\frac{d}{d r}(r\,\delta r)\right]^2 d m\,. \tag{46}$$

It can be shown that the foregoing equations give a minimum value for σ^2 when the true solution δr belonging to the lowest characteristic value of the pulsation equation is substituted; and any other function δr (satisfying the boundary conditions) will give a larger value for σ^2. These facts can clearly be made the basis of a variational procedure for determining σ^2.

In the theory of the adiabatic pulsations of ordinary stars, it is known[4] that we get a very good estimate of σ^2 (for the fundamental mode) by setting

$$\delta r = \text{Constant}\ r\,, \tag{47}$$

in an integral formula for σ^2 similar to equation (46). We shall assume that this will continue to be the case in our present problem. Therefore, making the substitution (47) in equation (46), we obtain

$$\sigma^2 \int_0^M r^2 d m = 4\gamma \int_0^M \frac{P}{\rho} d m - 2GM^2 + (2-\gamma)\int_0^R H^2 r\, d r\,. \tag{48}$$

---

[4] P. Ledoux and C. L. Pekeris, *Ap. J.*, **94**, 124 1941.

On the other hand,

$$\int_0^M \frac{P}{\rho}\, dm = 2\pi \int_0^R P r\, dr = -\pi \int_0^R r^2 \frac{dP}{dr}\, dr = G \int_0^M m\, dm = \tfrac{1}{2} G M^2 . \tag{49}$$

Hence

$$\sigma^2 \int_0^M r^2 dm = 2(\gamma - 1) G M^2 + (2 - \gamma) \int_0^R H^2 r\, dr . \tag{50}$$

An alternative form of this equation is (cf. eq. [23])

$$\begin{aligned} \sigma^2 \int_0^M r^2 dm &= 4(\gamma - 1)\left[\tfrac{1}{2} G M^2 - \mathfrak{M}\right] + 4\mathfrak{M} \\ &= 4\left[(\gamma - 1)^2 \mathfrak{U} + \mathfrak{M}\right] . \end{aligned} \tag{51}$$

III. THE GRAVITATIONAL INSTABILITY OF AN INFINITELY LONG CYLINDER WHEN A CONSTANT MAGNETIC FIELD IS ACTING IN THE DIRECTION OF THE AXIS

7. *The formulation of the problem.*—In Section II we have seen that an infinitely long cylinder in which there is a prevalent magnetic field in the direction of the axis is stable for radial oscillations. But the question was left open as to whether the cylinder may not be unstable for transverse or for longitudinal oscillations. In Section III we shall take up the discussion of the transverse oscillations; however, in order not to complicate an already difficult problem, we shall restrict ourselves to the case when the medium is incompressible in addition to being an infinitely good electrical conductor.

We picture to ourselves, then, an infinite cylinder of uniform circular cross-section of radius R_0, along the axis of which a constant magnetic field of intensity H_0 is acting. Since any transverse perturbation can be expressed as a superposition of waves of different wave lengths, the question of stability can be investigated by considering, individually, perturbations of different wave lengths. We suppose, then, that the cylinder is subject to a perturbation, the result of which is to deform the boundary into

$$r = R + a \cos kz . \tag{52}$$

Since the fluid is assumed to be incompressible, the mass per unit length must be the same before and after the deformation; this, clearly, requires that

$$R_0^2 = R^2 + \tfrac{1}{2} a^2 . \tag{53}$$

We shall see that, as a result of the deformation, the mean field in the z-direction is also changed by an amount of order a^2 (see eq. [87] below).

The investigation of the stability of the cylinder consists of two parts. First, we must calculate the change in the potential energy, $\Delta\Omega$, and the magnetic energy, $\Delta\mathfrak{M}$, per unit length resulting from the perturbation. Then, depending on whether $\Delta\Omega + \Delta\mathfrak{M}$ is positive or negative, we shall have stability or instability. We shall see presently that $\Delta\Omega + \Delta\mathfrak{M} < 0$ for all k less than a certain determinate value depending on H_0. In other words, the cylinder is unstable for all wave lengths exceeding a certain critical value λ_*. The determination of λ_* is the first problem in the investigation of stability. The second problem concerns the specification of the wave number k_m (say) for which the instability will develop at the maximum rate. We can determine this mode of maximum instability by considering the amplitude of the deformation (cf. eq. [52]) as a function of time, constructing a Lagrangian for the cylinder and determining the manner of increase of the amplitudes of the unstable modes. We shall find that whenever $\lambda > \lambda_*$ (or $k < k_*$), the amplitude increases like e^{qt}, where q is a function of k (and H_0). The mode of maximum instability is clearly the one which makes q (for a given H) a maximum.

Before proceeding to the details of the calculations, we may state that the method we have described derives from an early investigation of Rayleigh's[5] on the stability of liquid jets.

8. *The change in the potential energy per unit length caused by the deformation.*—Following the outline given in § 7, we shall first calculate the change in the potential energy, $\Delta\Omega$, per unit length caused by the deformation which makes the cross-section change from one of a constant radius R_0 to one whose boundary is given by equation (52). Since the potential energy per unit length of an infinite cylinder is infinite, the evaluation of $\Delta\Omega$ requires some care. We proceed as follows:

Let U and V denote the external and the internal gravitational potentials of the deformed cylinder. They satisfy the equations

$$\nabla^2 U = 0 \qquad \text{and} \qquad \nabla^2 V = -4\pi G\rho\,. \tag{54}$$

We shall first solve these equations to the first order in the amplitude a appropriately for the problem on hand. The solutions must clearly be of the forms

$$U = -2\pi G\rho R^2 \log r + aAK_0(kr)\cos kz + c_0 \tag{55}$$

and

$$V = -\pi G\rho r^2 + aBI_0(kr)\cos kz\,, \tag{55a}$$

where c_0 is an additive constant (with which we need not further concern ourselves), A and B are constants to be determined, and I_n and K_n are the Bessel functions of order n for a purely imaginary argument, which have no singularity at the origin and at infinity, respectively.

The constants A and B in solutions (55) are to be determined by the condition that U and V and $\partial U/\partial r$ and $\partial V/\partial r$ must be continuous on the boundary (52). Carrying out the calculations consistently to the first order in a, we find that the continuity conditions require

$$A\,K_0(kR) = B\,I_0(kR) \tag{56}$$

and

$$A\,K_1(kR) + B\,I_1(kR) = \frac{4\pi G\rho}{k}\,. \tag{56a}$$

Solving these equations, we find

$$A = 4\pi G\rho R I_0(kR) \qquad \text{and} \qquad B = 4\pi G\rho R K_0(kR)\,. \tag{57}$$

The required solution for V is, therefore,

$$V = -\pi G\rho r^2 + 4\pi G\rho R\, aK_0(kR)I_0(kr)\cos kz + O(a^2). \tag{58}$$

Now suppose that the amplitude of the deformation is increased by an *infinitesimal* amount from a to $a + \delta a$. The change in the potential energy, $\delta\Delta\Omega$, consequent to this infinitesimal increase in the amplitude, can be determined by evaluating the work done in the redistribution of the matter required to increase the amplitude. For evaluating this latter work, it is necessary to specify in a quantitative manner the redistribution which takes place; and we shall now do this.

An arbitrary deformation of an incompressible fluid can be thought of as resulting from a displacement $\boldsymbol{\xi}$ applied to each point of the fluid. The assumed incompressibility of the medium requires that div $\boldsymbol{\xi} = 0$; and, since no loss of generality is implied by supposing that the displacement is irrotational, we shall write

$$\boldsymbol{\xi} = \text{grad}\,\psi, \tag{59}$$

---

[5] Lord Rayleigh, *Scientific Papers* (Cambridge: At the University Press, 1900), **2**, 361; also *Theory of Sound* ("Dover Reprints" [New York, 1945]), **2**, 350–362.

and require that

$$\nabla^2\psi = 0. \tag{60}$$

A solution of equation (60) which is suitable for considering the deformation of a uniform cylinder into one whose boundary is given by (52) is

$$\psi = AI_0(kr)\cos kz, \tag{61}$$

where A is a constant. The corresponding radial and z-components of $\boldsymbol{\xi}$ are

$$\xi_r = AkI_1(kr)\cos kz \quad \text{and} \quad \xi_z = -AkI_0(kr)\sin kz. \tag{62}$$

Since at $r = R$, ξ_r must reduce to $a\cos kz$ (cf. eq. [52]), we must have

$$A = \frac{a}{kI_1(kR)}. \tag{63}$$

The displacements,

$$\xi_r = a\frac{I_1(kr)}{I_1(kR)}\cos kz \quad \text{and} \quad \xi_z = -a\frac{I_0(kr)}{I_1(kR)}\sin kz, \tag{64}$$

applied to each point of the cylinder will deform it into the required shape. The displacement $\delta\boldsymbol{\xi}$, which must be applied to increase the amplitude from a to $a + \delta a$, is therefore,

$$\delta\xi_r = \delta a\frac{I_1(kr)}{I_1(kR)}\cos kz \quad \text{and} \quad \delta\xi_z = -\delta a\frac{I_0(kr)}{I_1(kR)}\sin kz. \tag{65}$$

The change in the potential energy, $\delta\Delta\Omega$, per unit length involved in the infinitesimal deformation (65) can be obtained by integrating over the whole cylinder the work done by the displacement $\delta\boldsymbol{\xi}$ in the force field specified by the gravitational potential (58). It is therefore given by

$$\delta\Delta\Omega = -2\pi\rho\left\{\int_0^{R+a\cos kz}\delta\boldsymbol{\xi}\cdot\operatorname{grad}V\,r\,dr\right\}_{\text{av}}, \tag{66}$$

where the averaging is to be done with respect to z. Substituting for V and $\delta\boldsymbol{\xi}$ from equations (58) and (65), we obtain

$$\begin{aligned}\delta\Delta\Omega = -2\pi\rho\,\delta a\Bigg\{&\int_0^{R+a\cos kz}\cos kz\frac{I_1(kr)}{I_1(kR)}[-2\pi G\rho r\\ &+4\pi\rho GRakK_0(kR)I_1(kr)\cos kz]\,r\,dr\\ &+\int_0^{R+a\cos kz}\sin kz\frac{I_0(kr)}{I_1(kR)}[4\pi\rho GRakK_0(kR)I_0(kr)\sin kz]\,r\,dr\Bigg\}_{\text{av}}.\end{aligned} \tag{67}$$

Evaluating the foregoing expression consistently to the first order in a, we find

$$\delta\Delta\Omega = 2\pi^2\rho^2GR^2a\,\delta a - 4\pi^2\rho^2GRa\,\delta a\frac{kK_0(kR)}{I_1(kR)}\int_0^R[I_1^2(kr)+I_0^2(kr)]\,r\,dr, \tag{68}$$

or, using the readily verifiable result,

$$\int_0^R[I_1^2(kr)+I_0^2(kr)]\,r\,dr = \frac{R}{k}I_0(kR)\,I_1(kR), \tag{69}$$

we have

$$\delta\Delta\Omega = 4\pi^2\rho^2GR^2[\tfrac{1}{2} - I_0(x)K_0(x)]a\,\delta a, \tag{70}$$

where for the sake of brevity we have written

$$x = kR\,. \tag{71}$$

Finally, integrating equation (70) over a from 0 to a, we obtain

$$\Delta\Omega = 2\pi^2\rho^2 G R^2[\tfrac{1}{2} - I_0(x)K_0(x)]a^2\,. \tag{72}$$

This is the required expression for the change in the potential energy per unit length caused by the deformation.

9. *The change in the magnetic energy per unit length caused by the deformation.*—The changes in the magnetic field inside the cylinder can best be determined from the condition that the magnetic induction across any section normal to the axis of the cylinder must remain unaffected by the deformation. This condition follows from the assumed infinite electrical conductivity of the medium. Thus, if

$$H\mathbf{1}_z + \boldsymbol{h} \tag{73}$$

represents the magnetic field inside the cylinder (where $\mathbf{1}_z$ is a unit vector in the z-direction, $\boldsymbol{h}$ is a field, of order a, varying periodically with z, and H is the mean field), we must require that

$$N = \int_0^R H_0\, r\, d r = \int_0^{R + a\cos kz} (H + h_z)\, r\, d r = \text{Constant}\,. \tag{74}$$

Turning to the determination of H and $\boldsymbol{h}$, we may first observe that $\boldsymbol{h}$ can be derived from a magnetostatic potential ϕ satisfying the equation $\nabla^2\phi = 0$. For the problem on hand we can represent ϕ as a series in powers of a of the form

$$\phi = \sum_{n=1}^{\infty} \frac{a^n A_n}{nk} I_0(nkr) \sin nkz\,, \tag{75}$$

where the A_n's are constants to be determined. Retaining terms up to the second order in a, we have

$$h_r = aA_1 I_1(kr)\sin kz + a^2 A_2 I_1(2kr)\sin 2kz \tag{76}$$

and

$$h_z = aA_1 I_0(kr)\cos kz + a^2 A_2 I_0(2kr)\cos 2kz\,, \tag{77}$$

for the components of $\boldsymbol{h}$.

With h_z given by equation (77), the magnetic induction across a normal section of the cylinder is given by

$$N = \int_0^{R + a\cos kz} \{H + aA_1 I_0(kr)\cos kz + a^2 A_2 I_0(2kr)\cos 2kz\}\, r\, d r\,. \tag{78}$$

Evaluating N correct to the second order in a, we obtain

$$\begin{aligned} N = \tfrac{1}{2}H(R^2 + \tfrac{1}{2}a^2) + \tfrac{1}{2}a^2 A_1 R I_0(kR) + a\Big[HR + \frac{A_1}{k} I_1(kR)R\Big]\cos kz \\ + a^2\Big[\tfrac{1}{4}H + \tfrac{1}{2}A_1 R I_0(kR) + \frac{A_2}{2k} R I_1(2kR)\Big]\cos 2kz\,; \end{aligned} \tag{79}$$

and according to equation (74) this must be identically equal to (cf. eq. [53])

$$\tfrac{1}{2}H_0 R_0^2 = \tfrac{1}{2}H_0(R^2 + \tfrac{1}{2}a^2)\,. \tag{80}$$

Hence we must require that

$$\tfrac{1}{2}H(R^2+\tfrac{1}{2}a^2)+\tfrac{1}{2}a^2A_1RI_0(kR)=\tfrac{1}{2}H_0(R^2+\tfrac{1}{2}a^2)\,, \tag{81}$$

$$HR+\frac{A_1}{k}I_1(kR)R=0\,, \tag{82}$$

and

$$\tfrac{1}{4}H+\tfrac{1}{2}A_1RI_0(kR)+\frac{A_2}{2k}RI_1(2kR)=0\,. \tag{83}$$

From equations (82) and (83) we find:

$$A_1=-\frac{H}{R}\,\frac{x}{I_1(x)} \tag{84}$$

and

$$A_2=\frac{H}{R^2}\,\frac{x}{I_1(2x)}\left\{\frac{xI_0(x)}{I_1(x)}-\frac{1}{2}\right\}, \tag{85}$$

where $x=kR$ (cf. eq. [71]).

With A_1 given by equation (84), equation (81) gives (correct to order a^2)

$$H_0=H\left\{1-\frac{a^2}{R^2}\,\frac{xI_0(x)}{I_1(x)}\right\}, \tag{86}$$

or, equivalently,

$$H=H_0\left\{1+\frac{a^2}{R^2}\,\frac{xI_0(x)}{I_1(x)}\right\}. \tag{87}$$

This equation shows that the mean field inside the deformed cylinder is larger than that in the undeformed cylinder; the difference is of order a^2 and depends on the wave number of the deformation.

Equations (76), (77), (84), (85), and (87) determine the field inside the cylinder correct to the second order in a. It may be noted here that the same solution can also be derived from the alternative (but equivalent) condition that the magnetic lines of force follow the boundary of the cylinder (52).

With the field inside the cylinder determined, we can now evaluate the magnetic energy, $\mathfrak{M}$, per unit length. We have

$$\begin{aligned}\mathfrak{M}&=\frac{1}{4}\left\{\int_0^{R+a\cos kz}|\boldsymbol{H}|^2\,r\,dr\right\}_{\text{av}}\\&=\frac{1}{4}\left\{\int_0^{R+a\cos kz}(H^2+2Hh_z+h_z^2+h_r^2)\,r\,dr\right\}_{\text{av}}\,,\end{aligned} \tag{88}$$

where the averaging is to be done with respect to z. Substituting for h_r and h_z from equations (76) and (77) and evaluating $\mathfrak{M}$ correct to the second order in a, we obtain (cf. eq. [69])

$$\begin{aligned}\mathfrak{M}=&\tfrac{1}{8}H^2(R^2+\tfrac{1}{2}a^2)+\tfrac{1}{2}aH\left\{\cos kz\int_0^{R+a\cos kz}A_1I_0(kr)\,r\,dr\right\}_{\text{av}}\\&+\tfrac{1}{2}a^2HA_2\left\{\cos 2kz\int_0^{R+a\cos kz}I_0(2kr)\,r\,dr\right\}_{\text{av}}\\&+\tfrac{1}{8}a^2A_1^2\int_0^R[I_0^2(kr)+I_1^2(kr)]\,r\,dr\\=&\tfrac{1}{8}H^2(R^2+\tfrac{1}{2}a^2)+\tfrac{1}{4}a^2HA_1RI_0(kR)+\tfrac{1}{8}a^2A_1^2\frac{R}{k}I_0(kR)\,I_1(kR)\,.\end{aligned} \tag{89}$$

On making further use of equations (53), (84), and (87), we can reduce this last expression for $\mathfrak{M}$ to the form

$$\mathfrak{M} = \tfrac{1}{8} H_0^2 R_0^2 + \tfrac{1}{8} a^2 H^2 \frac{x I_0(x)}{I_1(x)} . \tag{90}$$

But the magnetic energy per unit length of the undeformed cylinder is $\frac{1}{8}H_0^2R_0^2$. Hence

$$\Delta \mathfrak{M} = \tfrac{1}{8} a^2 H^2 \frac{x I_0(x)}{I_1(x)} . \tag{91}$$

10. *The modes of deformation which are unstable.*—Combining the results of §§ 8 and 9, we have

$$\Delta\Omega + \Delta\mathfrak{M} = \left\{ 2\pi^2 \rho^2 G R^2 \left[\tfrac{1}{2} - I_0(x) K_0(x) \right] + \tfrac{1}{8} H^2 \frac{x I_0(x)}{I_1(x)} \right\} a^2 . \tag{92}$$

Letting

$$H_s^2 = 16\pi^2 \rho^2 R^2 G \qquad \text{or} \qquad H_s = 4\pi\rho R \sqrt{G} , \tag{93}$$

we can rewrite equation (92) more conveniently in the form

$$\Delta\Omega + \Delta\mathfrak{M} = 2\pi^2 \rho^2 R^2 G \left\{ \left[\tfrac{1}{2} - I_0(x) K_0(x) \right] + \frac{x I_0(x)}{I_1(x)} \left(\frac{H}{H_s} \right)^2 \right\} a^2 . \tag{94}$$

Whether the mode of deformation considered is stable or unstable will depend upon the sign of the quantity in braces in the foregoing expression.

Now the asymptotic behaviors of the Bessel functions which appear in equation (94) are:

$$I_0(x) \to 1, \quad I_1(x) \to \tfrac{1}{2}x, \quad \text{and} \quad K_0(x) \to -(\gamma + \log \tfrac{1}{2}x) \quad (x \to 0) , \tag{95}$$

where γ (not to be confused with the ratio of the specific heats) is Euler's constant 0.5772 . . . , and

$$I_0(x) \to \frac{e^x}{(2\pi x)^{1/2}} , \quad I_1(x) \to \frac{e^x}{(2\pi x)^{1/2}} , \quad \text{and} \quad K_0(x) \to \left(\frac{\pi}{2x} \right)^{1/2} e^{-x} \quad (x \to \infty) . \tag{96}$$

Hence $\Delta\Omega$ (cf. eq. [72]) tends to minus infinity logarithmically as $x \to 0$ and tends monotonically to the positive limit $\pi^2\rho^2R^2G$ as $x \to \infty$, while $\Delta\mathfrak{M}$ (cf. eq. [91]) tends to the positive limit $\frac{1}{4}a^2H^2$ as $x \to 0$ and increases monotonically to infinity (linearly) as $x \to \infty$. These behaviors of $\Delta\Omega$ and $\Delta\mathfrak{M}$ are illustrated in Figure 1, in which the functions $[\frac{1}{2} - I_0(x)K_0(x)]$ and $xI_0(x)/I_1(x)$ are plotted.

From the asymptotic behaviors of $\Delta\Omega$ and $\Delta\mathfrak{M}$ it follows that the equation

$$\tfrac{1}{2} - I_0(x) K_0(x) + \frac{x I_0(x)}{I_1(x)} \left(\frac{H}{H_s} \right)^2 = 0 \tag{97}$$

allows a single positive root. Let $x = x_*$ denote this root. Then

$$\Delta\Omega + \Delta\mathfrak{M} > 0 \qquad \text{for} \qquad x > x_* , \tag{98}$$

and

$$\Delta\Omega + \Delta\mathfrak{M} < 0 \qquad \text{for} \qquad x < x_* . \tag{98a}$$

Hence *all modes of deformation with $x < x_*$ are unstable*. Since $x = kR$, x_* specifies the minimum wave number (in units of $1/R$) for a stable deformation; alternatively, we could also say that *all modes of deformation with wave lengths exceeding*

$$\lambda_* = \frac{2\pi R}{x_*} \tag{99}$$

are unstable.

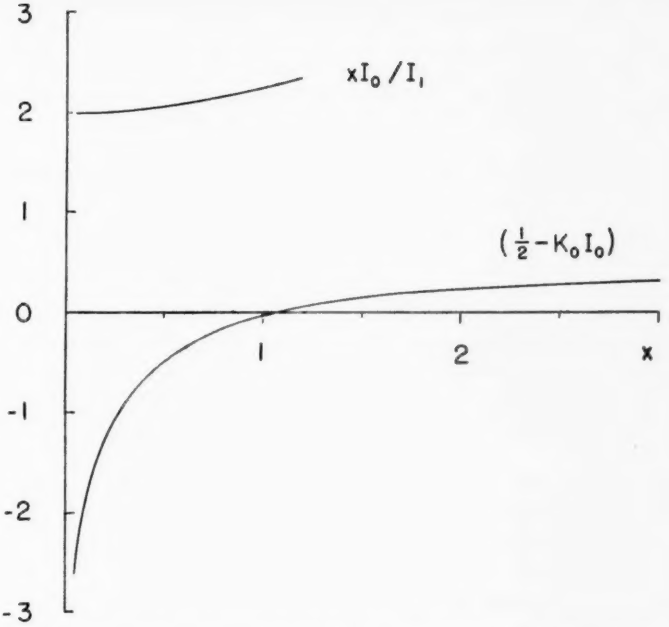

FIG. 1.—The dependence of the changes in the potential energy, $\Delta\Omega$, and magnetic energy, $\Delta\mathfrak{M}$, per unit length of an infinitely long cylinder on the wave number of the deformation; $\Delta\Omega$ is proportional to $[\frac{1}{2} - I_0(x)K_0(x)]$, while $\Delta\mathfrak{M}$ is proportional to $xI_0(x)/I_1(x)$, where x is the wave number measured in the unit $1/R$.

TABLE 1

DEPENDENCE OF WAVE NUMBERS x_* AND x_m AT WHICH INSTABILITY FIRST SETS IN AND AT WHICH IT IS MAXIMUM, ON PREVAILING MAGNETIC FIELD

H/H_s	x_*	x_m	$q_m/(4\pi G\rho)^{1/2}$
0	1.067	0.58	0.246
0.25	0.832	.47	.208
0.50	0.480	.28	.133
0.75	0.232	.14	.0685
1.00	0.092	.057	.0281
1.25	0.0299	.0182	.0091
1.50	0.00757	.00459	.00229
2.00	0.000228	0.000139	0.0000693

In Table 1 we have listed x_* for a few values of H/H_s. This table exhibits the strong stabilizing effect of the magnetic field: this is shown in the present connection by the very rapid increase, with increasing H, of the wave length at which instability sets in. In fact, for $H > H_s$ this increase becomes exponential; this can be shown in the following way: Since $x_* = 0.092$ already for $H = H_s$, for $H > H_s$ we may replace the Bessel functions which occur in equation (97) by their dominant terms for $x \to 0$; thus,

$$\tfrac{1}{2} + \gamma + \log \tfrac{1}{2} x_* + 2\left(\frac{H}{H_s}\right)^2 = 0 \qquad (H > H_s)\,. \tag{100}$$

Hence

$$x_* = 2 \exp\left\{ -\left[\gamma + \tfrac{1}{2} + 2\left(\frac{H}{H_s}\right)^2\right]\right\} \qquad (H > H_s)\,, \tag{101}$$

or, numerically,

$$x_* = 0.6811\, e^{-2(H/H_s)^2} \qquad (H > H_s)\,. \tag{102}$$

11. *The mode of maximum instability.*—In the preceding section we have seen that an infinite cylinder is gravitationally unstable for all modes of deformation with wave lengths exceeding a certain critical value. We shall now show that there exists a wave length for which the instability is a maximum. For this purpose we shall suppose that the amplitude, a, of the deformation is a function of time and seek an equation of motion for it.

We have already seen that the potential energy (gravitational plus magnetic) per unit length of the cylinder measured from the equilibrium state is

$$\mathfrak{V} = \Delta\mathfrak{M} + \Delta\Omega = -2\pi^2\rho^2R^2GF(x)a^2\,, \tag{103}$$

where

$$F(x) = I_0(x)\,K_0(x) - \tfrac{1}{2} - \left(\frac{H}{H_s}\right)^2 \frac{x\,I_0(x)}{I_1(x)}\,. \tag{104}$$

Defined in this manner, $F(x) > 0$ for $x < x_*$, i.e., it is positive for all unstable modes and negative for all stable modes.

To obtain the Lagrangian function for the cylinder, we must find the kinetic energy of the motion resulting from the varying amplitude. Since we have assumed that the fluid is incompressible, a velocity potential, ψ, exists which satisfies Laplace's equation. And the solution for the velocity potential appropriate to the problem on hand is

$$\psi = BI_0(kr)\cos kz\,, \tag{105}$$

where B is a constant to be determined. The components of the velocity derived from the foregoing potential are

$$u_r = \frac{\partial\psi}{\partial r} = +BkI_1(kr)\cos kz \tag{106}$$

and

$$u_z = \frac{\partial\psi}{\partial z} = -BkI_0(kr)\sin kz\,. \tag{106a}$$

The constant of proportionality, B, in the foregoing equations must be determined from the condition that the radial velocity, u_r, at $r = R$ must agree with that implied by equation (52); i.e., we should have

$$BkI_1(kR)\cos kz = \frac{da}{dt}\cos kz\,. \tag{107}$$

Hence

$$B = \frac{1}{kI_1(x)}\,\frac{da}{dt}\,. \tag{108}$$

From equations (106) we obtain, for the kinetic energy per unit length, the expression (cf. eq. [69])

$$\begin{aligned}\mathfrak{T} &= \tfrac{1}{2}\pi\rho B^2 k^2 \int_0^R [\, I_0^2(kr) + I_1^2(kr)\,]\, r\, dr \\ &= \tfrac{1}{2}\pi\rho B^2 k^2 \frac{R}{k}\, I_0(x)\, I_1(x)\,,\end{aligned} \tag{109}$$

or, substituting for B from equation (108), we have

$$\mathfrak{T} = \tfrac{1}{2}\pi\rho R^2 \frac{I_0(x)}{x\, I_1(x)} \left(\frac{da}{dt}\right)^2 . \tag{110}$$

The Lagrangian function (per unit length) for the infinite cylinder is therefore given by

$$\mathfrak{L} = \mathfrak{T} - \mathfrak{V} = \tfrac{1}{2}\pi\rho R^2 \frac{I_0(x)}{x\, I_1(x)} \left(\frac{da}{dt}\right)^2 + 2\pi^2\rho^2 R^2 G F(x)\, a^2 . \tag{111}$$

The equation of motion for a derived from the Lagrangian (111) is

$$\pi\rho R^2 \frac{I_0(x)}{x\, I_1(x)} \frac{d^2 a}{dt^2} = 4\pi^2\rho^2 R^2 G F(x)\, a\,, \tag{112}$$

or, alternatively,

$$\frac{d^2 a}{dt^2} = 4\pi G\rho \left\{ \frac{x\, I_1(x)}{I_0(x)} [\, I_0(x)\, K_0(x) - \tfrac{1}{2}\,] - \left(\frac{H}{H_s}\right)^2 x^2 \right\} a\,, \tag{113}$$

where we have substituted for $F(x)$ in accordance with equation (104). The solution for a is therefore of the form

$$a = \text{Constant}\; e^{\pm qt}\,, \tag{114}$$

where

$$q^2 = 4\pi G\rho \left\{ \frac{x\, I_1(x)}{I_0(x)} [\, I_0(x)\, K_0(x) - \tfrac{1}{2}\,] - \left(\frac{H}{H_s}\right)^2 x^2 \right\} . \tag{115}$$

Accordingly, q is purely imaginary for $x > x_*$ and is real for $x < x_*$; this is in agreement with the fact that all modes with $x > x_*$ are stable, while all modes with $x < x_*$ are unstable.

As defined by equation (115), $q = 0$ both for $x = 0$ and for $x = x_*$. There is, therefore, a determinate intermediate value of x—say, x_m—for which q attains a maximum—say, q_m. *The wave number x_m clearly represents the mode of maximum instability;* for it is the mode for which the amplitude of the deformation increases most rapidly. The wave length

$$\lambda_m = \frac{2\pi R}{x_m}\,, \tag{116}$$

corresponding to the wave number x_m, gives approximately the length of the "pieces" into which the cylinder will ultimately break up: for the component with the wave length λ_m, in the Fourier analysis of an arbitrary perturbation, is the one whose amplitude will increase most rapidly with time and, therefore, represents the mode in which the instability will first assert itself. Finally, it is clear that $1/q_m$ gives a measure of the time needed for the instability to make itself manifest.

In Table 1 the values of x_m and $q_m/(4\pi G\rho)^{1/2}$ are also listed. As in the case of x_* (§ 10), we can give explicit formulae for x_m and q_m for $H > H_s$. Since for $H > H_s$ we are concerned only with values of $x \ll 1$, we may replace the Bessel functions which occur in the expression for q^2 by their dominant terms for $x \rightarrow 0$. Thus

$$q^2 = 4\pi G\rho \left\{ -\tfrac{1}{2}x^2\left(\gamma + \tfrac{1}{2} + \log \tfrac{1}{2}x\right) - x^2\left(\frac{H}{H_s}\right)^2 \right\} \qquad (H > H_s) \,. \tag{117}$$

The expression on the right-hand side attains its maximum when

$$\left(\gamma + \tfrac{1}{2} + \log \tfrac{1}{2}x\right) + \tfrac{1}{2} + 2\left(\frac{H}{H_s}\right)^2 = 0 \,. \tag{118}$$

Hence

$$x_m = 2 \exp \left\{ -(\gamma + 1) - 2\left(\frac{H}{H_s}\right)^2 \right\} = 0.4131\, e^{-2(H/H_s)^2} \qquad (H > H_s) \,. \tag{119}$$

The corresponding expression for q_m is

$$q_m = \tfrac{1}{2}x_m(4\pi G\rho)^{1/2} \qquad (H > H_s) \,. \tag{120}$$

These formulae emphasize the fact, apparent from an examination of Table 1, that, as the strength of the magnetic field increases, not only does the wave length of the mode of maximum instability increase exponentially, but the time needed for the instability to manifest itself also increases exponentially.

TABLE 2

WAVE LENGTHS λ_* AND λ_m AT WHICH INSTABILITY SETS IN AND AT WHICH IT IS MAXIMUM AND CHARACTERISTIC TIME, q_m^{-1}, NEEDED FOR INSTABILITY TO MANIFEST ITSELF FOR CASE $R = 250$ PARSECS AND $\rho = 2 \times 10^{-24}$ GM/CM³

H (Gauss)	λ_* (Parsecs)	λ_m (Parsecs)	q_m^{-1} (Years)
0	1.5×10^3	2.7×10^3	1.0×10^8
1.25×10^{-6}	1.9×10^3	3.3×10^3	1.2×10^8
2.5×10^{-6}	3.3×10^3	5.6×10^3	1.8×10^8
3.75×10^{-6}	6.8×10^3	1.1×10^4	3.6×10^8
5.0×10^{-6}	1.7×10^4	2.8×10^4	8.7×10^8
6.25×10^{-6}	5.2×10^4	8.6×10^4	2.7×10^9
7.5×10^{-6}	2.1×10^5	3.4×10^5	1.1×10^{10}
10.0×10^{-6}	6.9×10^6	1.1×10^7	3.5×10^{11}

12. *Numerical illustrations.*—To illustrate the theory developed in the preceding sections we shall take, as typical of a spiral arm of a galaxy,

$$R = 250 \text{ parsecs} \qquad \text{and} \qquad \rho = 2 \times 10^{-24} \text{ gm/cm}^3 \,. \tag{121}$$

The corresponding value of H_s is (cf. eq. [93])

$$H_s = 5.0 \times 10^{-6} \text{ gauss} \,. \tag{122}$$

For these values of the physical parameters, the nondimensional results given in Table 1 can be converted into astronomical measures; they are given in Table 2. From the values given in this table it follows that between $H = H_s$ and $H = 2H_s$ the characteristic time of the instability becomes so long that, for all practical purposes, the instability is effectively removed by the presence of the magnetic field.

IV. THE FLATTENING OF A GRAVITATING FLUID SPHERE UNDER THE INFLUENCE OF A MAGNETIC FIELD

13. *The formulation of the problem.*—In this section we shall consider the gravitational equilibrium of an incompressible fluid sphere with a uniform magnetic field inside and a dipole field outside. We shall show that under these circumstances the sphere is not a configuration of equilibrium and that it will become oblate by contracting along the axis of symmetry.

We suppose, then, that initially the magnetic field in the interior of the sphere is uniform and of intensity H in the z-direction. In spherical polar co-ordinates (r, θ, φ) the components of $\boldsymbol{H}$ in the radial (r) and the transverse (θ) directions are

$$H_r^{(i)} = H\mu \qquad \text{and} \qquad H_\theta^{(i)} = -H(1-\mu^2)^{1/2} \qquad (r < R), \tag{123}$$

where $\mu = \cos\theta$ and the superscript i indicates that these are the components of the field *inside* the sphere.

When the field inside the sphere is uniform, that outside the sphere must be a dipole field given by

$$H_r^{(e)} = H\left(\frac{R}{r}\right)^3 \mu \qquad \text{and} \qquad H_\theta^{(e)} = \tfrac{1}{2} H\left(\frac{R}{r}\right)^3 (1-\mu^2)^{1/2}, \tag{124}$$

where R denotes the radius of the sphere.

The energy, $\mathfrak{M}$, of the magnetic field specified by equations (123) and (124) is given by

$$\begin{aligned} \mathfrak{M} &= \frac{H^2}{8\pi}\left(\tfrac{4}{3}\pi R^3\right) + \tfrac{1}{4}H^2 \int_R^\infty \int_{-1}^{+1} \left(\frac{R}{r}\right)^6 \{\mu^2 + \tfrac{1}{4}(1-\mu^2)\} r^2 dr\, d\mu \\ &= \tfrac{1}{4}H^2R^3 . \end{aligned} \tag{125}$$

Let the sphere be now deformed in such a way that the equation of the bounding surface is

$$r(\mu) = R + \epsilon P_l(\mu), \tag{126}$$

where $\epsilon \ll R$, $\mu = \cos\theta$ (θ being the polar angle), and $P_l(\mu)$ denotes, as usual, the Legendre polynomial of order l. We shall call such a deformation of the sphere a "P_l-deformation." We shall investigate the stability of the sphere by examining whether or not it is stable to a P_l-deformation.

14. *The change in the magnetic energy of the sphere due to a P_l-deformation.*—As we have already pointed out in § 8, an arbitrary deformation of an incompressible body can be thought of as the result of applying to each point of the body a displacement $\boldsymbol{\xi}$. And if, as in § 8 (eqs. [59] and [60]), we express $\boldsymbol{\xi}$ as the gradient of a scalar function, ψ, the solution of Laplace's equation satisfied by ψ appropriate to a P_l-deformation of a sphere is

$$\psi = A r^l P_l(\mu), \tag{127}$$

where A is a constant. The corresponding expressions for the components of $\boldsymbol{\xi}$ are

$$\xi_r = \frac{\partial\psi}{\partial r} = A l r^{l-1} P_l(\mu) \tag{128}$$

and

$$\xi_\theta = \frac{1}{r}\frac{\partial\psi}{\partial\theta} = -A r^{l-1}(1-\mu^2)^{1/2} P_l'(\mu), \tag{128a}$$

where a prime is used to denote differentiation with respect to μ. According to equation (126), at $r = R$, $\xi_r = \epsilon P_l(\mu)$; this determines A, and we have

$$\xi_r = \epsilon \left(\frac{r}{R}\right)^{l-1} P_l(\mu) \quad \text{and} \quad \xi_\theta = -\frac{\epsilon}{l}\left(\frac{r}{R}\right)^{l-1} (1-\mu^2)^{1/2} P_l'(\mu) \,. \tag{129}$$

Now the deformation of a body will alter the prevailing magnetic field; and, since in a medium of infinite electrical conductivity a change in the existing magnetic field can be effected only by bodily pushing aside the lines of force, it follows that

$$\delta \boldsymbol{H} = \text{curl}\,(\boldsymbol{\xi} \times \boldsymbol{H}) \,. \tag{130}$$

[The truth of this last relation can be established in the following way: Suppose that the displacement $\boldsymbol{\xi}$ takes place as a slow continuous movement so that if $\boldsymbol{u}$ denotes the velocity, $\boldsymbol{u} = \partial \boldsymbol{\xi}/\partial t$ (i.e., if quantities of the second order of smallness are neglected). On the other hand, when the electrical conductivity is infinite,

$$\delta \boldsymbol{E} = -\boldsymbol{u} \times \boldsymbol{H} \,,$$

where $\delta \boldsymbol{E}$ is the electrical field resulting from the changing magnetic field $\delta \boldsymbol{H}$ in accordance with Maxwell's equation,

$$\text{curl}\ \delta \boldsymbol{E} = -\frac{\partial}{\partial t}\,\delta \boldsymbol{H} \,.$$

Combining the last two equations, we have

$$\text{curl}\left(\frac{\partial \boldsymbol{\xi}}{\partial t} \times \boldsymbol{H}\right) = \frac{\partial}{\partial t}(\delta \boldsymbol{H}) \,.$$

The relation (130) is simply the integrated form of this equation.]

When the fluid is incompressible (i.e., when div $\boldsymbol{\xi} = 0$ in addition to div $\boldsymbol{H} = 0$), equation (130) can be written alternatively in the form

$$\delta \boldsymbol{H} = (\boldsymbol{H}\cdot\text{grad})\boldsymbol{\xi} - (\boldsymbol{\xi}\cdot\text{grad})\boldsymbol{H} \,. \tag{131}$$

And when the initial field is homogeneous, equation (131) simplifies still further to

$$\delta \boldsymbol{H} = (\boldsymbol{H}\cdot\text{grad})\boldsymbol{\xi} \,. \tag{132}$$

In spherical polar co-ordinates the foregoing equation is equivalent to

$$\delta H_r = \left(H_r \frac{\partial}{\partial r} + \frac{H_\theta}{r}\frac{\partial}{\partial \theta}\right)\xi_r - \frac{H_\theta \xi_\theta}{r} \tag{133}$$

and

$$\delta H_\theta = \left(H_r \frac{\partial}{\partial r} + \frac{H_\theta}{r}\frac{\partial}{\partial \theta}\right)\xi_\theta + \frac{H_\theta \xi_r}{r} \,. \tag{133a}$$

These equations in conjunction with equations (123) and (129) give

$$\delta H_r^{(i)} = \epsilon H\,(l-1)\frac{r^{l-2}}{R^{l-1}} P_{l-1}(\mu) \tag{134}$$

and

$$\delta H_\theta^{(i)} = -\epsilon H \frac{r^{l-2}}{R^{l-1}}(1-\mu^2)^{1/2} P_{l-1}'(\mu) \,. \tag{134a}$$

The corresponding change in the internal magnetic energy density is given by

$$\begin{aligned}\delta\left(\frac{|\boldsymbol{H}|^2}{8\pi}\right) &= \frac{1}{4\pi}\,\boldsymbol{H}^{(i)}\cdot\delta\boldsymbol{H}^{(i)}\\ &= \epsilon\,\frac{H^2}{4\pi}\,\frac{r^{l-2}}{R^{l-1}}\left\{(l-1)\,\mu P_{l-1}(\mu)+(1-\mu^2)P'_{l-1}(\mu)\right\}.\end{aligned} \tag{135}$$

On further simplification this reduces to

$$\delta\left(\frac{|\boldsymbol{H}|^2}{8\pi}\right)=\epsilon\,(l-1)\,\frac{H^2}{4\pi}\,\frac{r^{l-2}}{R^{l-1}}\,P_{l-2}(\mu)\;. \tag{136}$$

Hence, when averaged over all directions, this is zero except when $l = 2$, in which case

$$\delta\left(\frac{|\boldsymbol{H}|^2}{8\pi}\right)=\frac{\epsilon}{4\pi}\,\frac{H^2}{R}\qquad (l=2)\,; \tag{137}$$

the corresponding change in the internal magnetic energy, $\Delta\mathfrak{M}^{(i)}$, is given by

$$\Delta\mathfrak{M}^{(i)} = \tfrac{1}{3}\epsilon H^2R^2\,. \tag{138}$$

15. *The change in the external magnetic energy of the sphere due to a P_l-deformation.*— Writing the magnetic field outside the deformed sphere in the form

$$H_r^{(e)} = H\left(\frac{R}{r}\right)^3\mu+\delta H_r^{(e)} \tag{139}$$

and

$$H_\theta^{(e)} = \tfrac{1}{2}H\left(\frac{R}{r}\right)^3(1-\mu^2)^{1/2}+\delta H_\theta^{(e)}\,, \tag{139a}$$

we shall suppose that $\delta H_r^{(e)}$ and $\delta H_\theta^{(e)}$ are derivable from a magnetic potential $\delta\phi^{(e)}$. Since the magnetic potential satisfies Laplace's equation, the solution for $\delta\phi^{(e)}$ must be expressible as a linear combination of the fundamental solutions $P_j(\mu)\ r^{j+1}$, which vanish at infinity.

We shall find it convenient to write the solution for $\delta\phi^{(e)}$ in the form

$$\delta\phi^{(e)} = -\epsilon H\left\{\frac{l-1}{l}\left(\frac{R}{r}\right)^l P_{l-1}(\mu)+\Sigma A_j\left(\frac{R}{r}\right)^{j+1}P_j(\mu)\right\}, \tag{140}$$

where the A_j's are coefficients to be determined. The expressions for $\delta H_r^{(e)}$ and $\delta H_\theta^{(e)}$ derived from this potential are

$$\delta H_r^{(e)} = \epsilon H\left\{(l-1)\,\frac{R^l}{r^{l+1}}\,P_{l-1}(\mu)+\Sigma A_j\,(j+1)\,\frac{R^{j+1}}{r^{j+2}}\,P_j(\mu)\right\} \tag{141}$$

and

$$\delta H_\theta^{(e)} = \epsilon H\left\{\frac{l-1}{l}\,\frac{R^l}{r^{l+1}}\,P^1_{l-1}(\mu)+\Sigma A_j\,\frac{R^{j+1}}{r^{j+2}}\,P^1_j(\mu)\right\}. \tag{141a}$$

The coefficients A_j in equations (141) and (141a) can be determined from the condition that the component of the magnetic field normal to a bounding surface must be continuous. To the first order in ϵ this condition requires that

$$\begin{aligned}\{H_r^{(e)}\}_{R+\epsilon P_l}+\{H_\theta^{(e)}\}_R\,\frac{\epsilon}{R}(1-\mu^2)^{1/2}\,\frac{\partial P_l}{\partial\mu}&\\ =\{H_r^{(i)}\}_{R+\epsilon P_l}+\{H_\theta^{(i)}\}_R\,\frac{\epsilon}{R}(1-\mu^2)^{1/2}\,\frac{\partial P_l}{\partial\mu}&,\end{aligned} \tag{142}$$

where $-(\epsilon/R)(1-\mu^2)^{1/2}\partial P_l/\partial\mu$ is the angle (to the first order in ϵ) which the deformed boundary makes with the θ-direction; the terms in H_θ in the foregoing equation arise from this latter circumstance. Now, according to equations (124), (139), and (140),

$$\begin{aligned}\{H_r^{(e)}\}_{R+\epsilon P_l}+\{H_\theta^{(e)}\}_R\frac{\epsilon}{R}(1-\mu^2)^{1/2}\frac{\partial P_l}{\partial\mu}&=H\mu\left(1-3\frac{\epsilon}{R}P_l\right)\\&+\tfrac{1}{2}H\frac{\epsilon}{R}(1-\mu^2)\frac{\partial P_l}{\partial\mu}+\frac{\epsilon}{R}H\{(l-1)P_{l-1}+\Sigma A_j(j+1)P_j\}\,,\end{aligned}\qquad(143)$$

while, according to equations (123) and (134),

$$\begin{aligned}\{H_r^{(i)}\}_{R+\epsilon P_l}+\{H_\theta^{(i)}\}_R\frac{\epsilon}{R}(1-\mu^2)^{1/2}\frac{\partial P_l}{\partial\mu}&=H\mu\\&+\frac{\epsilon}{R}H(l-1)P_{l-1}-\frac{\epsilon}{R}H(1-\mu^2)\frac{\partial P_l}{\partial\mu}\,;\end{aligned}\qquad(143\text{a})$$

and the equality of the expressions on the right-hand sides of equations (143) and (143a) requires

$$\begin{aligned}\Sigma A_j(j+1)P_j&=3\mu P_l-\tfrac{3}{2}(1-\mu^2)\frac{\partial P_l}{\partial\mu}\\&=\frac{3}{2(2l+1)}\{(l+1)(l+2)P_{l+1}-l(l-1)P_{l-1}\}\,.\end{aligned}\qquad(144)$$

Hence

$$A_{l-1}=-\frac{3(l-1)}{2(2l+1)}\,,\qquad A_{l+1}=\frac{3(l+1)}{2(2l+1)}\,,\qquad(145)$$

and

$$A_j=0\qquad\text{for}\qquad j\neq l-1\qquad\text{or}\qquad l+1\,.\qquad\text{(145a}$$

Inserting these values of A in equations (141) and (141a), we obtain

$$\delta H_r^{(e)}=\epsilon H\left\{\frac{(l-1)(l+2)}{2(2l+1)}\frac{R^l}{r^{l+1}}P_{l-1}(\mu)+\frac{3(l+1)(l+2)}{2(2l+1)}\frac{R^{l+2}}{r^{l+3}}P_{l+1}(\mu)\right\}\qquad(146)$$

and

$$\delta H_\theta^{(e)}=\epsilon H\left\{\frac{(l-1)(l+2)}{2l(2l+1)}\frac{R^l}{r^{l+1}}P_{l-1}^1(\mu)+\frac{3(l+1)}{2(2l+1)}\frac{R^{l+2}}{r^{l+3}}P_{l+1}^1(\mu)\right\}.\qquad(146\text{a})$$

Returning to equations (139) and (139a), we can write the change in the external magnetic energy, $\Delta\mathfrak{M}^{(e)}$, to the first order in ϵ, in the form

$$\begin{aligned}\Delta\mathfrak{M}^{(e)}&=\frac{H^2}{8\pi}\iiint\limits_{R+\epsilon P_l\geq r\geq R}\left(\frac{R}{r}\right)^6\{\mu^2+\tfrac{1}{4}(1-\mu^2)\}r^2dr\,d\mu\,d\varphi\\&+\frac{H}{8\pi}\iiint\limits_{r>R}\left(\frac{R}{r}\right)^3\{2P_1(\mu)\,\delta H_r^{(e)}+P_1^1(\mu)\,\delta H_\theta^{(e)}\}r^2dr\,d\mu\,d\varphi\,.\end{aligned}\qquad(147)$$

After some minor reductions we find

$$\begin{aligned}\Delta\mathfrak{M}^{(e)} = {} & \tfrac{1}{4}\epsilon H^2R^2 \int_{-1}^{+1} \{ \tfrac{1}{2}P_2(\mu) + \tfrac{1}{2} \} P_l(\mu)\, d\mu \\ & + \tfrac{1}{2}\epsilon H^2 \int_R^\infty dr\, r^2 \int_{-1}^{+1} d\mu \left(\frac{R}{r}\right)^3 P_1(\mu) \left\{ \frac{(l-1)(l+2)}{2(2l+1)} \frac{R^l}{r^{l+1}} P_{l-1}(\mu) \right. \\ & \qquad \left. + \frac{3(l+1)(l+2)}{2(2l+1)} \frac{R^{l+2}}{r^{l+3}} P_{l+1}(\mu) \right\} \qquad (148) \\ & + \tfrac{1}{4}\epsilon H^2 \int_R^\infty dr\, r^2 \int_{-1}^{+1} d\mu \left(\frac{R}{r}\right)^3 P_1^1(\mu) \left\{ \frac{(l-1)(l+2)}{2l(2l+1)} \frac{R^l}{r^{l+1}} P_{l-1}^1(\mu) \right. \\ & \qquad \left. + \frac{3(l+1)}{2(2l+1)} \frac{R^{l+2}}{r^{l+3}} P_{l+1}^1(\mu) \right\} .\end{aligned}$$

From this equation it is evident that $\Delta\mathfrak{M}^{(e)}$ vanishes (to the first order in ϵ) for all deformations except a P_2-deformation. And for a P_2-deformation we have

$$\Delta\mathfrak{M}^{(e)} = \tfrac{1}{5}\epsilon H^2R^2 \int_{-1}^{+1} [P_2(\mu)]^2 d\mu + \tfrac{1}{5}\epsilon H^2R^5 \int_R^\infty \int_{-1}^{+1} \frac{dr}{r^4} \{ \tfrac{1}{2}P_2(\mu) + \tfrac{1}{2} \} d\mu \qquad (149)$$

or

$$\Delta\mathfrak{M}^{(e)} = \tfrac{7}{60}\, \epsilon H^2R^2 \qquad (l=2) . \qquad (150)$$

Finally, combining equations (138) and (150), we obtain

$$\Delta\mathfrak{M} = \Delta\mathfrak{M}^{(i)} + \Delta\mathfrak{M}^{(e)} = \tfrac{9}{20}\, \epsilon H^2R^2 , \qquad (151)$$

for the total change in the magnetic energy due to a P_2-deformation; it vanishes to this order for all higher deformations.

We have, therefore, shown that *the change in the magnetic energy is of the second order in* ϵ *for all deformations of the sphere except a* P_2*-deformation; and for a* P_2*-deformation it is of the first order in* ϵ *and is given by (151)*. Moreover, for a P_2-deformation $\Delta\mathfrak{M} > 0$ when the deformation is in the sense of making the sphere into a prolate spheroid; and $\Delta\mathfrak{M} < 0$ when the deformation is in the sense of making the sphere into an oblate spheroid.

16. *The change in the gravitational potential energy and the instability of the sphere to a* P_2*-deformation.*—The change in the potential energy, $\Delta\Omega$, due to a P_l-deformation can also be computed. The result is well known for a P_2-deformation. For a general P_l-deformation we can evaluate $\Delta\Omega$ by following the procedure used in § 8. We shall not give here the details of the calculations, which lead to the result

$$\Delta\Omega = \frac{3(l-1)}{(2l+1)^2} \left(\frac{\epsilon}{R}\right)^2 \frac{GM^2}{R} . \qquad (152)$$

The change in the potential energy is therefore always positive and is of the second order in ϵ. This is in contrast to $\Delta\mathfrak{M}$, which, as we have seen, is of the first order in ϵ for a P_2-deformation and is negative for a deformation which tends to make it oblate. We can therefore conclude that the sphere is unstable and that it will tend to collapse toward an oblate spheroidal shape. To estimate the extent to which this collapse may proceed, let us consider $\Delta\Omega + \Delta\mathfrak{M}$ for a P_2-deformation. We have (cf. eqs. [151] and [152])

$$\Delta\Omega + \Delta\mathfrak{M} = \frac{3}{25} \frac{GM^2}{R^3} \epsilon^2 + \tfrac{9}{20} H^2R^2\epsilon \qquad (l=2) . \qquad (153)$$

As a function of ϵ, $\Delta\Omega + \Delta\mathfrak{M}$ has a minimum which it takes when

$$\frac{6}{25}\frac{GM^2}{R^3}\epsilon + \tfrac{9}{20}H^2R^2 = 0\,, \tag{154}$$

or

$$\frac{\epsilon}{R} = -\frac{15}{8}\frac{H^2R^4}{GM^2}\,. \tag{155}$$

If H_* denotes the value of the constant magnetic field inside the sphere for which $\mathfrak{M}$ (given by eq. [125]) is equal to the numerical value of the gravitational potential energy $\Omega\ (= -3GM^2/5R)$, then

$$\tfrac{1}{4}H_*^2R^3 = \frac{3}{5}\frac{GM^2}{R}\,. \tag{156}$$

In terms of H_* defined in this manner, we can rewrite equation (155) in the form

$$\frac{\epsilon}{R} = -4.5\left(\frac{H}{H_*}\right)^2. \tag{157}$$

We may interpret this relation by saying that when a star has a magnetic field approaching the limit set by the virial theorem (cf. Sec. I), then it tends to become highly oblate; in this respect the magnetic field has the same effect as a rotation.

V. THE GRAVITATIONAL INSTABILITY OF AN INFINITE HOMOGENEOUS MEDIUM IN THE PRESENCE OF A MAGNETIC FIELD

17. *The statement of the problem.*—It is well known that, by considering the propagation of a wave in an infinite homogeneous medium and allowing for the gravitational effects of the density fluctuations, Jeans[6] showed that the velocity of wave propagation is given by

$$V_J = \sqrt{(c^2 - 4\pi G\rho/k^2)}\,, \tag{158}$$

where $c = \sqrt{(\gamma p/\rho)}$ denotes the convectional velocity of sound and k is the wave number. Accordingly, when

$$k < c(4\pi\rho G)^{-1/2}\,, \tag{159}$$

the velocity of wave propagation becomes imaginary; and under these circumstances the amplitude of the wave will increase exponentially with time. The inequality (159) is therefore the condition for gravitational instability; this is Jeans's result. In Section V we shall show that Jeans's condition (159) is unaffected by the presence of a magnetic field. The physical reason for this is evident for a deformation in which the density waves are perpendicular to the lines of force because the motion of the particles in this case will be parallel to the lines of force and therefore will not be impeded by the magnetic field. But also a density wave forming an angle with the lines of force may be obtained by particle motions parallel to the lines of force, as shown in Figure 2.

18. *The three modes of wave propagation in the presence of a magnetic field and the condition for gravitational instability.*—Consider an extended homogeneous gaseous medium of infinite electrical conductivity, and suppose that there is present a uniform magnetic

---

[6] *Astronomy and Cosmogony* (Cambridge: At the University Press, 1929), pp. 345–347.

field of intensity $\boldsymbol{H}$. Then the fluctuations in density ($\delta\rho$), pressure (δp), magnetic field ($\boldsymbol{h}$), and gravitational potential (δV) are governed by the equations

$$\rho\frac{\partial \boldsymbol{u}}{\partial t}=\frac{1}{4\pi}(\text{curl }\boldsymbol{h}\times\boldsymbol{H})-\text{grad }\delta p+\rho\text{ grad }\delta V\,,$$

$$\frac{\partial \boldsymbol{h}}{\partial t}=\text{curl }(\boldsymbol{u}\times\boldsymbol{H})\,, \tag{160}$$

$$\frac{\partial}{\partial t}\,\delta\rho=-\rho\text{ div }\boldsymbol{u}\,,$$

and

$$\nabla^2\delta V=-4\pi G\delta\rho\,.$$

If the changes in pressure and density are assumed to take place adiabatically, then

$$\delta p=c^2\delta\rho\,. \tag{161}$$

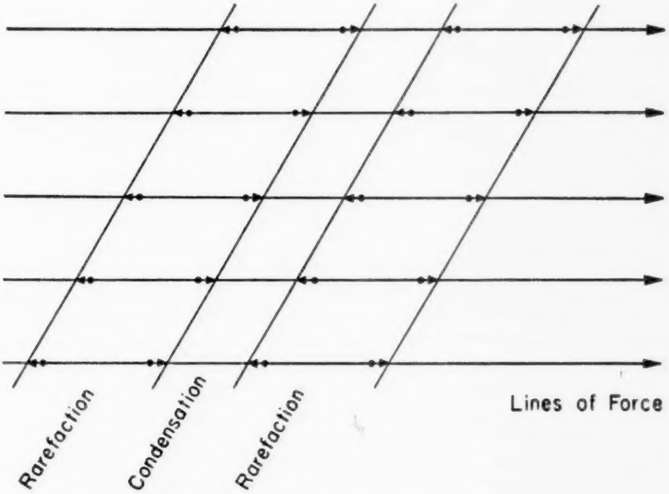

FIG. 2.—Illustrating why the presence of a magnetic field does not affect Jeans's condition for the gravitational instability of an infinite homogeneous medium.

We shall seek the solutions of equations (160) and (161) which correspond to the propagation of waves in the z-direction. Then $\partial/\partial z$ is the only nonvanishing component of the gradient. And if we further suppose that the orientation of the co-ordinate axes is so chosen that

$$\boldsymbol{H}=(0,\,H_y,\,H_z)\,, \tag{162}$$

it readily follows that $h_z=0$; and we find that equations (160) and (161) break up into the two noncombining systems:

$$\rho\frac{\partial u_x}{\partial t}=\frac{H_z}{4\pi}\frac{\partial h_x}{\partial z}\,,\qquad \frac{\partial h_x}{\partial t}=H_z\frac{\partial u_x}{\partial z}\,; \tag{163}$$

and

$$
\begin{aligned}
&\rho \frac{\partial u_y}{\partial t} - \frac{H_z}{4\pi} \frac{\partial h_y}{\partial z} = 0 \,, \\
&\rho \frac{\partial u_z}{\partial t} + \frac{H_y}{4\pi} \frac{\partial h_y}{\partial z} + c^2 \frac{\partial}{\partial z} \delta\rho - \rho \frac{\partial}{\partial z} \delta V = 0 \,, \\
&\frac{\partial h_y}{\partial t} + H_y \frac{\partial u_z}{\partial z} - H_z \frac{\partial u_y}{\partial z} = 0 \,, \\
&\frac{\partial}{\partial t} \delta\rho + \rho \frac{\partial u_z}{\partial z} = 0 \,, \\
&\frac{\partial^2}{\partial z^2} \delta V + 4\pi G \delta\rho = 0 \,.
\end{aligned}
\tag{164}
$$

Equations (163) can be combined to give

$$
\frac{\partial^2 h_x}{\partial t^2} = \frac{H_z^2}{4\pi\rho} \frac{\partial^2 h_x}{\partial z^2} \quad \text{and} \quad \frac{\partial^2 u_x}{\partial t^2} = \frac{H_z^2}{4\pi\rho} \frac{\partial^2 u_x}{\partial t^2} \,. \tag{165}
$$

These equations are the same as those leading to the ordinary hydromagnetic waves of Alfvén propagated with the velocity

$$
V_A = \frac{H_z}{\sqrt{(4\pi\rho)}} \,. \tag{166}
$$

This mode of wave propagation is therefore unaffected by gravitation and compressibility.

Turning next to solutions of equations (164), which also represent the propagation of waves in the z-direction, we can write

$$
\frac{\partial}{\partial t} = i\omega \quad \text{and} \quad \frac{\partial}{\partial z} = -ik \,, \tag{167}
$$

where ω denotes the frequency and k the wave number. Making the substitutions (167) in equations (164), we obtain a system of linear homogeneous equations which can be written in matrix notation in the following form:

$$
\begin{vmatrix}
\rho\omega & k \dfrac{H_z}{4\pi} & 0 & 0 & 0 \\
0 & -k \dfrac{H_y}{4\pi} & \rho\omega & -kc^2 & k\rho \\
kH_z & \omega & -kH_y & 0 & 0 \\
0 & 0 & -k\rho & \omega & 0 \\
0 & 0 & 0 & 4\pi G & -k^2
\end{vmatrix}
\begin{vmatrix}
u_y \\ h_y \\ u_z \\ \delta\rho \\ \delta V
\end{vmatrix}
= 0 \tag{168}
$$

The condition that equation (168) has a nontrivial solution is that the determinant of the matrix on the left-hand side should vanish. Expanding the determinant, we find that it can be reduced to the form

$$\left(\frac{\omega}{k}\right)^4 - \left\{\frac{H^2}{4\pi\rho} + \left(c^2 - \frac{4\pi G\rho}{k^2}\right)\right\}\left(\frac{\omega}{k}\right)^2 + \frac{H_z^2}{4\pi\rho}\left(c^2 - \frac{4\pi G\rho}{k^2}\right) = 0\,. \tag{169}$$

In terms of the velocity of wave propagation, $V = \omega/k$, we can rewrite equation (169) in the form

$$V^4 - (V_A^2 \sec^2\vartheta + V_J^2)V^2 + V_A^2 V_J^2 = 0\,, \tag{170}$$

where ϑ denotes the angle between the directions of $\boldsymbol{H}$ and of wave propagation and V_J and V_A have the same meanings as in equations (158) and (166).

It is seen that equation (170) allows two modes of wave propagation. If V_1 and V_2 denote the velocities of propagation of these two modes, we conclude from equation (170) that

$$V_1 V_2 = V_A V_J$$

and

$$V_1^2 + V_2^2 = V_A^2 \sec^2\vartheta + V_J^2\,. \tag{171}$$

Accordingly, *if V_J is imaginary, then either V_1 or V_2 must be imaginary.* In other words, one of the two modes of wave propagation will be unstable if Jeans's condition (159) is satisfied. The condition for gravitational instability is therefore unaffected by the presence of the magnetic field. However, as to which of the two modes will become unstable will depend on the strength of the magnetic field. Thus for $H \to 0$, the two modes given by equation (170) approach, respectively, Jeans's mode and Alfvén's mode. And if we suppose that

$$V_1 \to V_J \qquad \text{and} \qquad V_2 \to V_A \qquad \text{as} \qquad H \to 0\,, \tag{172}$$

then it follows from equation (170) that so long as $V_J^2 > 0$,

$$V_1 \to V_A \sec\vartheta \qquad \text{and} \qquad V_2 \to V_J \cos\vartheta \qquad \text{as} \qquad H \to \infty\,. \tag{173}$$

Hence, for $H \to \infty$, the mode which will become unstable when Jeans's condition is satisfied will be the mode which for $H \to 0$ is Alfvén's mode; and the mode which for $H \to 0$ is Jeans's mode becomes a hydromagnetic wave for $H \to \infty$ and is unaffected by gravitation. This "crossing-over" of the two modes with increasing strength of the magnetic field is in agreement with what is known[7] from the theory of wave propagation in a compressible medium in the absence of gravitation.

---

[7] Cf. H. van de Hulst, *Symposium: Problems of Cosmical Aerodynamics* (Dayton, Ohio: Central Air Documents Office, 1951), chap. vi; also N. Herlofson, *Nature*, **165**, 1020, 1950.

THE EFFECT OF ELECTRON SCREENING ON THERMONUCLEAR ENERGY GENERATION

GEOFFREY KELLER*
Perkins Observatory

Received December 19, 1952

ABSTRACT

It is known that thermonuclear reaction rates are sensitive to the heights of the intra-nuclear potential barriers. Since the height of a barrier will be reduced by the presence of screening electrons, computations have been made to determine the corresponding effect on the reaction rate of the carbon cycle. It has been found that, under conditions typical of the interior of the sun, the reaction rate should be increased by a factor of 1.54. Under conditions representative of a red dwarf interior, the increase is by a factor of 3 or more. Neither factor is likely to be important in the theory of stellar structure unless it should turn out that the proton-proton reaction is inoperative.

I. INTRODUCTION

It has been customary heretofore to neglect the effects of electronic forces when computing rates at which energy is generated within stars. In particular, this has been true when the carbon-cycle process has been considered. In that chain of reactions it will be recalled that (so far as is now known) the controlling reaction is

$$N^{14}+H^{1}\rightarrow O^{15}\,. \tag{1}$$

It is known that the rate at which this reaction occurs is very sensitive to the temperature of the protons which impinge upon the nitrogen nuclei. It was recently pointed out to the author by Dr. J. L. Greenstein that one might expect the small increment which these energies receive from the attraction between the proton and the electrons surrounding the nitrogen nucleus to affect the reaction rate greatly. A detailed calculation shows that the effect, while appreciable, is not so large as one might at first suppose. The reason seems to be that even though the energy increment due to electronic attraction is an appreciable portion of the thermal energy of an *average* proton, it is only a small fraction of the energy of the protons which most frequently penetrate the nuclear potential barrier.

II. REDUCTION IN HEIGHT OF POTENTIAL BARRIER

At the temperatures and pressures which are required to make energy generation by the carbon cycle an important process, one may expect to find carbon, nitrogen, and oxygen almost completely ionized. For example, at 11.6 million degrees and a density of 122 gm/cm^3 one finds an average of 0.6 electrons in the K shell of nitrogen. One will also find about 4.6 free electrons in the vicinity of the K orbits, so that electrons in K orbits are certainly highly perturbed by pressure effects and it is doubtful whether it is meaningful to speak of their existence at all.

In view of the general disorganization of the bound levels, one may expect that a statistical method for finding the average potential and electron density distribution should be reasonably accurate. Consequently, a generalized Thomas-Fermi method has been employed in which the effects of temperature and neighboring ion densities have been taken into account. The mathematical methods have been described in detail else-

---

* This research was supported in part by the Argonne National Laboratory under Consultant Subcontract No. 31-109-38-252.

where[1] and will not be recounted here. However, it should be stated that in the present case the generalized Thomas-Fermi equation has been solved by a series approximation near the nucleus and then integrated outward by numerical methods.

The most serious shortcoming of this procedure is that it gives a spuriously high density close to the nucleus of electrons of negative total energy. This difficulty occurs because the statistical method does not make provision for the fact that the potential well is too shallow and narrow to retain as "bound" any electron with a high negative total energy.

The primary effect of these spurious electrons is to make the radial electric field (especially near the nucleus) appear smaller than it should be, and thus an erroneous reduction in the height of the potential barrier is introduced. To eliminate this effect, an intercomparison was made between potential distributions obtained from a number of solutions of the GTF equation (obtained in connection with another problem) and potential distributions based on the assumption of hydrogen-like wave functions for the bound electrons. It was found that, over all, the generalized Thomas-Fermi potential barrier reduction should be corrected roughly by an amount given by the empirical expression

$$\Delta''(e_0 V) = -(4.1)Z^{0.77} \qquad \text{(Rydbergs)} \tag{2}$$

where Z is the atomic number of the nucleus and e_0 is the charge on a proton.

III. EFFECT OF REDUCTION OF BARRIER HEIGHT ON RATE OF PENETRATION OF NUCLEUS

In Figure 1 let the curve ABD be a plot of the potential energy of a proton in the neighborhood of an unscreened nitrogen nucleus. The nuclear potential well is not shown and would presumably lie very close to the origin. Distances r from the center are measured in Bohr radii. The probability that a proton impinging on the barrier with relative total energy E will penetrate the unscreened barrier is proportional to[2]

$$W = \exp\left\{ -2\left(\frac{2M_1M_2}{M_1+M_2}\right)^{1/2} \frac{\pi^2 Z_1 Z_2 e_0^2}{hE^{1/2}} \right\}. \tag{3}$$

The quantities M_1 and M_2 are the masses of the proton and nitrogen nucleus, and Z_1 and Z_2 are the corresponding atomic numbers. From the method of derivation of this expression, one can show that the value of W depends only on the quantity $e_0V - \mathrm{E}$ in the region to the left of G. The point G is that at which the proton would come to rest if it were a classical particle.

If shielding is now taken into account, the potential energy of a proton in the field of the nucleus and associated electrons has the form ABC. An impinging proton of energy E′ would classically come to rest at G, and the quantum-mechanical probability of penetration is still given by equation (3), wherein

$$E = E' + \Delta E \tag{4}$$

and where $\Delta E = \Delta(e_0 V)$ is the true reduction in barrier height.

Let us suppose that the number density of protons at $r = \infty$, $E' = 0$ is N_1; then the density at the point r_B is

$$N_1(r_B) = N_1 \exp\left\{\frac{-E'(r_B)}{kT}\right\}. \tag{5}$$

---

[1] Keller and Meyerott, *Argonne National Laboratory Report 4771* and *4856* (1952).

[2] Chandrasekhar, *Astrophysics*, ed. J. A. Hynek (New York: McGraw-Hill Book Co., Inc., 1951), chap. xiv, eq. (110).

We choose to consider the point r_B as a starting point for the bombarding protons, because inside this point they would travel with only infrequent collisions with electrons or other protons. The number of collisions between protons and nitrogen nuclei due to protons starting from r_B and having total energies in the range E' to $E' + dE'$ is given by[3]

$$\frac{N_1 N_2}{(kT)^{3/2}} \frac{h^2}{(2\pi)^3} \left[\frac{2\pi (M_1+M_2)}{M_1 M_2}\right]^{3/2} \exp\left\{\frac{-E'(r_B)}{kT}\right\} dE' \exp\left\{\frac{-[E'-E'(r_B)]}{kT}\right\}. \quad (6)$$

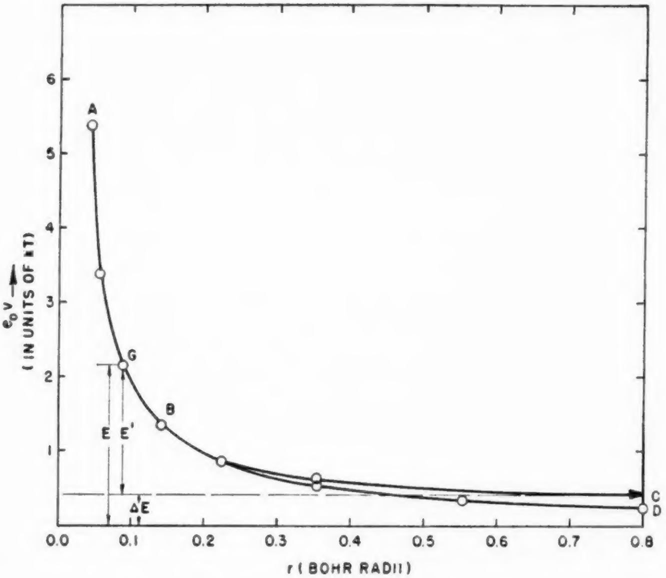

FIG. 1.—Potential energy of a proton in the neighborhood of a screened (ABC) and an unscreened (ABD) nitrogen nucleus.

Combining equations (3), (4), and (6) and making the substitutions

$$E = kTy, \quad (7)$$

and integrating, one obtains a quantity proportional to the number of penetrations per second,

$$\frac{N_1 N_2}{(kT)^{1/2}} \frac{h^2}{(2\pi)^3} \left[\frac{2\pi (M_1+M_2)}{M_1 M_2}\right]^{3/2} \exp\left[\frac{\Delta E}{kT}\right] \int_{y_c}^{\infty} \exp\left\{-y - 2Q^3 y^{-1/2}\right\} dy. \quad (8)$$

where

$$Q = 37.7 \left[\frac{A_1 A_2 Z_1^2 Z_2^2}{T(A_1 + A_2)}\right]^{1/6}. \quad (9)$$

The quantity

$$y_c = \frac{E'(r_B)}{kT} + \frac{\Delta E}{kT}. \quad (10)$$

---

[3] *Ibid.*, eqs. (113) and (114).

For reaction (1), at a temperature of 11.6×10^6 degrees and a density of 122 gm/cm, the unscreened ionization potential of the K shell divided by kT is 0.67; so it seems reasonable to assume that

$$\frac{E'(r_B)}{kT} < 1 . \tag{11}$$

For the same conditions it was found that $\Delta E/kT$ was equal to 0.40. Thus $y_i < 2$. Now, by substitution of actual values in the integrand of formula (8), it is easily shown that the maximum value of the integrand occurs near $y = 22$ and that contributions for $y < 2$ are comparatively negligible. In view of this, we may rewrite expression (8) for the number of barrier penetrations per second, making the substitution $y_i = 0$. The expression thus obtained is exactly equal to the penetration rate in the absence of screening,[4] multiplied by the factor

$$\exp\left[\frac{\Delta E}{kT}\right] . \tag{12}$$

It seems likely that the steps in the process of the nuclear reaction that follow the penetration are affected to a negligible extent by the reduction in the barrier height, since the amount of energy involved is so small compared to that liberated when the reaction occurs. For this reason, we may regard quantity (12) as the factor by which the reaction rate with unscreened nuclei should be increased to allow for screening.

IV. SAMPLE CALCULATIONS

Detailed calculations have been made for two cases:

Case I.—Condition representative of the interior of the sun. Temperature $11.6 \times 10^6\,^\circ K$, density 122 gm/cm^3. It is assumed that the nitrogen nuclei are immersed in a gas mixture containing at least 75 per cent of hydrogen and/or helium by weight. The reduction in the potential barrier height by the generalized Thomas-Fermi method is

$$\frac{\Delta'(e_0 V)}{kT} = 0.65 .$$

The correction for spurious electron densities near the nucleus is

$$\frac{\Delta''(e_0 V)}{kT} = -0.25 .$$

The factor which gives the increase in the reaction rate due to screening is thus

$$\exp[0.43] = 1.54 \pm 0.10 .$$

Case II.—Condition representative of the interior of a red dwarf. $T = 8.13 \times 10^6$, density = 443. Mixture the same as for Case I.

$$\frac{\Delta'(e_0 V)}{kT} = 1.55 , \qquad \frac{\Delta''(e_0 V)}{kT} = -0.36 .$$

The correction factor is $\exp[1.19] = 3.3 \pm 0.3$.

The limits of error represent the author's rough estimate of the inaccuracies inherent in the approximations which have been made.

---

[4] *Ibid.*, eq. (115).

V. CONCLUSIONS

It does not appear likely that the corrections computed here can be of major importance in the theory of the structure of most stars. The carbon-cycle reaction is so temperature-sensitive that small adjustments in T can readily be made to compensate for the increased rate of energy generation without affecting other properties of the gas appreciably. It is worth recalling, however, that it has been implied by Aller and his co-workers[5] that the proton-proton reaction may not be responsible for energy generation in red dwarf stars. If such is the case, these screening correction factors may be worth considering when studying such stars, since the factors are largest at low temperatures and high densities.

---

[5] *Ap. J.*, **115**, 328, 1952.

THE APSIDAL MOTION AND RADIUS OF GYRATION OF THE PROTON-PROTON SOLAR MODEL*

LLOYD MOTZ
Rutherford Observatory

Received January 12, 1953; revised January 21, 1953

ABSTRACT

The apsidal motion constant, k, and the radius of gyration, H/R, are calculated for the recently integrated proton-proton model of the sun. It is found that the apsidal-motion constant gives a value of the effective polytropic index which is smaller than one is led to expect from observational data. The value of the radius of gyration obtained places the model off the straight line that was previously found to exist between $-\log k$ and $-\log H/R$ for main-sequence stellar models.

INTRODUCTION

The development of a satisfactory solar model depends on the use of correct laws for the energy-generating process and for the opacity in the sun's interior. Although our knowledge of the opacity law for the stellar interiors is still incomplete, enough work has been done on nuclear reactions in stars[1] to indicate that the proton-proton chain reaction is predominantly responsible for the generation of energy in main-sequence stars in the neighborhood of the sun. Using the proton-proton chain, Epstein[1] derived a model for the solar interior that gave a hydrogen content in agreement with that observed in the solar atmosphere. Since then, the works of Frieman and Motz and that of Salpeter have shown that the rate of release of energy by the proton-proton chain reaction under conditions found inside the sun is larger than had been assumed by Epstein. For that reason a reinvestigation of the proton-proton solar model was recently undertaken,[2] using the corrected energy-generation law.

This new model gives a hydrogen content that is unreasonably high, so that one must conclude that the opacity law used in this model is incorrect. Although at present we are engaged in a redetermination of the opacity coefficient for the solar interior, it is worth while to see whether other parameters of the present model deviate from their expected values. Two parameters which we shall investigate in this paper are the apsidal-motion constant and the radius of gyration as defined by the author.[3]

These two quantities are of interest in the theory of stellar models because, on the one hand, the apsidal-motion constant is quite sensitive to a change of model and can be compared directly with observation and, on the other hand, there appears to be a linear relationship between the logarithm of the apsidal-motion constant and that of the radius of gyration for main-sequence stellar models.

APSIDAL-MOTION CONSTANT FOR PROTON-PROTON SOLAR MODEL

In a previous paper[4] (eqs [1]–[5]) the differential equations governing the first-order distortion of a surface of constant density in a binary star were expressed in a form suitable for integration in two-zone stellar models. Equation (10) in Paper I gives the

---

* This work was supported by the O.N.R., Contract Nonr-266(19).

[1] H. A. Bethe and C. L. Critchfield, *Phys. Rev.*, **54**, 248, 1938; E. Frieman and L. Motz, *Phys. Rev.*, **89**, 648, 1953; I. Epstein, *Ap. J.*, **114**, 438, 1951; E. E. Salpeter, *Phys. Rev.*, **88**, 549, 1952; H. Bondi and E. E. Salpeter, *Nature*, **169**, 304, 1952.

[2] I. Epstein and L. Motz (in press).

[3] L. Motz, *Ap. J.*, **115**, 562, 1952.

[4] L. Motz, *Ap. J.*, **112**, 434, 1950; hereinafter referred to as "Paper I."

form of the equation suitable for the convective core of our stellar model, and in the radiative-zone equation (5) of Paper I is replaced by

$$\frac{d^2W}{dx^2} - A^2\left(6.25 - UV\frac{n}{n+1}\right)W = 0\,, \tag{1}$$

where

$$x = \log_{10} r\,,\ U = \frac{d \log M(r)}{d \log r}\,, \qquad V = \frac{d \log P}{d \log r}\,, \qquad A = \log_e 10\,,$$

and n is the local polytropic index,

$$n + 1 = \frac{d \log P}{d \log T}\,.$$

The apsidal-motion constant k, which is a measure of the rate of precession of the line of apses of the binary system, is defined by equation (2) of Paper I in terms of the value of $W(x)$ at the surface, with η, which appears in that equation given by

$$\eta = \left[\frac{r\,e^{-Ax/2}}{W(x)}\,\frac{\partial}{\partial r}\left(e^{Ax}W[x]\right)\right]_{r=R}\,. \tag{2}$$

In the convective core of our present model we use the series-expansion solution and its first derivative given in Paper I.

Since equation (1) has to be integrated numerically through the radiative zone, we require two starting values for W. We first expand $W(x)$ in a power series in the neighborhood of the convective core–radiative zone interface, which lies at the point $x = 9.74$, and then impose the condition of continuity for the solution and its first derivative across the interface. This enables us to find the value of $W(x)$ at the interface itself and at the neighboring point $x = 9.76$. These two starting values are thus

$$W(9.74) = 0.12610\,, \qquad W(9.76) = 0.14069\,. \tag{3}$$

Using the method described in Paper I, we integrate equation (1) numerically through the radiative envelope out to the point $x = 10.82$, where $UVn/(n+1)$ is negligible. In the remaining portion of the radiative zone we use the solution

$$W = e^{-Ax/2}\left(c_1x^{-2} + c_2x^3\right)\,, \tag{4}$$

where c_1 and c_2 are constants in terms of which k is defined as follows:

$$k = \frac{c_1}{2\,c_2}\,. \tag{5}$$

The constants c_1 and c_2 can be found by comparing equation (4) with the numerical solution of equation (1) at $x = 10.82$. When we do this, we obtain

$$\eta(R) = 2.927\,,$$

so that

$$k = 0.007408\,.$$

This value of k is larger than that found by the writer[3] for the first proton-proton model integrated by Epstein. Corresponding to this value of k, we find an effective polytropic index of 3.3 for our present model. This value is considerably smaller than the average observed value of 3.7 obtained from the apsidal-motion data of main-sequence binary stars.

RADIUS OF GYRATION OF PROTON-PROTON SOLAR MODEL

It has been shown[3] that a linear relationship exists between $-\log k$ and $-\log H/R$ for simple polytropes and for various main-sequence models, where k is the apsidal-motion constant of the model and H, the radius of gyration, is defined as follows:

$$H = \frac{8\pi}{3M} \int_0^R \rho r^4 d r . \tag{6}$$

Since the hydrogen content of the present proton-proton model is unreasonably high, it is of interest to see whether the radius of gyration for this model falls on the straight line found for the polytropes and other main-sequence models.

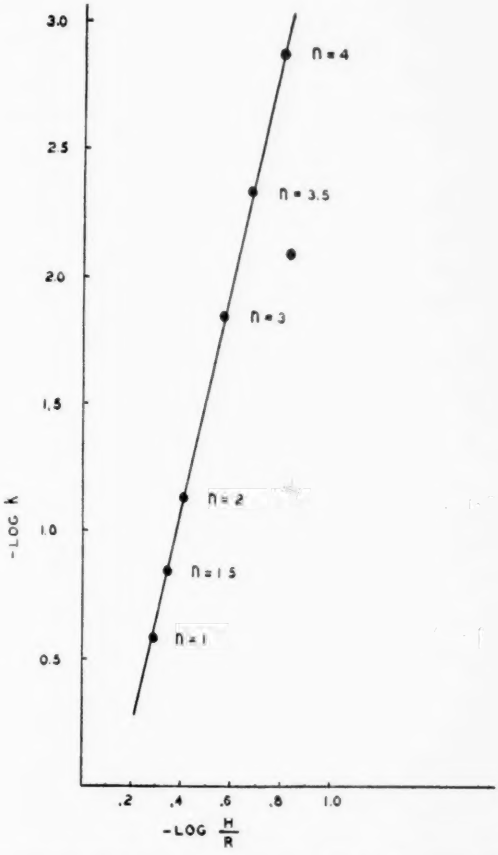

FIG. 1.—The linear relationship between log k and log (H/R) for polytropes. The small circle to the right of the line shows the position for the proton-proton model discussed in this paper.

For our two-zone model we have[3]

$$\left(\frac{H}{R}\right)^2=\frac{2}{3}\left[1+\frac{2\,(2.5)^{5/2}}{p_c^{3/2}}\,t_c^4\xi_j^3\vartheta_j-\frac{6\,(2.5)^{5/2}}{p_c^{3/2}}\,t_c^4\int_0^{\xi_j}\xi^2\vartheta\,d\xi-\frac{2}{MR^2}\int_{r_f}^{R} rM(r)\,\dot{d}r\right], \quad (7)$$

where t_c and p_c are the central values of the temperature and pressure on the scales $GM\mu\mathfrak{H}/kR$ and $GM^2/4\pi R^4$, respectively. A straightforward numerical integration of equation (7), using the data for the model given by Epstein and the author, gives

$$\left(\frac{H}{R}\right)^2=0.064894$$

or

$$\log\frac{H}{R}=-0.82022\,.$$

In Figure 1 the linear relationship between $-\log k$ and $-\log(H/R)$ is shown for typical polytropes. The small circle to the right of this line shows the position of the present proton-proton model.

The author is grateful to Mr. Laurence Sigler for doing the numerical integrations in this paper.

VARIATIONS IN ATMOSPHERIC ABSORPTION OVER THE DISKS OF JUPITER AND SATURN*

SEYMOUR L. HESS
Lowell Observatory and Florida State University

Received August 29, 1952; revised November 25, 1952

ABSTRACT

Variations in the strength of absorption of methane at 6190 A on Jupiter and Saturn, and ammonia at 6441 A on Jupiter, were studied. The absorptions decrease slightly toward the edges of Jupiter, but increase somewhat toward the edges of Saturn. The conclusion is drawn that the cloud surface on Jupiter rises toward the limbs, but is more nearly level on Saturn. The ammonia results indicate a decrease in temperature from equator to poles on Jupiter. The morning limb is found to be cooler than the evening limb.

I. INTRODUCTION

A considerable amount of work has been done on the atmospheric absorption bands in the spectra of the major planets, with the important result that methane and ammonia were identified as constituents.[1] It has also been found that the methane absorption increases as we pass from the nearer to the outer major planets, but the ammonia absorption reveals the opposite behavior: it is stronger on Jupiter than on Saturn and absent on Uranus and Neptune. It has been suggested that this is consistent with the decrease in temperature to be expected with increasing distance from the sun. The ammonia is thought to be more and more frozen out and deposited at the lower temperatures, thus explaining the decreasing ammonia absorption. The resulting lowering of the planetary cloud surface permits light to penetrate deeper into the atmosphere and so reveal more methane.[2]

Relatively little of a quantitative nature has been done, however, on the distribution of absorption strength over the surfaces of each of these planets. Jupiter is the largest and therefore the easiest object and so has received some attention. Saturn, Uranus, and Neptune have not been studied in this fashion. Elvey and Fairley[3] found that the methane absorption on Jupiter was the same at the limbs as at the center of the disk. Eropkin[4] worked at the edges of the planet and found about the same methane absorption at the pole as at the equatorial east limb but somewhat less ammonia at the pole. Bobrovnikoff[5] found no appreciable variation of methane over Jupiter's disk but did find indications of more ammonia over the dark belts than over the poles. Somewhat opposed to this is the earlier finding of V. M. Slipher,[6] who noted greater strength of ammonia at the equator than at the equatorial belts. He also noted slightly greater methane absorption at the equator as compared with the belts.

The investigations of Elvey and Fairley and of Eropkin were quantitative, since the spectra were photometered. The results of Bobrovnikoff and Slipher are from visual inspection only. The slight disagreements indicated may be due to the roughness inherent in eye estimates. Nevertheless, it should be remembered that Jupiter sometimes exhibits extraordinary visual changes in the structure of its cloud belts, so that changes from year to year in the distribution of methane and ammonia absorption certainly cannot be ruled out.

---

* Contribution No. 6 from the Project for the Study of Planetary Atmospheres. The research reported in this paper was sponsored by the Geophysics Research Division of the Air Force Cambridge Research Center under Contract No. AF 19(122)-162.

[1] Wildt, *Veröff. U. Sternw. Göttingen*, Vol. **22**, 1932.

[2] Russell, *The Solar System and Its Origin* (1935), p. 88.

[3] *Ap. J.*, **75**, 373, 1932.

[4] *Poulkova Obs. Circ.*, Nos. 10 and 15.

[5] *Pub. A.S.P.*, **45**, 171, 1933.

[6] *M.N.*, **93**, 657, 1933.

These observations are far from exhaustive; yet one fact stands out clearly. There seems to be little, if any, variation in absorption over the disk of Jupiter, especially between the center and the edges of the planet. This is contrary to expectation, because near the edges we are looking obliquely through the atmosphere and therefore the light should traverse a much longer absorbing path than it does near the center. This should result in considerably greater limb absorption. The importance of verifying and extending this surprising observational result was one reason for initiating the quantitative study of Jupiter and Saturn spectra reported in this paper. However, the major reason for such a study comes from the possibility of learning much about the relative heights and temperatures of various parts of the planetary cloud surface. This possibility arises from the following facts: the approximately known temperatures on Jupiter and Saturn are such as to insure that methane remains uncondensed at the visible surface, but that ammonia is almost certainly in equilibrium between the solid and gaseous states. Since this is the case, the amount of methane found above a given point is a measure of the elevation of that point. On the other hand, the amount of ammonia found is a function of the surface partial pressure of ammonia, and this, because of the condensation, is a function of the surface temperature only. The importance of such knowledge for an understanding of the structure and circulation of the Jovian and Saturnian atmospheres is so obvious as to require no elaboration.

II. OBSERVATIONS AND REDUCTIONS

The observations of Jupiter were carried out in October, 1949, after an earlier period of adjustment and test.[7] Spectra of Saturn were taken in April and May, 1950. The three-prism spectrograph of the Lowell Observatory was used, mounted on the 24-inch refractor. The technical data are given in Table 1.

TABLE 1

TECHNICAL DATA RELATING TO THE OBSERVATIONS

	Jupiter	Saturn
Eastman plate type	103*a*-E	103*a*-F
Exposure time	30–50 sec.	60–90 sec.
Aperture	24 in.	24 in.
Dispersion between C and D	43 A/mm	43 A/mm
Slit width	25 μ	25 μ
Calibration wave lengths	6100–6700 A	6100–6300 A

The Jupiter spectra were taken at the central meridian parallel to the latitude circles at the equator, the north and south equatorial belts (10° N. and S.), zones at 30° N. and S., and the north and south polar regions (60° N. and S.). The spectrograph was then rotated 90°, and spectra were obtained of the center of the disk and the morning and evening limbs (60° of longitude from the central meridian). On Saturn it was possible to take spectra of only the equator, north and south polar regions, and morning and evening limbs. The spectrograph slit was positioned on the planets by eye as carefully as possible.

The bands selected for study were the 6190 A methane band and the subband of ammonia centered at 6441 A. Photometric calibration was accomplished by exposing each plate to an incandescent lamp through a rotating sector wheel and a filter chosen so as to limit the wave lengths registering to the region in question (see Table 1). The use of a sector wheel permitted the possibility of error due to reciprocity failure, but this was minimized by using the *a* modification of the Eastman emulsions. Laboratory tests were made which indicated that reciprocity failure on these emulsions was negligible when the middle step of the sector scale was exposed for about the same total time as the spectra to be measured. Care was taken to meet this requirement. Similar spectra of the moon were measured to determine the nature of the continuum through the bands used.

---

[7] The assistance and guidance of V. M. Slipher and E. C. Slipher in this phase of the work are gratefully acknowledged.

A number of such plates was exposed, and the ones which were most free of defects of various sorts and which were obtained under the best seeing and guiding conditions were measured with a recording photoelectric microphotometer. From values of the absorption at intervals along the wide 6190 A band the contour of the band was plotted for each spectrum. The area inclosed by the contour was measured, and finally the equivalent width was computed. In the case of the slender 6441 A band the area inclosed on enlarged photometric traces was measured and the equivalent width computed from this area.

III. RESULTS FOR METHANE ON JUPITER

The average equivalent widths of the two bands studied are listed in Table 2 in terms of differences from the equatorial values. These are the absorption strengths in the line of sight and have not been corrected to absorptions along the vertical on the planet. Owing to the near-coincidence of the equatorial plane with the orbital plane of Jupiter, there are no large seasonal effects, and it was considered permissible to average together the results from the two hemispheres.

TABLE 2

EQUIVALENT WIDTHS OF ABSORPTIONS ON JUPITER

LATITUDE	6190 A METHANE BAND		6441 A AMMONIA BAND		NO. OF SPECTRA
	$W_{eq}-W$ (A)	Prob. Error (A)	$W_{eq}-W$ (A)	Prob. Error (A)	
10°	2.5	±1.4	0.08	±0.30	4
30°	4.0	±1.0	.34	±.17	4
60°	2.3	±2.2	.18	±.13	8
Morning limb	0.6	±0.8	.45	±.10	3
Evening limb	0.9	±1.4	0.06	±0.30	3
Equator	$W_{eq}=16.2\pm1.9$ A		$W_{eq}=1.16\pm0.16$ A		5

Since we are basically interested in the variation of absorption over the planet, these results have been expressed in terms of the difference of the equivalent width, W, from the equatorial equivalent width, W_{eq}. In some cases the mean difference is several times the probable error of the mean difference, so they are significant. The largest probable errors are mostly for spectra taken near the edges of the planet where guiding and seeing are most critical. The average equivalent width found here for the equator, 16.2 ± 1.9 A, is in excellent agreement with that found for the same band by Elvey and Fairley,[2] 15.9 A. The maximum absorption at the equator is found to be 16.6 per cent, while Elvey and Fairley found 17 per cent.

It is clear that these results are in broad agreement with the earlier findings, in that no very great variation in absorption over the disk is found. The small (but apparently sometimes significant) variations found here are in the direction of a *decrease* in absorption toward the edges rather than the expected increase. This means that when the obliquity of the light-path is taken into account, that is, when the amount of gas along the planetary vertical is considered, there must be much less methane near the edges than at the center. And, since the methane is probably well mixed with the other atmospheric constituents, this means that there must be less depth of atmosphere near the edges. This can come about only if the cloud surface rises toward the poles and limbs of the planet. It should be remembered, however, that the cloud layer need not have a sharp upper boundary. All that can be measured is the mean level of penetration of the light utilized. Hereafter this mean level of penetration will be referred to simply as the "cloud surface."

To convert these data to relative heights of the cloud surface, we need to know the form of the curve of growth and the planetocentric angle between the center of the disk and the point of measurement. The latter is known, but no determinations of the curve of growth for methane are available to the writer. We may proceed, however, on the assumption that methane behaves similarly to other gases in having a growth-curve in which absorption is proportional to the number of molecules in the path for relatively weak absorption (the linear part) and proportional to the square root of the number of molecules for stronger absorption (square-root part). These two usually encompass nearly all the range of gaseous absorption; so we shall make our computations on both assumptions and thus arrive at two results, one or the other of which is probably correct. Thus the number of molecules of methane is the path will be given by

$$N = KW^n \,, \tag{1}$$

where K is a constant, W is the equivalent width, and n is either 1 or 2. To correct to the number of molecules in a vertical planetary column, this must be multiplied by $\cos \theta$, where θ is the angle subtended at the center of the planet between the center of the disk and the point of measurement. As an approximation we may calculate pressure and N as functions of height under the assumption of an isothermal temperature. Then

$$\frac{p_1}{p_2} = \frac{N_1}{N_2} = e^{-(\bar{m}g/RT)z} \,. \tag{2}$$

Here z is the difference in height between the levels where the pressures are p_1 and p_2, and the numbers of absorbing molecules per unit area in the vertical are N_1 and N_2; $\bar{m}$ is the atmospheric mean molecular weight, g the acceleration of gravity, R the universal gas constant, and T the temperature. Substitution of equation (1) in equation (2), with the $\cos \theta$ correction to the vertical, and rearrangement yield:

$$z = \frac{RT}{\bar{m}g} \left[n \ln \frac{W_2}{W_1} + \ln \frac{\cos \theta_2}{\cos \theta_1} \right] . \tag{3}$$

Using this formula, we may compute the difference in the elevation of the cloud surface at two points on the planet at which methane absorptions W_1 and W_2 have been measured and which are at angles θ_1 and θ_2 from the center of the disk. The results of such a computation, together with the relative amounts of methane in the vertical column, are shown in Figure 1. Here all values are relative to the central meridian at the equator. The mean molecular weight was taken to be 4 and the temperature to be 150° K.

The choice of a value for the mean molecular weight is necessarily somewhat arbitrary. The mean density and moment of inertia of Jupiter indicate that the atmosphere must consist mostly of the light gases, hydrogen and helium. Since we lack any further definite knowledge, it is convenient to adopt a "Peek mixture" of 6 molecules of hydrogen to 1 molecule of methane.[8] Such a mixture provides for a reasonable excess of hydrogen and has a molecular weight of 4. As a consequence, the proportion of helium assumed to be present cannot affect the molecular weight of the atmosphere. The adopted molecular weight of 4 cannot be wrong by more than a factor of 2 and probably is much closer to the truth than this. We may further note that results from equation (3) are not critically dependent upon the adopted temperature. A change of 20° K would alter the computed heights by only 14 per cent.

---

[8] Peck, *M.N.*, **97**, 574, 1937.

Figure 1 shows quantitatively what we have already deduced qualitatively. The amount of methane along the vertical decreases markedly with latitude and is smaller at latitude 60° than at the equator by more than a factor of 2. It is worth noting that the assumed form of the curve of growth makes no essential difference. The result that the cloud layer is 10–12 km higher at 60° than at 0° is of an easily acceptable order of magnitude.

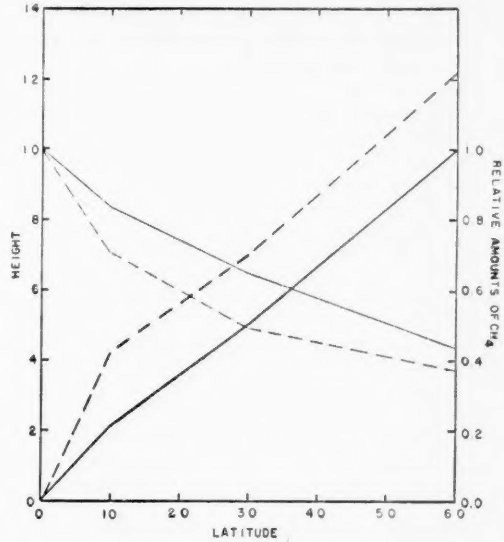

FIG. 1.—Height (km) of the visible cloud surface of Jupiter along the central meridian above the equatorial height as a function of latitude (*heavy lines*). The ratio of the amount of methane in a vertical column to the equatorial amount is given by the thin lines. The solid lines are for $n = 1$, and the dashed lines are for $n = 2$.

These results must be looked upon as supplementary rather than contradictory to Lyot's polarimetric data,[9] which indicate that poleward of 60° the cloud surface descends and the atmosphere becomes deeper. It was not feasible to check this spectrographically, since the region between 60° and the pole is so foreshortened that the spectrograph slit could not be set and kept there.

When the phase effect is taken into account, the morning and evening limbs are found to have about the same amount of methane in the vertical, but less than half of that over the center of the disk. Their relative heights are 10.2 and 9.2 km for the morning limb, and 9.2 and 13.0 km for the evening limb, for $n = 1$ and 2, respectively.

[9] Van de Hulst, in *The Atmospheres of the Earth and Planets*, ed. G. P. Kuiper (1949), p. 106.

Since these calculations indicate that the cloud surface is lowest at about the subsolar point and that it rises away from this point, the most obvious possible explanation is that the sun evaporates the ammonia cloud particles and causes the cloud surface to be lowest where solar heating is most intense. Where solar heating is less intense, the atmosphere is cooler, and condensation of ammonia takes place, which results in a thicker and higher cloud. Alternatively, it might be claimed that the cloud surface is actually level and the relative uniformity of methane absorption on Jupiter exists because the absorption falls on the portion of the curve of growth which lits between the linear and square-root absorption regions. In this intermediate region the slope of the curve of growth is often nearly zero, so that an increase in methane in the path would produce little or no increase in absorption. Although only a properly designed laboratory test could definitely settle this point, there are two arguments which may be advanced against this possibility. First, this transition region on the curve of growth occurs theoretically when the center of the line or band approaches complete absorption. This is far from the case for the 6190 A band on Jupiter for which the maximum absorption is 16.6 per cent at the equator. This also suggests that the linear assumption is more suitable than the square-root assumption. In this connection it should be pointed out that this band, which has been assigned the designation $6\nu_3$, consists of approximately 14 bands nearly superimposed, according to Adel and Slipher.[10] Thus it is probably unresolvable, since the continuum between any two lines is filled with the lines due to all the other component bands. This means that the composite band departs from complete absorption because the lines composing it are unsaturated, not because the instrument integrates saturated lines with the adjacent continuum. Thus the argument given above about the curve of growth, which is strictly applicable to a line, may be applied to the entire band. Second, Table 2 indicates a slight decrease in absorption away from the center rather than the complete uniformity or slight increase to be expected on this basis. Therefore, the explanation in terms of the height of the upper cloud surface seems preferable.

IV. RESULTS FOR AMMONIA ON JUPITER

The relative absorptions due to ammonia in the line of sight at various places on the planet are presented in Table 2. Here, too, the expected increase in absorption away from the center is absent. Instead, there are some definite decreases in absorption away from the center of the disk.

The ammonia measurements may be reduced to temperature differences by the following argument. If we assume the atmosphere to be completely mixed vertically, the partial pressure of ammonia at the Jovian surface will be

$$p=\frac{\bar{m}\mu g}{m}\cos\theta\,, \tag{4}$$

where $\bar{m}$ is the mean molecular weight of the atmosphere, m the molecular weight of NH_3, and μ the mass per unit area of NH_3 traversed by the light coming to us from the planet's surface. We shall again assume a curve of growth which is either linear or square root, so that

$$\mu=C_1W^n\,, \tag{5}$$

where C_1 is a constant and n is either 1 or 2. Equation (4) then becomes

$$p=\frac{\bar{m}C_1g}{m}\cos\theta W^n\,. \tag{6}$$

---

[10] *Phys. Rev.*, **46**, 902, 1934.

Since the temperature of the Jovian surface is low enough to cause condensation of NH_3 to solid cloud particles, we also have, from an integration of the Clausius-Clapeyron equation,

$$p = C_2 e^{-mL/RT}, \tag{7}$$

where C_2 is a constant and L is the latent heat of sublimation, which is assumed to be constant. Combination of equations (6) and (7) yields

$$\cos\,\theta W^n = \frac{C_3 m}{\bar{m} g}\, e^{-mL/RT}. \tag{8}$$

When we observe two points on the disk, denoted by 1 and 2, equation (8) applies to each point separately, and if we take ratios,

$$\frac{\cos\,\theta_1 W_1^n}{\cos\,\theta_2 W_2^n} = e^{(mL/R)(1/T_2 - 1/T_1)} \approx e^{(mL/RT^2)(T_1 - T_2)},$$

where T is the mean temperature of the surface. The temperature difference between the two points is then

$$T_1 - T_2 = \frac{RT^2}{mL}\left[n \ln \frac{W_1}{W_2} + \ln \frac{\cos\,\theta_1}{\cos\,\theta_2}\right].$$

When we insert the numerical values used before and L = 435 cal/gm, we get

$$T_1 - T_2 = 13.8\left[n \log_{10} \frac{W_1}{W_2} + \log_{10} \frac{\cos\,\theta_1}{\cos\,\theta_2}\right], \tag{9}$$

where $T_1 - T_2$ is in degrees Celsius.

Equation (9) has the important and fortunate property that easily detectable differences in absorption imply rather small differences in temperature. This gratifying sensitivity comes about because near the temperature of the Jovian surface the curve of saturation vapor pressure of ammonia versus temperature is very steep. Thus a small change in temperature means a large change in the saturation vapor pressure, and so a large change in absorption.

The relative amounts of ammonia in a vertical column and the calculated temperature distribution are given in Figure 2. If the cloud surface is diffuse, the temperatures are those of the mean level of penetration of the light. Again two curves are plotted in each case, one for each value of n, and again there is no great difference between the curves for $n = 1$ and $n = 2$. Two things are especially noteworthy. First, the temperature decreases toward the poles. This is consistent with expectation if solar heating is of primary importance on Jupiter. Second, the temperature difference between latitude 60° and the equator is rather small. It is only some 6° C, which is several times smaller than the corresponding terrestrial value. This is understandable in terms of the large diurnal variation in the height of the upper cloud surface at the equator. This variation suggests that much of the solar heat received goes toward sublimation of ammonia crystals rather than toward an increase in temperature. The more rapid sublimation at the equator keeps the temperature low and decreases the pole-to-equator temperature gradient.

The relative amounts of ammonia in the vertical at the equatorial limbs of the planet are given in Table 3, together with the calculated temperature differences. Since it is the effect of the total absorbing path as the light comes in from the sun and is reflected out again that is important, one must consider the phase effect in working near the limbs. This was included in computing the data of Table 3. Both limbs have less ammonia in the vertical than in the central meridian and therefore are cooler according to the physical interpretation proposed here. It is especially interesting to note that the morning limb, which had just undergone 5 hours of radiation to space with no compensating insolation, is calculated to be 4°–5°C cooler than the evening limb. This is what one would expect and constitutes support for the validity of the simple theory upon which these temperature calculations are based.

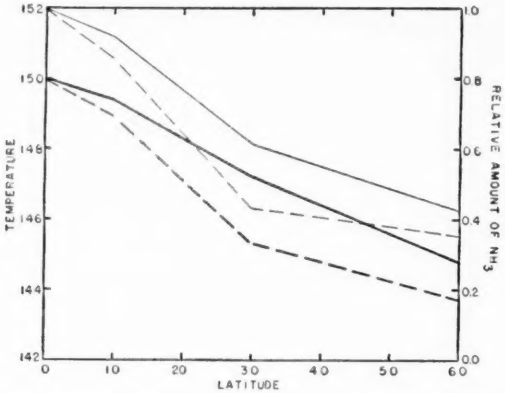

FIG. 2.—Temperature (° K) of the visible cloud surface of Jupiter along the central meridian as a function of latitude (*heavy lines*), assuming the equatorial temperature to be 150° K. The ratio of the amount of ammonia in a vertical column to the equatorial amount is given by the thin lines. The solid lines are for $n = 1$, and the dashed lines are for $n = 2$.

TABLE 3

RELATIVE AMOUNTS OF AMMONIA IN THE VERTICAL ALONG THE EQUATOR

LOCATION	AMOUNT OF NH_3 RELATIVE TO CENTRAL MERIDIAN		TEMPERATURE DEFICIT RELATIVE TO CENTRAL MERIDIAN (° C)	
	$n=1$	$n=2$	$n=1$	$n=2$
Central meridian . . . (long. = 0°)	1.00	1.00	0.0	0.0
Morning limb . . . . . (long. = 60°)	0.24	0.15	7.6	9.7
Evening limb . . . . . (long. = 60°)	0.54	0.51	3.9	4.8

V. RESULTS ON SATURN

Only the methane absorption could be dealt with quantitatively on Saturn, because the small amount of ammonia present produces too feeble an absorption for accurate measurement with the present procedures. The results are given in Table 4. Again these are the values in the line of sight, with no correction to the vertical. The results for the limbs have been omitted because of interference by Saturn's ring system. At this opposition the rings were seen nearly edge-on from earth and so were close to the equator.

Some years hence the rings will be more inclined to our line of sight, and it will be possible to make measurements at the morning and evening limbs.

Table 4 shows a quite different distribution of methane absorption than was found on Jupiter. The absorption clearly increases with latitude instead of decreasing slightly. Saturn, therefore, behaves according to expectation. The differences in absorption at various latitudes are more closely, but not completely, accounted for solely by the variation of path length with latitude. Thus at 55° S. there is 0.68 ($n = 1$) or 0.79 ($n = 2$) times as much methane in a vertical column as at 5° S., while at 45° N. there is 0.86 ($n = 1$) or 1.05 ($n = 2$) times as much methane in a vertical column as at 5° S. Thus, from equation (3), the cloud surface should be 5–8 km higher at 55° S., and not significantly different in elevation at 45° N., as compared to 5° S. These heights were computed using $m = 4$ and $T = 120°$ K. It must be remarked, however, that in correcting to a vertical column there is considerable dependence on the latitude at which the spectrograph slit is placed. The latitudes reported are estimates only, and on so small a disk as Saturn's the errors so introduced may not be negligible. Nevertheless, it seems valid to conclude that the observed increase in absorption toward the poles on Saturn indicates a more uniform atmospheric pressure along the cloud surface than is the case for Jupiter.

TABLE 4

EQUIVALENT WIDTHS OF ABSORPTION ON SATURN

Latitude	6190 A Methane Band (A)	Probable Error of $W_{eq}-W$ (A)	No. of Spectra
Equator (5° S.)	23.2±2.8	....	3
S. hem. (55° S.)	27.2	±0.7	3
N. hem. (45° N.)	28.2	±0.8	3

VI. CONCLUSION

The observations and their interpretation as presented here indicate that careful spectral analysis of various regions on Jupiter and Saturn may reveal gratifyingly small differences in elevation and temperature. The variation in methane absorption due to a difference in the height of the reflecting surface of as little as 10 km is easily detectable, and a difference in absorption of 10 per cent (which is probably close to the limit of accuracy of photographic photometry) corresponds to about 1 km difference in height on Jupiter. To bring home the potential sensitivity of this method, it may be noted that a feature on Jupiter which protrudes 10 km above its surroundings would, when viewed on the limb, extend outward by only 0″.004.

The accuracy of the calculations of height does not depend critically upon any of the following factors: (1) the assumption of vertical isothermalcy, (2) the value of temperature adopted, (3) the slope of the curve of growth. The calculated heights are inversely proportional to the mean molecular weight, which may be in error by as much as a factor of 2, probably less. Errors in height due to errors in estimating the planetocentric angle between the point of observation and the center of the disk are proportional to the tangent of this angle and so are far more serious near the edges than elsewhere. It is estimated that the error in placing the slit on Jupiter nowhere exceeded 5° of latitude. Even at latitude 60° this means an error in height of only 2 km. For Saturn with its smaller disk, this may have contributed appreciable error.

With respect to the determination of temperature differences from ammonia measurements, the results do not depend critically upon the adopted value of the temperature or the slope of the curve of growth. They depend upon the chosen mean molecular weight to the same extent as the height determinations discussed above. The most serious assumption underlying the method is that the ammonia vapor is completely mixed vertically, so that it constitutes the same fraction of the atmosphere at all elevations. The fact that condensation takes place at the cloud surface would tend to produce a gradient of the ammonia mixing ratio with height, just as condensation and precipitation of water near and at the surface of the earth produce a vertical gradient of water-vapor mixing ratio. If vertical turbulence is sufficiently intense on Jupiter, the NH_3 mixing ratio may be nearly constant, nevertheless.

We have no information at all on the vigor of vertical turbulence on Jupiter, nor can we deduce anything about it from the observed horizontal mixing processes. This is because turbulence in planetary atmospheres is almost certainly anisotropic, as it is on earth. Very little can be said, therefore, about the effect of this assumption on the temperature results. A factor which minimizes error from this source is that the method is a relative one, in which various regions are compared to one another. Thus it is not the departure from constant mixing ratio which is important, but rather it is whether the departure varies from place to place that matters.

NOTES

A PROBABLE CLUSTERING OF BLUE GIANTS IN CYGNUS

In the course of the general program of the classification of blue giants (OB stars) at the Tonantzintla Observatory, a clustering of eleven of these objects was noticed in an area of less than 1 square degree near $l = 47°$, $b = 0°$, about 2° northeast of γ Cygni.

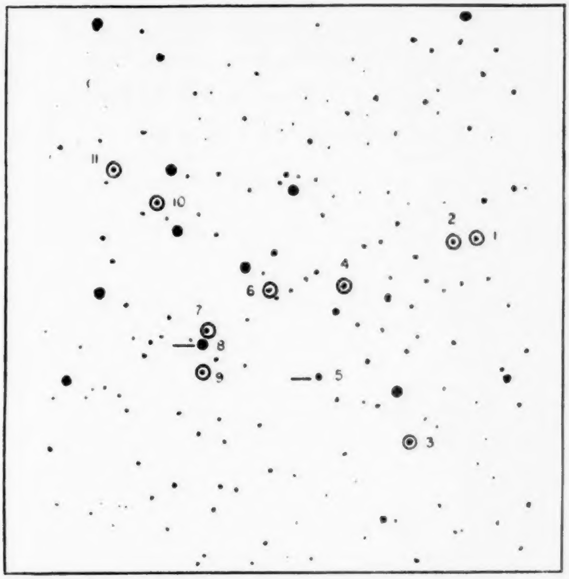

FIG. 1.—Identification of blue giants in clustering. The field is 50′ square. Star No. 8 is BD+40°4227. North is at top; east is at left.

TABLE 1

NEW OB STARS IN THE *Bonner Durchmusterung*

No.	BD	R.A. (1855)	Dec. (1855)	Mag. (*BD*)
3	+40°4212	20h26m5	+40° 43′	9.5
4	+40°4219	20 27.1	+40 57	9.5
10	+41°3804	20 28.6	+41 03	9.5
11	+41°3807	20 28.9	+41 07	9.5

Two of the eleven stars have already been published as of class OB; they are Nos. 5 (+40°4220; *Ap. J.*, **115,** 470, 1952) and 8 (+40°4227; *Ap. J.*, **113,** 149, 1951); the numbers are identified in Figure 1. The remainder are believed to be new.

Four of the other stars are also in the *Bonner Durchmusterung;* they are listed in Table 1.

The apparent visual magnitudes of the stars range from around 9 to 11. They are therefore fainter than the bright OB stars in the neighborhood of P Cygni.

The determination of spectroscopic absolute magnitudes and color excesses for the group would be of interest.

Luis Münch
W. W. Morgan

Observatorio de Tonantzintla
Puebla, México

Yerkes Observatory
Williams Bay, Wisconsin
March 18, 1953

THE NEBULA NEAR 10 LACERTAE

It is generally assumed that the ionized gas of the galaxy is found in a layer 200 psc in total thickness.[1] Several O stars are, however, farther than 100 psc from the galactic plane. Among them is the O9 star 10 Lacertae, with a true distance modulus[2] of $m_0 - M = 8^{m}8$ and $z = -170 + z_{\odot}$ psc, where $z_{\odot}$ is the distance of the sun from the plane. Recently the writer has observed that 10 Lacertae ionizes an *H* II region[3] near it. This emission nebula is unusually interesting for several reasons. First, the nebula is not in Gould's belt, unlike other diffuse galactic nebulae[4] known to be nearly as far from the galactic plane. One of the nodes of Gould's belt on the galactic plane is at longitude $l \simeq 70°$, while the longitude and latitude of 10 Lacertae are $l = 64^{\circ}.8$, $b = -17^{\circ}.3$. The second point of interest about the nebula is its complete freedom from other *H* II regions in the line of sight and from much interstellar absorption. The faintest stars on the *Franklin Adams Chart* of its area appear to be uniformly distributed. Also there are eleven stars in the list of Stebbins, Whitford, and Huffer[5] within 3° of 10 Lacertae.

TABLE 1

THE O AND B STARS WITHIN 3° OF 10 LACERTAE

HD No.	Lac	m_v	Sp.*	E_1 (Mag.)	R.V.$_*$ (Km/Sec)	R.V.$_{H,K}$ (Km/Sec)	Int.
212883		6.39	B2 V	+0.04	− 6.5	......	......
2978	...	6.07	B2 V	+ .01	−16.8	−86.3, −12.7	2, 10
3976	...	7.00	B1.5 V	+ .03	−17.2	......	......
4167	8 ft.	6.55	B2 V	− .04	−15.1	−32, −16.1	1, 6
4168	8 br.	5.83	B1 Vne	+ .05	− 1±6 (bin.)	−31.2, −13.9	1, 8
4263	...	6.75	B2 V	− .01	−19.5	......	......
4432	...	7.4	B3 V	+ .04	......	......	......
4652	..	6.67	B2:V	+ .04	+19±9 (bin.)	......	......
4680	10	4.91	O9 V	.00	− 9.5	−36.3, (−31.6), −27.3, −12.5	2, 2, 8
4993	12	5.18	B2 III	+ .01	−14.5	−33.4, −11.6	1b, 10
5191	......	6.22	B1 V	+0.05	−17.8	−12.8	8b

* W. W. Morgan.

---

[1] Cf. G. Westerhout and J. H. Oort, *B.A.N.*, **11**, 323, 1951.

[2] W. W. Morgan, unpublished.

[3] B. Strömgren, *Ap. J.*, **89**, 526, 1939; **108**, 242, 1948.

[4] E. Hubble, *Ap. J.*, **56**, 162, 1922; S. Cederblad, *Lund. Medd.*, II, No. 119, chap. iii, 1946.

[5] *Ap. J.*, **91**, 20, 1940.

Their color excesses E_1, given in Table 1, appear to be rather small and uniform. Variations in the apparent *emission measure*[3] EM of the nebula from point to point are therefore attributable to the nebula itself.

Observations of the nebula were made with the B spectrograph at the Yerkes Observatory during a program of spectrographic observations of galactic emission regions and nebulae which have already been described.[6] Table 2 gives data on seven spectrograms with positive results. The center of the E-W slit had nearly the same right ascension as 10 Lacertae throughout, while the difference between the declination of the center of the slit, δ_s, and the declination of 10 Lacertae, δ_*, is tabulated. The difference between the right ascension of the strongest $H\alpha$ emission on the slit α_n and of 10 Lacertae α_* is expressed in degrees in the last column.

The spectrograms show $H\alpha$ and sometimes [N II] 6584 and [S II] 6717. The $H\alpha$ emission extends as far as 2°0 = 20 psc from 10 Lacertae. Most of it is west of 10 Lacertae with abrupt changes in intensity along the slit, imitated rather closely by the emissions at λ 6584 and λ 6717. Figure 1 is a drawing of the nebula in the light of $H\alpha$ from the seven spectrograms of Table 2. The positions of 10 Lacertae and the ten B stars of Table 1 are marked on it. The picture may suggest an oval loop of emission, but 10 Lacertae is not at its center.

TABLE 2

SPECTROGRAMS OF THE NEBULA NEAR 10 LACERTAE

$\delta_s-\delta_*$	Exposure Time	U.T. 1952	Film B	$(\alpha_n-\alpha_*)\cos\delta_s$
+60′......	2^h38^m	Nov. 12	164	−0°1: center of diffuse segment
+28......	5 36	Nov. 22	166	−1.3
+ 8......	6 19	Nov. 13	165	−1.5: center of dense "knot"
− 5......	7 26	Oct. 22	127	−1.6: center of dense "knot"
− 7......	6 19	Nov. 11	163	−1.6: center of dense "knot"
−30......	4 25	Dec. 8	181	−1.6; −0.6: two segments
−60......	7 08	Oct. 24	131	−0.6: center of diffuse segment

On the assumption that the number of hydrogen atoms or ions per cubic centimeter N_H is uniform and that the ionization limit is $s_0 = 20$ psc from 10 Lacertae taken as the only source of radiation, the theory[3] of such regions leads to a density $N_H \simeq 3.5$ and a central $EM \simeq 2 \times s_0 N_H^2 = 490$. We can make another estimate of the central EM in the following way. Strömgren[7] has made intensity estimates of $H\beta$ emission which he reduces to a central $EM = 7200$ for IC 405. Preliminary spectrophotometric measures of the writer's plates of the central region of IC 405 and the nebula near 10 Lacertae give the intensity ratio of $H\alpha$ emission between them. This leads to a central $EM \simeq 400$ or 500 and $N_H \simeq 3.5$ in the Lacerta nebula. This is in fair agreement with the previous derivation. The measured intensity ratio between the $H\alpha$ emission knot 1°6 west of 10 Lacertae and the $H\alpha$ emission near 10 Lacertae is 3. Since the diameter of the H II region near 10 Lacertae appears to be about six times the thickness of the knot, the knot may be $\sqrt{3} \times 6 = 4$ times as dense as the mean gas density in the nebula.

The writer's measured intensity ratio between $H\alpha$ emission and [N II] 6584 emission in the nebula is 3. This is near the average of the values of the same ratio in a number of brighter nebulae,[8] including the Orion nebula, which has a central EM of the order of 10,000 times stronger than the EM of the Lacerta nebula.[7]

---

[6] H. M. Johnson, *Ap. J.*, **117**, 235, 1953.

[7] *Problems of Cosmical Aerodynamics* (Dayton, Ohio: Central Air Documents Office, 1951), p. 7.

[8] T. L. Page, *Ap. J.*, **108**, 157, 1948.

The volume of gas ionized by the ten B stars within 3° of 10 Lacertae, taken to act together,[3] is about one-quarter the volume ionized by 10 Lacertae, so that neglect of them in the computation of N_H seems justified. But it is evident that N_H is not uniform, so that the density derived by assuming it uniform should be an upper limit.[3] Moreover, the observed limit of the emission may be short of the range of ionization s_0. In this case our setting the observed limit equal to s_0 would again make the computed N_H an upper limit. Possibly the observed emission nebula is a concentration on a general stratum of gas. The emission nebula and the center of gravity of the eleven O or B stars of Table 1 are both displaced about 1° = 10 psc west of 10 Lacertae. A physical relationship between this configuration of stars and a mass of denser gas seems plausible: The mass of this nebula should exceed that of the eleven stars near it (about 110 ⊙) unless $N_H < \frac{1}{4}$.

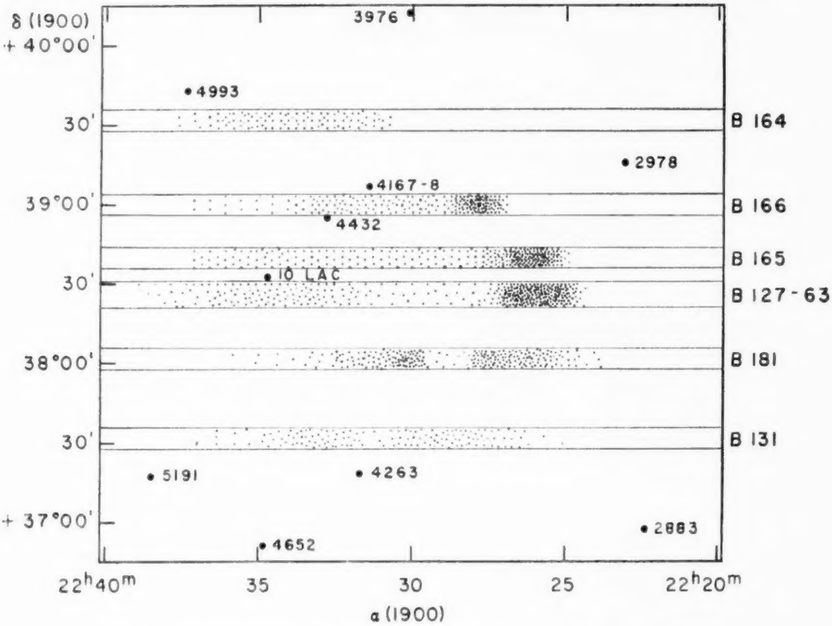

FIG. 1.—The nebula near 10 Lacertae in *Hα* with the near-by B stars of Table 1

Table 1 is completed with the radial velocity of each star from Moore's *General Catalogue*, the radial velocity of the interstellar H and K absorption lines of *Ca* II, and the intensity of the K line according to Adams.[9] The strongest K line in each case has a radial velocity nearly equal to the mean of the stellar radial velocities if HD 214652 is excepted. Thus it may be reasonable to associate this *Ca* II cloud with the gas known to be near 10 Lacertae. If this is done, however, the intensities of this *Ca* II K line appear to show much smaller fluctuations than the emission-line intensities of *Hα*. Furthermore, the calcium absorbs nearly uniformly over a considerably greater area of the sky than the $H\alpha$ emission covers. The calcium may be more evenly distributed than the hydrogen and/or closer to us than the nebula near 10 Lacertae.

---

[9] *Ap. J.*, **109**, 354, 1949; *Mt. W. Contr.*, No. 760, 1949.

We conclude that rather sharply defined clouds of gas occur near 10 Lacertae at $z \simeq -170$ psc with an over-all density $N_H \leqslant 3.5$; that the clouds may be concentrated toward the center of gravity of a configuration of several stars in the Lacerta aggregate[10] of early-type stars; and that the intensity ratio of $H\alpha$ emission to [N II] 6584 emission is about 3 in nebulae differing greatly in *EM*.

The writer wishes to thank Dr. B. Strömgren and Dr. W. W. Morgan for advice in the preparation of this note, and Dr. Morgan for the use of his unpublished spectroscopic distance moduli and spectral types.

HUGH M. JOHNSON

YERKES OBSERVATORY
February 3, 1953

[10] A. Blaauw and W. W. Morgan, *Ap. J.*, **117**, 256, 1953.

PHOTOELECTRIC MAGNITUDES AND COLORS IN NGC 6231

During five nights in October, 1950, fifty-five two-color observations were made on twenty stars in the galactic cluster NGC 6231. The observations were made with an unrefrigerated 1P21 photoelectric photometer mounted on the 24-inch (blue-corrected) component of the Victoria telescope at the Royal Observatory, Cape of Good Hope. A description of the apparatus has been given elsewhere.[1] The colors and magnitudes of the twenty stars listed by Struve[2] were tied to the colors and magnitudes of the stars D, H, K, and M in the near-by Harvard Standard Region E7 located at −45° declination. Transfers were made on each of the five nights, giving a total of nineteen observations made on the E7 stars. The probable errors of the mean zero points are ± 0.008 mag. for the blue; ± 0.006 mag. for the yellow; and ± 0.005 mag. for the color. One observation consisted of measures of the starlight with yellow and blue filters in this order: dark, yellow, blue, dark, blue, yellow, dark. The duration of each measure was 20 seconds. Most stars have only two observations; observing conditions were not ideal because of rather large hour angles. Frequent measures of the sky brightness were made.

The residuals from the final mean magnitudes for all the cluster stars give the probable errors of a single measure as ± 0.017 mag. for the blue, ± 0.015 mag. for the yellow, and ± 0.012 mag. for the color. The star HD 152248 was observed to be about 0.1 mag. fainter over a 2-hour period on October 6, 1950 (JD 2433561.25). It is perhaps an eclipsing binary, since it has already been identified by Struve as a spectroscopic binary.

An investigation of possible nonlinear color relations between various color systems due to ultraviolet transmission was made. When our filter-photomultiplier combination was used with the Victoria refractor, the blue response-curve was slightly altered from that previously published.[1] The result is a B filter almost identical with Johnson's $\boldsymbol{B}$ filter.[3] Since such a B filter has no troublesome ultraviolet transmission, linear relations are assumed in all cases.

The S' magnitudes and colors can be derived, using the following known relations[1] between the S' system and the natural color system (B, C) of the photometer: $S'Pg = B + 0.08\,C$; $S'Pv = V - 0.21\,C$; $S'CI = 1.29\,C$. These relations hold for observations taken at or near sec $z = 1.55$ to which all observations were corrected. The zero point of the final S' magnitudes is made to fit the provisional S' magnitudes of the E7 stars according to Stoy.[4] The S' system is related to the system of Stebbins, Whitford, and Johnson at the north pole by the relations: $\boldsymbol{P} = S'Pg + 0.10$; $\boldsymbol{V} = S'Pv + 0.10\ S'CI - 0.06$; $(\boldsymbol{P} - \boldsymbol{V}) = 0.90\ S'CI + 0.16$.[1] Observations of the colors of unreddened stars are available on the Cape photoelectric system and on the $(\boldsymbol{B}, \boldsymbol{V})$ system. In all probability, the Cape photoelectric system rejects light of wave length shorter than 3800 A, just as our B filter does.

---

[1] A. N. Cox, *Ap. J.*, **117**, 83, 1953.

[2] *Ap. J.*, **100**, 189, 1944.

[3] *Ap. J.*, **116**, 275, 1952.

[4] Private communication.

Table 1 contains for each cluster star its Struve number, its HD or CD number, the spectral type, $\boldsymbol{P}$, $(\boldsymbol{P} - \boldsymbol{V})$, $S'CI$, and $(\boldsymbol{B} - \boldsymbol{V})$. Dr. W. W. Morgan determined these spectral types from the Struve spectrograms,[2] and he has kindly supplied us with these classifications. Table 2 gives the observed S' magnitudes and colors for the E7 stars.

TABLE 1

MAGNITUDES AND COLORS OF 20 STARS IN NGC 6231

Struve No.	HD or CD	Sp. Type	$\boldsymbol{P}$	$\boldsymbol{P-V}$	$S'CI$	$\boldsymbol{B-V}$
1	152003	cB0	7.26	+0.26	+0.11	+0.40
2	152042	*	8.15	− .01	− .19	+ .15
3	152076	dB0	8.55	+ .11	− .06	+ .26
4	152147	cB0	7.55	+ .28	+ .13	+ .42
5	152218	dO9‡	7.64	+ .07	− .10	+ .22
6	152233	O6	6.50	+ .04	− .13	+ .20
7	152234	cB0.5	5.53	+ .10	− .07	+ .25
8	152235	cB1	6.75	+ .42	+ .29	+ .55
9	152247	O9	7.26	+ .10	− .07	+ .25
10	152248	O8‡	6.03	+ .02	− .16	+ .18
10†	....	....	6.16	+ .03	− .15	+ .19
11	152249	cO9	6.49	+ .07	− .10	+ .22
12	−41°11037	dO9	7.83	+ .04	− .13	+ .20
13	−41°11042	dO9	8.27	+ .11	− .06	+ .26
14	−41°11044	O8	7.45	+ .06	− .11	+ .21
15	152314	dO9	7.83	+ .09	− .08	+ .24
16	152424	cO9	6.57	+ .28	+ .13	+ .42
17	152408	O7–8fp	5.83	+ .04	− .13	+ .20
18	151804	O9f	5.15	− .06	− .24	+ .10
19	152270	Wolf-Rayet	6.64	− .02	− .20	+ .14
20	151932	Wolf-Rayet	6.61	+0.12	−0.04	+0.27

* No plates available.

† October 6–7, 1950.

‡ Double-lined spectroscopic binary.

TABLE 2

OBSERVED MAGNITUDES AND COLORS OF E7 STARS

Star (Region E7)	$S'Pg$	$S'CI$	Star (Region E7)	$S'Pg$	$S'CI$
D	7.58	−0.37	K	8.69	+1.13
H	8.11	−0.04	M	8.73	+0.07

In order to obtain a distance for the cluster, attention is fixed only on the main-sequence stars whose Struve numbers are 3, 5, 12, 13, and 15. Stoy has kindly communicated the colors of many early-type stars on the Cape photoelectric system.[5] The normal color of a main-sequence O9 star converted to the S' system is about -0.63 mag. The mean *observed* color index of the main-sequence cluster stars on the S' system indicates a color excess of 0.54.

Recent work by Johnson indicates that O9 V stars have a $(B - V)$ color of about -0.32.[6] Using the known relation: $(P - V) = 1.09\,(B - V - 0.16)$, the normal unreddened $(P - V)$ color is -0.52. The average color of the cluster stars on the (P, V) system is $+0.08$, giving a color excess of 0.60.

It is assumed here that color excesses on two different systems are related in the same way as are the color indices. Converting the S' color excess to the (P, V) system, the two methods result in the values 0.49 and 0.60. The ratio of total absorption in visual light to selective absorption on the (P, V) system is assumed to be 2.8.[7] The visual absorption, therefore, is about 1.5 mag.

TABLE 3

DISTANCE DETERMINATION DATA

Struve No.	Sp. Type	M_V	$(V - M_V)$ Approx.	$(V - M_V)$ True	Distance (Parsecs)
3	dB0	−4.0	12.4	10.9	1510
5	dO9	−4.3	12.6*	11.1	1660
12	dO9	−4.3	12.1	10.6	1320
13	dO9	−4.3	12.5	11.0	1590
15	dO9	−4.3	12.0	10.5	1260
Mean					1470†

* The double-lined spectroscopic binary, 5, has been corrected for duplicity. Stars 12 and 13 are also spectroscopic binaries, but the uncertain correction has been omitted.

† The formal probable error of the mean is ± 60 parsecs. This does not allow for errors in the assumed value of either the total absorption or the absolute magnitudes.

Table 3 gives the data on the distance determination. For the five main-sequence stars are given the spectral type, the absolute magnitude, the apparent distance modulus, the true distance modulus, and the distance. The absolute visual magnitudes from Morgan were systematically changed by 0.1 mag. to get them on the V system. The mean distance to the cluster is 1470 ± 150 parsecs. Absorption in this region of the sky is rather spotty, as can be seen from a picture published by MacRae.[8] Our distance and our value for the photographic absorption (2.2 mag.) can be compared with those determined by Kholopoff,[9] which were 1400 ± 300 parsecs and 3.0 mag., respectively.

Figure 1 shows a color-luminosity array of the data in Table 1.

The following statement concerning the spectral types is by W. W. Morgan:

> The spectral types listed in Table 1 are approximate values determined from a series of spectrograms obtained by Struve for radial velocity measurements; they are on the system of the Yerkes spectral atlas, as revised for supergiants (*Ap. J.*, **112,** 363, 1950). The prefixes "c" and

---

[5] Some of this information was published in preliminary form in *Observatory*, **71,** 201, 1951.

[6] H. L. Johnson and W. W. Morgan, *Ap. J.*, **117,** 346, 1953.

[7] This ratio is based upon recent observations by D. L. Harris and H. L. Johnson (in press).

[8] *Harvard Bull.*, **914,** 21, 1940.

[9] *Astr. Zhur.*, **28,** 491, 1951.

"d" have been preferred to luminosity classes because of the preliminary nature of the classification; the plates were not intended for the determination of accurate spectral types.

From the point of view of the stellar astronomer, the stars in the neighborhood of NGC 6231 are of especial interest, since they afford the opportunity for an accurate calibration of the O and early B supergiants from the cluster parallax, which could be determined from the fainter main-sequence objects. A detailed investigation of this cluster would be of the greatest interest.[10]

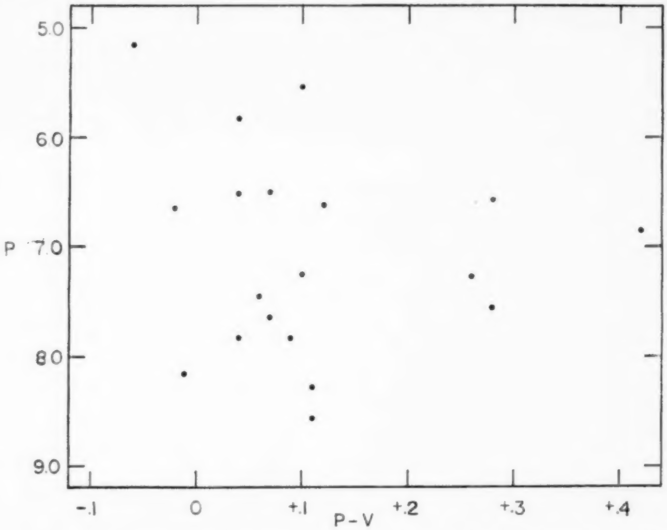

FIG. 1.—The color-luminosity array for the nineteen nonvariable stars in NGC 6231

It is a pleasure to thank H.M. Astronomer, R. H. Stoy, and his staff at the Royal Observatory for their generous hospitality and assistance in the observational aspects of this program. The project has been supported by the Graduate School of Indiana University. Some of the photoelectric equipment was constructed from a Research Corporation grant.

ROBERT R. BROWNLEE
ARTHUR N. COX

GOETHE LINK OBSERVATORY
INDIANA UNIVERSITY

March 10, 1953; revised April 6, 1953

[10] Private communication.

THE OBSERVATORY

FOUNDED 1877

* * *

A Magazine presenting current developments in Astronomy by means of Articles, Correspondence, Notes on discoveries and Reviews of important astronomical books. The papers read at the Meetings (Astronomical & Geophysical) of the Royal Astronomical Society and the discussions which follow are also fully reported.

* * *

Annual subscription for 6 issues, post free, £1 (U.S.A. and Canada, $3.00) should be sent to

***The Editors,* ROYAL GREENWICH OBSERVATORY**
Herstmonceux Castle, Hailsham, Sussex, England

THE ASTROPHYSICAL JOURNAL

announces the publication of

A GENERAL INDEX, Volumes 76–100

Price: $5.00*

ORDERS NOW ACCEPTED

Also available:

GENERAL INDEX, Volumes 1–25 ....$2.50
GENERAL INDEX, Volumes 26–50 ....$2.50
GENERAL INDEX, Volumes 51–75 ....$2.50

*** Postage $0.15 per copy extra to foreign addresses.**

THE UNIVERSITY OF CHICAGO PRESS
5750 ELLIS AVENUE CHICAGO 37 · ILLINOIS

IMPORTANT BOOKS IN THE HISTORY OF ASTRONOMY

THE ARYABHATIYA OF ARYABHATA

An Ancient Indian Work on Mathematics and Astronomy

Translated with Notes by WALTER EUGENE CLARK

Aryabhata's work, which was composed in A.D. 499, is probably the earliest preserved Indian mathematical and astronomical text bearing the name of an individual author; the earliest Indian text to deal specifically with mathematics; and the earliest preserved astronomical text from the third or scientific period of Indian astronomy. This is the first complete translation from the Sanskrit of this historical document.

120 pages *7¾ × 5¼* *$2.50*

LATIN TREATISES ON COMETS BETWEEN 1238 and 1368 A.D.

By LYNN THORNDIKE

This volume publishes for the first time the Latin texts of important tracts on comets observed between 1238 and 1368 A.D. Among the treatises are works by Aegidius of Lessines, Gerardus de Silteo, Peter of Limoges, Geoffrey of Meaux, and John of Legnano. As a summary of the Aristotelian doctrine of comets, the commentaries of Thomas Aquinas and of Albertus Magnus on Aristotle's *Meteorology* are included in English translation.

286 pages *6 × 9* *Index* *$5.00*

THE SPHERE OF SACROBOSCO AND ITS COMMENTATORS

By LYNN THORNDIKE

A critical edition of the Latin text, together with an English translation, of the SPHERE of John of Sacrobosco—for centuries the best and best known manual of astronomy by a Western author. Also included is the hitherto unpublished commentary by Robert of England, with an English translation. In addition, the commentary of Cecco d'Ascoli and the commentary ascribed to Michael Scot are made available for the first time outside of rare books printed in abbreviated Latin.

506 pages *6 × 9* *Index* *$10.00*

THE UNIVERSITY OF CHICAGO PRESS